UNIVERSITAT POLITÈCNICA DE VALÈNCIA

ETS INGENIERÍA DE CAMINOS, CANALES Y PUERTOS

TRABAJO DE FIN DE MÁSTER

Probabilistic structural evaluation of a cable-suspended concrete roof: the Braga Stadium (Portugal)

Presentado por

Roberto Gerussi

Para la obtención del

Máster Universitario en Ingeniería de Caminos, Canales y Puertos

Curso: *2021/2022*

Fecha: *Diciembre de 2021*

Tutor: *Prof. Carlos R. Sánchez Carratalá (*)*

Cotutor: *Prof. Marco Ballerini (**)*

Cotutor: *Prof. Marco Broccardo (**)*

(*) Universitat Politècnica de Valéncia

(**) Università degli Studi di Trento

Acknowledgments

I would like to mention all the people without whom this Thesis could not have been completed.
First of all, I would like to express my thanks to my supervisors: Professor Marco Ballerini and Professor Marco Broccardo of the University of Trento, Professor Carlos Rafael Sánchez Carratalá of the Polytechnic University of Valencia, who in these lasts months have wisely guided and advised me in the development and drafting of this document.
A special acknowledgment also to engineer Giovanni Berti, engineer Massimo Majowiecki and to the staff of MJW structures, who provided information and technical material that was crucial for the realization of this thesis.
A special mention to Professor Lucia Simeoni, to the staff of the International Mobility Office for Science and Technology of the University of Trento, to Professor Julian Alcalá González and to the personnel of the Oficina de Relaciones Internacionales ETSICCP of the Polytechnic University of Valencia, for their kindness, their patience and their availability during this Double Degree program.
I would like to sincerely and warmly thank my family, in particular Ennio, Lauretta and Nicola, for the relief and unconditional trust shown throughout all my life. I also wish to thank my fiancee Martina, for its trust, patience and the confidence that she has always instilled in me through the most difficult moments.
Finally, a special word of thanks to my friends: Matteo, Edoardo and Alessandro, who accompanied and helped me over the years at the University of Trento, as well as Francesco and Geremia, with whom I shared fortunes and misfortunes of an unforgettable year in Valencia.

Abstract

Cable structures often pose a significant challenge, particularly due to the struggle in foreseeing the structural response during the design. Because of this we rely on finite element models, despite their complexity, especially when facing dynamic forces. Hence the need of simplified models, optimized to retrace specific behaviours of the structure and reduce the computational burden. This Master's degree thesis deals with the case of the Braga Stadium, characterised by a roof of concrete shells supported by suspended cables. The aim is to assess whether reliable results regarding its seismic response can be obtained from simplified models.

Starting from the provided designs and information, we calculate the cables geometry and performed a static analysis of the cables and the East stand, whose results re exploited to calibrate the simplified models. The structural layout on parallel elements allows us to simplify the structure as a planar one: we have assembled three models with increasing amount of simplification, that include the cables and the East stand upright. The West stand is not included as on its side the cables are anchored directly to the rock.

The models are evaluated through a multi-support analysis, considering the two uttermost cases: with perfectly correlated accelerograms and with uncorrelated accelerograms. We perform several simulations, extrapolating from each one the peak values of the maximum cable force and the maximum relative displacement of its ends. We then processed these data, calculating the main statistical parameters and the empirical distribution functions for each model.

The comparison shows that using simplified models we can obtain reliable results for the maximum cable forces, but not for the maximum relative displacements. Furthermore, cable modelling cannot be ignored: any simplification must be applied solely to the support structures. Finally, the use of uncorrelated accelerograms causes a significant increase of cable forces, even if a realistic scenario would be intermediate to the two considered. This result enhances the need of a multi-support analysis in this kind of structures, especially in case of large span suspended roofs like the one studied here.

Contents

List of Figures

List of Tables

Chapter 1

Introduction

Mechanics of tensile structures is characterized by an accentuated geometric non-linearity since for such structures the tangential stiffness increases along the load-displacement curve, thus resembling a non-linear geometric hardening behaviour. This means that the internal forces do not increase evenly with the applied loads. Furthermore, as their components undergo only tension, there are no issues with buckling instability phenomena, so that the applicable loads are considerably higher and the material strength can be fully exploited (given the stress state to which these elements are subjected). This evidence allows an higher structural efficiency, as we are able to reduce the ratio between dead loads and live loads. In doing so, it is possible to design surprisingly light structures, with low own weights and therefore higher load-bearing capacity.

Since cable elements have neither bending nor shear stiffness, they can resist only tensile forces, and thereby are able to transmit the external loads only by adapting their shape accordingly: due to this, they can be defined as partially constrained elements, or elements with variable geometry. Thereby, any variation of the applied loads leads to a subsequent variation of the cable geometry and internal forces, according to the hardening behavior already mentioned. This relation between shape, applied loads and internal forces results in a particularly challenging structure for any designer, especially due to the difficulty in foreseeing the structural response during the design, that grows when dynamic forces are considered.

Because of these reasons we often rely on finite element models, that allow to apply numerical methods instead of finding the exact solution to the static and dynamic problems. These can be easily programmed and executed on a computer, with an undoubted advantage in terms of efficiency and precision. Despite this, the accentuated geometric non-linearity and the general complexity of tensile structures dramatically increase the computational load, and consequently also the time required for each analysis cycle and the size of the output data, not to mention the risk of bugs and errors that could compromise the final result. Hence the need of simplified models, that are optimized to model only specific behaviors of the real structure, thus reducing the total

amount and the sophistication of the calculations to be faced.

In this Thesis we want to evaluate the ability of purposely developed simplified models to replicate the seismic response of an existing cable structure. The study case is represented by the Braga Municipal Stadium, characterized by a cable-suspended concrete shell roof, that provides a perfect practical example of the aforementioned structural typology. Further reasons of interest in choosing this structure were the large span of the roof and its layout as parallel suspended cables without damping devices, so that the stabilization against seismic or wind actions is only due to its own weight. Regarding the seismic action, we focused only on its horizontal component directed parallelly to the cables (to which we also refer as longitudinal component), thus optimizing the simplified models according to this action and carrying out a comparative study, to assess whether they can provide reliable results with respect to a realistic model, that acted as reference case.

As established by the design codes, structural elements are designed and checked to support the loads acting over them. Particularly in case of external actions affected by high uncertainty and variability, such as seismic ground motions, the designer does not size the structural elements according to the maximum force related to a specific event, as it is not predictable. Instead, he faces the design process from a probabilistic standpoint, with the aim to maintain the failure probability for an ensemble of several different events under a certain, yet significantly low, value. Consequently, the design forces established according to the seismic design codes are determined by the legislators in compliance with this principle. When comparing the different simplified models with the reference case we kept the same approach, thus considering several simulations of the seismic action to assess their overall behaviour.

Another aspect that we have considered in the evaluation of the simplified models is related to the possible alterations in the transmission of seismic waves through the terrain. During the same seismic event, the different soil characteristics between the supporting structures could give rise to different ground motions on the surface. Due to their structural layout, large span roofs could be extremely sensitive to this phenomenon: to account this aspect we performed a multi-support analysis, applying different ground motions at the base of the two stands of the stadium. Because of the lack of information about the soil characteristics, as well as because of the time required to run and process the numerous simulations, we considered only the two uttermost scenarios: with perfectly correlated accelerograms and with uncorrelated accelerograms. Although these cases are not realistic, they still allow us to understand how the structural response changes because of this problem.

This thesis is divided into the following chapters:

- **Chapter 1**, contains a brief introduction, describing the main reasons of interest about this topic and summarizing the work hereby presented.
- **Chapter 2** contains a literature review, with a complete summary of what was studied in preparation for this thesis and the theories applied in the analysis of the study case.
- **Chapter 3** describes in detail the study case, examining the main characteristics of the structure and summarizing some of the most interesting publications about it.
- **Chapter 4** illustrates the static analysis of the cable, from the loads assessment to the calculation of the resulting forces for various load combinations, also describing the simplification hypotheses assumed.
- **Chapter 5** presents the static analysis and the modal analysis of the East stand, performed using a simplified 2D model.
- **Chapter 6** describes in detail the finite element models developed for this work, from the more realistic model (taken as a reference) up to the simplified ones. A detailed setup of the simulations performed for the multi-support analysis is also included.
- **Chapter 7** briefly describes the data processing of the analysis outputs and the comparison of the results for each model, evaluating their reliability with respect to the reference case.
- **Chapter 8** finally presents the achieved conclusions, summarizing the most significant outcomes.

The attached annexes contain the tables with the numerical results of the analyses, the project drawings that we took as reference, and some brief considerations about some analyses that have been omitted from the main document for the sake of synthesis.

Chapter 2

Literature review

The aim of this chapter is to propose a literature review of some interesting books about tensile structures in general. We will present the theoretical formulations on which their design is founded, with special regard to cable-suspended roofs (since the study case belongs to this category). The review is structured as a summary of the main concepts presented in these books [19] [27] presented in reference, starting from the preliminary design (with some useful approximate formulations), up to the static and dynamic analysis formulas. The chapter will end with a recap of the technical characteristics of the main components of a tensile structure.

2.1 Preliminary and conceptual design

Conceptual design is the first phase of the project, and in the case of tensile structures assumes particular importance as the stress state determines their geometry, and vice versa. This means that the shape itself is determined during the structural design, and not before (as is the case for other structural types), thus raising the need to define all those elements presented in this section: the State 0, approximate formulations, mathematical and physical models testing.

2.1.1 Design process

While talking about a tensile structure, the design is a heuristic decision-making process that comprehends the choice of both geometry and physics of the structural systems, depending on the initial design hypothesis [19]. This can be described as a logical sequence of model making, where each model aims to represent the expected behaviour of the structure by refining and detailing the previous one. The first phase is the conceptual design and relies mainly on the basic knowledge of the engineer. It is in an iterative process to determine the conceptual model by defining the structural typology, the loads that will act over it and its materials.

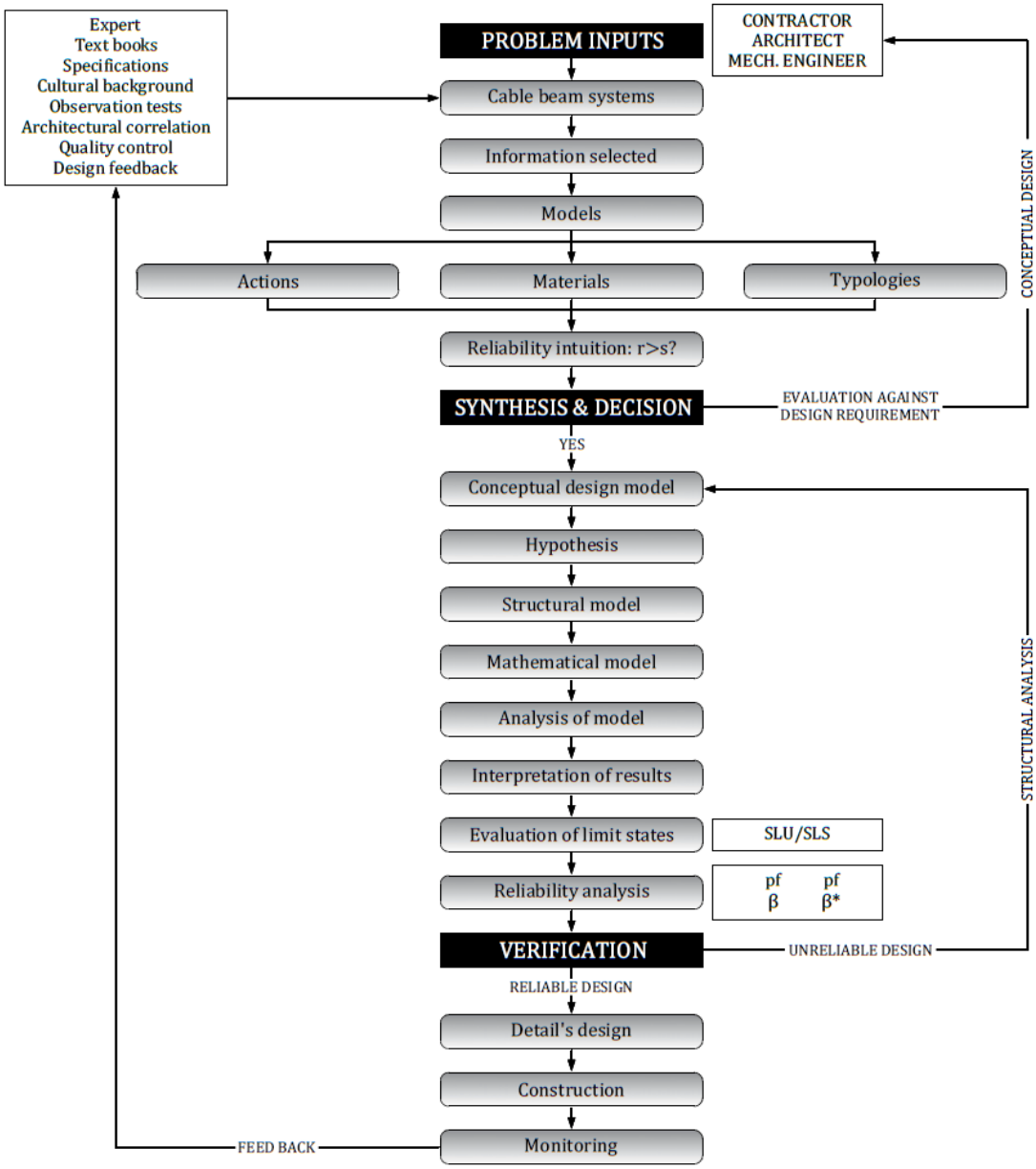

Figure 2.1: Different phases of the design process for a tensile structure. Source: [19]

Once the conceptual model is defined, it is possible to introduce more hypothesis over its mechanical behaviour, thus defining the "structural model". This will be then converted into a mathematical model, eventually applying data from a physical model. The mathematical model is then analysed, to obtain the stress state and strain state: from these we can assess the structural behaviour of the system, as well as verify the stability and strength of each component. The last phase of the structural analysis is the design of the constructive details. Once the execution project is completed, we can finally define the building process and the monitoring systems. The phases thus illustrated are strictly related to the different operative steps of the project definition,

which can be developed as follows:

1. Conceptual proposal and feasibility analysis.
2. Outline proposal.
3. Preliminary design.
4. Final design.
5. Execution design.

The first two steps are more focused on satisfying the architectural requirements and rely mainly on the designer experience and knowledge. The preliminary project consists in the definition of the structural geometry and the stress conditions, and in the overall sizing of the main elements. Then, during the final design the sizing of each component is refined, and its resistance is compared to the serviceability and ultimate limit states to meet the structural requirements. The final phases are the design of the constructive details, the building process, the calculation of both construction and maintenance costs, and the definition of the construction timetable. All these aspects are included in the execution design, which will finally be carried out by the manufacturer.

2.1.2 The State 0

One of the main aspects that affect the design process of a tensile structure is that its geometric configuration depends on both the pre-solicitation status and the border conditions. Because of this, the geometry is not a given data of the design problem. Therefore, the design methodology is characterized by the determination of the state 0, that according to M. Majowiecki can be defined as a geometrical configuration associated with a prestress state that allows to satisfy the static equilibrium in each part of the structure, that can guarantee both static and dynamic stability for the different load conditions, while the geometry of the structural surface satisfies the architectonic requirements [19].

The definition of the state 0 can be carried out in two phases:

- Throughout the preparation and analysis of an architectural model.
- By defining a mathematical model, eventually using the data obtained from the architectural model.

This process is often iterative, with continuous corrections, as it involves the problems related with the non-linearity that characterizes tensile structures.

2.1.3 Architectural models

Architectonic models are often prepared during the first stages of the preliminary design process. Their main purpose is to define and study the geometric features of the roofing system, as well as his functional and aesthetic qualities. We can distinguish three main typologies of architectural models, that rely on different physical principles:

- **Models made from soap bubbles**

  These exploit the fact that a soapy water membrane, defined around a closed perimeter, defines a surface where every point has a uniform distribution of stress: this principle allows to realize models quite closer to the final design. Once the model has been realized, we can track its surface using photogrammetric mapping devices. The main shortcomings are the weakness of the model itself, as well as the small scale, which reduces its precision. The main example of this technique are the studies carried out by Frei Otto on the subject of form finding 2.2.

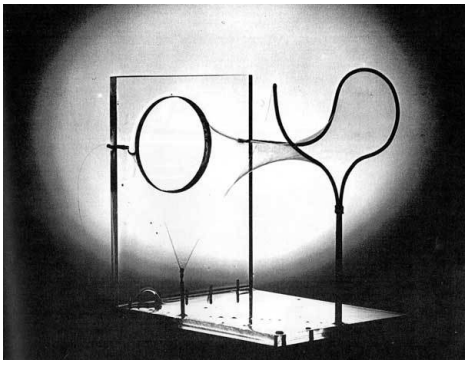

Figure 2.2: Frei Otto was a pioneer with his studies on form finding. These images show some of his models from soap bubbles Source: www.researchgate.net

- **Models made from foam or other elastic material**

  These models are realized using a grid of elastic orthotropic material or elastic foam, which allows to create curved surfaces. They are particularly suited for the studies of the aerodynamic effects carried out in the wind tunnel, as it was the case of the Braga Municipal Stadium 2.3. Another interesting aspect is that they clearly define the volumetric distribution of the spaces under the cover system, which is particularly helpful during the first phases of the architectonic design.

Figure 2.3: Aeroelastic model of the Braga Stadium (Braga, Portugal) developed at the Politecnico di Milano wind tunnel. Source: [15]

- **Models made from steel wires**

  This technique is mainly used to obtain information about the stress and deformation states of the structure subjected to prestress and live loads. These basically rely on the similitude principle, for which the model and the structure should have similar behaviour in terms of geometric characteristics and static performance. Nevertheless, a small measurement error over a scaled model could lead to a severe mistake in the estimation of that value in the reality. This possibility prompted the improvement of interactive software, that develop a reliable mathematical model with the same purposes.

Figure 2.4: Steel wire model of the German pavilion at the 1967 Montreal Expo, designed by Frei Otto. Source: www.archdaily.com

The main disadvantage of all is that the development cost of an architectural model development costs can reach up to the 50% of the value of the total design costs. This fact, combined with their other drawbacks, makes their realization too expensive. Today there are modern interactive design techniques (such as C.A.D., C.A.A.D. and C.A.S.D) that allow to define a reliable mathematical models already during the first stages. Despite that, architectural models can still be used to verify the results of these interactive techniques.

2.1.4 Mathematical models

Mathematical models are defined with the aim of obtaining the geometric configuration that satisfies both static and dynamic balances, in every point of the surface. In this problem load conditions and architectonic restraints over the structure are known, while we must determine in detail its geometry and its stress state. To do that, there are two possible ways:

a) By solving the equilibrium equations for an infinitesimal portion of the membrane.

b) By adopting a discretization of the surface and solving the equilibrium numerically.

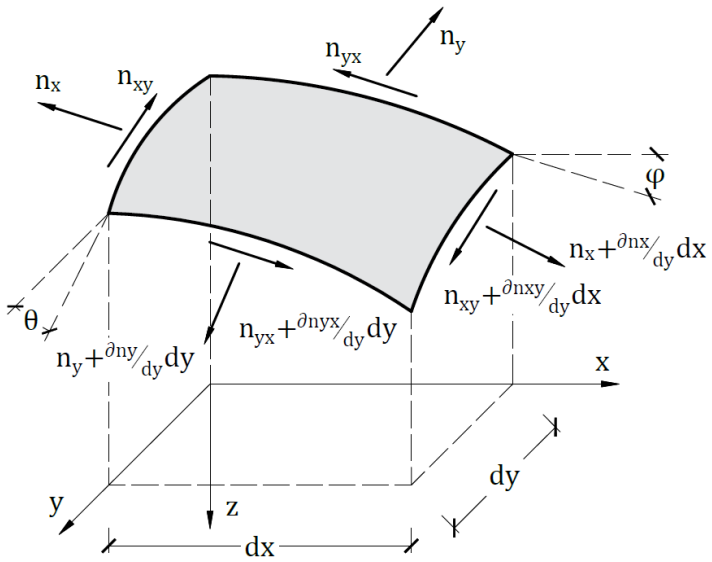

Figure 2.5: Conceptual sketch of a generic infinitesimal membrane portion, along with the stresses acting over it. Source: AutoCAD, own elaboration.

Talking about case a) we can refer to the imagine 2.5, that represents an infinitesimal portion of the membrane.Its equilibrium can be written as shown in equation2.1:

$$\begin{cases} \dfrac{\partial \bar{n}_x}{\partial x} + \dfrac{\partial \bar{t}}{\partial y} + \bar{p}_x = 0 \\ \dfrac{\partial \bar{n}_y}{\partial y} + \dfrac{\partial \bar{t}}{\partial x} + \bar{p}_y = 0 \\ \bar{n}_x \dfrac{\partial^2 z}{\partial x^2} + \bar{n}_y \dfrac{\partial^2 z}{\partial y^2} + 2\bar{t} \dfrac{\partial^2 z}{\partial x \partial y} + \bar{p}_z + \bar{p}_x \dfrac{\partial z}{\partial x} + \bar{p}_y \dfrac{\partial z}{\partial y} = 0 \end{cases} \tag{2.1}$$

where $\bar{n}_x$ and $\bar{n}_y$ are the projection of the normal tension according to their respective direction x and y over the base plane $z = 0$, t is the projection of the shear tension over the base plane $z = 0$, and finally $\bar{p}_x$, $\bar{p}_y$ and $\bar{p}_z$ are the components of the external force

per unit of surface p projected over the planes yz, xz and xy respectively. The relation between the projected tensions and the membrane stresses is defined as:

$$\bar{n}_x = n_x \frac{\sqrt{1+\left(\frac{\partial z}{\partial y}\right)^2}}{\sqrt{1+\left(\frac{\partial z}{\partial x}\right)^2}} \quad \text{and} \quad \bar{n}_y = n_y \frac{\sqrt{1+\left(\frac{\partial z}{\partial x}\right)^2}}{\sqrt{1+\left(\frac{\partial z}{\partial y}\right)^2}} \tag{2.2}$$

Moreover, the hypothesis for which the structure must be in tension results as:

$$n_{min} = \frac{1}{2}\left(n_x + n_y + \sqrt{(n_x - n_y)^2 + 4t^2}\right) \geq 0 \tag{2.3}$$

This system of differential equations can be solved once combined with the boundary conditions associated. We can distinguish two possible cases:

- The geometry is imposed in form of a function $f(x, y) = z$, and the stress state needs to be determined. This is the most difficult case, as it is almost impossible to find a surface that satisfies all the imposed conditions.

- Assuming a known stress state, the unknown is the function $f(x, y) = z$ and the system can be written as a 2^{nd} order PDE with variable coefficients.

Note that the sign of the discriminant term (defined as: $\bar{t}^2 - \bar{n}_x \bar{n}_y$) is invariant for any continuous, real, and differentiable coordinate transformation with nonzero Jac. Because of that it is possible to define a coordinate system for which $\bar{t} = 0$ and the main directions of the internal forces are n_1 and n_2. They can be, depending on their signs:

- $n_1 n_2 = 0 \Longrightarrow$ parabolic PDE.

- $n_1 n_2 > 0 \Longrightarrow$ elliptic PDE.

- $n_1 n_2 < 0 \Longrightarrow$ hyperbolic PDE.

Considering the expression for the Gaussian curvature (defined as $K = k_1 k_2$) the structural surface can be defined as:

- $k_1 k_2 = 0 \Longrightarrow$ parabolic surface.

- $k_1 k_2 > 0 \Longrightarrow$ elliptic surface.

- $k_1 k_2 < 0 \Longrightarrow$ hyperbolic surface.

The synthetic expression for membrane equilibrium without external loads, together with the hypothesis of tension-only stress regime, implies that:

$$\begin{cases} \bar{n}_1 k_1 + \bar{n}_2 k_2 = 0 \\ n_1 n_2 > 0 \end{cases} \longrightarrow \; k_1 k_2 < 0 \tag{2.4}$$

A tensile structure can therefore be defined as a structure with hyperbolic geometry and elliptical stress regime.

The membrane problem can be solved analytically (only in the simplest cases) or numerically (using computers). In such case the membrane equation is approximated using the finite differences method: the surface is discretized and the partial derivative is approximated with a 2^{nd} order formula. The problem obtained by combining to the boundary conditions to the discretized equilibrium equation can then be solved using iterative methods, such as Gauss-Siedel.

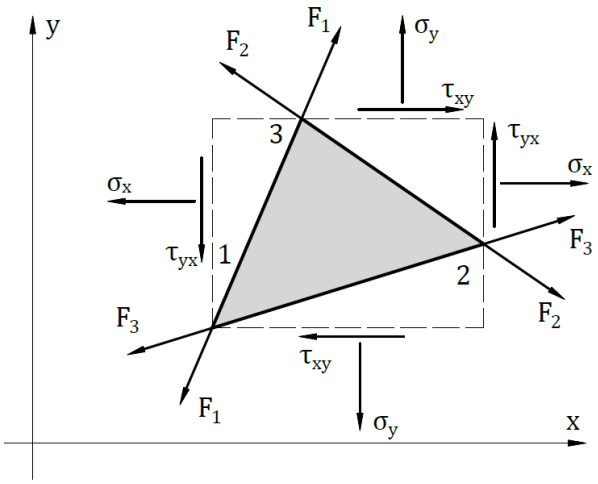

Figure 2.6: Representation on local coordinate system of a generic triangular FE and the forces acting over it. Cable FE stresses can be defined by aggregating the sides of adjacent elements. Source: AutoCAD, own elaboration.

Talking about case b), the finite element method has been developed to avoid the issues that come by finding the State 0 through the resolution of equilibrium equations. Specifically, the representation of complex boundary conditions, and the definition of a suitable geometric reference grid. The FEM method is based on the definition of a generic triangular surface element, to which we apply the external loads and the forces forwarded by adjacent elements. Then we solve the system formed by the balance equations for each finite element, combined with the boundary conditions. The initial surface is divided into triangular elements (such as the one shown in figure 2.6), whose edges define k nodes. We then apply the hypothesis of a constant stress state

within every element. Over each side of every element, we apply a force F_i directed along it. The sum of the two coincident sides of adjacent elements defines a cable, while the hypothesis of constant stress makes each node subjected only to the forces F_i. Because of that, the structure is represented by a set of rods and nodes linked together: by balancing each one of them we can define a statically balanced surface. Then, considering the generic triangular element, the stress state can be determined using the formula:

$$\begin{bmatrix} \sigma_x \\ \sigma_y \\ \sigma_{xy} \end{bmatrix} = \frac{2}{t} \begin{bmatrix} \frac{l_{12}^2}{h_3} & \frac{l_{23}^2}{h_1} & \frac{l_{31}^2}{h_2} \\ \frac{m_{12}^2}{h_3} & \frac{m_{23}^2}{h_1} & \frac{m_{31}^2}{h_2} \\ \frac{l_{12}m_{12}}{h_3} & \frac{l_{23}m_{23}}{h_1} & \frac{l_{31}m_{31}}{h_2} \end{bmatrix} \begin{bmatrix} F_1 \\ F_2 \\ F_3 \end{bmatrix} \tag{2.5}$$

Where σ_x, σ_y and $\sigma_x y$ represent internal forces, $m_k i$ and $l_k i$ are the directional cosines for the side ki, t is the membrane thickness, F_i are the forces along their respective side, h_i is the triangle height with respect to the edge i. Once given the border conditions we can the determine the stress state by calculating the forces over each cable. We therefore write the equilibrium equation for every node as follows:

$$\sum_{i=1\rightarrow}^{m} S_{ki} = p_i \sum_{i=1\rightarrow}^{m} \bar{n} A_{ki} + \bar{p}_k = \bar{p}_k^0 \quad \text{for: } k = 1, 2, \ldots, n \tag{2.6}$$

where n is the number of internal nodes, m is the number of cable elements, p_i is the normal distributed load acting over the surface i, P_k is the concentrated load acting over the generic node k, $S_k i$ is the equivalent force acting along the cable element ki, $A_k i$ is the area of the triangular element i, and $\bar{n}$ is the normal unitary vector of the surface with an edge in the node k. The equation can be rewritten in its scalar form. Then, considering a set of 3 equations for each node, we define a system of $3n$ equations that can be expressed in the matrix form:

$$[A]_{3n \times m} \left\{ S^0 \right\}_m = \{P\}_{3n} \tag{2.7}$$

where $[A]$ is the matrix of the cosine directors, $[S_0]$ is the vector of the cable forces, $[P]$ is the vector of the external loads. In this situation there are m-unknown terms for the values of the $S_k i$ forces, and $3n$ unknown terms for the nodes coordinates. In the end, there are three possible ways to solve the whole system:

- Supposing the $S_k i$ already known, we solve the system to calculate the $3n$ coordinates. This procedure is rarely used, as it is almost impossible to find a solution

that satisfies all the initial design hypothesis. It could be carried out by adding more restrictions, such as imposing a uniform stress state over specific areas or finding the closest solution to a given geometry.

- We assume a given geometry, and we solve the system by determining the $S_k i$ forces. As $m < 3n$, the problem is non-determined, and we have to define ourselves $3n-m$ unknowns to be able to solve it, relying on the design hypothesis.

- We can face a global design problem by finding all the $3n + m$ unknowns. This can be obtained by re-writing the equilibrium for the whole cable and nodes set. At first, we write the expression for the potential energy of the system $U(t)$. This formula is combined with the border conditions, that are expressed in terms of requirements over the initial geometry, over the length of the cables, or over their deformation and stress values.

  Then, the solution can be found as a minimum of the function $U(t)$ by applying the Lagrange multiplier method. We can also set this as an optimization problem: the aim is to find the closest solution to an assigned geometry, while respecting other requirements over the stress and strain states.

2.1.5 Preliminary design formulas

As seen in the previous section, there are different available methods that allow to determine the structural geometry and the stress status (the so-called state 0, which is the first phase of proper structural definition). Once determined, we can proceed to the proper preliminary design phase, which is exploited using simplified methods to obtain an overall sizing of the main components of the structure.

The optimal solution is usually defined throughout comparative studies over different preliminary designs. These studies consider other aspects than the sole structural requirements, such as building and maintenance costs: hence the need to apply approximations that simplify and accelerate this burdensome process. Regarding these simplifications, the modern techniques of computational analysis and numerical calculation allow to automatize the design processes previously described. Because of this, the methods based on discretization are generally preferred. Other methods, based on the continuum analysis, are still used to verify the structure's performances obtained during the design phase in terms of order of magnitude. Regarding the load analysis, the resulting loads are classified in the same way as ordinary structures, using the geometric configuration obtained by studying the state 0 of the structure. Specific attention must be paid to the determination of live loads and their behaviour, due to the shapes that characterize this kind of structures.

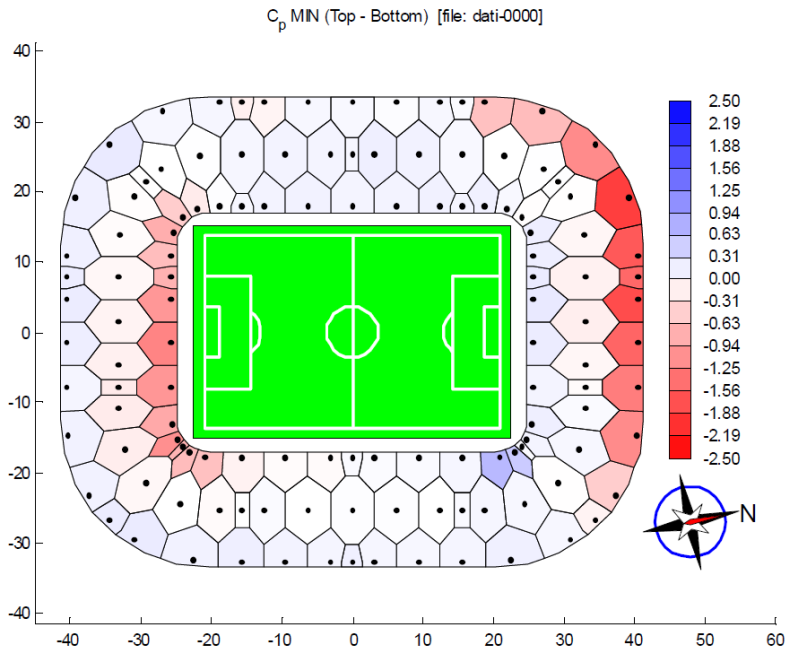

Figure 2.7: Maximum and minimum values of the net pressure coefficients due to wind action over the roof of the Olimpiakos Stadium (Athens, Greece), determined through wind tunnel analysis. Source: [17]

Snow load can cause several damages, especially in case of snowdrifts. To prevent this, different load distribution should be considered. Wind load is usually determined following extensive wind tunnel studies over physical models, with the aim to define both static and dynamic effects over the structure. The loads thus defined are grouped into different load combinations (specifically defined by the Eurocode and by national regulations), to be able to proceed with the rough sizing and structural checks over the structure. In this phase, deformations are also considered: deformation compatibility between the structure and the roofing material must be obtained, to prevent possible damage to the latter.

The rough sizing is based on simplified methods, that approximate the geometric configuration of the structure and its behaviour. Ropes are subjected to tension-only forces and, in this phase, mechanical non-linearity phenomena are neglected. In the case of a suspended single rope, we can consider the following geometric basic configurations, each one linked to a specific load typology.

2.1.5.1 The catenary

The geometry assumed for a load uniformly distributed along the length of the rope is the catenary curve. This represents the most generic case, as it is the geometry assumed by a generic cable subjected to its own weight, such as the one in figure 2.8.

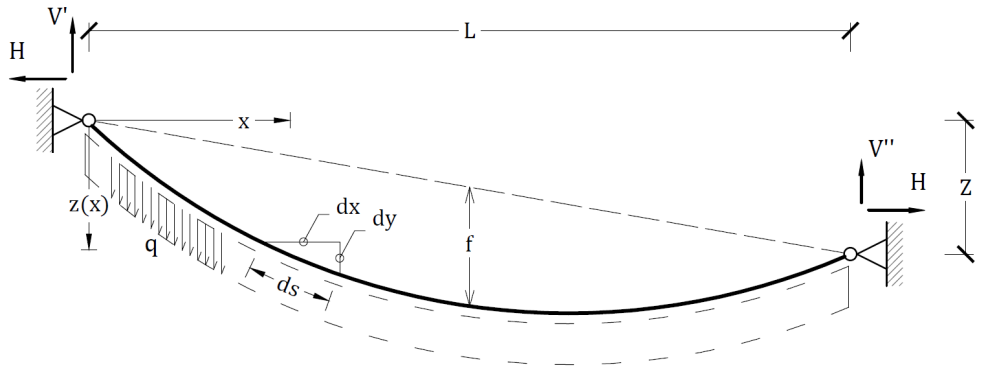

Figure 2.8: Reference scheme for a generic cable subjected only to its own weight, that assumes the geometry of a catenary curve. Source: AutoCAD, own elaboration

The differential equation that governs its equilibrium is:

$$H\frac{\partial^2 z}{\partial x^2} + q\frac{\partial s}{\partial x} = 0 \tag{2.8}$$

where H is the horizontal tension component, q is the cable own weight per unit length, s is the length of an infinitesimal part of the cable, x and z are the horizontal and vertical directions (we consider z positive downwards).

By integrating the equation twice, we can determine the solution, and by applying the boundary conditions (that represents the position of the cable's ends) the geometric configuration is determined as follows:

$$z\left(0\right) = 0 \text{ and } z\left(L\right) = Z \;\longrightarrow\; z\left(x\right) = \frac{H}{q}\left[\cosh\left(\alpha\right) - \cosh\left(\frac{2\beta x}{L} - \alpha\right)\right]$$
$$\text{with: } \beta = \frac{qL}{2H} \text{ and } \alpha = \sinh^{-1}\left(\frac{\beta\dfrac{Z}{L}}{\sinh\left(\beta\right)}\right) + \beta \tag{2.9}$$

where L is the span of the cable and Z is the difference in height between the ends. Note that the horizontal component of the tension H is constant along the cable, while the vertical component of the tension is variable, and so is the tension itself. Therefore, once H is assigned the problem is solved as we can define the geometry and the reactions. The cable's total length l can defined as:

$$l = \frac{2H}{q}\sinh\left(\alpha\right)\coth\left(\alpha - \beta\right) \tag{2.10}$$

The vertical components of the constraint forces are:

$$V' = H \sinh(\alpha) \quad \text{and} \quad V'' = \frac{q}{2}[Z \coth(\beta) - l] \tag{2.11}$$

And finally, the support forces are:

$$S' = H \cosh \alpha \quad \text{and} \quad S'' = \frac{q}{2}[l \coth \beta - Z] \tag{2.12}$$

The elastic elongation due to the applied tension is:

$$\Delta l_e = \frac{Hl}{L}\frac{l}{EA} \tag{2.13}$$

where E is the elastic modulus of the cable material, A is the area of the transversal section. A common situation is the condition for which the ends of the cable are at the same level (expressed as: $z(0) = z(L) = 0$). In this case the formulation is simplified, as:

$$\alpha = \beta = \frac{qL}{2H} \tag{2.14}$$

so that the geometry can is described by the equation:

$$z(x) = \frac{H}{q}\left[\cosh(\alpha) - \cosh\left(\frac{qx}{H} - \alpha\right)\right] \tag{2.15}$$

Now the maximum vertical displacement f (also called maximum sag) is exactly in the middle of the cable. We can easily define a relation between it and the applied horizontal tension H:

$$f = \frac{H}{q}[\cosh(\alpha) - 1] \tag{2.16}$$

This formula clearly shows the distinctive feature of suspended structures: as the geometry is undefined, to solve the equilibrium problem we must:

- Predefine the geometry of the structure (in this case by assigning f).
- Assign the applied force H, and then calculate the consequent geometry assumed by the cable.

2.1.5.2 Parabolic geometry under uniformly distributed load

Another notable configuration is the one of a cable subjected to a uniformly distributed load along the horizontal direction. This is case of a snow load, or the wind equivalent static pressure. Moreover, since the catenary equation might be difficult to solve, the parabolic curve is often used to approximate it. According to M. Majowiecki in [19],

this assumption is usually acceptable as long as the ratio between the applied load q and the equivalent distributed load over the span q' is less than 3%.

$$\frac{q\prime}{q} < 3\% \quad \text{with: } q' = q\frac{l}{L} \tag{2.17}$$

Where l is the length of the cable, and L its span. This occurs in two situations:

- When the ratio between the maximum deflection and the cable span is low. Due to this the difference between the length and the span is negligible, and so it is also the difference between the parabolic and catenary curves related to q and q' respectively.

- When the weight of the cable is significantly lower than the distributed load applied over its span. This is the case of suspension bridges, where the cable weight does not affect the geometric configuration assumed by the structure itself.

Thanks to that we can often use the parabolic curve to determine either the applied pretension or the geometry of the structure, particularly during the preliminary design phase as it would be preferable to simplify the calculations.

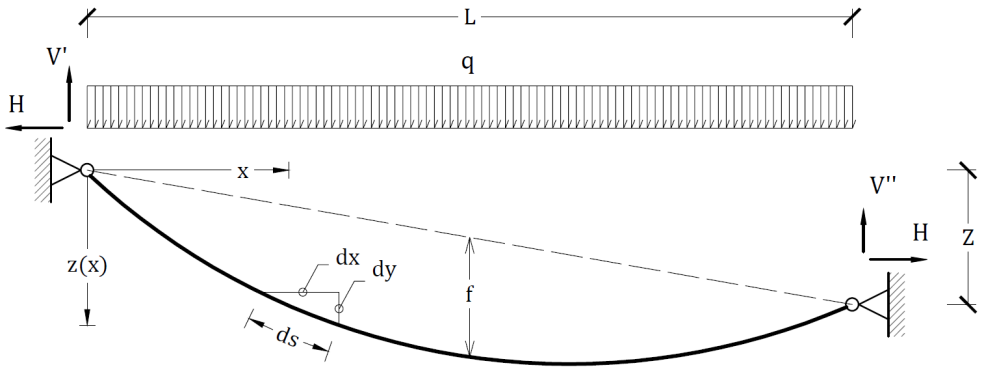

Figure 2.9: Reference scheme for a generic cable subjected to a uniformly distributed load along its span, that assumes the geometry of a parabolic curve. Source: AutoCAD, own elaboration.

The differential equation that governs the equilibrium is the following:

$$H\frac{\partial^2 z}{\partial x} + q = 0 \tag{2.18}$$

where, H is the cable horizontal tension, while q now stands for the uniformly distributed load along the horizontal direction. By integrating it and applying the boundary

conditions, the geometric configuration is obtained:

$$z\left(0\right)=0 \text{ and } z\left(L\right)=Z \quad \longrightarrow \quad z\left(x\right)=\frac{qx}{2H}\left[L-x\right]+\frac{Z}{L}x \tag{2.19}$$

As in the catenary curve, also in the parabolic curve the horizontal tension H is constant along the cable. The solution of the equilibrium problem is then ruled by the ratio between H and maximum sag f as:

$$H=\frac{qL^2}{8f} \tag{2.20}$$

Therefore, the support forces are determined as:

$$\begin{aligned} V'=\frac{qL}{2}+H\frac{Z}{L} \quad \text{and} \quad V''=\frac{qL}{2}-H\frac{Z}{L} \\ S'=\sqrt{H^2+V'^2} \quad \text{and} \quad S''=\sqrt{H^2+V''^2} \end{aligned} \tag{2.21}$$

while the length of the cable is calculated by substituting the relation for H, developing the binomial expression and then integrating it:

$$l=L\left[1+\frac{8f^2}{3L^2}+\frac{Z^2}{2L^2}\right] \tag{2.22}$$

These formulas can be consequently simplified if both ends of the cable have the same level (this condition is expressed as: $z(0)=z(L)=0$). In this case the relations become:

$$z(x)=\frac{qx}{2H}(L-x) \tag{2.23}$$

$$V_1=V_2=\frac{qL}{2} \tag{2.24}$$

$$l=L\left[1+\frac{8f^2}{3L^2}\right] \tag{2.25}$$

while the relation between the maximum deflection f and the horizontal tension remains the same, as well as the one for the total tension.

Note that when the loads are applied over the projected length, we can easily determine the cable geometry through the static analysis of an "equivalent" beam. The cable assumes the form of a parabolic curve, whose bending moment is zero in every point: this condition can be exploited to determine the value of z that satisfies it, thus finding the unknown equation. As an example, we apply this method to the previously shown case of the cable under a uniform load acting over its span. Making reference to the same notation, we can approximate the cable static scheme with the "equivalent"

presented in figure 2.10.

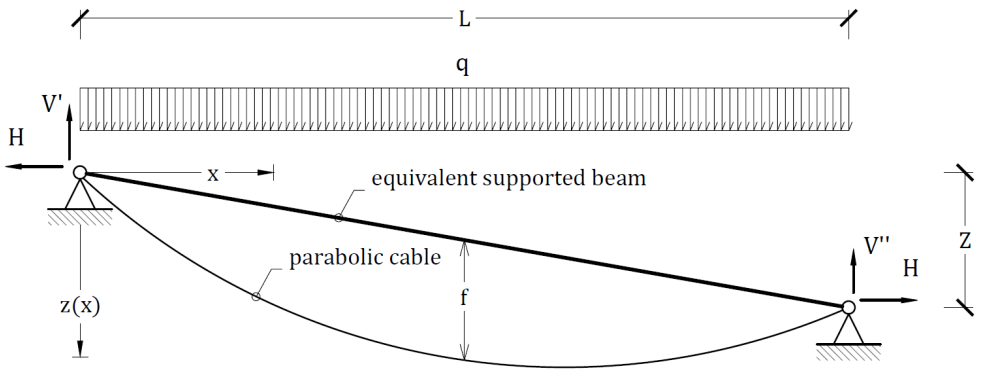

Figure 2.10: Static system "equivalent" to a cable subjected to a uniformly distributed load along its span. Source: AutoCAD, own elaboration.

Its reactions can be easily determined through a static equilibrium equation.

$$V_1 = \frac{qL}{2} + H\frac{Z}{L} \text{ and } V_2 = \frac{qL}{2} - H\frac{Z}{L} \tag{2.26}$$

We can now write the function of the cable bending moment at a generic point x:

$$M(x) = V_1 x - \frac{qx^2}{2} - Hz = \frac{qL}{2}x + H\frac{Z}{L}x - \frac{qx^2}{2} - Hz \tag{2.27}$$

where z is the sag at that point. Since the function must be equal to zero in every point, it can be wrote also as:

$$M(x) = 0 \longrightarrow Hz = V_1 x - \frac{qx^2}{2} - Hz = \frac{qL}{2}x + H\frac{Z}{L}x - \frac{qx^2}{2} \tag{2.28}$$

Therefore:

$$z = \frac{qL}{2H}x + \frac{Z}{L}x - \frac{qx^2}{2H} \tag{2.29}$$

which is the parabolic function of the cable geometry. Note that the resolution process is much more simple, as it no longer requires to solve the Cauchy problem: we can simply study the static scheme of a hinged beam. This method, combined with the superposition property, is particularly useful with complex load configurations, for which the resolution of the PDEs is not so immediate.

2.1.5.3 Other notable parabolic geometries

We want now to present some notable parabolic geometries, as they will also be applied in the analysis of study case. These equations can be easily obtained with the procedures presented in the previous part, and therefore the detailed resolution steps will be omitted,

showing only the main results. To simplify the formulation, we assume a parabolic curve to represent the geometry of the cable. Moreover, we will also consider only an elastic behaviour regarding the material, and we will assume that both cable ends are at the same level.

Cable subjected to a concentrated load:

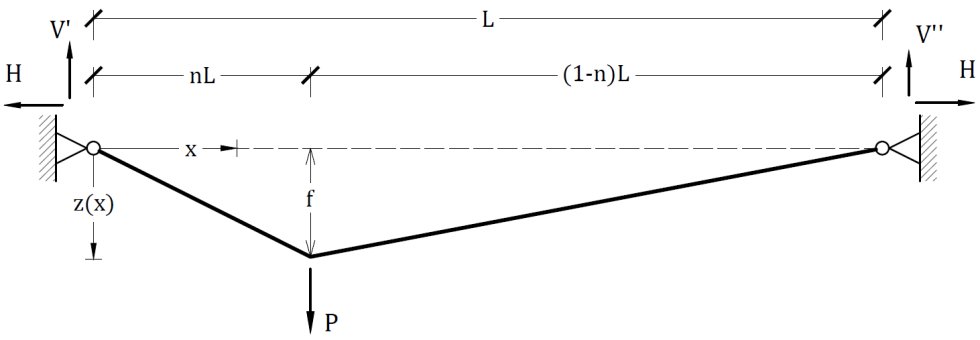

Figure 2.11: Cable subjected to a generic concentrated load, that assumes the geometry of a polygonal line. Source: AutoCAD, own elaboration.

Making reference to the static scheme presented in figure 2.11, we consider the basic case of a cable subjected to a concentrated load, whose ends are at the same level. The vertical reactions can be expressed as:

$$V_1 = (1-n)P \quad \text{and} \quad V_2 = nP \tag{2.30}$$

Assuming the maximum sag as f, the horizontal component of the cable tension is:

$$H = P\frac{(1-n)nL}{f} \tag{2.31}$$

While the geometry is expressed by the equations:

$$z(x) = \begin{cases} \dfrac{P(1-n)}{H}x & \text{for: } 0 < x/L < n \\ \dfrac{nP}{H}(L-x) & \text{for: } n < x/L < 1 \end{cases} \tag{2.32}$$

We can observe an interesting consequence of applying a concentrated load, as it introduces a discontinuity in the cable geometry, and therefore more equations are needed (one for each section): this is the case of any load variation along the cable. The same discontinuity can be found discontinuity in the 1^{st} derivative of $z(x)$, while the 2^{nd} derivative is zero anyway, as the geometry now is linear.

Cable subjected to both uniformly distributed and concentrated loads:

Making reference to the static scheme presented in figure 2.12, we consider the basic case of a cable subjected to both uniformly distributed and concentrated loads, whose ends are at the same level.

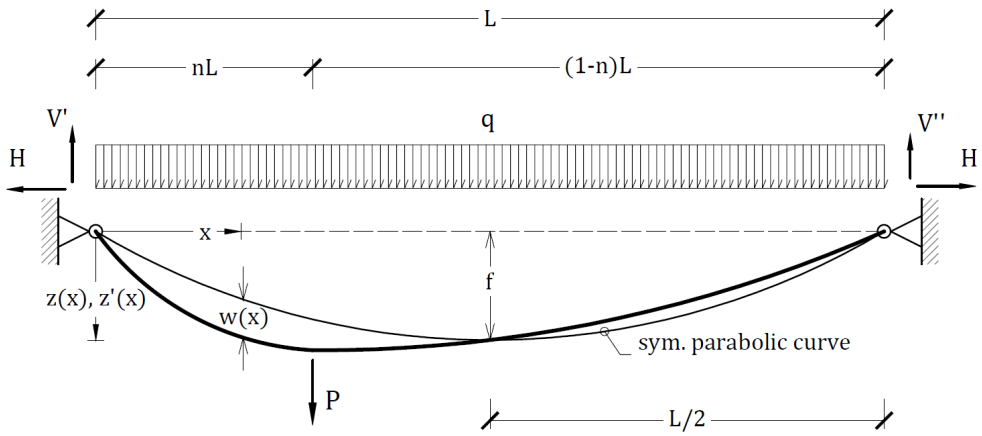

Figure 2.12: Cable subjected to its own weight plus a concentrated load, that assumes the geometry of 2 successive parabolic curves. Source: AutoCAD, own elaboration

As already shown, the vertical reactions can be defined from a static equilibrium equation.

$$V_1 = (1-n)P + qnL\left(1 - \frac{n}{2}\right) \quad \text{and} \quad V_2 = nP + \frac{qn^2L}{2} \tag{2.33}$$

The equations for the geometry are:

$$\begin{cases} \dfrac{qx}{2H'}(L-x) + \dfrac{P(1-n)}{H'} & \text{for: } 0 < x/L < n \\ \dfrac{qx}{2H'}(L-x) + \dfrac{nP}{H'}(L-x) & \text{for: } n < x/L < 1 \end{cases} \tag{2.34}$$

Note how the solution can also be obtained by superposing the parabolic curve found for the case of uniformly distributed load and the linear equations of the concentrated load case. Now we need to determine the relation between the term H' and the middle sag f, which is the parameter usually adopted (although it does not necessarily correspond to the maximum sag). To do this we rely on the equation:

$$l_{tot} = l_{AB} + l_{BC} \tag{2.35}$$

where l_{tot} can be determined with the already known relation for a uniformly distributed load.

$$l = L\left[1 + \frac{8}{3}\frac{f^2}{L^2} - \frac{32}{5}\frac{f^4}{L^4}\right] \tag{2.36}$$

while the other terms l_{AB} and l_{BC} can be determined from the expressions for $z(x)$: these are integrated to obtain the length of each parabolic curve as a function of the term H'. Once the equation for the cable's length is developed, it can be finally solved to find the relation between H' and f:

$$H' = \frac{qL^2}{8f}\left[1 - 3n(1-n) + 3n(1-n)\left(1 + 2\frac{P}{qL}\right)^2\right]^{\frac{1}{2}} \tag{2.37}$$

These relations do not consider the elastic elongation. This term can be neglected only with small loads, otherwise the elasticity must be considered. In this case the elongation can be expressed as:

$$\Delta l \cong \frac{\Delta H L}{EA}\left(1 + \frac{16}{3}\frac{f^2}{L^2}\right) \tag{2.38}$$

where ΔH represent the tension variation due to the concentrated load, and is equal to $\Delta H = H' - H$, where H is the horizontal tension due to the uniformly distributed load q. Therefore, the compatibility equation becomes:

$$l_{tot} + \Delta l = l_{AB} + l_{BC} \tag{2.39}$$

By substituting all the terms and developing the equation we determine the relation:

$$L\left(1 + \frac{16}{3}\frac{f^2}{L^2}\right)\left[1 + \frac{H - H'}{EA}\left(1 + \frac{16}{3}\frac{f^2}{L^2}\right)\right] = \tag{2.40}$$

$$= L\left[1 + \frac{q^2L^2}{24H'^2}(1 - 3n + 3n^2) + \frac{q^2L^2}{8H'^2}n(1-n)\left(1 + 2\frac{P}{qL}\right)\right] \tag{2.41}$$

Which is a cubic equation for H'. To solve it we first need to assign f, thus determining H using the equation 2.20. Then it is possible to calculate also H' and so the final geometry of the cable, also considering the elastic elongation.

Cable subjected to both uniformly distributed and concentrated loads:

Another useful example is the parabolic curve generated by a distributed overload acting in proximity to one end. This load configuration introduces a discontinuity in the $2^n d$ derivate, as the first portion of the cable where has a positive curvature, while its second portion has linear geometry. Making reference to the static scheme presented in figure 2.13, its reactions can be expressed by the equations:

$$V_1 = \frac{qL}{2} + pnL\left(1 - \frac{n}{2}\right) \quad \text{and} \quad V_2 = \frac{qL}{2} + \frac{pn^2L}{2} \tag{2.42}$$

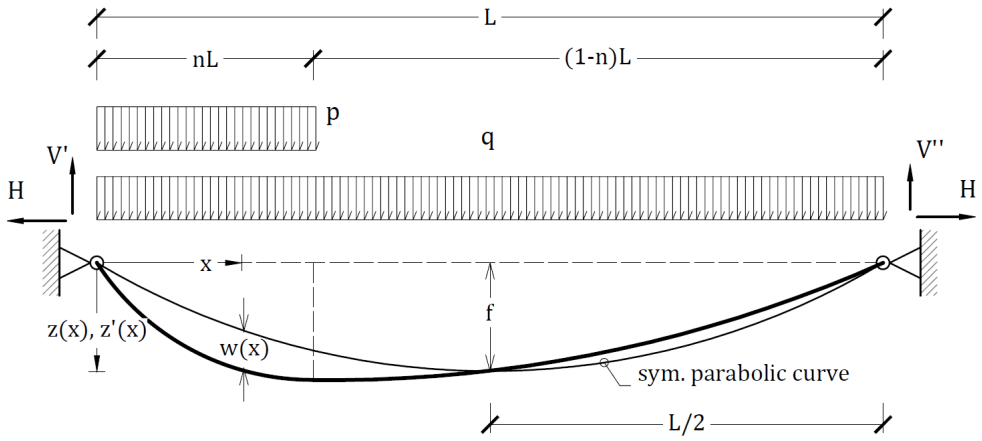

Figure 2.13: Cable subjected to its own weight plus a distributed overload next to its end, that assumes the geometry of 2 successive parabolic curves. Source: AutoCAD, own elaboration

The equations of the two parabolic sections are:

$$\begin{cases} \frac{qx}{2H'}(L-x) + \frac{px}{2H'}(L-x) - \frac{px}{2H'}(1-n)^2 L & \text{for: } 0 < x/L < n \\ \frac{qx}{2H'}(L-x) + \frac{p}{2H'}L^2 n^2 \left(1 - \frac{x}{L}\right) & \text{for: } n < x/L < 1 \end{cases} \tag{2.43}$$

As previously seen, H' can be determined by applying the equation for the cable's length for which:

$$l_{tot} = l_{AB} + l_{BC} \tag{2.44}$$

Therefore, we obtain the formula:

$$H' = \frac{qL^2}{8f}\left[1 + 2\frac{p}{q}(3-2n)n^2 + \frac{p}{q}n^2(4-3n)\right]^{\frac{1}{2}} \tag{2.45}$$

Thanks to these equations, and given the structure geometry, we can define the tension as a function of the applied load and then perform a rough sizing. In case of simpler geometries this procedure can be carried out manually, allowing to check the orders of magnitude of stresses and deformations of the structure. These simplified methods are therefore based on the equations and hypotheses just described and aim to directly relate the main parameters that characterize the rough sizing.

2.2 Static analysis

Once the preliminary project has been defined we proceed to the proper static analysis of the structure. In this phase, we usually do not resort on approximations, since we want to assess phenomena such as geometric and mechanical non-linearity, relaxation effects, elastic deformations and eventually large displacements. This requires considerable computational capacity, for which finite elements models and specially developed structural calculation programs are needed. However, it is necessary to know the principles and calculation methods on which rely these software.

2.2.1 Mathematical models of cable and truss elements

As previously said, the geometry of the structure is determined from the prestress state and the boundary conditions. Once this is known, we can move on to the static analysis of the physical-mathematical model, to check the validity of the preliminary design and the static stability of the structure. The physical-mathematical model is based on the cable finite element (schematized in figure 2.14), which is simplified as a linear mono-dimensional rod with constant section, placed between two successive nodes. It can undergo only tension forces. This element is characterized by mechanical and geometric parameters, such as the elasticity modulus E, the section area A and the length l.

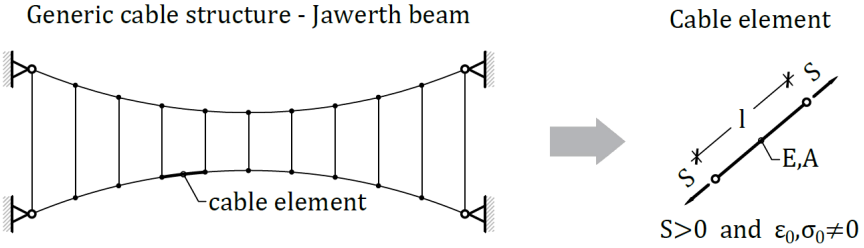

Figure 2.14: Schematization of the cable FE: part of a larger network, defined between 2 nodes, can undergo only tension forces. It is characterised by its section A, elastic module E, length l and assigned initial stress and strain states. Source: [19]

The initial tension state σ_0 and deformation state ε_0 are also assigned. In some cases, it can be replaced with the conrod finite element, which is characterized by the same parameters, but can be subjected to both traction and compression stresses. The stress-strain function of the material can be assumed as linear-elastic, linear-elastic perfectly-plastic, or we can even consider a viscoelastic or time-dependent deformation regime.

The cable element is subjected to the action of its own weight, to thermal variations, to imposed length variations and to all the possible external actions that the structure

will undergo. Cable elements and conrod elements are particularly versatile, and prone to depict a wide range of components such as cable networks, suspended cables, edge cables, tendons, and columns. Generally talking, the mathematical model must be suitable for the analysis of the main structural problems:

- Representation of the state 0 geometric configuration.
- Phenomena of both geometric and material non-linearity.
- Regime of one-side internal force.
- Visco-elasticity.
- Short and long term creeping phenomena.
- Dynamic effects induced by wind or earthquake.
- Interaction between tensile structure and anchoring system.
- Instability effects.
- Collapsing phenomena due to high temperatures.
- Static analysis of Ultimate Limit State and Serviceability Limit State.

Regarding the analysis methods, we can distinguish two main categories: displacements method and forces method. Force method (also called flexibility method) is rarely used, given the difficulty in coding it. On the other hand, the displacements method (also called stiffness method) is widespread, especially in software for automatic analysis due to its easy coding process. However, in case of large deformations it could still have some difficulties with the numerical calculation techniques. To overcome this problem, a mixed analysis method has been developed. Since the equations are usually quite complicated, we always apply numerical calculation techniques to get a valid solution. The most widely used are direct, iterative, or incremental methods with matrix formulation, or iterative methods with vectors.

2.2.2 Analysis of cable structures with the displacement method

The displacements method is hereby illustrated. It will be referred to a generic rope network, consisting of m cable elements connected by n nodes. To ease the discussion, we consider some simplifying assumptions while outlining the structure:

- The cable element does not have bending stiffness.
- The stress-strain function is assumed as linear elastic. No instability or loosening phenomena, nor plastic or viscous deformations are allowed.
- There are only small deformations.
- Nodes are treated as perfect hinges.
- There are no stiffening contributions from the other elements of the roof.
- We assume that the loads are only applied to nodes. From previous experiences over suspended cable structures, it has been seen that this approximation generates a small error (about 3%). Because of this, we apply this assumption even if it is possible to study the case of uniformly distributed loads over the cables.

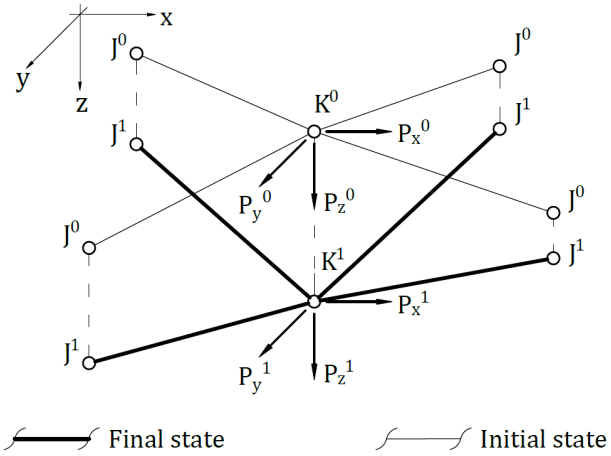

Figure 2.15: Reference scheme for the displacement method applied to a generic node. Source: [19]

Considering the scheme shown in figure 2.15, in the State "0" the configuration of the network in equilibrium conditions is described by the following known parameters:

- Node coordinates, that are collected in the hyper-vector X^0:

$$\{X\}^0 = \begin{Bmatrix} X_1 \\ \vdots \\ X_n \end{Bmatrix}^0 \; ; \; \{X_k\}^0 = \begin{Bmatrix} x \\ y \\ z \end{Bmatrix}^0 \qquad \text{with: } k = 1, 2, \ldots, n \tag{2.46}$$

- Rod forces. We name S^0_{kj} the effort in the cable element between the nodes k and j.

- The loads applied in the State "0", defined as $\{P\}_k^0$.

While applying the external loads we need to establish a new equilibrium configuration, called Final state. It is represented by these parameters:

- Geometric state variation, where with u, v, w we represent the nodal displacements along to the directions x, y, z respectively.

$$X_k^F = \{X^0 + U\}; \quad \text{with: } U = \{f(u,\ v, w)\}_k \tag{2.47}$$

- Internal force variation, where ΔS_{kj} is the internal force variation of the rod between nodes k and j.

$$\{S\}_{kj}^F = \left\{S^0 + \Delta S\right\}_{kj} \tag{2.48}$$

- Load variation, where ΔP_k represents the load variation over the node k.

$$\{P\}_k^F = \left\{P^0 + \Delta P\right\}_k \tag{2.49}$$

With reference to the proposed scheme, we consider the k-th node which is connected to other nodes i. In state "0", the nodal equilibrium equations and the formula for the element's length can be written as shown in equation 2.50.

$$\begin{cases} \sum_1^i \frac{S_{kj}^0}{l_{kj}^0} \Delta x_{kj}^0 = -P_{xk}^0 \\ \sum_1^i \frac{S_{kj}^0}{l_{kj}^0} \Delta y_{kj}^0 = -P_{yk}^0 \\ \sum_1^i \frac{S_{kj}^0}{l_{kj}^0} \Delta z_{kj}^0 = -P_{zk}^0 \end{cases} \tag{2.50}$$

$$l_{kj}^0 = \left(\Delta x_{kj}^2 + \Delta y_{kj}^2 + \Delta z_{kj}^2\right)^{\frac{1}{2}} \tag{2.51}$$

While in the final state these equations become:

$$\begin{cases} \sum_1^i \left[\frac{(S^0 + \Delta S)_{kj}}{(l^0 + \Delta l)_{kj}} (\Delta x^0 + \Delta u)_{kj}\right]_{kj} = -\left(P^0 + \Delta P\right)_{xk} \\ \sum_1^i \left[\frac{(S^0 + \Delta S)_{kj}}{(l^0 + \Delta l)_{kj}} (\Delta y^0 + \Delta v)_{kj}\right]_{kj} = -\left(P^0 + \Delta P\right)_{yk} \\ \sum_1^i \left[\frac{(S^0 + \Delta S)_{kj}}{(l^0 + \Delta l)_{kj}} (\Delta z^0 + \Delta w)_{kj}\right]_{kj} = -\left(P^0 + \Delta P\right)_{zk} \end{cases} \tag{2.52}$$

$$l_{kj}^{F} = \left(l^{0} + \Delta l\right)_{kj} = \left(\left(\Delta x^{0} + \Delta u\right)_{kj}^{2} + \left(\Delta y^{0} + \Delta v\right)_{kj}^{2} + \left(\Delta z^{0} + \Delta w\right)_{kj}^{2}\right)^{\frac{1}{2}} \quad (2.53)$$

Then, in the equilibrium equations we want to express the term ΔS_{kj} as a function of the displacements. The assumed stress-strain relation is therefore applied in equation 2.54.

$$\Delta S_{kj} = EA_{kj}\varepsilon_{kj} = EA_{kj}\frac{\Delta l_{kj}}{l_{kj}^{0}} = EA_{kj}\left(\frac{l_{kj}^{F}}{l_{kj}^{0}} - 1\right) \quad (2.54)$$

Where E is the elasticity modulus, A_{kj} is the cross-section area of the kj-th cable element. We develop the system of equations that define the final state. Then, we further process the vector products by substituting the expression for ΔS_{kj}: it is therefore possible to define the resolutive non-linear equations system 2.55.

$$\begin{cases} \sum_{1}^{i}\left[S_{kj}^{0}\dfrac{\Delta u_{kj}}{l_{kj}^{0}} + \left(EA_{kj} - S_{kj}^{0}\right)\dfrac{\Delta x_{kj}}{l_{kj}^{0}}a_{kj}\right]_{kj} = -\left(P^{0} + \Delta P\right)_{xk} + R_{xk} \\ \sum_{1}^{i}\left[S_{kj}^{0}\dfrac{\Delta v_{kj}}{l_{kj}^{0}} + \left(EA_{kj} - S_{kj}^{0}\right)\dfrac{\Delta y_{kj}}{l_{kj}^{0}}a_{kj}\right]_{kj} = -\left(P^{0} + \Delta P\right)_{yk} + R_{yk} \\ \sum_{1}^{i}\left[S_{kj}^{0}\dfrac{\Delta w_{kj}}{l_{kj}^{0}} + \left(EA_{kj} - S_{kj}^{0}\right)\dfrac{\Delta z_{kj}}{l_{kj}^{0}}a_{kj}\right]_{kj} = -\left(P^{0} + \Delta P\right)_{zk} + R_{zk} \end{cases} \quad (2.55)$$

with:

$$\begin{cases} R_{xk} = -\sum_{1}^{i}\left[EA_{kj} - S_{kj}^{0}\right]_{kj} \cdot \left[\dfrac{\Delta u_{kj}}{l_{kj}^{0}}c_{kj} + \dfrac{\Delta x_{kj}}{2l_{kj}^{0}}d_{kj}\right] \\ R_{yk} = -\sum_{1}^{i}\left[EA_{kj} - S_{kj}^{0}\right]_{kj} \cdot \left[\dfrac{\Delta v_{kj}}{l_{kj}^{0}}c_{kj} + \dfrac{\Delta y_{kj}}{2l_{kj}^{0}}d_{kj}\right] \\ R_{zk} = -\sum_{1}^{i}\left[EA_{kj} - S_{kj}^{0}\right]_{kj} \cdot \left[\dfrac{\Delta w_{kj}}{l_{kj}^{0}}c_{kj} + \dfrac{\Delta z_{kj}}{2l_{kj}^{0}}d_{kj}\right] \end{cases}$$

$$a_{kj} = \Delta X_{kj}\Delta U_{kj} = \left\{X_{k}^{0} - X_{j}^{0}\right\}\left\{U_{k} - U_{j}\right\} = \\ = \frac{1}{\left(l_{kj}^{0}\right)^{2}}\left(\Delta x_{kj}\Delta u_{kj} + \Delta y_{kj}\Delta v_{kj} + \Delta z_{kj}\Delta w_{kj}\right)$$

$$b_{kj} = \frac{1}{\left(l_{kj}^{0}\right)^{2}}\left(\Delta u_{kj}^{2} + \Delta v_{kj}^{2} + \Delta w_{kj}^{2}\right)$$

$$c_{kj} = a_{kj} + \frac{1}{2}b_{kj} - \frac{3}{2}a_{kj}^{2}$$

$$d_{kj} = 3a_{kj}^{2} - 3a_{kj}b_{kj} - 5a_{kj}^{3}$$

The equations 2.2.2 for R_{ik} are obtained by considering only the terms up to the 3^{rd} degree in the relations for u, v, w. For a generic structure of n nodes, a system of $3n$ simultaneous equations would result. These are solved with numerical algorithms,

thus determining the values of the displacements u, v and w. Finally, by applying the correct displacements to the formulas for ΔS_{kj} we obtain the internal force of the cable elements. The whole system can be rewritten in the compact matrix form:

$$[K]\{U\} = \{P\} + \{R\} \tag{2.56}$$

where:

- $[K]$ is the global stiffness matrix.
- $\{U\}$ is the unknown displacement vector.
- $\{P\}$ is the external load vector.
- $\{R\}$ is the cable's residual forces vector, containing the terms R_{xk}, R_{yk} and R_{zk}.

With the same nonlinear equations, we can define the stiffness coefficients matrix of the single cable element. These are obtained by developing the right part of the equations of that same system for $\sum X = 0$, $\sum Y = 0$ and $\sum Z = 0$. The expressions are then rewritten by developing and rearranging their terms. The matrix is defined by separating the coefficients from their respective unknown displacement terms:.

$$[K] = \begin{bmatrix} [M] & [-M] \\ [-M] & [M] \end{bmatrix} \tag{2.57}$$

where:

$$[M] = \begin{bmatrix} \frac{EA_{kj} - S^0_{kj}}{l^0_{kj}} n_x^2 + \frac{S^0_{kj}}{l^0_{kj}} & \frac{EA_{kj} - S^0_{kj}}{l^0_{kj}} n_x n_y & \frac{EA_{kj} - S^0_{kj}}{l^0_{kj}} n_x n_z \\ \vdots & \frac{EA_{kj} - S^0_{kj}}{l^0_{kj}} n_y^2 + \frac{S^0_{kj}}{l^0_{kj}} & \frac{EA_{kj} - S^0_{kj}}{l^0_{kj}} n_y n_z \\ \text{sym.} & \dots & \frac{EA_{kj} - S^0_{kj}}{l^0_{kj}} n_z^2 + \frac{S^0_{kj}}{l^0_{kj}} \end{bmatrix}$$

where n_x, n_y and n_z are the directional cosines of the cable element. When considering non-linear geometric effects, the stiffness matrix can be rewritten as a combination of two terms.

$$[K_E] + [K_G] = [K] \tag{2.58}$$

where K_E is the elastic stiffness matrix and is directly related with the elongation of the cable element. K_G is the geometric stiffness matrix, for which the nodal equilibrium is affected by the variation of the geometric configuration. The stiffness matrices are

referred to a single element kj, so that when considering a system made by several elements they must be calculated separately and then assembled.

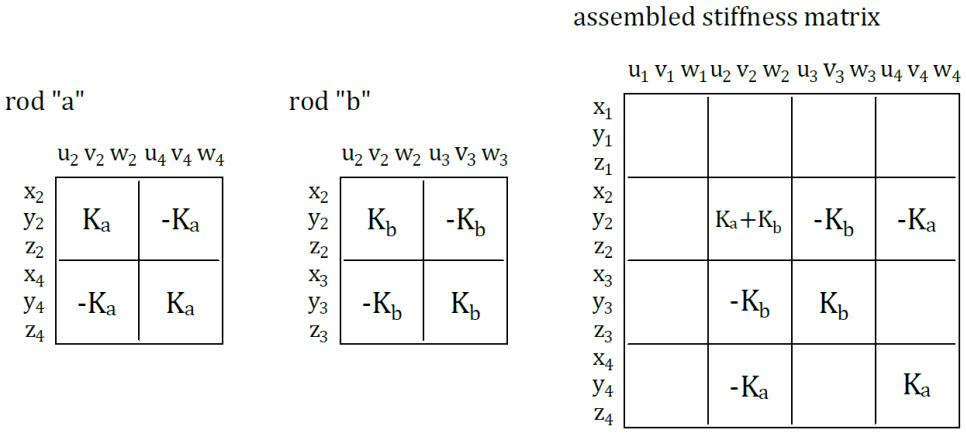

Figure 2.16: An example of the assembling process for the global stiffness matrix, with the assembled matrix on the right, obtained from 2 elements "a" and "b", whose stiffness matrices are shown on the left. Source: [19]

2.2.3 Consequences of thermal solicitations

Tensile structures can undergo daily or seasonal thermal variations that induce internal forces. These will combine with the prestress: for instance, a temperature rise will cause the cable elongation, thus decreasing its initial prestress. Because of this, thermal variations must be properly considered while checking the structural stability and strength.

- When temperature rises, we must verify that the residual prestress is adequate.

- When temperature drops, we must check the element's resistance, taking also into account the maximum variable loads.

To introduce thermal effects, we consider an additional term in the expression for the axial force variation ΔS_{kj}:

$$\Delta S_{kj} = EA_{kj}\varepsilon_{kj} + \Delta S_{kj}^{\Delta t} = EA_{kj}\varepsilon_{kj} + EA_{kj}\alpha\Delta t_{kj} \tag{2.59}$$

where α is the thermal elongation coefficient, Δt_{kj} is the temperature variation of the element. The equilibrium equation will then be solved as previously shown.

2.2.4 Approximations for numerical models

For a large 3D tensile structure the equilibrium equations could be extremely onerous, even for a modern software. Nevertheless, we can introduce some approximations and simplify the model, thus reducing the number of calculations without compromising the correctness of the results. Some notable cases are:

- Low-curvature tensile structures (i.e., with low values of the f/L ratio). In this situation the plane displacements are negligible with respect to the vertical displacement w. The problem is therefore simplified by not considering the terms related to u and v, reducing the number of equations from $3n$ to n.

- In hypostatic structures, such as free ropes, rigid kinematic motions are much higher than elastic ones. We can assume the cables as non-extensible, and thereby facilitate calculation by neglecting the elongation terms.

- For remarkably rigid structures we can neglect the residual term R, that contains the nonlinear terms. Due to this we can perform a linear analysis and eliminate the iterative part of the resolution method.

- When studying rope networks with numerous nodes the calculations become excessive. Whenever possible, we can get around the problem by analysing an equivalent thinner mesh network, thus reducing the number of nodes and equations.

Finally, a last note: some structures can be particularly complex and challenging, even for a modern calculation software. In these situations, even if none of the aforementioned cases are involved, the designer must simplify the structural model to reduce the computational costs, without however committing approximations for which the data obtained are no longer reliable.

2.2.5 Numerical methods for non-linear static equations

There are several available methods to solve the nonlinear systems seen above. Generally, the unknown terms are determined through iterative analysis procedures. These methods can be divided into three main categories:

- Direct methods.

- Non-direct methods.

- Methods based on functional minimization.

2.2.5.1 Direct methods

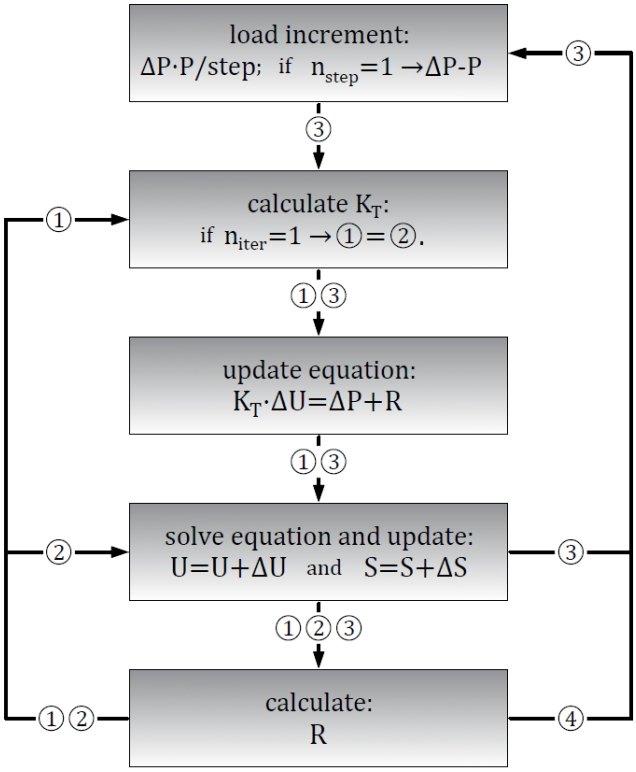

Figure 2.17: Confrontation between the most common direct methods:1-Newton-Raphson, 2-Modified N-R, 3-Incremental, 4-Modified N-R and Incremental. Source: [19]

There are several methods based on this type of procedure such as Newton-Raphson, its modified version, or the incremental method. These roughly apply the same process, with some differences that are shown in figure 2.17. Regarding the resolution process, the nonlinear equations system is outlined as follows:

$$[K_E + K_G + K_{NL}]\,[U] = [P] \tag{2.60}$$

Where K_E is the elastic stiffness matrix and K_G is the geometric stiffness matrix. K_{NL} is the nonlinear matrix, that contains the terms that depend on the displacement according to nonlinear functions. The resolutive system for the displacement method can therefore be rewritten as shown in equation 2.61.

$$[K_E + K_G]\,[U] = [P] + [R] \tag{2.61}$$

By developing and rewriting the equations, the nonlinear terms have been grouped into the residual vector $[R]$. The resolution procedure is the following one.

1. The system is initially solved by assuming $[R] = 0$, thus calculating $[U]$ with a linear analysis.

2. Once $[U]$ is known it is possible to determine the residue vector $[R]$ for the current iteration.

3. We can then solve the whole complete system:

$$[K]\,[U] = -\,[P] + [R] \tag{2.62}$$

So that the value of $[U]$ for the 2^{nd} iteration is determined. This process is repeated, until the difference between the $[U]$ values from two successive iterations falls below a certain tolerance.

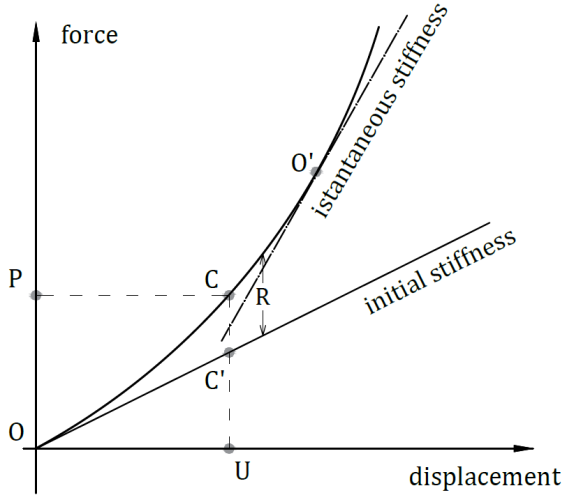

Figure 2.18: Hardening process of a tensile structure, with a generic representation of the direct resolution method. Source: [19]

When applying direct resolution methods, we operate along the load-displacement curve of the structure. The tangent at the origin represents the system's initial stiffness K, while K' is the instantaneous stiffness for the applied load P and the corresponding displacement U.

The nonlinear vector is then calculated as an unbalanced load.

$$-\,[P] + \sum [K']\,[U'] = [R] \tag{2.63}$$

The aim is to determine the exact value of the stiffness K for which there are no residual terms. We can therefore write the iterative resolution procedure as:

$$R^i = K^i U^{i+1} = \sum K^i U^i - P \;\longrightarrow\; U^{i+1} = U^i + \Delta U^{i+1} \tag{2.64}$$

2.2.5.2 Non-direct methods

Indirect integration methods are quite suitable in case of scattered stiffness matrices. The solution of the problem is sought by decoupling the equations, through the continuous iteration of a recurring expression to approach the exact solution.

$$u_j^{i+1} = u_j^i - \frac{1}{a_{jj}} \left(\sum_{j=1}^{n} a_{kj} u_j^i - P' \right) \tag{2.65}$$

Where j and k are the different rows and columns indexes of the stiffness matrix, a_{jj} and a_{kj} are the stiffness matrix coefficients, P' is the generalized load (which comprehends both external and dummy loads from the residual terms).

This expression is obtained from the non-linear equations of the displacement method, by making explicit the displacement terms. Since we consider each row separately, we have the decoupling of the equations. Then we apply an iterative procedure to find the solution, cyclically analysing all the nodes one by one. Each node displacement is determined by locking the adjacent ones in the positions obtained with the previous iteration, thus gradually refining the result at every iteration. This procedure works well as long as the coefficient matrix is diagonally predominant, and the equations are weakly nonlinear. Convergence is slow, so under-relaxation factors might be useful to reduce the number of iterations.

2.2.5.3 Methods based on functional minimization

In this part we introduce a further category, which is based on the pursuit of the equilibrium by minimizing the total potential energy of the system. Since this method is based on the minimum potential energy theorem (as shown in equation 2.67), it can only be applied in case of linear elastic behaviour. The potential energy is defined as follows.

$$W_T = W_D + W_P \tag{2.66}$$

Where W_D is the deformation energy and W_P is the external loads potential energy. The aim is to express them in terms of the displacements U, and them minimize the resulting function. This condition can be found by solving the equation:

$$g_i = \frac{\partial W_T}{\partial u_i} = 0 \tag{2.67}$$

To identify a global minimum of energy it is also necessary to prove that the second derivative of W_T is positive. The total energy of the analysed system can be expressed

as:

$$W_T = \sum W_{D,i} - \{P\}^T \{U\} \tag{2.68}$$

Where P is the external loads vector, U is the nodal displacement vector and $W_{D,i}$ is the deformation energy of every i-th element of the structure. For instance, we take into account a generic system with 3 degrees of liberty, for which there is a generic node j linked with other k nodes through n finite elements. We can then define the nodal displacement vector and the external load vector as:

$$\{U\} = \begin{Bmatrix} u_j \\ v_j \\ w_j \end{Bmatrix} \quad \text{and} \quad \{P\} = \begin{Bmatrix} P_{xj} \\ P_{yj} \\ P_{zj} \end{Bmatrix} \tag{2.69}$$

It is possible to define to the equilibrium equations from the expression of the potential energy of the system. To do so we need to differentiate this expression relatively to the displacements at the considered node:

$$\begin{cases} \dfrac{\partial W_T}{\partial u_j} = -\sum_{k=1}^{n} \dfrac{\partial W_{D,jk}}{\partial u_j} - p_{xj} \\ \dfrac{\partial W_T}{\partial v_j} = -\sum_{k=1}^{n} \dfrac{\partial W_{D,jk}}{\partial v_j} - p_{yj} \\ \dfrac{\partial W_T}{\partial w_j} = -\sum_{k=1}^{n} \dfrac{\partial W_{D,jk}}{\partial w_j} - p_{zj} \end{cases} \tag{2.70}$$

We define S_{jk} the generic effort at the element between the nodes j and k, while e_{jk} represents its elongation. Then, we want to write the deformation energy as a function of the displacements, so we start by defining it in terms of S_{jk} and e_{jk}, as shown in equation 2.71.

$$dW_{D;j} = S_{jk} e_{jk} \quad \longrightarrow \quad \frac{\partial W_{D,jk}}{\partial u_j} = \frac{\partial W_{D,jk}}{\partial e_{jk}} \frac{\partial e_{jk}}{\partial u_j} = S_{jk} \frac{\partial e_{jk}}{\partial u_j} \tag{2.71}$$

The length of the deformed element can be written as:

$$\begin{aligned} (l_{jk} + e_{jk})^2 = {} & [(x_k - x_j) + (u_k - u_j)]^2 + \\ & + [(y_k - y_j) + (v_k - v_j)]^2 + [(z_k - z_j) + (w_k - w_j)]^2 \end{aligned} \tag{2.72}$$

By differentiating it for u_j we can obtain the relation for $\partial e_{jk}/\partial u_j$. This expression is substituted into $\partial W_{D,jk}/\partial u_j$, which is then substituted into $\partial W_T/\partial u_j$, thus obtaining the equilibrium equation for u_j. This procedure is shown using the term u_j, however it

is the same for v_j and w_j. At the end, we obtain the whole system .

$$\begin{cases} \dfrac{\partial W_T}{\partial u_j} = -\sum_{k=1}^{n} t_j k \left[(x_k - x_j) + (u_k - u_j)\right] - p_x j \\ \dfrac{\partial W_T}{\partial v_j} = -\sum_{k=1}^{n} t_j k \left[(y_k - y_j) + (v_k - v_j)\right] - p_y j \\ \dfrac{\partial W_T}{\partial w_j} = -\sum_{k=1}^{n} t_j k \left[(z_k - z_j) + (w_k - w_j)\right] - p_z \end{cases} \tag{2.73}$$

$$t_{jk} = \frac{S_{kj}}{l_{kj} + e_{kj}}$$

For a generic iteration cycle r, to which corresponds the displacement vector $\{U\}_r$, we consider s as the step amplitude along the direction d. The minimization procedure is then defined by the expressions:

$$\{U\}_{r+1} = \{U\}_r + \{\Delta U\}_r \quad \text{where: } \{\Delta U\}_r = s_r \{d\}_r \tag{2.74}$$

Where $\{\Delta U\}_r$ represent the vector of the displacement variations between two successive iterations. After a certain number of cycles, we obtain the displacement as:

$$\{U\} = \sum_{r=1}^{N} s_r \{d\}_r \tag{2.75}$$

The most widely used minimization methods are:

- Steepest descent method.
- Relaxed steepest descent method.
- Conjugate gradient method.
- Newton-Raphson method.

The energetic methods are generally stable and really accurate, although they have a handicap due to the limited number of variables and the fact that they can only be used in case of linear elastic behaviour. On the other hand, iterative methods are not always stable, while incremental methods are less accurate. To overcome these problems, we can combine the two, thus defining stable and very accurate algorithms that are comparable with energy methods. Energy methods are very useful especially in case of strong geometric nonlinearities, or poorly conditioned stiffness matrices. In these situations, iterative and incremental methods require specific measures that significantly increase the computational costs.

2.3 Analysis of dynamic effects

Due to its sensitiveness to dynamic actions, this is a crucial phase of the tensile structure design process. However, the variability of wind and seismic forces, together with the structural complexity, make particularly challenging the study of these effects. This section summarizes the main principles and methods of dynamic analysis, with a brief digression on the principles on which relies the mathematical modelling of wind and seismic actions. This last part plays an important role in the design, as it affects the design actions and the definition of monitoring procedures and on-site tests.

2.3.1 Importance of dynamic effects

One of the main characteristics of tensile structures is the low ratio between their own weight and the variable external loads. This causes a strong sensitivity to dynamic efforts, which means larger oscillations and deformations when compared to other conventional structures. Because of this, wind or seismic solicitations could make a tensile structure unusable and potentially lead to its collapse. This problem is usually solved with these procedures:

- By applying pretension stresses to the structure's elements, thus reducing their flexibility to dynamic actions.
- By adding energy dissipation devices, such as damping or ballasting systems.
- During the design stages, by carrying out accurate analyses of the interaction with dynamic actions accompanied by tests on aeroelastic models. This allows defining the most suitable geometry to limit the extent of dynamic effects.

The aim of all these countermeasures is to reduce the vibration period of the structure itself. Another key factor of tensile structures is the relevance of geometric non-linearity, that should not be neglected. It is worthy of mention the resonance escape effect: large displacements and geometric non-linearity make the deformation modes to diverge from that same resonance state that caused the phenomenon. This has a clear beneficial impact in limiting the effects due to self-excited vibrations. The main sources of dynamic stress over suspended roofs are wind and earthquakes. Given their variability and unpredictability, they must be studied with a semi probabilistic approach: accurate data regarding past events are available only in rare cases. The main characteristics of these dynamic stresses will be presented below, by briefly defining how to generate a mathematical model and the main methods for analysing and determining the effects induced.

2.3.2 Modelling of wind behaviour

Although wind is mainly linked to the atmospheric and geographical characteristics of the site, its effects are also related with the geometric configuration of the stressed structure. The wind flow is altered by the roof shape, thus generating aerodynamic phenomena that cause differential pressure stresses over its surface. These stresses in turn cause a deformation of the surface itself: the wind flow is again modified and so are the related stresses. From an analytical perspective we can classify these effects into two categories:

- Statics: these are pressure effects generated on the surface affected by the aerodynamic flow and acting normally to it. Tangential effects might also be considerable in some cases, as they are linked to phenomena of friction and alteration of the wind boundary layer.

- Dynamics: these are vibration phenomena generated by the continuous deformation of the surface and by the aerodynamic flows of the wind itself. According to [19], we can identify 3 main sources:

    - Critical frequencies caused by a succession of gusts: they lead to longitudinal oscillations and turbulence.
    - Critical speeds with uniform winds: they give rise to transversal oscillations and to Karman-Bernard alternating turbulence effects.
    - Critical speeds of aerodynamic instability: the structure has problems of lateral-torsional instability, due to its own shape.

The consequences are rhythmic and prolonged oscillations over time, with possible resonance effects of the structure. It is notable that these phenomena could also occur with low intensity winds. Due to a numerical analysis the wind mathematical model is structured as follows:

$$(t) = \bar{v} + \bar{v}_i(t); \quad \text{for: } i = x, y, z \tag{2.76}$$

where $\bar{v}$ is the term of constant average horizontal speed, equal to the mean of the instantaneous speeds over a given time interval. It is therefore a stationary phenomenon, linked to static effects. $\bar{v}_i(t)$ is the fluctuating component of speed, (linked to the dynamic response) which can be seen as a stochastic phenomenon. It can be determined for several orthogonal directions, by combining a certain number of sinusoidal fluctuations of different amplitude and frequency.

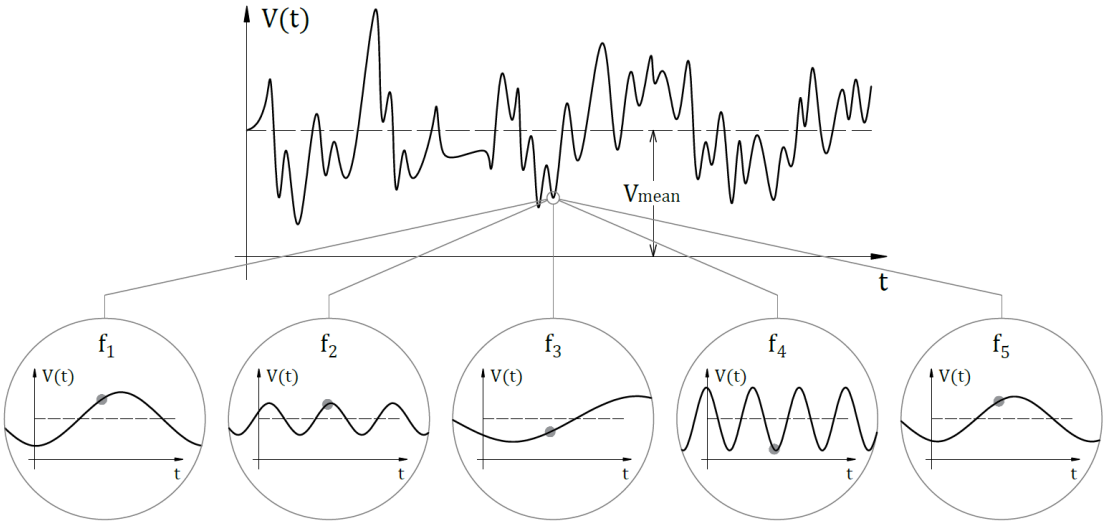

Figure 2.19: Conceptual representation of the wind action as a combination of different sinusoidal fluctuations. Source: AutoCAD, own elaboration.

Hence, to determine the fluctuating component a spectral analysis is needed. In a few words, the wind speed for a generic direction can be expressed as a sum of contributions with different frequency:

$$v\left(t\right)=\bar{v}+A_1\sin\left(\theta\right)+A_2\sin\left(2\theta\right)+\ldots+A_n\sin\left(n\theta\right)=\bar{v}+\sum_{i=1}^{n}A_i\sin\left(\frac{2\pi t}{f_i}\right) \quad (2.77)$$

Then, we can define the wind speed standard deviation as:

$$\sigma^2\left(v\right)=\bar{v}^2-\bar{v}^2(t) \quad (2.78)$$

where the first term $\bar{v}^2$ is the root-mean square value (the arithmetic mean of the squared values), while the second term $\bar{v}^2(t)$ is the squared mean value of the variable wind speed components. That same deviation can be rewritten as follows.

$$\sigma^2\left(v\right)=\int_0^\infty S_v\left(f\right)\ df \quad (2.79)$$

where the term $S_v\left(f\right)$ represents the speed spectral density, which is a function of the frequency. By doing so we can describe the wind speed through a certain frequency domain. Its representation is provided by a frequency spectral diagram.

According to [19], when representing the horizontal wind speed the spectral density diagram should be characterized by 3 frequency peaks: the first is related to annual wind variation (caused by seasonal variations), while the third one is related to 12 hours wind variations (caused by day/night cycles). The second peak could be related to wind

variations along a period of 4 to 6 days (caused by meteorological cycles), although wind speed during this interval should not be considered a stationary process. There should also be a "spectral gap" between the second and third peak, that leads to some observations:

- Wind speed variations can be divided into slow variations, linked to meteorological phenomena, and rapid variations, linked to fluid turbulence and local conditions.
- For rapid variations, mean wind speed can be represented by the hourly average, as for intervals of this order of magnitude the average speed does not change with the duration of the survey.
- The effects of low frequency variations of the variable wind speed component can be well represented by the variations obtained on the hourly average.

These are relevant in deciding when and for how long we should carry out the necessary on-site surveys of wind-related parameters such as speed and pressure coefficients. We can deduce that the definition of mathematical models for wind behaviour influences the monitoring process of tensile structures, before and after their construction. As we will see in chapter 3, several on-site surveys have been performed over the study case: even if not presented in detail, the data of this studies refer precisely to periodic hourly surveys, concentrated in the periods of the year in which the greatest wind phenomena are expected.

2.3.3 Analysis of wind solicitation

Having defined the mathematical model that describes the speed trend, we can move on to the study of the effects induced over the surface. Usually, the aeroelastic behaviour of the structure is studied as that of a body surrounded by a moving fluid. There are different ways to undergo these studies, that will be briefly illustrated below.

2.3.3.1 Static equivalent analysis

The analysis is simply reduced to the determination of the pressure field acting over the surface. Because of this, the solution of the stress and strain problems can be obtained by solving the static equilibrium equations. The actions due to the average wind speed and due to its fluctuating component are calculated separately, then they are combined with each other. In the simplest cases we can resort to a direct calculation of the equivalent action, using data that are already known and referred to notable cases.

In order to obtain the values related to our specific problem, we have to apply corrective parameters for ground roughness, ground relative elevation, orientation and shape of the roof, internal pressure and other factors. This is the specific procedure proposed by the Eurocode and by numerous national regulations. However, in most cases the pressure field should be determined from accurate studies on scale models in wind tunnel, as we usually treat unique and elaborate surfaces. This method could be useful for a preliminary design, while on the following stages it is preferable to take into account the dynamic effects.

2.3.3.2 Dynamic analysis

The Davenport procedure is hereby applied to get the maximum displacements and stresses due to the wind action, starting from an analytical speed spectrum. This process can be briefly illustrated with the following steps.

1. Determination of the analytical wind speed spectrum for a certain quote.
2. Introduction of the turbulence effects caused by the analysed surface.
3. Determination of the wind-induced force spectrum.
4. Determination of the structure response spectrum.
5. Determination of the maximum displacement and the induced efforts over the surface.

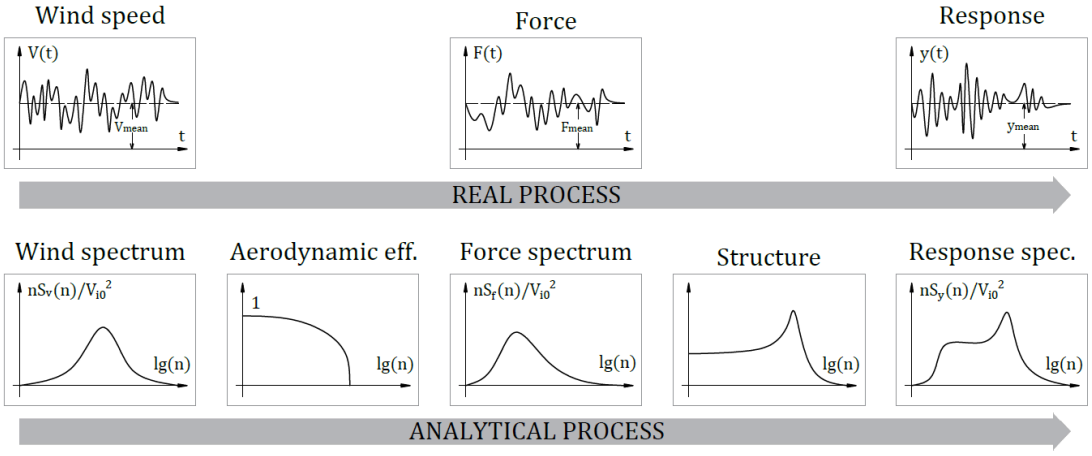

Figure 2.20: Schematic representation of the real effect of wind turbulent action and of the Davenport procedure applied for the response spectrum. Source: [19]

Although easy to apply, this method (shown also in figure 2.20) only gives information about the maximum displacements induced by both static and dynamic wind

effects. The next step in terms of accuracy is to consider the development of these effects over a period, thus determining the dynamic solicitation.

2.3.3.3 Dynamic solicitation

In this section we will see how to obtain the dynamic solicitation due to the wind, so that we can then apply it in a dynamic analysis method. In this case, the main shortcoming is that there is no information on its effective duration. The orthogonal decomposition technique is particularly effective on defining this dynamic solicitation:

1. This procedure starts from experimental data, from which we measure the instantaneous pressure for several points over the surface (located within a mutual range of $d \leq 0.1v/f$).

2. By developing those data, we can determine the eigenvalues $a_j\,(t)$ and their relative eigenvectors $p_j(x, y,\ t)$ for each vibration mode. We usually consider only the modes that cause considerable pressure variation over the surface, to reduce the number of calculations.

3. We can then apply the orthogonal decomposition relation, for which the pressure over a generic point at given time is expressed as a weighted mean between the considered modes.

$$p_i\,(x, y, t) = \sum_{j=1}^{N} a_j\,(t)\, p_j(x_i, y_i,\ t) \quad \text{with:} \quad a_j a_k = 0\ \forall\ j \neq k \tag{2.80}$$

   Where we have imposed a condition to eliminate all the non-orthogonal modes.

4. Having defined only orthogonal modes, we can analyse each one of them separately. Once the response is known for every mode and every point, we can apply the same formula to get the structure response to the dynamic solicitation as:

$$R_i\,(t) = \sum_{j=1}^{N} a_j\,(t)\, R_j(x_i, y_i) \tag{2.81}$$

2.3.4 Analysis of seismic solicitation

In this case the equivalent static analysis cannot be applied due to the geometric and structural irregularities that always characterize tensile structures. It is preferable to define a dynamic solicitation, and then apply one of the available dynamic analysis methods through a dedicated software. In case of seismic solicitations, the dynamic

forcing is related to the ground acceleration and to the mobilized masses.

$$P(t) = -ma_g(t) \tag{2.82}$$

The procedure that defines the response spectrum is similar to what we have seen for the wind solicitation. In case of new buildings, the Eurocode provides a specific procedure for the spectral parameters, and after them for the design spectrum. Whenever specific acceleration spectra related to past seismic events are available, we can also use them instead of calculating new ones.

2.3.5 Solutions for the motion equations

We will now briefly see some of the most widely used dynamic analysis techniques for tensile structures. These are summarized below, and we will present their main application principles.

2.3.5.1 Linear dynamic analysis

We take as a reference the case shown in figure 2.21, consisting of a suspended cable in which all the mass is concentrated at the middle point. It is a rather basic example, even though it is still a realistic approximation of some suspended structures. This structure can be traced back to the equivalent system in figure 2.22: a mass suspended from a spring and a viscous piston, subjected to gravitational forces and a generic external dynamic impulse. The motion equation can be obtained by writing the equilibrium equation for the vertical displacement w_{tot}, and by then developing it.

$$m\ddot{w} + c\dot{w} + kw = P_t \tag{2.83}$$

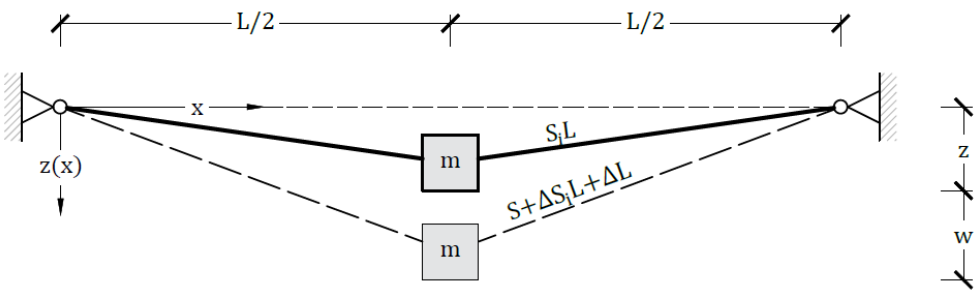

Figure 2.21: Reference structure taken as example to show the linear dynamic analysis of a simple suspended cable whose mass is concentrated at the middle point. Source: AutoCAD, own elaboration.

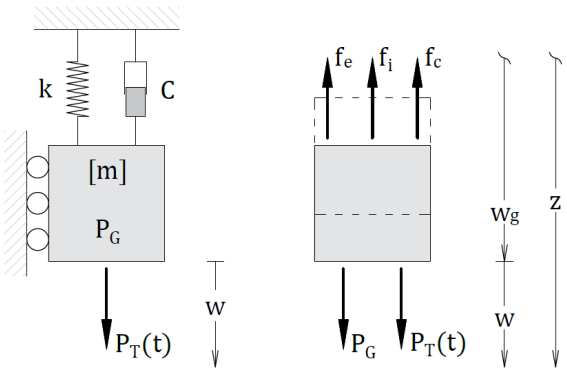

Figure 2.22: Representation of the mass damper system, equivalent to the reference structure, along with the forces acting over it. Source: AutoCAD, own elaboration.

where in equation 2.83: $m\ddot{w} = f_i$ are the inertial forces, $c\dot{w} = f_c$ are the damping forces, $kw = f_e$ are the elastic forces, P_g represents the gravitational loads, P_t represents the external dynamic solicitation. This is a 2^{nd} order differential equation that describes the displacement component $w(t)$ due to the dynamic force. The global solution is obtained by combining the solution of the associated homogeneous equation with the specific solution for the applied loads. The associated homogeneous equation corresponds to the case of free damped oscillation, whose solution is related to the damping ratio:

$$\xi = \frac{c}{c_{cr}} = \frac{c}{2m\omega} \tag{2.84}$$

Where c_{cr} is the critical damping factor, namely the value of the damping c for which the system response does not have any oscillation, ω is the natural pulsation. The damping capability of tensile structures is generally low (usually $\xi < 0.2$) due to their lightweight. Because of this the structure response consists of successive oscillations with decreasing amplitude. The solution is given by this expression:

$$w_o(t) = \exp(-\xi\omega t)\left(A\sin(\omega_d t) + B\cos(\omega_d t)\right) \tag{2.85}$$

Where $\omega_d = \omega\sqrt{1-\xi^2}$, while A and B are constant values related to the system initial conditions of displacement $w(0)$ and speed $\dot{w}(0)$. The logarithmic decrease is a useful parameter that describes the trend of damped free vibrations, and can be calculated from the amplitude of two successive vibrations:

$$\delta = \ln\left(\frac{a_n}{a_{n+1}}\right) = \ln\left(exp\left(\frac{2\pi\omega}{\omega_d}\right)\right) = \frac{2\pi\xi}{\sqrt{1-\xi^2}} \tag{2.86}$$

Hence, by carrying out free vibration tests and by measuring the amplitude of two successive oscillations we can determine the damping ratio of the structure.

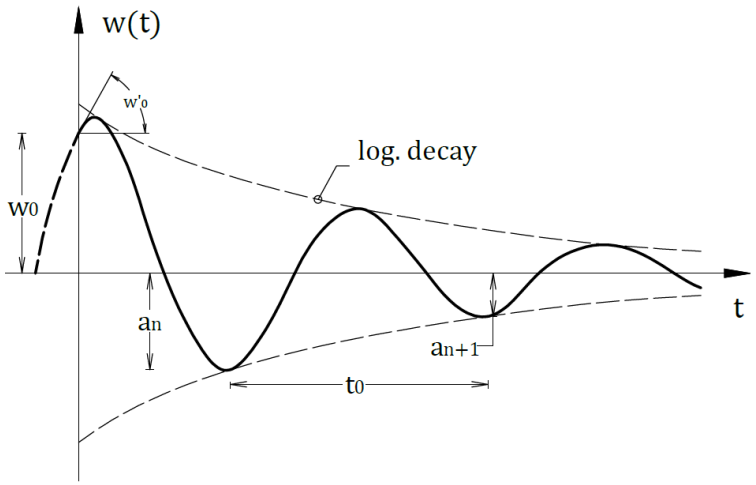

Figure 2.23: An example of damped sinusoidal motion, whose oscillations decrease according to a logarithmic scale. Source: [19]

The specific solution is related to the external dynamic load. Exact solutions of the motion equation are available only for some notable cases, such as sinusoidal forcing or linear load increase. However, when facing a generic loading function, we can always apply the Duhamel integral technique. In this method the load function $P(t)$ is treated as a series of successive impulses of short duration: for an infinitesimal impulse $P(\tau)$, with a duration $d\tau$, the response can be expressed as:

$$dw_p = \frac{P(\tau)\, d\tau}{m\omega_d} \exp\left(-\xi\omega\left(t-\tau\right)\right) \sin\left(\omega_d\left(t-\tau\right)\right) \tag{2.87}$$

The response produced by a series of infinitesimal impulses can therefore be written as:

$$w_p(t) = \frac{1}{m\omega_d} \int_0^t P(\tau) \exp\left(-\xi\omega\left(t-\tau\right)\right) \sin\left(\omega_d\left(t-\tau\right)\right) d\tau \tag{2.88}$$

This technique is particularly suitable for seismic solicitations, as the irregularity of the seismic acceleration $a_g(t)$ can be well approximated by the Duhamel integral. The method exploits the superposition principle to combine the responses to several successive impulses, therefore it can be applied only in linear systems. When both the solutions are finally known, the global solution to the motion equation can be obtained as:

$$w(t) = w_p(t) + w_o(t) \tag{2.89}$$

With reference to the initial case, the total vertical translation is finally obtained as:

$$w_{TOT} = w_g + w \tag{2.90}$$

Where w_g represents the static displacement due to gravitational forces. Within a dynamic regime the displacements are meant as incremental displacements, relatively to the configuration induced by static actions. As already stated, this method can only be applied to linear systems since the Duhamel integral is based on the superposition principle. Another limitation occurs since in the motion equation the stiffness k is treated as a constant: this is an acceptable approximation only with small displacements. Furthermore, when the natural and the solicitation frequencies are close enough, the system falls into resonance.

The damping ratio of tensile structures is generally low, which leads to an exponential increase in the amplitude of the induced oscillations. This aspect is even more influential in the case of structures suspended on cables, in which usually the only form of damping is represented by the mass of the structure itself. In this situation the hypotheses of small displacements and constant stiffness are no longer applicable, leading to some interesting conclusions:

- To analyse the behaviour of the structure in proximity of resonance phenomena, non-linearity aspects must be considered.

- In case of large displacements, the stiffness non-linearity causes a change in the natural frequency ω of the structure. Therefore, now it differs from that of the solicitation, thus preventing the resonance itself.

2.3.5.2 Modal superposition

When facing a multi degree of freedom system we have a set of motion equations, linked within each other. Considering what has been seen in the previous sections, this system can be written in its matrix form as:

$$[M]\{\ddot{U}\} + [C]\{\dot{U}\} + [K]\{U\} = \{P(t)\} \tag{2.91}$$

That, if the system is linear, can be solved with the modal superposition method. Such procedure is based on the decoupling of the various vibration modes, and on the calculation of their natural frequencies and relative displacements, as seen above. The motion of the system is described by combining these different modes:

$$\{U(t)\} = X_1\Phi_1 + X_2\Phi_2 + \ldots + X_n\Phi_n = \sum_{i=1}^{n} X_i(t)\,\Phi_i = [\Phi]X(t) \tag{2.92}$$

Where Φ_i is the i-modal vector. Hence, $[\Phi]$ is the modal matrix that transforms the displacement vector from normalized coordinates to geometric coordinates. $X_i(t)$ is

normalized coordinate or a scalar term dependent on t, that can be considered as a participation coefficient to the i-th mode. Usually, we consider only a limited number of modes (those which mobilize the larger mass). The vector $\{X(t)\}$ includes all these scalars for the modes considered. We can assume zero damping (which is a realistic hypothesis, since tensile structures have generally low values of the damping ratio), and then apply the change of variables to the motion equation. Finally, by multiplying each term for $[\Phi]^T$ the system can be rewritten as:

$$[\Phi]^T [M] [\Phi] \{X(t)\} + [\Phi]^T [K] [\Phi] \{X(t)\} = [\Phi]^T \{P(t)\} \tag{2.93}$$

The stiffness and mass matrices are therefore transformed into normal coordinates:

$$\begin{aligned} \{\Phi\}_i^T [M] \{\Phi\}_i = \bar{M}_i \quad \text{where:} \quad \{\Phi\}_j^T [M] \{\Phi\}_i = 0 \quad \forall\, i \neq j \\ \{\Phi\}_i^T [K] \{\Phi\}_i = \bar{K}_i \quad \text{where:} \quad \{\Phi\}_j^T [K] \{\Phi\}_i = 0 \quad \forall\, i \neq j \\ \{\Phi\}_i^T \{P(t)\} = \bar{P}_i \end{aligned} \tag{2.94}$$

Where, due to the orthogonality of the vibration modes, all the terms outside of the diagonal are null. The motion equations are hereby decoupled: it is now possible to write an equation referred only to the i-th vibration mode:

$$\bar{M}_i \ddot{X}_i(t) + \bar{K}_i X_i(t) = \bar{P}_i \tag{2.95}$$

There are N-decoupled equations. As every mode can be orthonormalized with respect to the mass matrix, it is possible to write the relation:

$$[\Phi]^T [M] [\Phi] = [I_N] \qquad [\Phi]^T [K] [\Phi] = \left[\omega^2\right] \tag{2.96}$$

$$\{\ddot{X}(t)\} + \left[\omega^2\right] \{X(t)\} = [\Phi]^T P(t) \tag{2.97}$$

The calculation of the frequency comes down to an eigenvalues problem, in the following form:

$$\det\left([K] - \omega^2 [M]\right) = 0 \tag{2.98}$$

Once the frequencies are known, the dynamic response is determined by solving separately the decoupled motion equations, referred to a single degree of freedom. Then, once the modal response of each normalized coordinate is obtained the results are combined, to obtain the response in geometric coordinates. While applying this method, it might be useful to reduce the degrees of freedom of the structure, thus reducing the number of dynamic responses to be calculated. Such operation is called static condensation and can be carried out with the Guyan method, which is based

on the subdivision of the degrees of freedom into Master (to be kept) and Slave (to be eliminated). The degrees of freedom to be eliminated are those characterized by a high ratio between the respective stiffness and the associated mass. As already mentioned, the method is linear and therefore has a limited field of action. To get around this problem, we proceed to solve the system of equations of motion with implicit or explicit direct integration methods.

2.3.5.3 Direct integration

An incremental and non-linear dynamic analysis is performed. To do this, it is necessary to rewrite the equation of motion for a specific time interval Δt, and therefore to know the equilibrium at instants t and $t + \Delta t$. Recalling all the various terms of the equations expressed for the linear dynamic analysis, it is possible to write the equilibrium as:

$$\begin{cases} F_I(t) + F_C(t) + F_E(t) = P(t) \\ F_T(t + \Delta t) + F_c(t + \Delta t) + F_E(t + \Delta t) = P(t + \Delta t) \end{cases} \tag{2.99}$$

From which comes the incremental expression for the time interval Δt:

$$\Delta F_I(t) + \Delta F_C(t) + \Delta F_E(t) = \Delta P(t) \tag{2.100}$$

whose terms can be developed as:

- $\Delta F_I(t) = M\Delta\ddot{U}(t)$
- $\Delta F_C(t) = C\Delta\dot{U}(t)$
- $\Delta F_E(t) = K\Delta U(t)$
- $\Delta P(t) = P(t + \Delta t) - P(t)$

It must be remembered that $\Delta\ddot{U}(t)$, $\Delta\dot{U}(t)$, and $\Delta U(t)$ respectively express variations in acceleration, speed, and displacement for the considered interval. Regarding the other terms, some clarifications need to be made:

- M represents the matrix of the masses, which are all considered concentrated at the nodes. If there are only translational degrees of freedom this matrix is diagonal. While calculating its components for a real structure, we can associate a given area of influence to each node to obtain the related mass.
- C is the damping matrix, the parameters of which are usually determined from the logarithmic decrease. Usually, considering the different phenomena of structural,

material, and aerodynamic damping, it is assumed as proportional to the masses and stiffness according to the relation:

$$C = \alpha M + \beta K \tag{2.101}$$

The coefficients are named weighting constants. Alternatively, we can consider that same matrix as proportional to the modal frequencies, according to their damping factors.

- The global stiffness matrix is defined as the sum of the elastic stiffness and geometric stiffness matrices:

$$K\left(t\right) = K_E\left(t\right) + K_G\left(t\right) \tag{2.102}$$

The non-linear part is continuously updated in the known terms vector.

- $\Delta P\left(t\right)$ is the known terms vector, containing the applied loads. If we want to consider geometric or material non-linearity effects, we need to add a non-linear component to it. This is obtained starting from the vector of unbalanced dummy loads, which are updated from the previous iteration:

$$\Delta P\left(t\right) = \Delta \bar{P}^{i}\left(t\right) + \Delta \bar{P}_{NL}^{i-1}\left(t\right) \tag{2.103}$$

The solution is obtained as an incremental solution to the motion equations. These are converted into a system of algebraic equations, introducing a relationship between acceleration, speed, and displacement for the considered interval Δt. In doing so, the unknown components are reduced to a single vector. However, this procedure is possible only when we assume a prior relation to describe the variation of one of the unknown vectors.

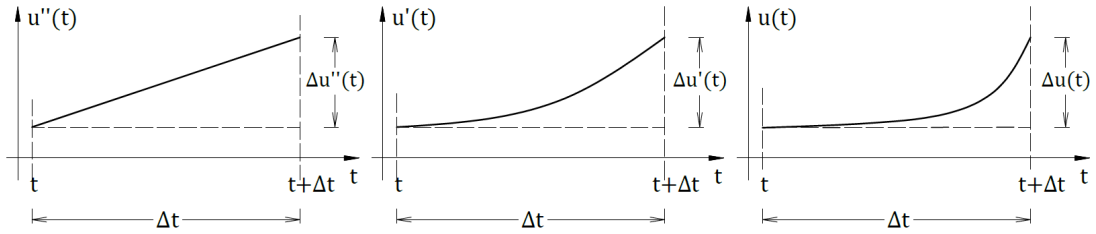

Figure 2.24: Example of correlation between speed, acceleration and displacement functions. This was defined by assuming a linear variation for the acceleration. Source: AutoCAD, own elaboration.

For instance, we can assume that the acceleration term $\ddot{U}(t)$ changes linearly (figure 2.24): consequently, we can also deduce the relations for both $\dot{U}(t)$ and $U(t)$ (speed will have quadratic variation, while the displacement variation will be cubic). By assessing the displacement at the end of the interval Δt, we can therefore define the expressions for $\Delta\dot{U}(t)$ and $\Delta U(t)$ within the same. Finally, by assuming the vector $\Delta U(t)$ as unknown term, we then develop the expressions for $\Delta\dot{U}(t)$ and $\Delta\ddot{U}(t)$ as functions of $\Delta U(t)$, $U(t)$, $\dot{U}(t)$ and $\ddot{U}(t)$. These will be substituted into the motion equations, and by isolating the known terms we obtain a system of pseudo static equations, which is solved for $\Delta U(t)$:

$$\bar{K}(t) \cdot \Delta U(t) = \Delta\bar{P}(t) \tag{2.104}$$

The expression for the effective stiffness is expressed as a function of the stiffness, mass, and damping matrices. The effective incremental load vector is defined as a function of the mass matrix and the known terms $U(t)$, $\dot{U}(t)$ and $\ddot{U}(t)$. Beginning from the initial moment t_0, and for every time interval Δt, we then apply the following procedure:

1. The initial values of $U(t)$ and $\dot{U}(t)$ are already known, as well as the mechanical properties of the structure (defined by $C(t)$ and $K(t)$).

2. Starting from the known terms, we determine the elastic forces $F_E(t)$ and the damping forces $F_C(t)$.

3. The initial acceleration is calculated as:

$$\ddot{U}(t) = M^{-1}[P(t) - F_C(t) - F_E(t)] \tag{2.105}$$

4. We then determine the terms representing the effective incremental load and the effective stiffness. It is therefore possible to solve the pseudo static equation:

$$\bar{K}(t)\,\Delta U(t) = \Delta\bar{P}(t) \tag{2.106}$$

   Thus obtaining the incremental displacement $\Delta U(t)$, as well as the incremental speed $\Delta\dot{U}(t)$.

5. Speed and displacement values at the end of the time interval Δt are calculated as:

$$\begin{aligned} U(t+\Delta t) &= U(t) + \Delta U(t+\Delta t) \\ \dot{U}(t+\Delta t) &= \dot{U}(t) + \Delta\dot{U}(t+\Delta t) \end{aligned} \tag{2.107}$$

6. The process is repeated for the following interval Δt.

The procedure leads itself quite well to the study of tensile structures, which usually present considerable phenomena of geometric non-linearity. Furthermore, it must be considered that simply suspended cables can resist only to traction efforts, presenting a further non-linearity. The method is not exempt from flaws: it is necessary to prearrange the function that describes the variation $\ddot{U}(t)$. Another approximation is made considering constant damping and stiffness during the time interval Δt. This last shortcoming can be avoided by calibrating the integration parameters, for example by exploiting the measurements obtained from physical models. In the specific case of tensile structures, the comparison and interaction between analyzes on physical models and computer simulations is an essential aspect to obtain good results in the design phase.

2.3.5.4 Other available methods

Throughout the continuous processing of the motion differential equations, it is possible to define simple and synthetic formulations for the analysis and resolution of the dynamic problem. The solutions thus obtained are easy to understand, and allow the control of the structural dynamic characteristics during the preliminary design. However, this system is practicable only with relatively simple problems, such as free suspended ropes (also with damping systems), or cables with bending stiffness properties. On the other side, when we face more complex structures, we could still refer to a simplified case by making appropriate assumptions. The results thus obtained could be used to broadly validate those provided by computer analysis.

2.3.6 About the dynamic stability of tensile structures

The first data related to the aerodynamic instability phenomena in tensile structures were produced following the famous collapse of the Tacoma Bridge. Since that moment, several studies have been produced. However, there is still a lot to discover, particularly regarding the effects of seismic stresses over large, suspended structures. Lev Zetlin, in one of the first studies, asserts that the frequency resonance occurs when the frequency of the external dynamic loads equals the natural frequencies of the structure. This implies an exponential increase in the amplitude of oscillation, and consequently in the stresses induced on the structural elements. Due to the unpredictability of natural phenomena that cause such dynamic stresses, it is not possible to obtain sufficiently accurate values of its frequency ω. Therefore, it is not possible to design the structure so that the value of the ratio ω_n/ω is far from unity, thus avoiding the resonance caused by external loads.

The best ways to prevent the resonance therefore remain the use of energy dissipation systems (such as tuned mass damper or viscous shock absorbers), or prestressed stabilizing cables. Regarding the use of stabilizing ropes, the exact values of the natural frequency for the single cable does not have much importance from the engineer's perspective. The frequencies calculated under the same conditions differ from each other, so that the ropes vibrate in different modes when applying an external force. Consequently, the frequency resonance is eliminated. Instead, it is the designer's responsibility to ensure that under permanent loads the frequencies of supporting and stabilizing elements are different, and that they diverge as the loads grow in magnitude.

When variable loads are applied, the stresses induced on the cables are different, hence the resulting geometry consists of a superposition of different vibration modes. Under the action of an external dynamic force, the geometries of the supporting and stabilizing elements will therefore be different, and the energy transfer from one cable to the other will make self-damping the overall system. This concept is useful to improve the dynamic properties of the structure already during the preliminary design. Nevertheless, the problem is more complicated: it has been proved that the natural frequencies of stabilizing and supporting elements can coincide with low or medium variable loads. In conclusion, the design rule remains valid, but the validation of the project is not immediate. It is therefore necessary to study the development of the dynamic phenomena over the time (here modern analysis techniques come into play).

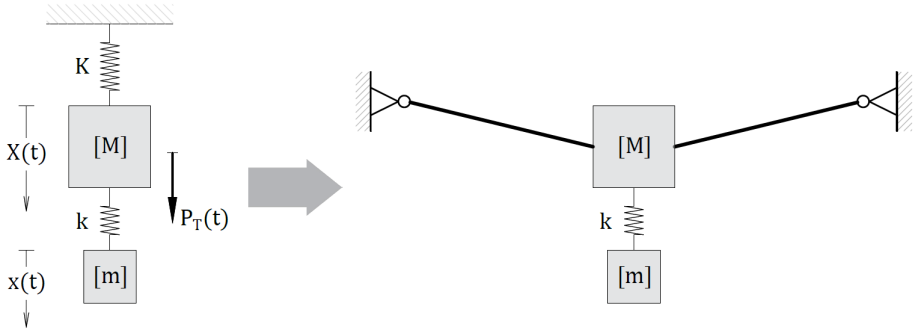

Figure 2.25: An example of a generic tensile structure, formed by a suspended cable with a tuned mass damper, together with its equivalent damped system. Source: AutoCAD, own elaboration

When designing structures based on suspended cables, such as walkways or electrical distribution cables, we can apply stabilizing systems based on suspended masses to control their dynamic behaviour. Figure 2.25 shows a basic example, where a suspended mass has been added to the main structure by means of a damping device. The secondary system is characterized by the parameters k (stiffness of the damping device) and m (added mass). By neglecting the damping contribution, the motion equations for

the primary and secondary systems respectively result:

$$M\ddot{X} = -KX - k\,(X - x) + P\,(t) \quad \text{and} \quad m\ddot{x} = k(X - x) \tag{2.108}$$

From these we obtain two values (Ω_1 and Ω_2) of the resonance pulsation, which means that the system has two natural frequencies, as shown in figure 2.26. By imposing the initial conditions, and then by integrating the equations, we can determine the counter-phase displacement of the 2 masses. The system is calibrated by calculating the values of k and m which eliminate the resonance that would occur for a non-stabilized structure at a solicitation frequency of $\omega = (K/M)^{1/2}$. The qualitative diagram of the dynamic response shows that there is a doubling in the resonance frequencies, which move away from the one of the non-stabilized structure.

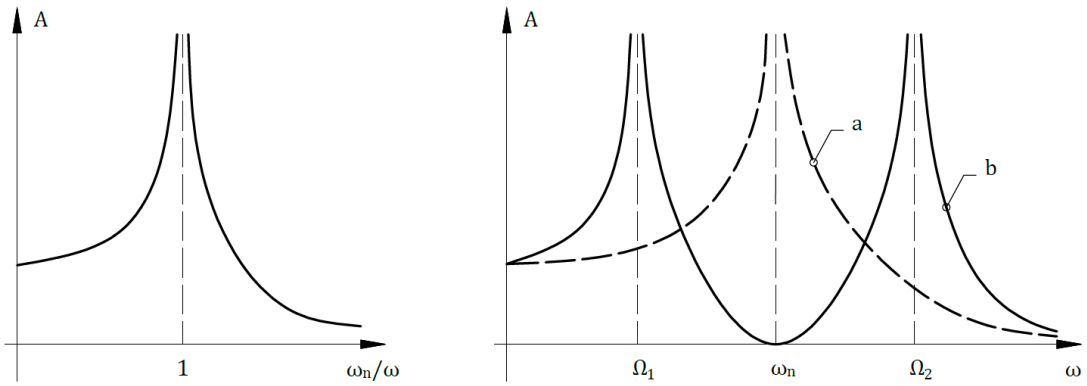

Figure 2.26: Tuned mass damper effect over the resonance behaviour of the structure: a doubling in the resonance frequencies (b), that move away from the solicitation frequency (a). Source: AutoCAD, own elaboration

The formulation just illustrated can also be applied to design a prestressed damping system with stabilizing cables. This would be treated as an undamped system with mutual absorption of vibrations between the supporting and stabilizing cables. The more the primary system is loaded and the secondary one is unloaded, the more this equivalent scheme is reliable. However, a further problem arises, as low values of the m/M ratio imply that the values of Ω_1 and Ω_2 are slightly different from each other, as we can see in figure 2.27.

Consequently, in case of a dynamic force with a wide frequencies spectrum, the damped structure might be excited close to both the values of its natural frequencies, thus generating a "double effect" system. Fortunately, as described by Zetlin, the cases in which this phenomenon occurs are limited. In addition, also the self-damping effect comes to help. Due to the large displacements caused by the resonance, the geometric configuration of the structure changes, and so do its natural frequencies. This effect is

as consistent as the system is deformable and as lower are its natural frequencies.

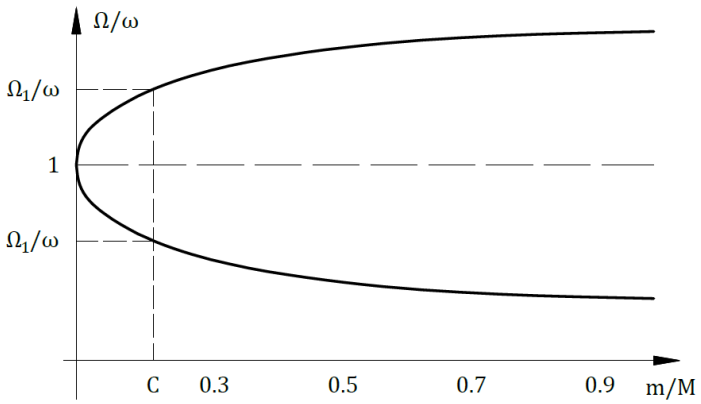

Figure 2.27: Effects of the ratio between tuning and structure masses over the resonance frequencies: the more the structure is loaded, the closer they are. Source: [19]

2.4 Materials and construction details

This section is intended to provide an overview of the main technical characteristics of cable-based structural systems. The various types of cables, their constitution and the parameters that characterize them will be presented. The same will be done for other construction components, such as anchors, covers, clamps and connections.

2.4.1 Cable's main characteristics

The rope section is not a single solid steel element; instead it consists of wires, cores and strands (as shown in figure 2.28). The wire is the basic component: it is usually a single unalloyed carbon steel filament, with a diameter between 0.5mm and 7mm. This is manufactured from squared steel bars, processed with a cold profiling treatment and then with a progressive reduction of their section to obtain the wire.

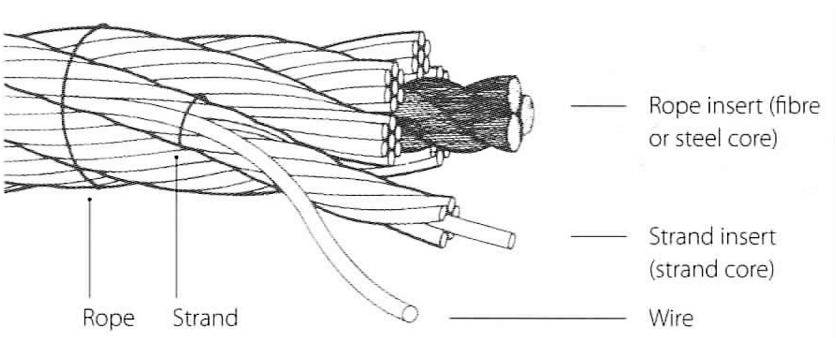

Figure 2.28: Different components of a rope. Source: [27]

Numerous wires are then helically wounded around a central wire core to form a strand. When the rope is made up of a single strand we can refer to it as a spiral rope, however in most cases strands are spun helically around an insert, called rope core (that can be either one wire or a spun yarn) to form a larger rope. Furthermore, single parallel members of wires or strands can also be combined to form larger units, called bundles (differentiated into parallel wire bundles and parallel strand bundles), which are held together using clamps or iron bounds. Parallel single members as ropes or bundles can be then combined to form proper cables.

Steel cables are characterized by specific technical parameters, which are presented below:

- **Diameter**: this value is the external diameter of the cable, to which the data sheets are usually referred. It must not be confused with the diameter of the metallic section of the rope.

- **Formation**: there are different formation types available, but the main distinction is between parallel and cross laid strands, shown in figure 2.29. To make cross-laid strands we use wires with the same diameter wounded in a multi-stage process, so that their number increases in the external layers. The resistance is lower due to the point-like contact area between the strands, that increase the local stresses. Parallel laid strands are obtained through a single stranding operation, that ensures a linear and continuous contact between different wires, thus improving the load distribution.

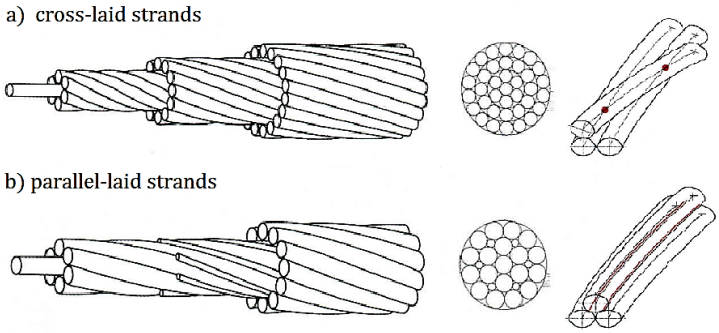

Figure 2.29: Differences between parallel-laid and cross-laid strands. Source: [27]

- **Lay direction**: with "z" and "s" we refer to the lay direction (clockwise or counterclockwise) of the outer wires of a single strand, while with "Z" and "S" we refer to the lay direction of the outer strands of a rope. The type of lay describe the combination of the lay directions of wires and strands in a rope: when they have opposite lay direction it is called regular lay, while when they have the same lay direction it is called Lang's lay. This last type is more hard-wearing and flexible, on the other site the regular lay is less susceptible to twist and spring.

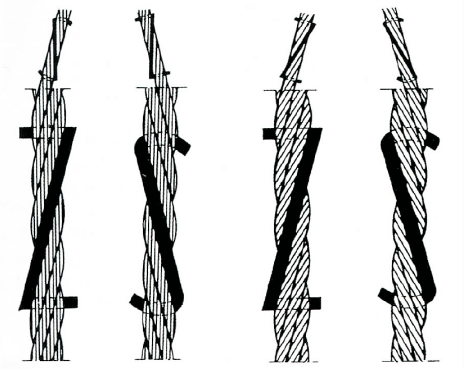

Figure 2.30: Lay type and directions. From the left: regular lay and right-turning (sZ), regular lay and-left turning (zS), Lang's lay and right-turning (zZ), Lang's lay and left-turning (sS). Source: [27]

- **Metallic area**: this is the sum of the areas of each wire transversal section. By neglecting the contributions of protective coatings and inserts, this can be considered as the resistant area of the cable, even if it is then necessary to take into account also the various phenomena of compressibility of the strands.

- **Rated Breaking Load**: this is the minimum breaking load guaranteed by the manufacturer. It is defined by the formula:

$$F_r = K' d^2 \sigma_r \tag{2.109}$$

  Where K' is a specific coefficient related to the cable formation, d represents the nominal diameter of the cable, and σ_r stands for the unitary wire strength. This value is then compared with the effective breaking load, determined from a traction test. The maximum permissible tensile load is defined from this parameter, usually around 30% and 50% of the effective breaking load.

- **Linear weight**: this is obtained from the formula:

$$W = K'' d^2 \tag{2.110}$$

  Where K'' is a specific coefficient related to the cable formation, while d stands for the nominal diameter of the cable.

- **External protective coating**: the steel wires are usually protected by applying a lubricant, while in case of aggressive environment factors they can also be galvanized. A further protection is provided by external paints and coatings with specific additives.

We must note that traditional ropes have a slight tendency to untwist under load. This phenomenon is caused by two factors: the manufacturing twist, that leaves residual stresses, and the loading twist, as loading induces an axial deformation along the wire, which leads to a reduction of the lay angle, thus generating a twist. Manufacturing twist is inevitable yet moderate, while load twist can be limited by spinning individual layers of wire in opposite directions. The cable can therefore be defined as rotation-free when its end does not tend to rotate under load, or does not produces torque when hinged. Regarding their behaviour under bending, another distinction is made between parallel and wounded strands: in the first type bending causes an elongation of the external fibers and a shortening of the internal ones. On the other side, in spirally wounded strands each strand is only stretched or compressed in places, thus relieving the bending effects.

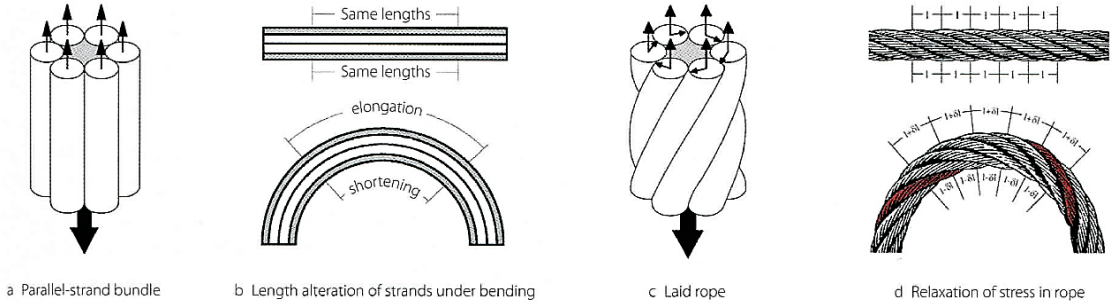

Figure 2.31: Length alterations and stress relaxations in deflected ropes. Source: [27]

Another useful parameter is the elasticity modulus (or Young modulus), provided by the following relation.

$$E = \frac{\Delta S l}{A \delta l} \tag{2.111}$$

Where ΔS represents the traction increase, l is the length of the rope, A is the metallic cross-section area, and δl stands for the elongation caused by ΔS. This value is determined through the assessment of the elongation caused by loads between 10% and 90% of the rated breaking load. It essentially depends on two factors:

- The elasticity of each wire.
- Compressibility of the cable core: the wires tend to adjust themselves following an elongation, thickening towards the section centre, and thus reducing its diameter. To reduce this effect, we can apply a prestress by subjecting the cable to a predetermined load (usually around 55% of the breaking load).

Once the technical characteristics have been exposed, we can make a summary of the main cable types currently available. There are many possible configurations, however the most widespread are:

- **Open spiral strands** (figure 2.32-a). They consist of spirally spun wires around a core wire, with many layers usually spun in alternate directions. Open spiral strands ropes are frequently employed for load-bearing elements, anchoring systems, edge ropes in membrane structures or supporting ropes in rope trusses, since they are particularly suitable for light to medium forces.
- **Half and Full-locked coil strands** (figure 2.32-b,c). When the number of wires increases, the geometrical strength of the rope bonding decreases: in this case half and full-locked coil strands are the most suitable solution. These are a specific type of spiral strand characterized by the maximum value of the ratio between metallic and nominal sections. This result is achieved through the use of a core

of round wires with one or more external layers of shaped wires, thus improving also the corrosion protection. Because of this they have higher breaking loads and lower flexibility than other cable typologies. Due to their high elastic modulus, they are suitable for uses with low elastic deformability requirements, such as cableways and suspension bridges.

- **Round spiral strand ropes** (figure 2.32-d), formed of many strands spun spirally in one or more layers around an insert. This type of cables can be manufactured using different laying techniques. They have high flexibility with low density, but they are quite susceptible to corrosion and wear. Their main uses are as stay wires, low-level truss tension members, handrail ropes in stairs or parapets.

- **Rope inserts**. For static wire ropes steel inserts are often used: these are made out of fibre, and are arranged between individual layers to prevent sliding.

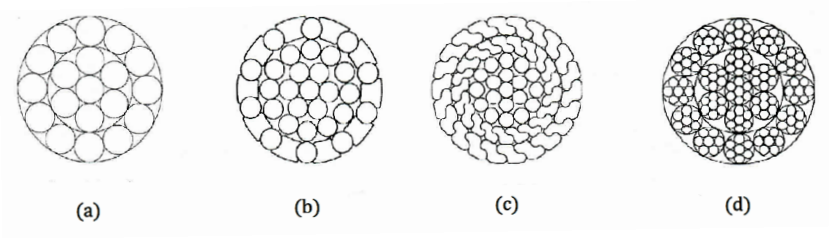

Figure 2.32: Most common types of wire rope: (a) open spiral strand, (b) half-locked spiral strand, (c) fully-locked spiral strand, (d) round spiral strand rope. Source: [27]

Finally, note that thermal actions cause considerable length variations over the cable, changing their geometric configuration and thus influencing the stresses, especially on hyperstatic structural systems. Another critical point for the stress increase occurs with strong bends (that could make necessary to wind several cables into a coil). The problem of excessive bending must also be carefully monitored during the assembly phases, as it could induce permanent deformation of the wires, with a consequent reduction in resistance.

2.4.2 Connection devices

As regards the anchoring terminals, two types of cable lugs are available:

- **Molten zinc**: the wire's ends are inserted into the cone of the cable lug, while the molten zinc is poured on the other side. Alternatively, shell casting is also available: in this case the cast block is inserted into the cone-shaped sleeve only after the casting process is ended. The effectiveness is generally very high, and the result can also be evaluated with X-ray scans.

- **Hammered**: the end of the cable is inserted into a steel sleeve, which is subsequently tightened inside with the aid of an hydraulic socket. The cable terminal thus wraps and definitively fixes the cable wires. The main shortcoming of this typology is that the breaking load at the terminal lug is usually lower than that of the proper cable.

Then, there are also numerous devices dedicated to the connection between cables: these are generally steel devices that are installed using tightened bolts and that operate by friction. The various standards impose specific dimensional limitations both for the devices and for the angles of attack between cables, also defining the necessary verification and controls. The variants and models available are so numerous that is impossible to show them all in detail. For the sake of synthesis we only list the various typologies, according to the intended use. The main types of connections are:

- **Cable connectors and network clamps**.

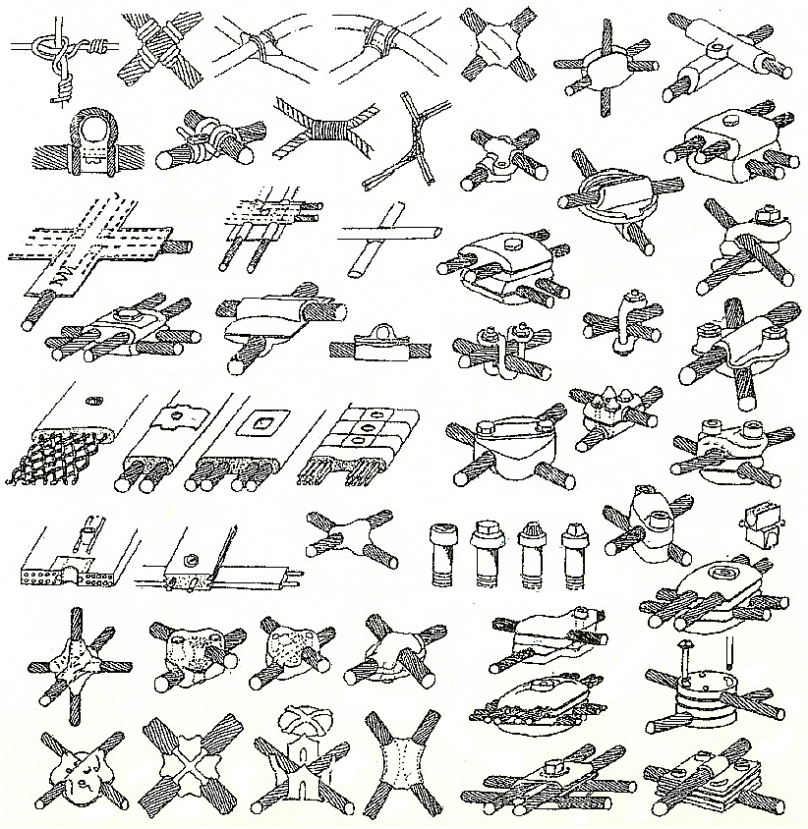

Figure 2.33: Various solutions for cable connectors and network clamps. Source: [19]

- **Longitudinal junctions and border junctions**.

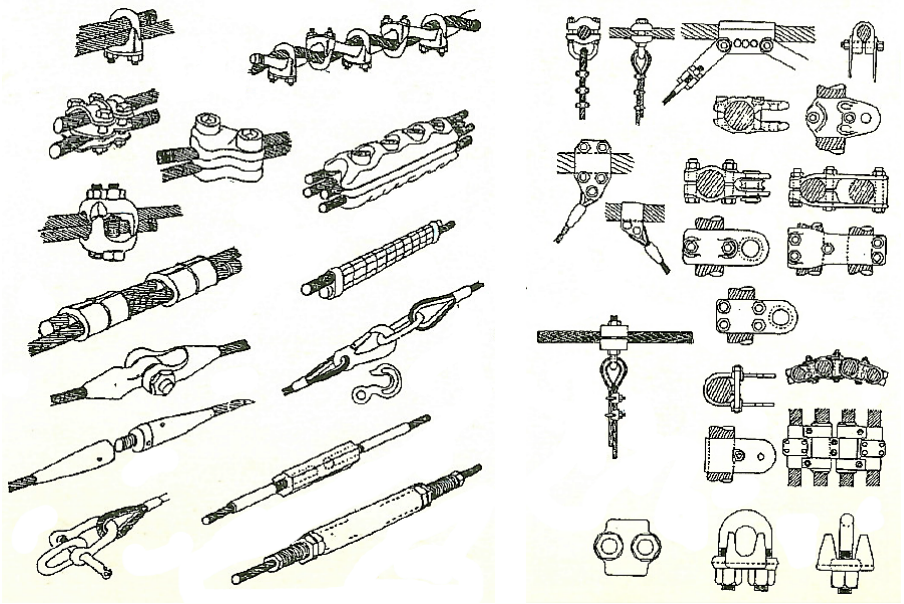

Figure 2.34: Various solutions for longitudinal junctions and border junctions. Source: [19]

- **Node switches**.

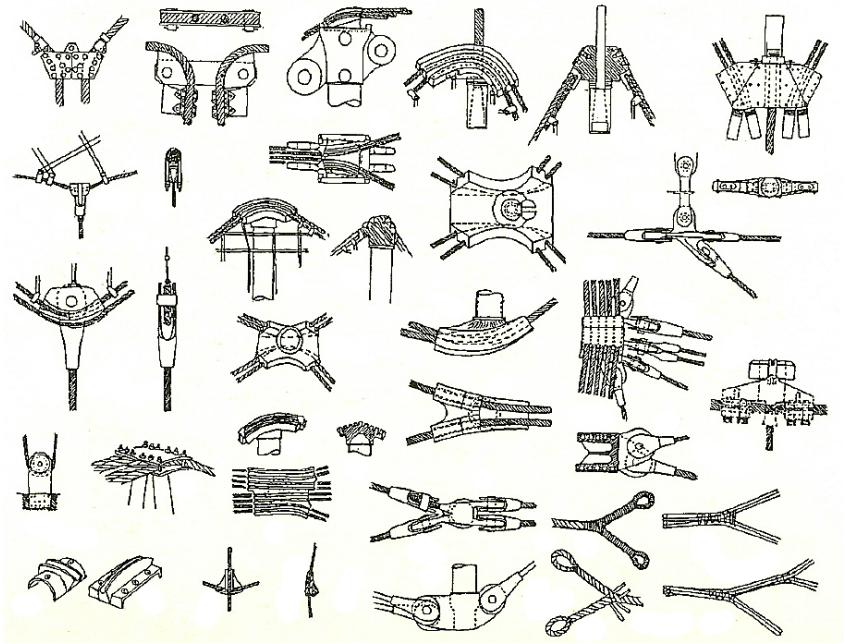

Figure 2.35: Various solutions for nodal switches. Source: [19]

To get an even clearer idea we can refer to figures 2.33, 2.34 and 2.35, bearing in mind that they contain only some of the available models. Their application depends on many

parameters: material of the clamp, type of rope, applied tension, use of the structure and others. In the case of networks consisting of wire meshes, the economic factor is also important, since a large number of terminals will be required. These components are usually placed on the ground. Once the mesh has been assembled, it is raised and tensioned: once the final geometry is reached, the last corrections are made and the final tightening is carried out. The main problems are loosening and wear due to environmental factors, such as rust. It is also important to pay attention to the local damage that the wires can undergo during tightening, in particular for those joining components that operate by mutual deformation.

2.4.3 Roofing typologies

As for the clamps, numerous types of roofing membranes and cable connection systems are also available here. Here too, for synthesis reasons, a simple summary will be provided, explaining their main characteristics. We can mainly distinguish:

- **Roofs with corrugated sheet metal**. There are various design solutions available:
    - The corrugated sheet is hooked directly to the cables by mean of clamps. The insulating and waterproofing mantles are placed above the sheet. Alternatively, the mantle can also be suspended below the rope structure.
    - The sheet is hooked to the cables by means of purlins. A space is created between those and the sheet, where the insulating mantle and the waterproofing can be placed.
    - Both the sheet metal and the insulating mantle are suspended below the rope system. This solution appears to be the most complex due to the difficult waterproofing near the suspension joints, however it allows to limit the volumes of the covered areas.
- **Transparent covers made with plexiglass, perspex or other transparent material**. In this case it is necessary to make joints able to prevent breaking and failures caused by the movements between the panels, due to the deformations of the roof.
- **Concrete roofing**. This typology saw a certain initial diffusion since its weight contributes to the stabilization of the roof, while now the same effect is sought by setting up tensile structures with overlapping roofing. These roofs can be realized on site, by building the slabs using temporary formwork, even if the

most common solution is the use of prefabricated panels. These are put in place once the cables have been laid, and connected within each other by means of special joints, hinges or clamps.

- **Covers with fabric materials**, which are particularly suitable for membrane and pneumatic structures. There are different materials available and the most common types of structural fabric are: polyester fiber, vinyl-components fiber, fiberglass, polyamide compounds. These are then coated with a protective coating, usually PVC, synthetic rubber or PTFE. The mechanical properties and characteristics are referred to a given specific model, and are determined starting from uni-axial and bi-axial and tear tests, performed on flaps of a given width.

2.4.4 Anchor systems

Tensile structures are inherently very economical, as they use the base material most efficiently. Processing, execution, assembly and maintenance costs are also very low. The most expensive components from this point of view are the anchoring structures to the ground, which are prefigured as special foundation works specific for this construction system. In the case of closed structural systems this problem does not arise: anchoring is obtained by exploiting their geometry (using rings, arches or other closed geometries) or by gravity (as in the case of the Braga Stadium stands, which tend to balance the forces transmitted). Open systems, on the other hand, require special anchoring structures to the ground, which can be classified as follows:

- **Gravity anchors** (2.36-a,b), where the vertical force transmitted by the cable is opposed by the weight of the foundation, and possibly of the ground placed above it.

- **Plate anchors** (2.36-c,f): in this case the cable is anchored to a plate, thus exploiting the weight of the ground above it and the friction between the soil breaking surfaces to counteract the action transmitted by the superstructure. This type of foundations is usually evaluated with the Meyerhof theory, based both on theoretical premises, on tests over models, and on-site experiences. Basically, the evaluation of the lifting capacity is performed on a simplified model, assuming a failure surface detected by experimental or on-site tests. The bearing capacity can be expressed as:

$$P_u = F + W \tag{2.112}$$

Where F is the friction contribution and W is the weight of the ground and the foundation. This formulation is developed in specific semi-empirical expressions

for the various cases of continuous, discrete, rectangular or circular, superficial or deep foundations.

- **Foundations on piles or micropiles** (2.36-d,e). For cable structures the poles are inclined, so that the force transmitted by the cable coincides with its geometric axis. By doing this, we can exploit the maximum reactant section possible, avoiding the formation of internal moments that can damage the pole itself. The resistance in this case is obtained by friction between the pole and the ground, while the weight of the pole has a reduced contribution.

- It is also possible to generate **mixed anchoring systems** with plate and micropiles, so as to further increase the contribution of resistance. The resistant mechanism is obtained by combining those mentioned above for the two types respectively.

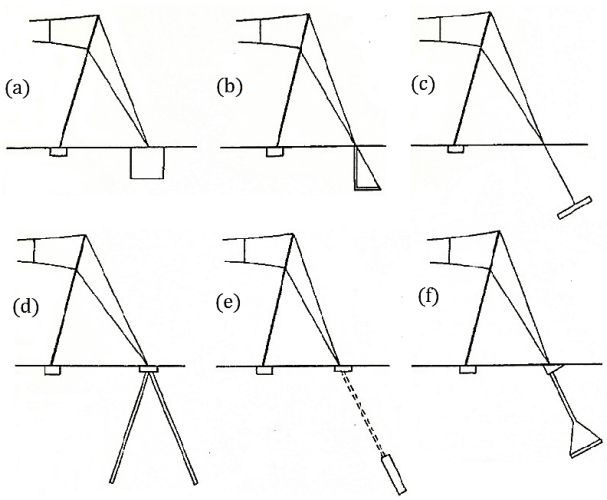

Figure 2.36: Various solutions for ground anchors. Source: [19]

The choice of the foundation type is affected by numerous factors, that are inherent to the structure itself, to the type of transmitted load (static, cyclically variable or dynamic), and to the soil characteristics. With regard to these last ones, the soil type (sandy or clayey), its stratigraphy, the presence of an aquifer and its possible variations are particularly relevant. It is therefore necessary to perform a series of tests and analyses on the ground (such as coring, tri-axial tests, edometric tests) already from the early design stages, and not infrequently, pilot tests are used in order to verify the expected performances from the foundation on site, before realizing the proper structure.

2.5 Notes about the construction process

When compared to conventional structures, assembling is an even more important process in tensile structures. We must bear in mind that the final static behavior is determined from the outcome of this process, and must be as similar as possible to what determined during the design phase. In fact, there is no predetermined geometry of the structure, since this depends on the load and mounting conditions. In this process, it is necessary to take into account the fact that cable structures are more deformable than traditional ones: this fact becomes significant when the roofing systems and other overloads are also added. It is almost always necessary to calculate the value of pretension forces to be applied on the structural elements during the various stages of installation, so that the stresses remain consistent with what is foreseen in the project. For this reason, usually for built-up structures, the assembly phase gives rise to the most severe load condition.

Once the installation technique has been chosen, the precise geometric configuration of the structure must therefore be determined for each phase, starting from the final one up to the initial one. The pretension forces are then calculated, as well as any possible correction during installation. It is also necessary to foresee the possibility of having to adjust some connections, so as to easily modify the geometry during the assembly. These requirements translate into precise technical choices regarding the ropes: these are usually equipped with a fixed and a mobile cable terminal, with which the initial draft and subsequent adjustments are carried out. It is also necessary to set up monitoring tools that allow to measure forces, lengths and deformations as the construction progresses, and therefore to continuously determine the geometric state of the cable system.

The construction process is heavily conditioned by the characteristics of the structure itself, and it is almost impossible to describe it correctly without referring to a specific building. However, it is possible to define common assembly phases for a given type of structure. For example, in the case of structures constituted by in-series components the process generally occurs according to these steps:

1. The cables are transported to the construction site and unrolled.

2. Friction joints are applied and clamps and connections are fixed between the different cables that make up the structure.

3. The cable system is hooked up by means of the cable lugs, is lifted and put into position, fixing it to the anchors.

4. The cables are tensioned using the mobile cable terminals. In this operation, hydraulic jacks and other suitable measuring instruments are usually used.

5. The roof is positioned according to a predetermined sequence and by continuously monitoring elongation and displacement of the structure.

To check the stresses of the cables different techniques are applied, in order to have redundant data. Readings are performed on the jacks during the pretension phases, geometric surveys of the in-place elements are carried out, direct measurements of the forces in some elements of the structure are performed. In the case of radial tensile structures it is no longer possible to tension the cables separately, as they interact within each other. A precise pretension sequence is established for each element of the structure, and often multiple steps are carried out for a single element due to the interaction with the others. In the case of rope network structures, things are even more complicated: after the first lifting, the various elements are hooked up, and as the pretension phase proceeds, any corrections and tightening of the terminals are made.

Chapter 3

Presentation of the study case: the Braga Municipal Stadium

In this chapter we will discuss the study case of this thesis, introducing the different elements that characterise it: the east and west stands, the roof, the pitch. We will also discuss their most peculiar aspects, trying to explain how the structure works. Finally, a summary of some publications that have been examined will also be presented. In this chapter, as well as in chapters 4, 5 and 6, for technical data, dimensions and information about the structure we will refer to the information included in the designs provided by MJW-Structures (annex A) and in [15], [16], [22], [18], [10] and [17]).

3.1 General description

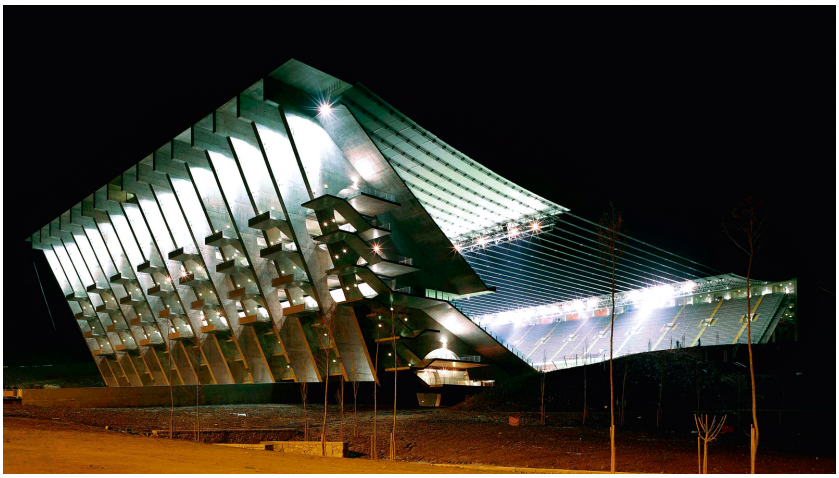

Figure 3.1: Night view of the Braga Municipal Stadium, Braga (Portugal). Source: [15]

The structure is located in Braga, Portugal, and is part of a large complex of sports facilities built for the 2004 European football championship [28]. The architecture is from Eduardo Souto de Moura, that designed this 30.000-seat Stadium on the site of the dismissed Monte do Castro quarry. He imagined a stadium with only two stands: one

would stand up from the ground and one would be carved in the hillside. Its goal was to keep the structure light and clean, integrating it with the surrounding environment. A suspended roof came as the most suitable solution. The structural design was provided by the Portuguese firm AFAssociados, while the roof analyses came from Eng. Massimo Majowiecki and other institutions: Danish Maritime Institute, Politecnico di Milano, RWDI, University of Porto and others. The characteristics described in the following sections are based on the information reported in [15] and [16].

3.1.1 The East stand

Figure 3.2: View of the works over the supporting beams for the horizontal slabs (a), armouring of the uprights (b), completed structure (c). Source: [15]

The East stand is a standalone structure that rises from ground level at +98m above sea level. It is supported by sixteen cantilever uprights in reinforced concrete (C35/45 + A500), with a thickness of 1m and an height of 55m, spaced 7.5m within each other. The cables of the suspended roof are anchored to the stand more than 50m above the foundations. The transition between cables and stand is ensured through an extremely stiff concrete beam, placed on top of the uprights and following the direction of the roof cables. It was therefore necessary to adjust the geometry of the uprights, so that the resulting combinations of gravitational actions of the stand and the horizontal forces transmitted by the roof would minimise the unbalanced moments at the foundations. The uprights are linked within each other via continuous concrete slabs, with a length

of about 125m, that pass though three large circular openings made inside them (one with a diameter of 14m and the other with a diameter of 8.5m).

These floor slabs are supported on paired metal beams (HE360B, HE450B, HE500B and HE600B) along the circular openings. The flight of stairs are in reinforced concrete, placed between the uprights and spanning an open bay of 6.5m. Structurally, the entire stand works without dilatation joints, therefore the set of uprights and slabs stabilise itself against both horizontal and vertical actions. The foundations are three types of geological-geotechnical strata, whose heterogeneity was particularly important. Due to the sensitiveness to subsidence shown by the structure it has been decided to replace the lesser quality terrain with concrete. The seismicity heavily conditioned the design of the vertical elements, mainly due to the weight of the cable anchoring beam which is placed at the top of them. Given the absence of dilatation joints, temperature variations and shrinkage proved to be influential for the project. Because of these actions, the first floor at +93.24m asl was completely disconnected from the uprights and sustained with a system of independent frames.

3.1.2 The West stand

Figure 3.3: View of the hinges at the top of the pillars (a), an inside foyer (b) and a general overview (c). Source: [15]

The West stand is "carved" in a granite massif, whose upper level correspond with the hill summit where a square give access to it. The horizontal floors are made with

a layered system: steel beams and reinforced concrete slabs provide support to an upper concrete slab, which act as the actual floor, while the 65cm in-between gap allows a clean passage for pipes and other installations. The steps are prefabricated and supported on prestressed and reinforced concrete angled beams, aligned with the sixteen middle uprights, to which they are hinged. The floors and the inclined beams are supported through concrete columns and partitions, whose foundations are on footings directly placed on the rocky basement. In zones with fragmented or cracked massif, anchorages were also added. Moreover, the second and third floors work also as rigid diaphragms, as the structure needs to be reinforced against horizontal actions due to the slenderness of the columns and the eccentric supports of the angled beams.

As the hilltop is at the same level of the roof, the horizontal actions transmitted by the cables were stabilised by anchoring it directly to the massif. Eighteen concrete uprights were placed between the anchoring beam and the rock and adjusted to the embankment irregularities. They support the roof actions and the horizontal component of the stands reaction, which heavily influenced their design. The rock anchors are divided on two levels: the upper one transmits directly the majority of the roof horizontal load to the rock massif, while the lower one helps correcting the direction of the upright reactions over the hillside.

3.1.3 The roof

The roof consists of a structure supported by a series of 68 suspended cables with a total span of 202m. These are coupled, with a space of 3.75m between each pair. They support two concrete shells, which have an thickness of 25cm and cover the two stands for a length of 57m (while in the middle section of 88m the cables are free). These shells are composite, made out of standardised slabs of 1.8m by 3.75m: each portion is connected to the cables by means of clamps, that allow relative tangential movements, while the connections between two successive slab sections are by mean of bolts and hinges. This choice helped to improve the response to thermal actions, shrinkage, wind effects, and also the predictability of the roof behaviour.

A steel truss beam is hanging along the inner border of each shell, bound both to the cables and the slabs. This beam is made up of independent portions bolted on site, and contributes to the stabilization of the roof against transverse oscillations. Rainwater is drained off the roof towards the east embankment, where the entire collector system is located. This was achieved by giving a 1%-slope to the roof surface by varying the length of the cables. Because of this the cable tension varies through the length of the roof, and therefore the cables have different diameter, ranging between 80mm and 86mm. Two stainless steel spouts are suspended at the end, and channel the water

towards the collection manifolds.

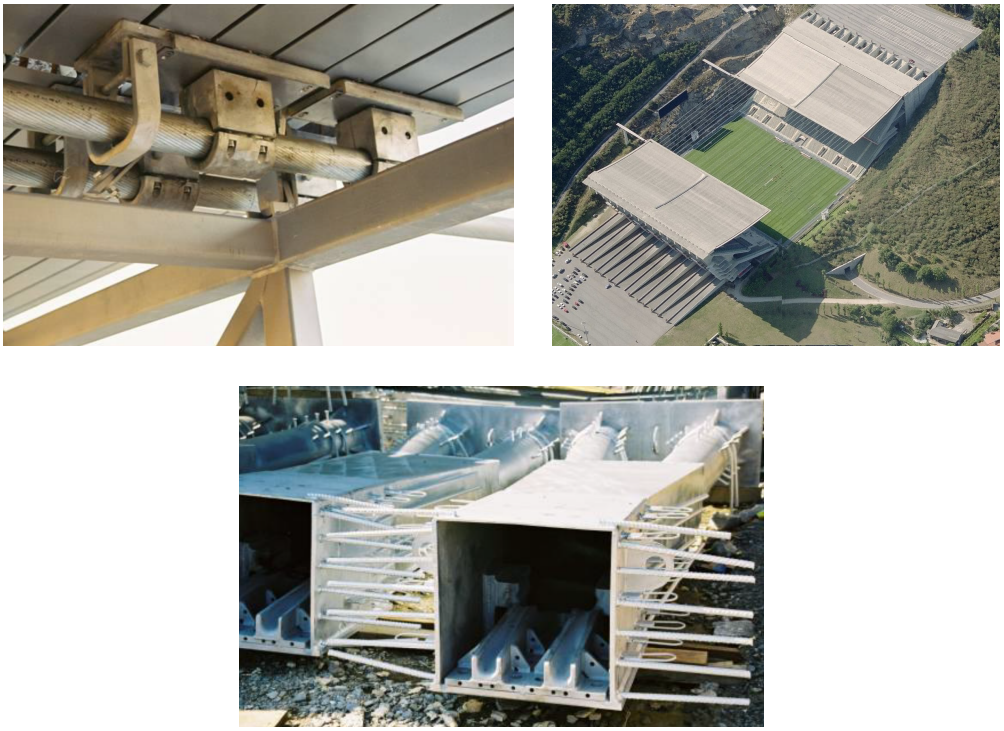

Figure 3.4: Details of the cable clamps (a) and the anchors (b), aerial view of the roof (c). Source: [15]

Given its peculiarity, it was not possible to design the roof relying on codes, recommended values or previous experiences. It was therefore necessary to carry out experimentation and modelling works, which started from the assessment of the actions needed to forecast the structural interaction and response. A combination of physical scaled models and mathematical models was used, proceeding with a series of independent calculations and tests, that also influenced the cable selection process just described. These studies were focused specifically on the wind action, and on finding the optimal design that would mitigate its effects. The roof structure was crucial also in the conceptual design of the stands: while the west one benefits from the presence of the granite massif at the level of the cable anchors, for the east one it was necessary to adapt its shape in order to counterbalance the cables action.

The cable selection process is worth of mention: these were initially expected to be equidistant with a spacing of 1,875m. The selection of the correct typology was extremely important, as it would affect the shape and technological characteristics of the whole roof. Given the vital role of the manufacturer's technical capabilities, it was decided for the cables to adopt a design/build contract, for which the manufacturer would have more involvement, being able to propose changes to the initial design by AFAssociados. The winner was the Tensoteci consortium (today Redaelli-Tecna), and

some notable changes to the initial project resulted from this collaboration. The slabs were standardized, and it was decided to couple the cables. The chosen technology is full locked coil cable, with galvanized protection.

3.1.4 The pitch

The pitch has been built as an independent structure, with the football field at its top and different services underneath. The pitch is at level +98m asl and cover a surface of about 10000m^2, while at floor -1 and floor -2 (at a level of +93.24m and +87.80m respectively) we can find a car park, restrooms, conference rooms and other services. The drainage water is channelled along a peripheral tunnel, thus avoiding annoying infiltrations. Electrical and hydraulic devices, such as light and fire-fighting systems, are embedded inside slabs and columns, as in the east and west stands.

The structure is realised with concrete circular columns and slabs. The columns are capped, thus avoiding punching phenomena and supporting the concrete slabs. Each column is spaced 9.35m in one direction and 7.50m in the other, while the slabs have a thickness of 0.35m, with the exception of the top one. This has a thickness of 0.5m and the whole set of slab, playing field, drainage and waterproofing counts for 1.10m of thickness. The column foundations are on plinths. Neoprene bearings have been placed on top of the most stiff columns to prevent strong forces generated by shrinkage and thermal variations.

3.1.5 Excavations and preparatory works

As the stadium would have been realised on the side of a rocky hill, slope excavations and stabilisation were required in order to fit all the facilities: in the end it was necessary to extract around 1700000m^3 of rock and gravel. During this excavation process it was also possible to check the geological and geotechnical conditions of the soil. The east side was found to be extremely fractured, sloping in the direction of the embankment itself. Because of this it was not possible to obtain a vertical wall, as in the first design idea, and were adopted contention measures such as ledges, anchors, nets and high resistance bolts. Moreover, a continuous slipping and a fault detected in the North-West side caused the stadium to be shifted 20m west from the planned location.

The west side embankment was much smaller and easier to stabilise. Due to these difficulties the designers decided to install a monitoring system, consisting of 10 load cells in the anchoring and 4 in-place inclinometers, each one of a total length of 20m. This system was lately integrated with the permanent monitoring system of the structure, that automatically and permanently manages all these sensors.

3.2 Construction and monitoring

3.2.1 Construction process

After the completion of the preparatory excavations, the stands and the pitch were built. As for the west stand, the structure was very sensitive to settlements, and in addition there were numerous prestressed components. The reports [15] and [16] state that due to this it was necessary to define the construction phases in advance during the design process.

Figure 3.5: Different construction stages: (from the left) initial excavations (a), east (b) and west (c) stand works, laying of the cables (d) and composite slabs (e). Source: [16]

It was decided to apply only 20% of the force over the anchors before realizing the roof, and the rest once it was completed. Five of the uprights have been laid on hard core, for which was necessary a foundation beam, in order to apply immediately the entire force and begin their construction after the subsidence process. The other uprights, laid on rock, were realized using provisional anchors, that generated a prestress state that minimised the settlement consequences.

There were many doubts on how to realize the roof. The designers took as reference the building process of stress-ribbon bridges and the Dulles Airport building in Washington. In this cases, the slabs were slid along the cables into their final position. A similar procedure was adopted for this stadium, with some expedients to avoid the use of props and formwork. It was therefore decided to use precast panels, whose lower faces are lined in steel sheeting. This acts as a proper form-work, and also has metal parts that allow the use of bolts, thus facilitating the assembly procedure on site. In the end, such process was carried out according to the following phases [15]:

1. The suspended cables were laid using a provisional guide cable, starting from the west stand towards the east stand, as shown in figure 3.5 (d).

2. The cables were permanently anchored to the East stand, while a temporary anchor was applied to the West stand.

3. The prefabricated slabs of the shells were then assembled near the anchor points, at the top of their respective stands.

4. As the slabs were ready, they were slid into position along the cables using gravity and connected to the adjacent panels by bolts. Once all the panels were in place, the joints between each one were concreted.

5. The different parts of the truss beams were lifted into position and bolted to the slabs and to the adjacent elements.

6. The geometry of the roof was finally adjusted by varying the length of the cables. This phase was carried out using an hydraulic jack on top of the west stand. Once finished, they were permanently anchored also to the West stand.

The intrinsic characteristics of these structures (roofs supported on suspended cables) do not allow an optimal control of the various structural parameters during construction. Therefore, analysis and monitoring of the finished structure are necessary to verify that its performances are consistent with what was assessed during the design phase.

3.2.2 Geometry control and permanent monitoring

As described in [15] and [10], the monitoring process of the structural response began already during the construction phase, as the application of cables and prefabricated slabs constituted a proper "load test" for the structural elements of the stands. As a result, cables stresses and strains were carefully monitored, and the verification of these values with the expected behavior ensured that the geometry was as desired in the design. In addition, there still was the verification of the roof geometry by means of topographic surveys.

These data were integrated with the ones provided by the structure monitoring system, to study its behavior during the assembly of the roof. This instrumentation consists of: load cells on the roof cables, strain gauges and tiltmeters on the uprights, inclinometers on the embankments and on the foundations, load cells applied to the rock anchors. Thanks to these data it was possible to check the predictions of the mathematical models, which were eventually corrected and improved with the measurements obtained on site during the construction phase. This enhanced the theoretical reference of the roof geometry, that was used for the final adjustments at the end of the

construction. Since the completion of the stadium, permanent monitoring of the various structural parameters, both static and dynamic, has been carried out. In addition to the static sensors already mentioned, there are also 6 tri-axial accelerometers on the roof, placed at the inner border of the slabs (where the largest oscillation amplitudes are expected). The field processor samples time series of 60 minutes: this duration resulted from a compromise between the goals of obtaining reliable estimates of modal damping ratios and a characterisation of the daily variations of the model parameters. Regarding the wind actions, these are constantly checked through a meteorological station and 3 anemometers located on top of the West shell.

3.3 Studies and research on the cable-suspended roof

Numerous independent entities have conducted research and studies about the dynamic behavior of the roof, with special regard to the wind action and its effects. Several academic articles and publications have emerged from these collaborations, talking about the mathematical modelling of the wind action, the effectiveness of the finite element models and the dynamic properties of the structure. We want to hereby propose a brief summary of some of the most interesting ones, focusing on the tests and analysis performed after the construction of the roof.

3.3.1 Wind tunnel models and tests

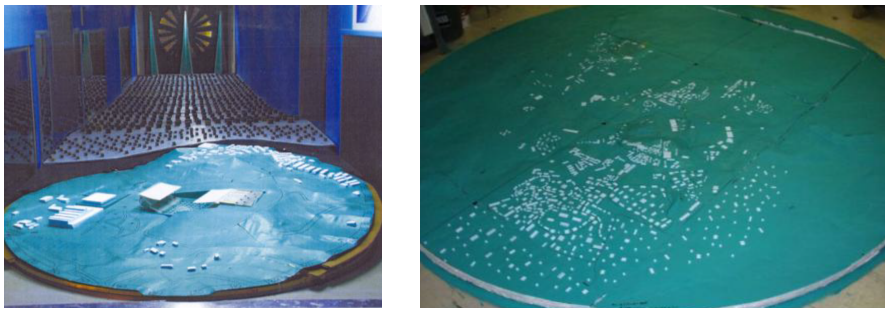

Figure 3.6: Rigid scaled models of the stadium and its surroundings developed by RWDI. Source: [16]

The main wind tunnel tests over the stadium were developed independently at RWDI [26] and the Politecnico di Milano [13] wind tunnels. In the first case the tests were performed on a rigid model, with the aim of determining the wind pressure field related to various directions. The flexible model of the Politecnico di Milano was instead developed to test the aerodynamic stability of the roof and a preliminary design of a damping system.

For the first model, wind speed and directions (measured by a nearby weather station) were applied in a series of tests over a 1:500 scaled model of the stadium and its surroundings, shown in figure 3.6 (a). Having obtained the actual wind speed over the roof, another rigid model in 1:400 scale was studied to determine the static pressure fields. These were measured at different points on both sides of the slabs and collected into time history series for each wind directions, then the net pressure coefficients were then obtained through an interpolation of these data.

The structural response was assessed by evaluating separately its mean, quasi-steady (through a POD) and resonant components (that consider dynamic amplification of structural vibration modes). The obtained pressure coefficients were lower than those reported by standards for similar geometries. Large values were located near the roof borders due to local vortex effects, while very high resonant effects have been found: as they are related to inherent structural damping, this result [20] prompted the need of deep studies over an aeroelastic model.

Figure 3.7: Aeroelastic scaled model tested in the Politecnico di Milano wind tunnel. Source: [21]

A 1:70 scaled aeroelastic model was tested at the Politecnico di Milano (figure 3.7). These analyses were performed both under laminar and turbulent flows (in this case with a reconstruction of the surrounding environment), verifying the aeroelastic stability at full scale (58m/s). From these tests emerged that the resonant response is dominant, with oscillation amplitudes up to 50cm in full scale. According to [21], the on site turbulence values were affected by high uncertainties and quite different from the ones found in the models, so a more accurate evaluation of the structural damping properties was necessary, leading to the development of full-scale tests in order to confirm the theoretical estimations previously obtained.

3.3.2 Reliability analysis

The roof was also subjected to a sensibility analysis [4] under random wind loads (without considering structural dynamic amplification), using the data from RWDI wind tunnel tests. The aim was to evaluate the sensibility of failure probability to spatial random distribution of wind loads, the wind direction with the highest probability to cause a failure, the roof points that would fail with most probability and the spacial distribution of wind loads that drive the structure to fail with most probability. This study was developed to overcome the uncertainties regarding numerous factors that could affect the structural response: cables elastic modulus, long term creeping phenomena, fabrications tolerances, construction tolerances and others.

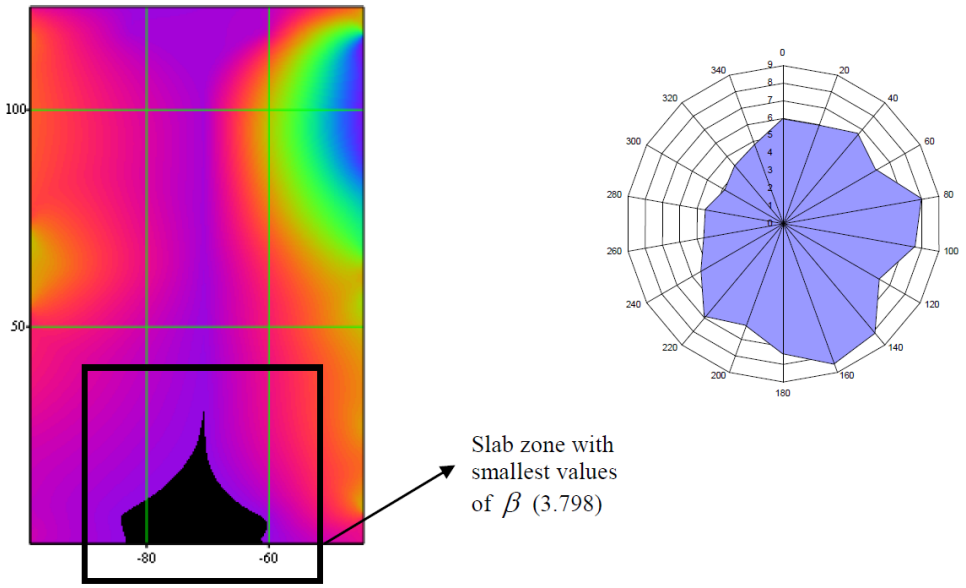

Figure 3.8: Mapping of the β values for a 300° North wind direction (a) and minimum β values for each direction (b) Source: [20]

The reported results [17] proved that the structural response is sensitive to the standard deviations of the cable strain variations, and that the most likely failure mechanism would involve the border cables, allowing a proper local dimensioning to prevent chain failure. The most dangerous wind direction was determined by evaluating the reliability index β, considering different pressure distributions (related to different directions) at Ultimate Limit State. The same index was also evaluated for various points of the slab surfaces, thus defining the areas with the highest failure probability. The worst wind direction resulted to be 300° North, while the worst area is located near the slab border, where the bending moment reaches the maximum values, and therefore the β index reaches its minimum. As said in reference [20], this type of analysis can provide better results than the POD method applied to wind tunnel data, since it relates

the wind loads spatial distribution to the roof weakness. Finally, it was also found that the worst wind distribution is quite different from the one assumed in design codes.

3.3.3 Full-scale testing program

The testing program on structure is part of a design and verification strategy, according to the Eurocode "Basis of Structural Design" that gives general indications about the Design Assisted by Testing [29]. Full scale testing, applying both artificial and ambient vibrations, has been performed to reduce the uncertainties about dynamic damping performances and to check vibration modes and frequencies. These test were carried out by VIBEST (Laboratory of Vibrations and Monitoring of University of Porto).

3.3.3.1 Induced vibration test

The high flexibility and the mass of the roof generate low frequency values for the first vibration modes, hence the need of a special excitation system capable to produce oscillations in the range 0.2 to 1 Hertz [22].

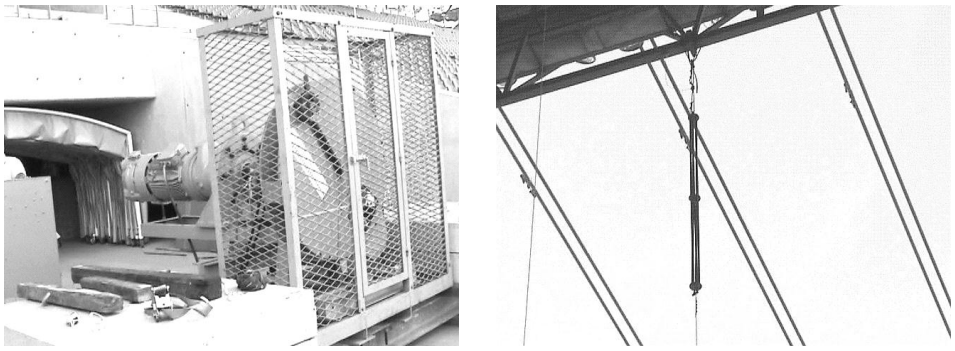

Figure 3.9: View of the electric engine (a) and the girder linked spring (b). Source: [23]

Two different setups were used:

- During the first stage the structure was excited by impulsive loads, with the aim to identify the main natural frequencies. The loads were generated by releasing a 5 tons mass suspended to the roof edge truss beam by mean of a cable.

- During the second stage the structure was excited with periodic loads, with the purpose to excite the main natural vibration modes using resonant harmonic forces. These were provided with a cable and a prestressed spring, connected to an electric engine through an eccentric link.

For each setup 2 different solicitation points at the inner border of the slabs have been considered, while the measuring arrangement consisted of 6 accelerometers that

were already part of the permanent monitoring system. The setup is outlined in image 3.10. Note that since the acceleration horizontal components are negligible when compared to the vertical ones, only these have been measured and considered in the analyses.

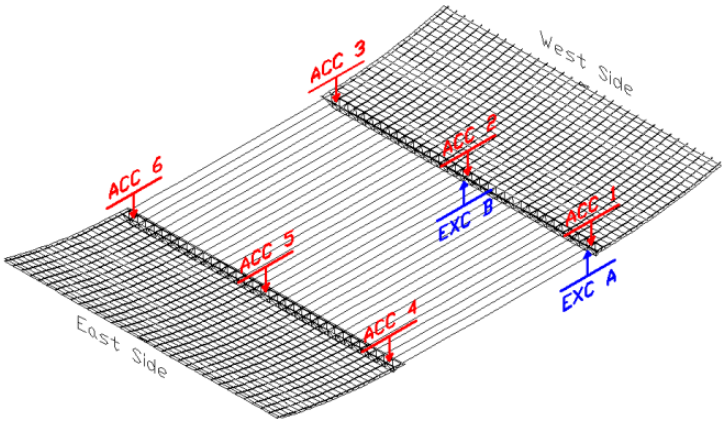

Figure 3.10: Roof view with the accelerometers and the exciting system positions. Source: [23]

3.3.3.2 Ambient vibration tests

The ambient vibration tests on the completed roof produced the data used to determine modal damping ratios, by implementing the Enhanced Frequency Domain Method and Stochastic Subspace Identification Methods. These analyses were carried out in two days, by measuring the vertical acceleration to the roof in 42 points on the two slabs using motion recorders.

The 42 points were organized in different setups, keeping only one measurement point as a reference among all. For each setup, time series of 16 minutes were recorded at the sampling frequency of 100Hz. This analysis [2] was strongly influenced by the action of the wind, as it was the only significant dynamic stress, and influenced the oscillation amplitudes during the tests.

3.3.4 Estimations of modal parameters and damping ratios

Different methods have been applied to determine the natural frequencies, shapes and damping ratios from the output of full-scale tests. Their results have been compared within each other and with the estimations from a FEM model, trying to prove the consistency of previous calculations and of these proper methods. In the end, the experimental evaluation of modal damping ratios allowed to increase the reliability

of the previous theoretical evaluations, with special regards to the response against dynamic wind loads.

3.3.4.1 Proper Orthogonal Decomposition

The induced vibration decay time series were processed. The recorded acceleration fields have been treated first with a frequency filtering between 0.05Hz and 30Hz, and then with a Proper Orthogonal Decomposition (POD) [12]. From the free vibration intervals it was then possible to evaluate the logarithmic decay and the consequent damping ratio. The results [22] show that different modes have been identified, and as they involve all the main roof deformation modes they are sufficient to characterize its dynamic behaviour. The comparison between experimental data and FEM model outputs revealed that the anti-symmetric modes are well represented by the theoretical calculations, while the symmetric ones in reality are lightly stiffer.

3.3.4.2 Frequency domain decomposition

The ambient vibration response was initially processed with the Frequency Domain Decomposition (FDD) [7] to obtain the modal shapes. The method is based on the spectral matrices of the ambient response, whose columns contain the mode shapes.

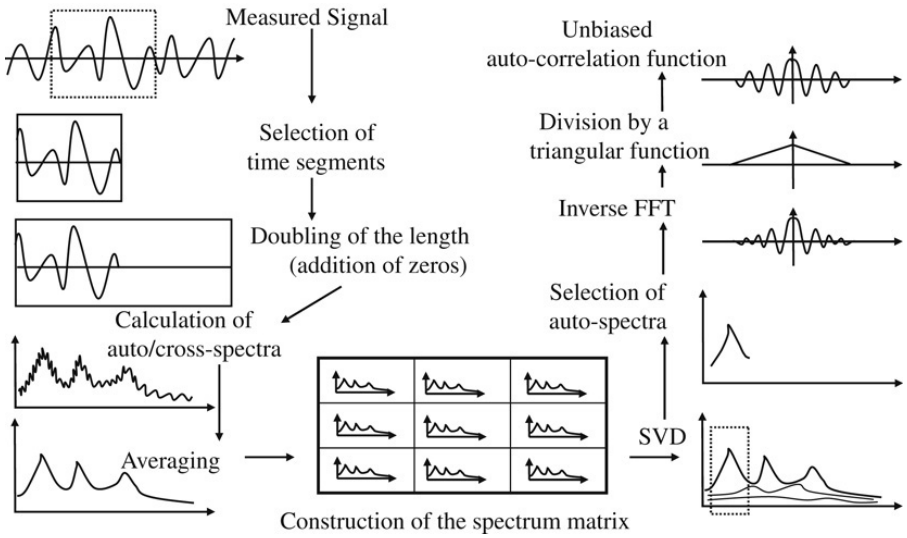

Figure 3.11: Procedure for the estimation of modal damping ratios. Source: [18]

The modal damping ratios have then been assessed using the Enhanced Frequency Domain Decomposition Method [6]. Due to the low frequencies and the small values of damping expected, the duration of each setup time series was not sufficient to have an accurate estimation. Therefore, to increase the accuracy, the auto-correlation functions were determined using an alternative procedure with regard to that presented

in reference [1] based on the Fast Fourier Transform, and whose steps are summarized in figure 3.11.

3.3.4.3 Stochastic subspace identification

The Stochastic Subspace Identification methods have been applied over the ambient vibration response data, with the aim of comparing the modal damping ratios obtained through different output-only identification procedures. The Stochastic Subspace Identification Method [39] relies on a stochastic space model to identify the modal parameters, where the excitation is assumed as a white noise. Two type of analysis were carried out:

- Co-variance driven Stochastic Subspace Identification Method (SSI-COV), where the white noise matrices are identified from the correlation functions of the measured time series. The method was applied using MatLab routines developed by the University of Porto [14], using direct definition to estimate the correlation functions.

- Data driven Stochastic Subspace Identification Method (SSI-DATA), where the identification of the matrices is performed from the time series using the concept of projection of subspace. The method was applied using the Artemis software [38].

Since for real structures is not possible to predict the order of the model that fits better the experimental data, modal parameters were estimated using models with an order defined within a previously fixed interval. Such procedure [18] has been developed after applying a low pass filter, that eliminated the contribution of modes with higher frequency. For the SSI-COV method, the dynamic behaviour was well represented by state-space models of orders between 20 and 40, while for the SSI-DATA method models with orders between 30 and 50 proved to be sufficiently accurate. Other comments about the results (in terms of mode shapes, natural frequencies and damping ratios) can be found in section 3.3.4.5, where they will be grouped and compared with the ones obtained from other methods.

3.3.4.4 Estimation through finite element modelling

In addition to the previous theoretical models, developed in collaboration with VIBEST since the early design phase [2], another 3D finite element model was developed to analyse the static and dynamic behaviour of the roof. The model, described in [18], was formed by 34 cables, spaced 3.75m within each others, idealised with 89 truss elements

each. These cables were linked to shell elements to replicate the slabs effects, and were also linked by transversal truss girders at the end of each slab. Sliding between cables and slabs was allowed, and the 1% transversal slope was recreated by modifying the cable's length. Modal parameters were calculated using the tangent stiffness matrix after the application of permanent loads, considering also the geometric non-linear properties of the cables. It was also simulated the construction process, by gradually activating the shell elements loads.

3.3.4.5 Correlation between different methods

According to different reports [18] [22], the structure was extremely challenging as it was characterised by closely spaced modes, low damping ratios (with a magnitude of around 0.3%) and numerous natural frequencies under 1Hz. The presence of pairs of closely spaced frequencies is justified by the 1% transversal slope, that breaks the structural symmetry. The identified modes are represented in image 3.12.

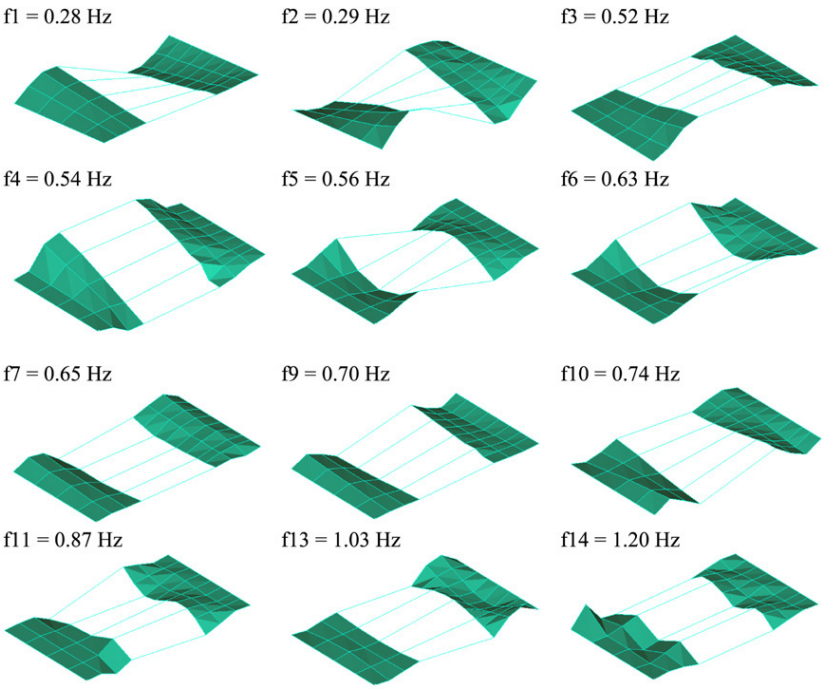

Figure 3.12: Mode shapes and frequencies estimated with through FDD (whose results were confirmed by other methods) Source: [18]

Still, there are some problems, as stated in [18]. The POD applied to induced vibration response was affected by the low excitation level of some modes, and by the difficulty in isolating the contribution of the modes with close natural frequencies. This led to the non-estimation of the damping ratios related to these modes, and enhanced the need of an alternative method to find the missing values and confirm the theoretical

predictions. The SSI-COV and SSI-DATA method applied to ambient vibration response were affected by an high scattering of the damping values estimates, mainly because of the damping varying with the oscillation amplitude. The comparison with the damping coefficients obtained from the FEM model showed an increasing difference at lower frequencies, due to the low damping values and the aerodynamic damping component (which affects more the low frequency modes). Despite this, the results provided by FDD, EFDD, SSI-COV and SSI-DATA methods were close within each other and with the modes identified with POD, thus proving to be consistent [18].

Summary of all the identified modal damping coefficients (%)

Mode	Free vib.	SSI-COV	Harmonic exc.	Ambient vibration		
				FDD	SSI-COV	SSI-DATA
1	-	0.29	0.28	0.58	0.50	0.51
2	-	0.37	0.27	0.52	0.42	0.48
3	0.28	0.32	0.22	0.47	0.44	0.39
4	0.25	0.22	-	-	0.40	0.33
5	-	0.44	-	-	0.47	0.53
6	0.34	0.36	0.43	0.35	0.54	0.47
7	-	0.29	-	-	0.28	0.73
8	-	0.11	0.20	-	0.27	0.30
9	-	0.18	-	-	0.26	0.31
10	0.20	0.18	-	0.25	0.26	0.29
11	-	-	-	0.36	0.41	0.38

Table 3.1: Brief summary of all the identified modal damping coefficients obtained with different experimental methods. Source: [18]

Table 3.1 summarizes the modal damping coefficients identified with different methods. In the end, both operational modal analysis and procedures based on artificial excitation could provide good estimations of the order of magnitude of modal damping ratios. Finally, it is worth of mention a conference paper [10] published in 2014, based on a study conducted over the resulting data from continuous monitoring between December 2011 and August 2012. The analysis was focused on characterising the wind action, establishing correlations with the structural response and assessing the influence of wind and temperature on the variation of modal parameters. Regarding the estimated damping ratios, it was possible to evidence the dominant influence of wind and confirm previous estimates based on free and forced vibration tests.

3.3.5 Mitigation of wind induced vibrations

The analysis of the wind action has shown that the induced vibrations can reach considerable amplitudes. Furthermore, the damping factor found with both theoretical and experimental analyses is quite low, thus not contributing in mitigating these effects. It seemed important to think about a damping system, and it was carried out a preliminary design to determine the optimal properties for such device, described in [22] and [20]. As the first natural modes have their maximum amplitude near the ends of the truss beams, the damping system was preliminary designed with 4 linear viscous dampers placed on the ground and anchored to these point via tensile strands. No added masses or stiffness were considered to prevent compression on these strands.

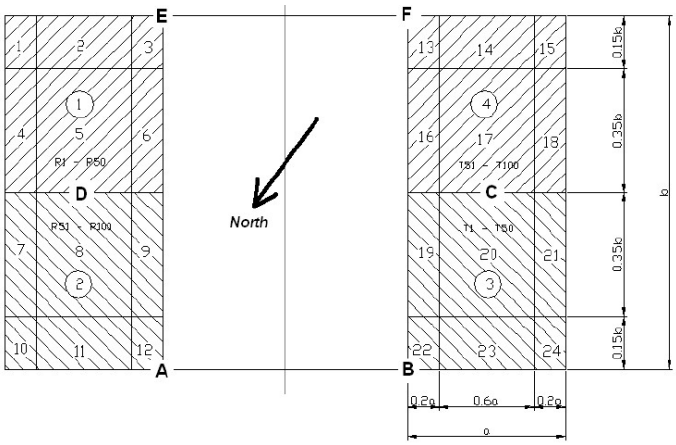

Figure 3.13: Reference scheme for the evaluation of structural response with and without external dampers. [22]

Comparison of the structural responses in absence and with external dampers

	$\xi_l = 1\% - \mathbf{C = 0\ kg_f\ s/m}$				$\xi_l = 1\% - \mathbf{C = 15000\ kg_f\ s/m}$				
	min [cm]	max [cm]	μ [cm]	σ [cm]	min [cm]	max [cm]	μ [cm]	σ [cm]	$V_{max,damp}$ [m/s]
A	-34	+32	+2	10.6	-11	+14	+2	3.8	≈ 0.27
B	-46	+39	-6	11.1	-24	+10	-6	4.9	≈ 0.37
E	-35	+48	+8	16.4	-13	+31	+8	6.0	≈ 0.41
F	-60	+26	-15	16.2	-38	+3	-15	6.8	≈ 0.34

Table 3.2: Comparison of the structural response (vertical displacements) with and without external dampers for various points. Source: [22]

Table 3.2 summarize the results published in [22] and [17] (making reference to the scheme in figure 3.13). An initial estimation was performed using an eigenvalue analysis of the damped system. The problem was defined considering the first 10 vibration modes

of the original structure and the added dampers, analyzing the resulting 4 complex modes. The dynamic behavior was also assessed through wind tunnel tests carried out over an aeroelastic model (whose results are reported in [13]), which was subjected to the pressure fields derived from RWDI wind tunnel tests [26]. The output data presented in [22], proved that with a damping coefficient of 150kNs/m an additional damping ratio between 4% and 10% could be obtained, producing a significant reduction of the oscillation amplitudes. However, a more accurate design process should consider other possible problems, as well as other possible damping technologies.

Chapter 4

Structural analysis of the cable-suspended roof

In this chapter we will present a simplified static analysis of the cable-suspended roof, whose results will be exploited in the definition of simplified models. At first, we will determine the external loads acting over the roof (although with some approximations), then we will perform a simplified static analysis of the suspended cables under permanent loads, calculating their geometry and tension. We will also evaluate their behaviour in case of loads or net span variations. Finally, we will also assess the effects of the elastic elongation.

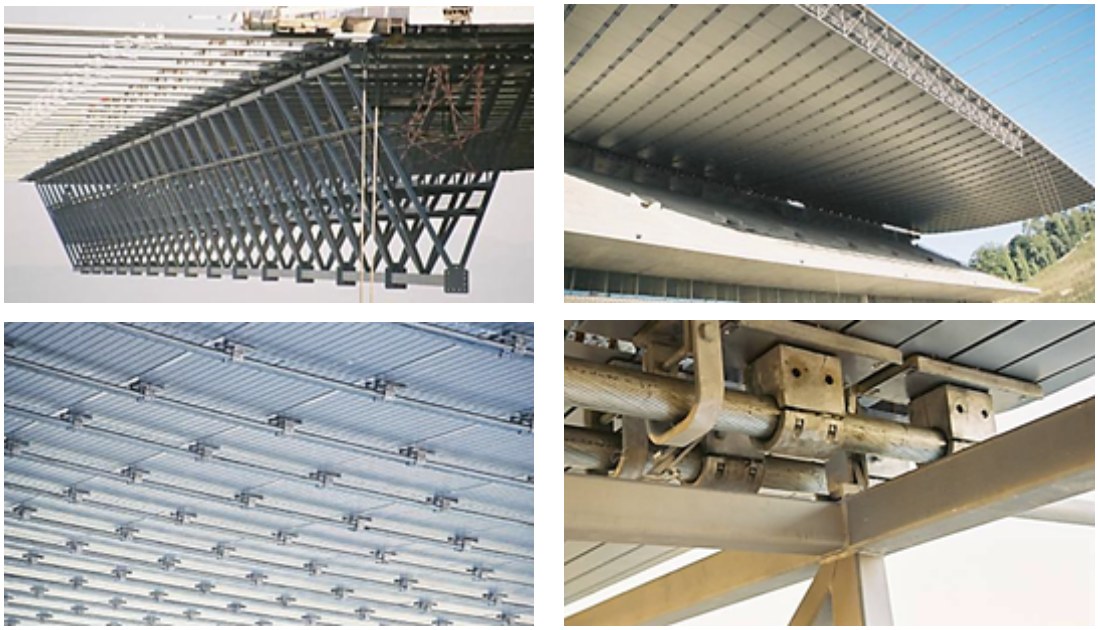

Figure 4.1: Details of the suspended roof (clockwise from above): the truss beam, the truss beam and the slabs during constructions, clamps between slabs and cables, clamps between slabs, cables and truss beam. Source: [16]

4.1 Load evaluation

In this section we will assess the loads acting over the roof. These will be calculated according to the Eurocode prescriptions ([30], [31], [32] and [33]) but, due to the peculiarities of this structure we will discuss some simplifying assumptions, when necessary. Permanent loads will be used to evaluate the tension of each cable at the State 0 and will also be considered to estimate the mobilized mass and the Seismic Limit State for the dynamic analysis with the simplified models. Live loads will be considered only to estimate the maximum tension of the cables under Ultimate Limit State and Serviceability Limit State.

4.1.1 Permanent structural loads

The structural loads over the roofing system are of two types: the loads of the cable itself and the loads of the concrete shell. Regarding the cable's weight we consider the data provided by the manufacturer Redaelli-Tecna: table 4.1 shows the weights of each cable depending on its diameter. It should be noted that the cables are paired, with a distance between one pair and the next of 3.75m, with a total number of 34 couples for 68 cables. The designs (provided by MJW Structures) show that the shell is made from reinforced concrete with a thickness of 25cm. As previously said, each pair of cables has a spacing of 3.75m. Thus, considering a unit weight of25 kN/m^3, the load per unit length of the shell over a single cable will result as:

$$q_{shell} = (25kN/m^3 \cdot 0.25m \cdot 3.75m)/2 = 11.719\, kN/m \tag{4.1}$$

Table 4.1: Technical data and performances of the roof cables according to the manufacturer. Source: [15] and www.Redaelli.com

Redaelli Tecna - full locked coil strands

Φ [mm]	A [mm^2]	MBL [kN]	N$_{rD}$ [kN]	Weight [kg/m]	Weight [kN/m]	EA [MN]
80	4679	7380	4922	35,9	0,352	785
82	4902	7720	5146	37,8	0,371	821
84	5127	8055	5370	39,6	0,388	856
86	5348	8385	5591	41,6	0,408	891

Finally, we evaluate the weight of the transversal truss beam. This value has been calculated from the designs provided by MJW-Structures, considering a specific weight for the steel of 78.5kN/m3. The truss beam has a own weight of roughly 2.781kN/m.

Considering a spacing of 3.75m between each pair of cables we obtain an equivalent concentrated load of:

$$P_{truss} = \frac{2.781kN/m \cdot 3.75m}{2} = 5.214\ kN \tag{4.2}$$

4.1.2 Permanent beared loads

In this case the permanent non-structural loads consist of:

- Weight of the lighting and sound systems over the transversal truss beam. Since it was not possible to define them precisely, they have been approximated with a linear uniformly distributed load of 0.5kN/m. Considering a spacing of 3.75m between each pair of cables, this results in a concentrated load over each cable of:

$$P_{systems} = \frac{0.5kN/m \cdot 3.75m}{2} = 0.938\ kN \tag{4.3}$$

- Weight of the maintenance walkway, located at the centre of the roof over the cables 33, 34, 35, 36. It is formed by 2 concrete curbs with a section of 20x20cm, and by other security devices whose load has not been considered. The loads of this walkway over each one of the aforementioned cables is:

$$q_{walkway} = \frac{0.2m \cdot 0.2m \cdot 25kN/m}{2} = 0.500\ kN/m \tag{4.4}$$

Figure 4.2: Detail of the rainwater discharge pod. Source: [15]

- Weight of the steel drains of the rainwater discharge system, shown in figure 4.2 This has a mass of 385kg and has been considered equally distributed between cables 65, 66, 67 and 68. The concentrated load due to this component, acting over each cable is of:

$$q_{drains} = \frac{385kg \cdot 9.81m/s^2 \cdot 10^{-3}}{4} = 0.944\ kN \tag{4.5}$$

4.1.3 Cat. H accidental overload

Due to its conformation, the roof is accessible only for inspection and maintenance purposes. According to the Eurocode prescriptions [30], the surface overload for cat. H is 0.5kN/m^2, thus resulting in a linear overload over each cable of:

$$q_{cat.\ K} = \frac{0.5kN/m^2 \cdot 3.75m}{2} = 0.938\ kN/m \tag{4.6}$$

4.1.4 Snow load

Although it is considered only for comparison purposes, and it will not affect the further seismic simulations, the roof variable slope snow has been approximated as a uniformly distributed load over the horizontal. According to the Eurocode prescriptions [31], the snow load can be calculated as:

$$s = \mu_i \cdot c_e \cdot c_t \cdot S_k \tag{4.7}$$

- μ_i is the roof shape coefficient. For a plane roof (or in any case with an angle of less than 30°) is equal to 0.8. The roof slope ranges from 0° to 16.57°, so this value can be assumed as constant over all its surface.

- c_e is the exposition coefficient. Considering the worst scenario, with a sheltered surface where snowdrifts could occur, is equal to 1.2.

- c_t is the thermal coefficient. Considering the worst scenario, where no melting occurs, is equal to 1.

- S_k is the characteristic value of the snow load at ground level and depends on the location and its altitude. The city of Braga, Portugal, is classified as Z2 zone, and has a snow basic load of 0.22kN/m^2.

Moreover, we also consider the possibility of an exceptional snowdrift, for which we must add another coefficient to the formula, c_{esi}. The suggested value for it by the Eurocode [31] is 2. Because of this, the snow load is equal to:

$$s = \mu_i \cdot c_e \cdot c_t \cdot c_{esi} \cdot S_k = 0.8 \cdot 1.2 \cdot 1 \cdot 2 \cdot 0.22 = 0.422\ kN/m^2 \tag{4.8}$$

Considering a spacing of 3.75m between each pair of cables, the equivalent linear uniformly distributed load is of:

$$q_{snow} = \frac{0.422kN/m^2 \cdot 3.75m}{2} = 0.792kN/m \tag{4.9}$$

4.1.5 Static equivalent wind pressure load

As stated in [20], due to the complex geometry of the roof and the structure itself, wind effects could not be defined through the codes prescriptions. Therefore, they have been studied extensively by the designers using FEM models and physical models on wind tunnels, so that the wind load distribution should not be assumed as a simple static uniform pressure. Still, wind effects will not be relevant for this thesis aim and will be used only for comparison purposes. Because of this we have tried to determine a uniform pressure distribution that could represent the worst possible scenario, by applying simplifying assumptions that always act with a safety margin.

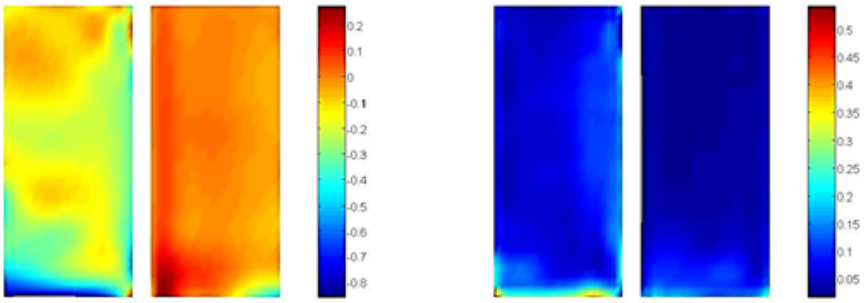

Figure 4.3: Mean value (on the left) and standard deviation (on the right) of the net pressure coefficients for a 270°N wind direction, that causes the highest values over the slab surfaces. Source: [20]

While the basic wind pressure depends on the location and its altitude and is assigned by the Eurocode [32], the net pressure coefficient has yet to be determined. As stated in [20], to do this the designers could not rely on the Eurocode prescriptions due to the peculiar roof shape. Therefore, we have considered the data published on that same article, showing the mean value and standard deviation of the net pressure coefficients for each point of the surface. These were determined with a POD (Proper Orthogonal Decomposition) of the data from a series of wind tunnel tests. To further simplify the analysis, we have considered only the cable that undergoes the worst pressure, and then we have applied the assessed value over the rest of the surface.

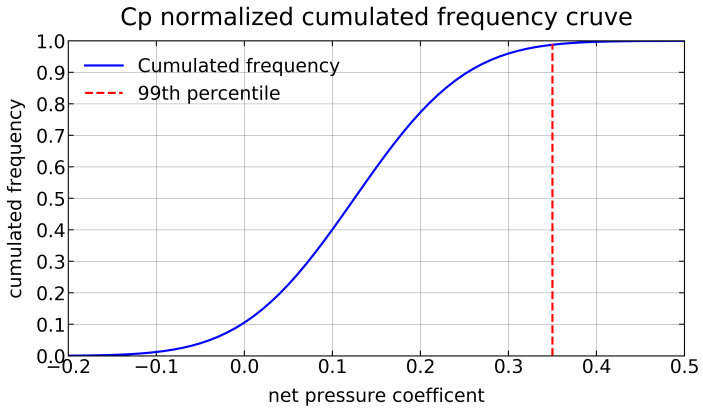

Figure 4.4: Estimated normal cumulative distribution of net c_p on the concrete shells (mean: 0.125, std. dev: 0.100), with the 99^{th} percentile marked on the red line. Source: Excel, own elaboration

From figure 4.3 we have calculated the mean value of the c_p's and their standard deviation on the border cable, considering different points along it and obtaining a mean value of 0.125 and a standard deviation of 0.1. Supposing a normal distribution (as it is done in reference [20]), we can obtain the pressure coefficient c_p that corresponds to the 99^{th} percentile, thus including most of the worst-case scenarios that the cable might undergo. From this procedure, whose result is shown in figure 4.4, we got c_p=0.35. The wind equivalent uniform load can be estimated as:

$$w = q_p\left(z\right) \cdot c_p \tag{4.10}$$

Where:

- $q_p\left(z\right)$ stands for the wind pressure at the roof level, and can be determined as:

$$q_p\left(z\right) = q_b \cdot c_e(z) \tag{4.11}$$

  Where q_b is the basic wind load for the location at ground level. For the city of Braga, Portugal, this value is equal to 0.46kN/m^2. $c_e(z)$ is the exposition coefficient: due to the difficulty in evaluating it, we consider the worst possible value, which corresponds to 4. Therefore:

$$q_p\left(z\right) = \frac{0.46kN}{m^2} \cdot 4 = 1.84kN/m^2 \tag{4.12}$$

- As previously said, c_p=0.35.

We obtain:

$$w = \frac{1.84kN}{m^2} \cdot 0.35 = 0.64kN/m^2 \tag{4.13}$$

Considering a spacing of 3.75m between each pair of cables, we obtain an equivalent uniformly distributed load over each cable of:

$$q_{wind} = \frac{0.64kN/m^2 \cdot 3.75m}{2} = 1.2\ kN/m \tag{4.14}$$

4.1.6 Thermal effects over the cables

In this section we will present some considerations about the thermal effects on cables. As stated in [33], the thermal distribution in a building element can be decomposed into essential components:

1. Uniform thermal component.

2. Uniformly linear thermal variation, defined in the two components along the vertical and horizontal axis.

3. Non-linear thermal variation.

Due to the cable reduced section, these first two contributions are negligible. Considering this specific case, we can identify two possible outcomes:

- A uniform positive variation of temperature would produce a cable elongation and an increase of the maximum sag. There would be a decrease of the horizontal tension component, therefore this situation is not useful for the cable ULS verification.

- A uniform temperature decrease would instead produce a shortening, with a reduction of the maximum sag. This would cause an increase in the horizontal tension component, and it is therefore the situation that we are interested in investigating.

Referring to the requirements of [33], the uniform temperature variation can be defined as:

$$\Delta T_U = T - T_0 \tag{4.15}$$

Where T_0 is the temperature of the cable at the time of application of the restrains. Since we do not have information about, we apply the suggested value of 10°C. T is the average temperature of a structural element. Since the cable is exposed to atmospheric conditions, we can assume T as T_{out}, that is the temperature of the outer environment. Referring to table 5.2 of [33], this is assessed for the two limit situations:

- On winter we can assume:

$$T_{out} = T_{min}$$

  Where T_{min} is the value of minimum air temperature with 50 year return period. This value was obtained from the Portuguese legislation, and is assumed as -16°C.

- On summer we refer to the case of a light colored surface facing south-west. In this case $T_{out} = T_{max} + T_4$. For T_4 we considered the recommended value, that is 30°C, while T_{max} was assessed as T_{min} and is equal to 41°C.

Consequently, we define the two limit situations:

$$\Delta T_U = \begin{cases} 71°C & \text{in summer} \\ -26°C & \text{in winter} \end{cases} \tag{4.16}$$

For the sake of synthesis, we opted for an analysis on a simple 2D finite element model of the cable with SAP2000 defined as done for the simplified models B1, B2 and C in section 6.1.3. The positive thermal variation causes roughly a 120kN decrease of the cable maximum tension (which, as already mentioned, is not relevant for the verification). The negative thermal variation leads to a 34kN increase of the cable maximum tension: that is around 1% of the 3000kN maximum cable tension under permanent loads. Consequently, when compared to other variable loads, the thermal action is not relevant in the ULS verification. Therefore, it was decided to neglect it in the load combinations.

4.1.7 State 0, ULS and SLS combinations for the roof

Considering the Eurocode prescriptions [30], we can determine the loads related to each section of the cable according to Ultimate Limit State (ULS), Serviceability Limit State (SLS), Seismic Limit State that maximize the tension over the cables. We have reported only the combination for irreversible SLS, as the others (reversible and long term) gave load values close to the State 0 ones, for which the difference in terms of cable tension and elongation is not appreciable from the graphs proposed. The generic expressions for these combinations are:

- Ultimate Limit State:

$$\gamma_{G1} \cdot G_1 + \gamma_{G2} \cdot G_2 + \gamma_p \cdot P + \gamma_{Q1} \cdot Q_1 + \sum_i \gamma_{Qi} \cdot \psi_{0i} \cdot Q_i + \dots \tag{4.17}$$

- Serviceability Limit State - irreversible:

$$G_1 + G_2 + P + Q_1 + \sum_i \psi_{0i} \cdot Q_i + \dots \tag{4.18}$$

- Seismic Limit State:

$$E + G_1 + G_2 + P + \sum_i \psi_{2i} \cdot Q_i + \dots \tag{4.19}$$

Where G_1 are the permanent structural actions, G_2 are the permanent non-structural actions, Q_i are the accidental loads, γ_i are the partial coefficients and ψ_i are the coefficients for concomitant actions. In additions to these we will also consider the combinations that defines the State 0, that defines the basic tension of the cable under permanent loads:

- State "0" - permanent loads:

$$G_1 + G_2 + P \tag{4.20}$$

The partial coefficients applied for this case are summarized in table 4.2, while the coefficients for concomitant actions are resumed in table 4.3.

Table 4.2: Partial coefficients for load combinations, according to Eurocode [30]

Partial coefficients

load type	action	coef. id	EQU	A1	A2
Permanent load	fav.	γ_{G1}	0,90	1,00	1,00
	unfav.		1,10	1,35	1,00
Non-structural permanent load	fav.	γ_{G2}	0,80	0,80	0,80
	unfav.		1,50	1,50	1,35
Variable load	fav.	γ_{Q}	0,00	0,00	0,00
	unfav.		1,50	1,50	1,35

Table 4.3: Coefficients for concomitant variable actions, according to Eurocode [30]

Coefficents for concomitant actions

load type	id.	Ψ_{0i}	Ψ_{1i}	Ψ_{2i}
Cat. H - inspection and maintenance	Q_H	0,0	0,0	0,0
Cat. C - crowd	Q_C	0,7	0,7	0,6
Wind	Q_W	0,6	0,2	0,0
Thermal variations	$Q_{term.}$	0,6	0,5	0,0
Snow under 1000m	Q_S	0,5	0,2	0,0

We must also consider that the first and last pair of cables are submitted only to half of the loads, since they have only half of the spacing. In the end, the combinations that provides the worst situation for the cables are the ones that maximize the applied loads, thus maximizing their tension.The maximum loads determined are directly shown below in table 4.4, without showing the whole calculation and choice process for each possible combination.

Table 4.4: Actions resulting from the application of load combinations. Source: Excel, own elaboration

Applied load combinations - part. 1

comb.	load	cable id. 1-2	3-...-8	9-...-24	25-...-32	33-...-36
State "0"	q_c [kN/m]	0,408	0,408	0,388	0,371	0,371
	$q_{l,sx}$ [kN/m]	5,860	11,719	11,719	11,719	12,219
	$q_{l,dx}$ [kN/m]	5,860	11,719	11,719	11,719	12,219
	P_t [kN]	3,076	6,152	6,152	6,152	6,152
SLS	q_c [kN/m]	0,408	0,408	0,388	0,371	0,371
	$q_{l,sx}$ [kN/m]	6,887	13,773	13,773	13,773	14,273
	$q_{l,dx}$ [kN/m]	6,887	13,773	13,773	13,773	14,273
	P_t [kN]	3,076	6,152	6,152	6,152	6,152
ULS	q_c [kN/m]	0,551	0,551	0,524	0,501	0,501
	$q_{l,sx}$ [kN/m]	10,200	20,399	20,399	20,399	21,149
	$q_{l,dx}$ [kN/m]	10,200	20,399	20,399	20,399	21,149
	P_t [kN]	4,223	8,446	8,446	8,446	8,446

Applied load combinations - part. 2

comb.	load	cable id. 33-...-36	37-...-42	43-...-64	65-66	67-68
State "0"	q_c [kN/m]	0,371	0,371	0,352	0,352	0,352
	$q_{l,sx}$ [kN/m]	12,219	11,719	11,719	11,719	5,860
	$q_{l,dx}$ [kN/m]	12,219	11,719	11,719	11,719	5,860
	P_t [kN]	6,152	6,152	6,152	7,096	4,020
SLS	q_c [kN/m]	0,371	0,371	0,352	0,352	0,352
	$q_{l,sx}$ [kN/m]	14,273	13,773	13,773	13,773	6,887
	$q_{l,dx}$ [kN/m]	14,273	13,773	13,773	13,773	6,887
	P_t [kN]	6,152	6,152	6,152	7,096	4,020
ULS	q_c [kN/m]	0,501	0,501	0,475	0,475	0,475
	$q_{l,sx}$ [kN/m]	21,149	20,399	20,399	20,399	10,200
	$q_{l,dx}$ [kN/m]	21,149	20,399	20,399	20,399	10,200
	P_t [kN]	8,446	8,446	8,446	9,862	5,639

The coefficients for concomitant actions for a seismic combination related to the variable loads are zero for all the variable loads acting on the roof, therefore the seismic combination includes only the permanent loads, as in the State 0 combination. For the sake of brevity we summarized on table only the results related to State 0. Moreover, the Eurocode [30] also assigns the masses that should be considered doing the seismic analysis, according to the expression:

$$G_1 + G_2 + \sum_i \psi_{2i} \cdot Q_i + \dots \tag{4.21}$$

The loads that have a favourable effect on the verification must be omitted. In this case thermal action, wind, snow and maintenance loads are not considered since their coefficients for concomitant actions ψ_{2i} is zero. In the end we consider only permanent loads, which are the same that are applied in the State 0. The mass distribution will be determined specifically for each model, according to the accuracy degree to be obtained, therefore this topic will be exposed in detail later.

4.2 Static analysis of the roof

In this section we will determine analytically the geometry of the cable for different situations: State 0 (permanent loads only), ULS, SLS and for a net span increase. To simplify the analysis we will apply the parabolic approximation, and we will determine the solution to the static problem through an iterative process defined on different Excel sheets. For each case considered we will discuss the analytical solution, and then we will briefly present the results obtained using some graphs, while the tables with all the data are shown in annexes C and D.

4.2.1 Resolution of the static problem with simplified formulation

In the real case the roof is constituted by a series of cables, on which 2 concrete shells are placed, consisting of prefabricated slabs connected within each other by hinges. These sections rest on the cable by means of sleeves, so that the static action transmitted translates into a series of concentrated loads at the support points. The exact geometry of the cable is a series of catenary curves, defined between one sleeve and the next. The same goes for the truss. however, it is possible to simplify this discussion by means of some assumptions:

- The action of the transversal truss acts as a concentrated load placed at the

innermost edge of the concrete shell.

- The slabs are treated as a distributed load acting along the length of the cable sections over which they are placed.

- We will simplify the analysis considering only a 2D model, and so we will consider each cable separately.

Therefore, we can define the static scheme shown in figure 4.5. Since the cable has a symmetric geometry, we show only one half of it. Under these assumptions, the geometry of the cable is that of 3 successive catenary curves. However, the ratio between the maximum sag and the total span is between 0.035 and 0.045: in this case we can approximate the catenary with a parabolic curve, thus simplifying the analysis. Furthermore, by considering the weight of the shell and the cable acting along the net span rather than along the length of the cable itself we introduce an error of around 1.25% in the resultant vertical force, which is negligible.

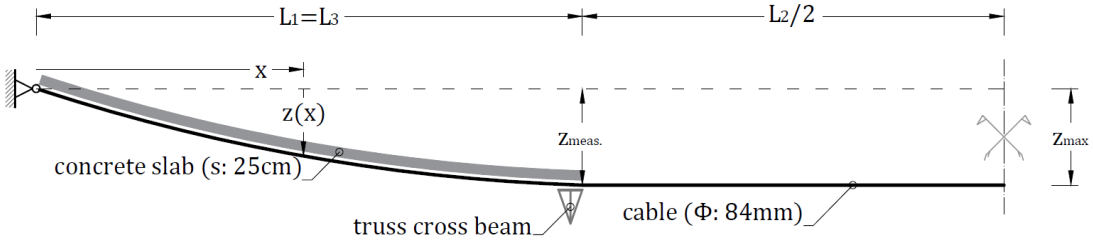

Figure 4.5: Reference simplified scheme for the cable geometric configuration. Source: AutoCAD, own elaboration

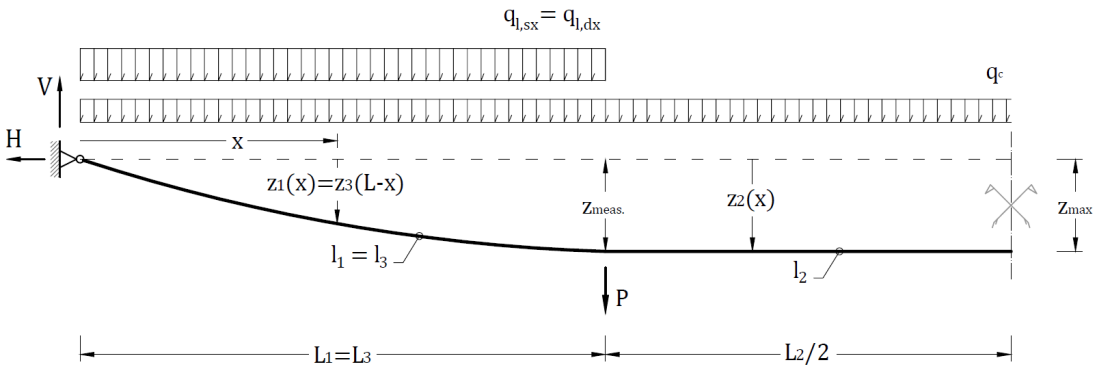

Figure 4.6: Reference static scheme for the single cable, with the loads acting over it. Source: AutoCAD, own elaboration

As previously said, with the parabolic approximation the distributed loads are considered acting over the span, thus defining the static scheme shown in figure 4.6, that will be taken as reference. Because of this the cable geometry function follows the

bending moment function, so that at each point the tension is directed along the cable and the resultant moment is zero.

We can also apply the superposition principle and determine the cable geometry by considering separately each load. Each load contribution can be analysed separately with the approach shown in chapter 2 at point 2.1.5.3:

- The contribution of the cable's own weight, which is approximated as a distributed load acting over the whole span. The resulting geometry is:

$$z_c\left(x\right) = \frac{q_c x}{2H} x\left(L - x\right). \tag{4.22}$$

- The contribution of each one of the concrete slabs, which are approximated as distributed loads acting over part of the cable span. The resulting geometry is defined by two equations for each load, for the left shell:

$$z_{l,sx}(x) = \begin{cases} \frac{q_{l,sx} x}{2H} x\left(L - x\right) - \frac{q_{l,sx} L}{2H} x\left(1 - n\right)^2; & \text{for: } x \in [0;\ nL] \\ \frac{q_{l,sx} L^2}{2H} n^2 \left(1 - \frac{x}{L}\right); & \text{for: } x \in [nL;\ L] \end{cases} \tag{4.23}$$

While for the right shell:

$$z_{l,dx}(x) = \begin{cases} \frac{q_{l,dx} L^2}{2H} n^2 \frac{x}{L}; & \text{for: } x \in [0; (1-n)L] \\ \frac{x^2 q_{l,dx}}{2H}\left(L - x\right) - \frac{q_{l,dx} L}{2H}(L - x)\left(1 - n\right)^2; & \text{for: } x \in [(1-n)L;\ L] \end{cases} \tag{4.24}$$

- The contribution of the two concentrated loads due to the transversal beams. In this case the geometry is a simple polygonal defined by the 3 equations:

$$z_p(x) = \begin{cases} \frac{P}{H} x; & \text{for: } x \in [0;\ nL] \\ \frac{P}{H} nL; & \text{for: } x \in [nL;\ (1-n)\,L] \\ \frac{P}{H}\left(L - x\right); & \text{for: } x \in [(1-n)\,L;\ L] \end{cases} \tag{4.25}$$

where L is the cable span, H is the horizontal tension, q_c is the distributed load over all the cable, $q_{l,sx}$ and $q_{l,dx}$ are the distributed loads over part of the cable, P is the concentrated load. The resulting geometry is obtained by combining these equations

for each part of the cable:

$$z(x) = \begin{cases} z_1(x); & \text{for: } x \in [0;\ nL] \\ z_2(x); & \text{for: } x \in [nL;\ (1-n)L \\ z_3(x); & \text{for: } x \in [(1-n)L;\ L] \end{cases} \tag{4.26}$$

where:

$$\begin{aligned} z_1(x) &= \frac{q_c x}{2H}(L-x) + \frac{q_{l,sx} x}{2H}(L-x) - \frac{q_{l,sx} L}{2H} x (1-n)^2 + \frac{q_{l,dx} L^2}{2H} n^2 \frac{x}{L} + \frac{P}{H} x. \\ z_2(x) &= \frac{q_c x}{2H}(L-x) + q_{l,sx} L^2 2H n^2 \left(1 - \frac{x}{L}\right) + \frac{q_{l,dx} L^2}{2H} n^2 \frac{x}{L} + \frac{P}{H} nL. \\ z_3(x) &= \frac{q_c x}{2H}(L-x) + \frac{q_{l,sx} L^2}{2H} n^2 \left(1 - \frac{x}{L}\right) + \frac{q_{l,dx} x}{2H}(L-x) - \\ &\quad - \frac{q_{l,dx} L}{2H}(L-x)(1-n)^2 + \frac{P}{H}(L-x). \end{aligned}$$

The unknown term of this equation is represented by the horizontal tension H, while both the deformed geometry and the external loads are known. From these we can also calculate the vertical reactions as:

$$\begin{aligned} V_I &= \frac{q_c L}{2} + \frac{q_{l,sx} n^2 L}{2} + q_{l,dx} nL \left(1 - \frac{n}{2}\right) + P. \\ V_{II} &= \frac{q_c L}{2} + q_{l,sx} nL \left(1 - \frac{n}{2}\right) + \frac{q_{l,dx} n^2 L}{2} + P. \end{aligned} \tag{4.27}$$

Since the cable geometry has been approximated as a succession of 3 parabolas, its length can be calculated as the length of these curves. The formula can be defined by considering an infinitesimal portion ds of the cable for which:

$$ds = \sqrt{dx^2 + dz^2} = \sqrt{1 + \frac{dz^2}{dx^2}} \cdot dx = \sqrt{1 + z'(x)^2} \cdot dx. \tag{4.28}$$

where dx and dz are the projections of ds along their respective axes. The length can be calculated by solving the following integral for the 3 segments of the cable:

$$\begin{aligned} l_{tot} &= l_1 + l_2 + l_3 = \\ &= \int_0^{nL} \sqrt{1 + z_1'(x)^2}\, dx + \int_{nL}^{(1-n)L} \sqrt{1 + z_2'(x)^2}\, dx + \int_{(1-n)L}^{L} \sqrt{1 + z_3'(x)^2}\, dx. \end{aligned} \tag{4.29}$$

The generic expression for the elastic deformation due to an axial solicitation is:

$$\varepsilon(x) = \frac{N(x)}{EA} = \frac{\sqrt{H^2 + V^2(x)}}{EA}. \tag{4.30}$$

However, in this case the solution is not immediate since $V(x)$ varies along the cable, and so does the tension $N(x)$. The elastic elongation is therefore determined by integrating the deformation formula.

$$\Delta l_{el} = \int_0^l \varepsilon(x)\, dx = \int_0^l \frac{N(x)}{EA} dx = \int_0^l \frac{\sqrt{H^2 + V^2(x)}}{EA} dx. \tag{4.31}$$

Since the resulting relation would be too complicated, and since the geometry of the cable in this case is calculated by discretizing the parabolic curve, we can approximate $\varepsilon(x)$ using the average value of $N(x)$ calculated at each point.

$$\Delta l_{el} = \int_0^l \frac{N(x)}{EA} dx \cong \int_0^l \frac{\widetilde{N}}{EA} dx = \frac{\widetilde{N}}{EA} l. \tag{4.32}$$

where:

$$\widetilde{N} = \frac{\sum_{i=1}^{n} N(x_i)}{n}. \tag{4.33}$$

Given the deformed geometry and given the elastic elongation it is then possible to evaluate the cable initial length, before it was subjected to State 0 loads.

$$l_0 = l_{tot} - \Delta l_{el} = l_{tot} \left(1 - \frac{\widetilde{N}}{EA}\right). \tag{4.34}$$

4.2.2 Analysis of State "0"

In this section we will determine the tension that undergoes each cable under permanent loads (the so called State 0). Since the external loads are and the geometric configuration are already known, the only unknown is the horizontal tension H. As the equations defined in the previous section cannot be solved explicitly, the applied horizontal tension has been determined using an iterative process on an Excel spreadsheet.

Table 4.5: Horizontal length of each section of the cable. Source: Excel, own elaboration

Total net span of the cable and of each portion				
L_{TOT} [m]	L_1 [m]	L_2 [m]	L_3 [m]	n
202	57	88	57	0,282

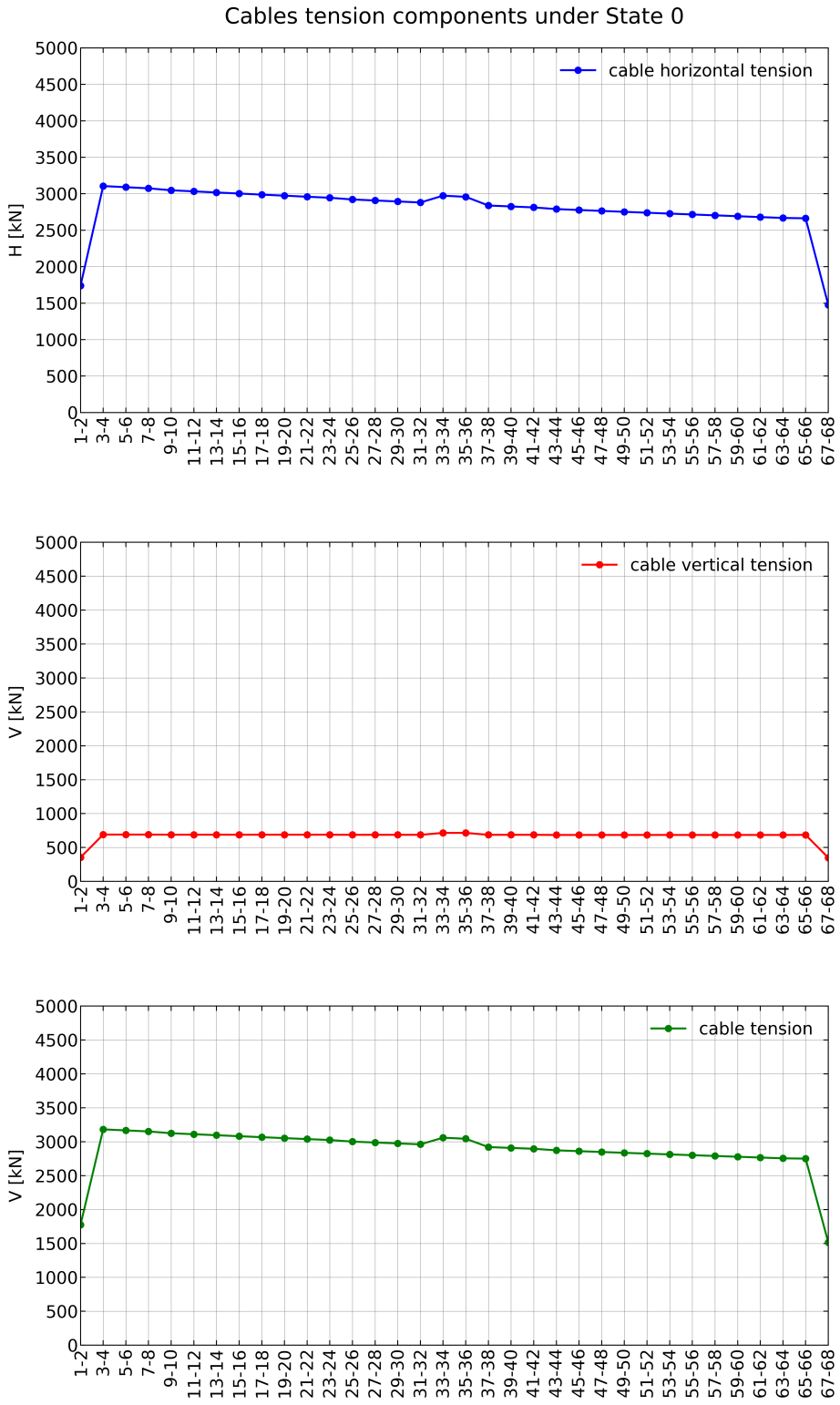

Figure 4.7: (from above) Horizontal, vertical and resultant restraint reactions for each pair of cables under State "0" conditions. Source: Excel, own elaboration

The equations for $z_i(x)$ have been solved by assigning the values of the applied loads for the State 0 (summarized in table 4.4), the net span (table 4.5), and by setting

an initial value of H. The vertical displacement at a predetermined point is then calculated and compared with the measured value from the provided designs. H is then assessed with the "goal seek" Excel function, as the value that minimizes the difference between calculated and measured sag. Once the static problem has been solved, the deformed geometry is then determined by calculating the vertical displacement at defined intervals. The results are summarized in the table attached on the annex, while the restrain reactions for each pair of cable are briefly shown in graphs 4.7. Because of the transversal slope the maximum sag is different for each pair: this results in a decreasing cable tension along the roof. Without considering the first and last pair of cables and the cables that bear the walkway, the horizontal tension ranges between 3105kN (on cables 3 and 4) and 2663kN (on cables 65 and 66).

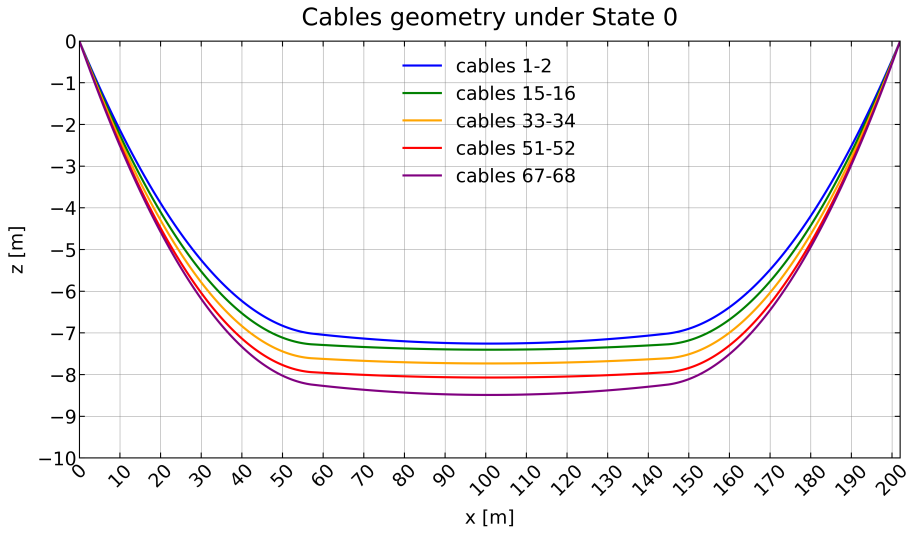

Figure 4.8: Geometric configuration of some cables with the parabolic curve approximation. Vertical and horizontal axes are not equally scaled, to show the increasing sag of each pair. Source: Excel, own elaboration

Once the horizontal tension is known, the geometric configuration of each cable is defined by calculating $z_i(x)$ for intervals of 0,5m. The geometry is approximated with 3 successive parabolic curves. The first one and the last one (which are symmetrical, and above which lies the concrete slab) have a maximum sag between 1.65m and 1.99m. The central section is almost horizontal, as it has a maximum sag between 0.13m and 0.19m, compared to a span of 88m: this happens because of the high tension compared to the low applied load (which corresponds to the own cable's weight).

The length of each cable is determined by approximating the integral with the Cavalieri-Simpson's method. This rule provides for the subdivision of the integration interval into sub-intervals and the substitution of the integrand function by means of

quadratic polynomials. In our case:

$$l_j = \int_0^{L_j} \sqrt{1 + z_j'(x)^2}dx = \int_0^{L_j} f_j(x)dx \quad \text{where: } f_j(x_i) = \sqrt{1 + z_j'(x_i)^2} = y_i. \tag{4.35}$$

The Cavalieri-Simpson rule is defined by the formula:

$$l_j = \int_0^{L_j} \sqrt{1 + z_j'(x)^2}dx \cong \frac{\Delta x}{3}\left(y_0 + 4y_1 + 2y_2 + \ldots + 2y_{n-2} + 4y_{n-1} + y_n\right). \tag{4.36}$$

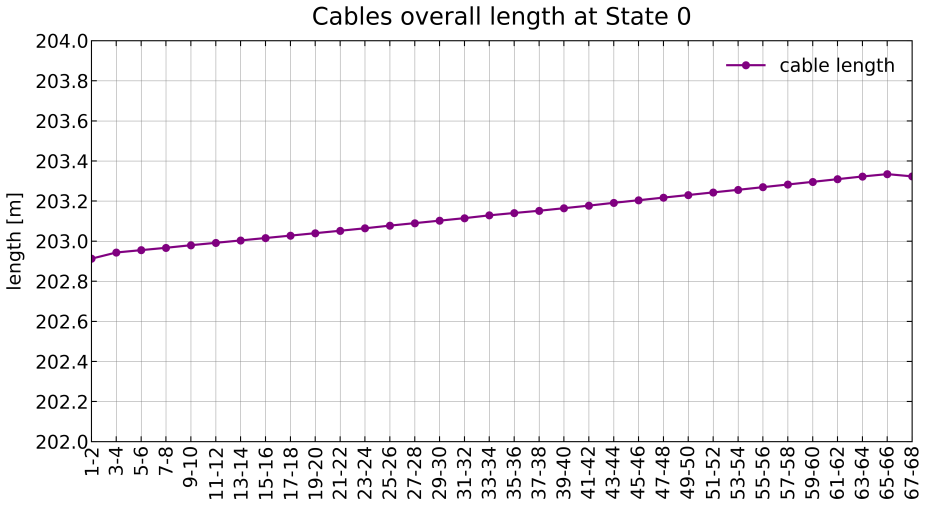

Figure 4.9: Deformed length of cables under permanent loads. Source: Excel, own design

The numerical method has been applied with steps of $\Delta x = 10\ cm$. The results are resumed in figure 4.9, that shows how the transversal slope is obtained by varying the length of the cables. The deformation under permanent loads (the State 0) is obtained by considering the mean value of the tension along each cable (in this case $N(x)$ has been calculated every 0.5m). The cable elongation is therefore calculated as:

$$\Delta l_{el} = \frac{\widetilde{N}}{EA}l; \quad \text{where: } \widetilde{N} = \frac{\sum_{i=1}^{n} N(x_i)}{n}. \tag{4.37}$$

The initial length of the unstressed cable can be determined from these values as:

$$l_{0,tot} = l_{tot} - \Delta l_{el}. \tag{4.38}$$

The cable's length has been adjusted several times during the construction process to meet the desired geometry of the roof and was fixed only at the end. Because of this these are only gross estimations and the exact values are not reported here.

4.2.3 Variations due to a load increase

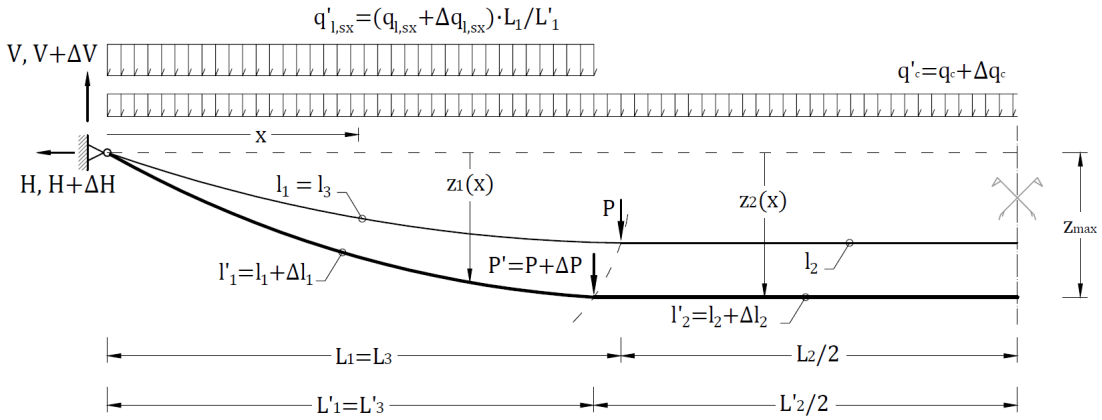

Figure 4.10: Reference static scheme for the cable subjected to a load increase. Source: AutoCAD, own elaboration

Following the determination of the State 0 a new problem comes out, as we need to define how the tension of each cable will change due to a load variation. This will occur when applying the various load combinations selected for each limit state, as they also comprehend variable loads such as wind and snow. To find a solution to this problem we have applied equation 4.39, for which the sum of the initial cable length and the elongation produced by a load increase must be equal to the total cable length calculated for the assigned load increment.

$$l_{tot} + \Delta l_{el} = l'_{tot} \tag{4.39}$$

where l_{tot} is the initial length of the cable. In this case we take as a reference the length at the State "0" which has already been determined in the previous section, Δl_{el} is the elastic elongation produced by the load increment. As previously said, this term is equal to:

$$\Delta l_{el} = \int_0^l \varepsilon\,(x)\,dx = \int_0^l \frac{\Delta N\,(x)}{EA} dx \tag{4.40}$$

However, since the integral could be quite complicated to be solved we consider. as before, the mean value of the tension variation, thus simplifying the problem:

$$\Delta l_{el} = \int_0^l \frac{\Delta N\,(x)}{EA} dx \cong \int_0^l \frac{\Delta \widetilde{N}}{EA} dx = \frac{\Delta \widetilde{N}}{EA} l. \tag{4.41}$$

where $\Delta \widetilde{N}$ is the mean value of the tension variation between the State "0" and the considered limit state.

This term can be developed as:

$$\Delta\widetilde{N} = \frac{\sum_{i=1}^{n} \Delta N\left(x_i\right)}{n} \tag{4.42}$$

At each point the tension variation is equal to:

$$\Delta N\left(x_i\right) = N'\left(x_i\right) - N\left(x_i\right) = \sqrt{H'^2 + V'^2\left(x_i\right)} - \sqrt{H^2 + V^2\left(x_i\right)} \tag{4.43}$$

The term $N\left(x_i\right)$ is already known from the determination of the State "0", while the term $N'\left(x_i\right)$ represents the increased cable tension and can be expressed as a function of the horizontal and vertical component of the tension variation:

$$N'\left(x_i\right) = \sqrt{H'^2 + V'^2\left(x_i\right)} = \sqrt{\left(H + \Delta H\right)^2 + \left(V\left(x_i\right) + \Delta V\left(x_i\right)\right)^2} \tag{4.44}$$

The term $\Delta V\left(x_i\right)$ is known for each point (hence also $V'\left(x_i\right)$), as it related to the load variation, while ΔH is the only unknown of the problem. As seen in section 4.2.1, the cable can be divided into 3 different sections with the shape of a parabolic curve. Because of this the elongation term can be expressed as:

$$\begin{aligned}
\Delta l_{el} &= \Delta l_{el,1} + \Delta l_{el,2} + \Delta l_{el,3} = \\
&= \int_0^{l_1} \frac{\Delta N_1\left(x\right)}{EA} dx + \int_0^{l_2} \frac{\Delta N_2\left(x\right)}{EA} dx + \int_0^{l_3} \frac{\Delta N_3\left(x\right)}{EA} dx = \\
&\cong \int_0^{l_1} \frac{\Delta\widetilde{N_1}}{EA} dx + \int_0^{l_2} \frac{\Delta\widetilde{N_2}}{EA} dx + \int_0^{l_3} \frac{\Delta\widetilde{N_3}}{EA} dx = \\
&= \frac{\Delta\widetilde{N_1}}{EA} l_1 + \frac{\Delta\widetilde{N_2}}{EA} l_2 + \frac{\Delta\widetilde{N_3}}{EA} l_3
\end{aligned} \tag{4.45}$$

where $\Delta\widetilde{N_1}$ and $\Delta\widetilde{N_2}$ are the mean values of the tension variation along their respective sections, that can be calculated as previously shown:

$$\Delta\widetilde{N_j} = \frac{\sum_{i=1}^{m<n} \Delta N_j\left(x_i\right)}{m}$$

$$\begin{aligned}
\Delta N_j\left(x_i\right) &= N'_j\left(x_i\right) - N_j\left(x_i\right) = \\
&= \sqrt{H'^2 + V'^2_j\left(x_i\right)} - \sqrt{H^2 + V^2_j\left(x_i\right)} = \\
&= \sqrt{\left(H + \Delta H\right)^2 + \left(V_j\left(x_i\right) + \Delta V_j\left(x_i\right)\right)^2} - \sqrt{H^2 + V^2_j\left(x_i\right)}
\end{aligned} \tag{4.46}$$

l'_{tot} is the total cable length under the increased loads, expressed as a function of the horizontal tension $H\prime$, and therefore as a function of the horizontal tension variation

ΔH. This term can be calculated as the length of a parabola by solving the integral:

$$l = \int ds = \int_0^L \sqrt{1 + \left(\frac{\partial z_(x)}{\partial x}\right)^2} dx. \tag{4.47}$$

This can be decomposed for each section of the cable:

$$\begin{aligned} l_{tot} &= l_1 + l_2 + l_3 = \\ &= \int_0^{L\prime_1} \sqrt{1 + \left(\frac{\partial z_1(x)}{\partial x}\right)^2} dx + \int_{L'_1}^{L'_1+L'_2} \sqrt{1 + \left(\frac{\partial z_z(x)}{\partial x}\right)^2} dx + \\ &+ \int_{L'_1+L'_2}^{L} \sqrt{1 + \left(\frac{\partial z_3(x)}{\partial x}\right)^2} dx \end{aligned} \tag{4.48}$$

where the terms $\partial z_1(x)/\partial x$, $\partial z_2(x)/\partial x$ and $\partial z_3(x)/\partial x$ can be obtained from the expression of the parabolic geometry of the cable. Regarding these terms it is necessary to make a brief digression. The concrete shells are made up of separate sections, free to rotate reciprocally and placed on the cables adapting to their geometry. They are free to slide along it, and the only constraint to the horizontal translation is the upper linking point, near the linking point of the cable itself. On the other hand, the transverse trusses are hung on the cable in two places near the inner edges of the shells. They too can slide along the cable and are therefore attached to the slabs immediately above. In this way the relative displacement between shells and truss beams is prevented. For this reason, the applied loads follow the variations in the cable geometry, with a redistribution of their action, without however corresponding the same elastic elongation. Consequently, a load increase would cause a variation of the cable configuration and therefore a variation in its geometry. However, this aspect is negligible if compared to the approximation level assumed up to now for both load configuration and cable geometry. It is therefore considered that the geometry of the cable does not change following load variations, thus simplifying the discussion. The cable is still defined with the same successive parabolic curves; therefore, the formula has the same structure of the one seen initially.

$$
\begin{aligned}
z_1(x) &= \frac{q\prime_c x}{2H\prime}(L-x) + \frac{q\prime_{l,sx} x}{2H\prime}(L-x) - \frac{q\prime_{l,sx} L}{2H\prime} x\,(1-n\prime)^2 + \frac{q\prime_{l,dx} L^2}{2H\prime} n\prime^2 \frac{x}{L} + \frac{P\prime}{H\prime} x \\
z_2(x) &= \frac{q\prime_c x}{2H\prime}(L-x) + \frac{q'_{l,sx} L^2}{2H'} n'^2 \left(1-\frac{x}{L}\right) + \frac{q'_{l,dx} L^2}{2H'} n'^2 \frac{x}{L} + \frac{P'}{H'} n\prime L \\
z_3(x) &= \frac{q\prime_c x}{2H\prime}(L-x) + \frac{q\prime_{l,sx} L^2}{2H\prime} n\prime^2 \left(1-\frac{x}{L}\right) + \frac{q\prime_{l,dx} x}{2H\prime}(L-x) - \\
&\quad - \frac{q\prime_{l,dx} L}{2H\prime}(L-x)(1-n\prime)^2 + \frac{P\prime}{H\prime}(L-x)
\end{aligned}
\tag{4.49}
$$

The terms that differ from the State "0" are the increased loads (q'_c, $q'_{l,sx}$, $q'_{l,dx}$ and P'), the increased horizontal tension H', that can be expressed as $H' = H + \Delta H$, and the non-dimensional parameter n'. By differentiating these equations, we obtain:

$$
\begin{aligned}
\frac{\partial z_1(x)}{\partial x} &= \frac{q\prime_c}{2H\prime}(L-2x) + \frac{q\prime_{l,sx}}{2H\prime}(L-2x) - \frac{q\prime_{l,sx} L}{2H\prime}(1-n\prime)^2 + \frac{q\prime_{l,dx} L}{2H\prime} n\prime^2 + \frac{P\prime}{H\prime} \\
\frac{\partial z_2(x)}{\partial x} &= \frac{q\prime_c}{2H\prime}(L-2x) + \frac{q\prime_{l,sx} L^2}{2H\prime} n\prime^2 \left(-\frac{1}{L}\right) + \frac{q\prime_{l,dx} L}{2H\prime} n\prime^2 \\
\frac{\partial z_3(x)}{\partial x} &= \frac{q\prime_c}{2H\prime}(L-2x) + \frac{q\prime_{l,sx} L^2}{2H\prime} n\prime^2 \left(-\frac{1}{L}\right) + \frac{q\prime_{l,dx}}{2H\prime}(L-2x) - \\
&\quad - \frac{q\prime_{l,dx} L}{2H\prime}(-1)(1-n\prime)^2 + \frac{P\prime}{H\prime}(-1)
\end{aligned}
\tag{4.50}
$$

Note also that the integration limits of the integral formula for l_{tot} have not been specified. This is because they have changed due to the elastic elongation produced by the load variation. In fact, now the length of each section is changed due to the elastic elongation, and so does also their projection over the span.

$$
L = L'_1 + L'_2 + L'_3 \tag{4.51}
$$

Where the terms L'_1, L'_2 and L'_3 stands for the net span of each section and can be expressed as the sum of the initial span and the projected elongation on the chord.

$$
L'_i = l_i + \Delta L_i(\Delta l_{el,i}) \tag{4.52}
$$

Defining exactly this term would require an iterative process since ΔL_i is not known. However, we can simply approximate it: after determining the State 0 we have seen that the central section of the cable has a span of 88m, with a length of around 88.005m and a maximum sag of around 15cm, depending on what cable we are considering.

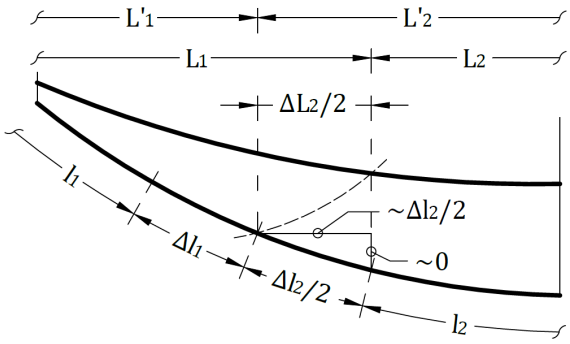

Figure 4.11: Scheme showing the approximation of the central section cable elongation with its horizontal projection. Source: AutoCAD, own elaboration

Because of that we can consider this section as sub-horizontal without producing a significant error, thus approximating ΔL_2 with $\Delta l_{el,2}$ (as shown in figure 4.11). Therefore, the integration limits can be obtained as:

$$\begin{aligned} L_1' &= L_1 - \frac{\Delta l_{el,2}}{2} = L_1 - \frac{1}{2}\frac{\Delta \widetilde{N_2}}{EA} l_2 \\ L_2' &= L_2 + \Delta l_{el,2} = L_2 + \frac{\Delta \widetilde{N_2}}{EA} l_2 \\ L_3' &= L_3 - \frac{\Delta l_{el,2}}{2} = L_3 - \frac{1}{2}\frac{\Delta \widetilde{N_2}}{EA} l_2 \end{aligned} \tag{4.53}$$

Note that this assumption becomes more consistent as the load increases, because this produces a tension increment and therefore a reduction of the cable sag. Due to the mutual variation of L_1', L_2' and L_3', even the n' needs to be redefined as:

$$n' = \frac{L_1'}{L} \tag{4.54}$$

Another problem that we must consider is that both permanent and variable loads are referred to the State 0. Since we have approximated the catenary with a parabolic curve, $q'_{l,sx}$ and $q'_{l,dx}$ are applied over the initial span of the shells, that is L_1 and L_2. The loads are redistributed on a different span as the applied horizontal tension varies. For this reason, once a value for ΔH has been assigned to each iteration, the redistributed

load must be recalculated as:

$$\begin{aligned} {q'^1}_{l,sx} &= q'_{l,sx}\frac{L_1}{L'_1} = q'_{l,sx}\frac{l_1}{L_1 - \frac{1}{2}\frac{\Delta\widetilde{N_2}}{EA}l_2}. \\ {q'^1}_{l,dx} &= q'_{l,dx}\frac{L_3}{L'_3} = q'_{l,sx}\frac{l_3}{L_3 - \frac{1}{2}\frac{\Delta\widetilde{N_2}}{EA}l_2} \end{aligned} \tag{4.55}$$

Now considering the geometric symmetry of the cable, the problem can be simplified. The equation for the cable's length can be developed as:

$$\begin{aligned} l_{tot} + \Delta l_{el} &= l'_{tot} \\ l_1 + l_2 + l_3 + \Delta l_{el,1} + \Delta l_{el,2} + \Delta l_{el,3} &= l'_1 + l'_2 + l'_3 \end{aligned} \tag{4.56}$$

Because of the symmetry we can simplify it as:

$$l_1 + \frac{l_2}{2} + \Delta l_{el,1} + \frac{\Delta l_{el,2}}{2} = l'_1 + \frac{l'_2}{2} \tag{4.57}$$

l_1 and l_2 are already known, while the other terms are a function of the only unknown ΔH. However, it is quite difficult to express it as a function of the load variation. Moreover, the integration limits are not directly known since they are dependent on the elongation of the middle section, which is a function of ΔH. Therefore, it is necessary to define an iterative process based on assigning an initial value of ΔH, with which we can define all the other terms of the equation for the cable's length. This is redefined to provide a residual term, that we want to nullify:

$$l_1 + \frac{l_2}{2} + \Delta l_{el,1} + \frac{\Delta l_{el,2}}{2} - l'_1 + \frac{l'_2}{2} = 0 \tag{4.58}$$

4.2.4 Analysis of ULS and SLS

In this section we will determine the tension that undergoes each cable according to the Ultimate Limit State and the irreversible Serviceability Limit State, under combinations that maximize its tension. This happens well all loads are maximized, so that the considered combinations have been already determined and are summarized in table 4.4 (while the net span is summarized in table 4.5). Since the external loads are already known following the load analysis, and since the tension under permanent loads is already known from the State 0 (determined in section 4.2.2), the only unknown is the horizontal tension variation ΔH.

As the equations defined in the previous section cannot be solved explicitly, the

applied horizontal tension has been determined with an iterative process defined on an Excel spreadsheet. Equation 4.58 has been solved by assigning the values of the applied loads and by setting an initial value of ΔH. The aim is to minimize the residual term of the congruence equation, using the "goal seek" Excel function to obtain the correct value of the only unknown ΔH.

Once the static problem has been solved, the maximum design tension as been calculated from the data provided by the cable manufacturer, according to Eurocode prescriptions.

$$N_{Rd} = \frac{N_{Uk}}{\gamma_r} = \frac{MBL}{1.5\gamma_r} = \frac{MBL}{1.5 \cdot 1} \tag{4.59}$$

Where:

- N_{Rd} is the maximum design tensile strength.
- N_{Uk} is the characteristic tensile strength.
- MBL is the minimum breaking force, guaranteed by the manufacturer.
- γ_r is the safety factor, which is equal to 1 according to that same code [35], section 6.2, table 6.2 (here displayed in figure 4.12)

Table 6.2: Recommended γ_R – values

Measures to minimise bending stresses at the anchorage	γ_R
Yes	0,90
No	1,00

Figure 4.12: Eurocode 3-1-11, section 6.2, table 6.2: security coefficient γ_r for group B elements. Source: [35]

> Since we do not have further information about, we consider the recommended value in case of absence of measures to minimise bending stresses at the anchorage.

The results can be seen in the 4^{th} column of table 4.1. The maximum tension is variable along the structure since the designer has chosen cables of different diameters. The maximum stress is the same for all the cables, around 1570MPa, while the maximum design stress is around 1050MPa.

We must precise that, by considering both the partial coefficient γ_i for variable loads and the reduction factor in the equation for N_{Rd} equal to 1.5, we obtain a safety coefficient of 2.25. In reality, cable structures are designed with higher values (at least 3):

therefore it would be more appropriate to not strictly apply the Eurocode requirements, and assume a reduction factor of at least 2.

However, considering the uncertainties that affect the data regarding the applied loads, specifically the wind action, we have chosen to assume the Eurocode value. According to the same section of the Eurocode, the verification is accomplished when:

$$\frac{N_{Rd}}{N_{Ed}} \geq 1 \tag{4.60}$$

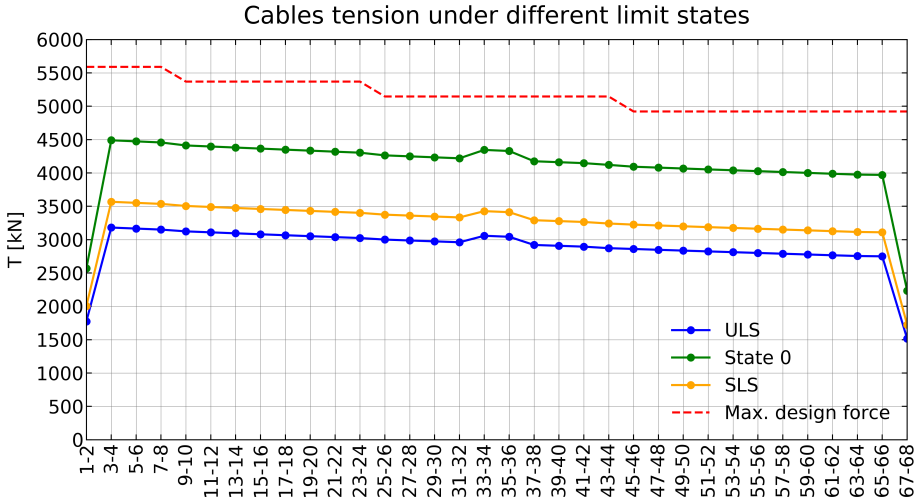

Figure 4.13: Maximum tension of each pair of cables under State 0, ULS and SLS, against the maximum design tension according to Eurocode prescriptions. Source: Excel, own elaboration

The results showed that all the cables are verified. To have a clearer idea, we can look at figure 4.13, that shows the comparison between the maximum cable tension for each cable under ULS, under irreversible SLS, and under permanent loads (State 0), compared to the design strength. As previously done, the length of each cable is determined by approximating the integral with the Cavalieri-Simpson's method.

Once the horizontal tension is known, the geometric configuration of each cable is defined by calculating $z_i(x)$ for intervals of 0,5m. As previously said, the geometry is approximated with 3 successive parabolic curves. In this case is useful to compare the sag variation with the state 0 and note that, as expected, each cable has a lower sag.

Figure 4.14 shows the geometry variation for ULS, SLS and State 0 (the scale between horizontal and vertical axis is not the same, to enhance the sag between different cable pairs). We have also seen that the variation of the projected length of each section between ULS and State 0 in the worst case (cables 33-34) is less than 10cm. This is a negligible value when compared to the net span (57m for the first section and 88m for

the second one): less than 0.5%. Therefore, we can conclude that the approximations adopted considering the geometry invariant are acceptable.

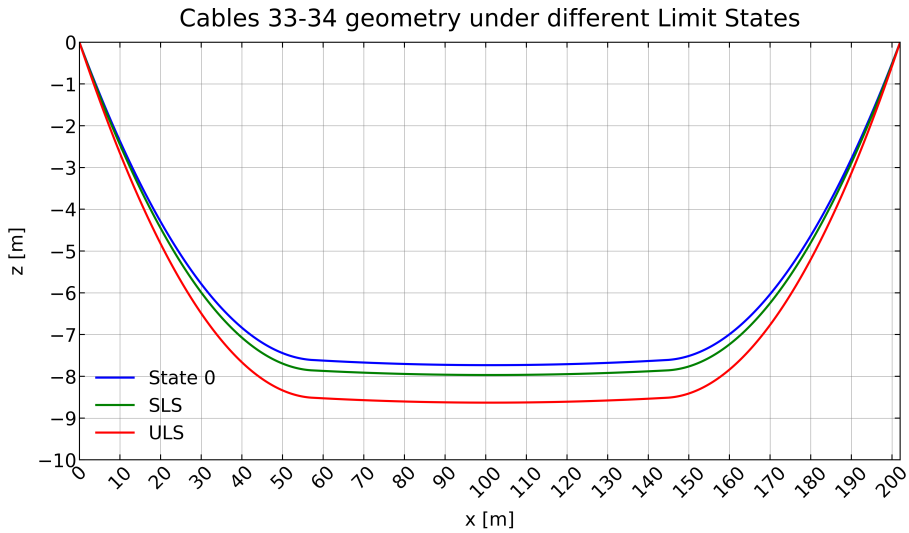

Figure 4.14: Comparison of the geometric configuration of cables 33 and 34 under permanent loads and under ULS conditions. Source: Excel, own elaboration

4.2.5 Variations due to a restraint horizontal displacement

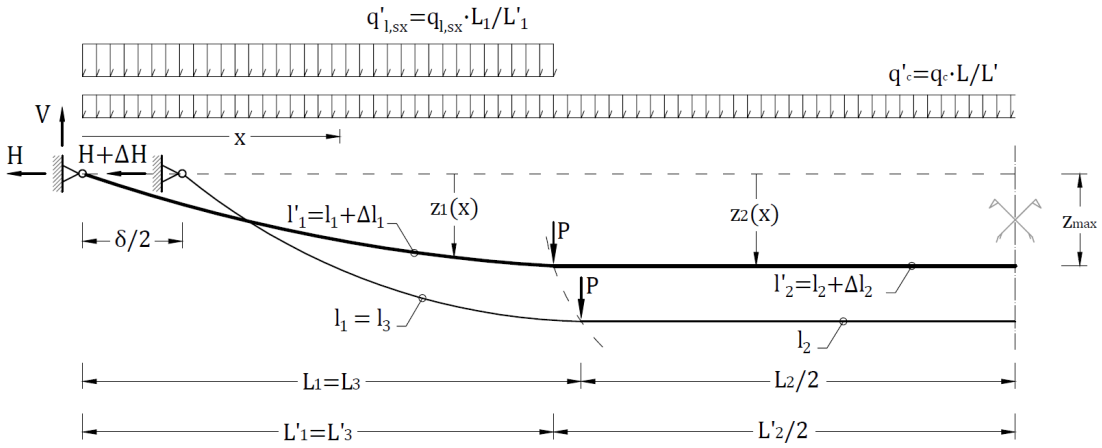

Figure 4.15: Reference static scheme for the cable under a horizontal displacement of one support. Source: AutoCAD, own elaboration

In this section we will consider the case of a horizontal displacement of one of the attachment points, that causes an increase of the total span of the cable, while the applied loads do not change. The static analysis is carried out by calculating the horizontal tension variation caused by an assigned displacement. We assume the hypothesis that despite the displacement, the cable will stay symmetric. To solve the problem, we can

apply the same congruence equation seen previously.

$$l_{tot} + \Delta l_{el} = l'_{tot} \tag{4.61}$$

l_{tot} is the cable length for the initial situation with zero displacement, in this case the State 0, for which the cable length is already known. Δl_{el} represents the elastic elongation due to the span, and the consequent tension increase: this last term can be approximated using the mean value of the tension variation.

$$\Delta l_{el} = \int_0^l \frac{\Delta N\left(x\right)}{EA} \cong \int_0^l \frac{\Delta \widetilde{N}}{EA} dx = \frac{\Delta \widetilde{N}}{EA} l \quad \text{where: } \Delta \widetilde{N} = \frac{\sum_{i=1}^{n} \Delta N\left(x_i\right)}{n} \tag{4.62}$$

However, in this case the tension variation is caused only by a variation of the horizontal component, while the vertical component remains the same.

$$\Delta \widetilde{N} = \sqrt{H'^2 + V\left(x\right)^2} = \sqrt{\left(H + \Delta H\right)^2 + V\left(x\right)^2} \tag{4.63}$$

Also for $V(x)$ there is a small variation due to the load redistribution, but this aspect will be presented in detail later. In the end we can express the elastic elongation as:

$$\Delta l_{el} = \Delta l_{el,1} + \Delta l_{el,2} + \Delta l_{el,3} \cong \frac{\Delta \widetilde{N_1}}{EA} l_1 + \frac{\Delta \widetilde{N_2}}{EA} l_2 + \frac{\Delta \widetilde{N_3}}{EA} l_3 \tag{4.64}$$

Where:

$$\Delta \widetilde{N_j} = \frac{\sum_{i=1}^{m<n} \Delta N_j\left(x_i\right)}{m} = \frac{\sum_{i=1}^{m<n} \sqrt{\left(H + \Delta H\right)^2 + V\left(x\right)^2}}{m}$$

l'_{tot} is the total cable length expressed as a function of the horizontal tension H', and therefore as a function of the increased horizontal tension variation ΔH. As seen previously, this term can be calculated as the length of a parabola by solving the integral:

$$\begin{aligned} l_{tot} &= l_1 + l_2 + l_3 = \\ &\int_0^{L'_1} \sqrt{1 + \left(\frac{\partial z_1(x)}{\partial x}\right)^2} dx + \int_{L'_1}^{L'_1 + L'_2} \sqrt{1 + \left(\frac{\partial z_2(x)}{\partial x}\right)^2} dx + \\ &+ \int_{L'_1 + L'_2}^{L} \sqrt{1 + \left(\frac{\partial z_3(x)}{\partial x}\right)^2} dx. \end{aligned} \tag{4.65}$$

Where the terms $\partial z_1(x)/\partial x$, $\partial z_2(x)/\partial x$ and $\partial z_3(x)/\partial x$ can be obtained from their respective expression of the parabolic geometry of the cable:

$$
\begin{aligned}
z_1(x) &= \frac{q'_c x}{2H'}(L'-x) + \frac{q'_{l,sx} x}{2H'}(L'-x) - \frac{q'_{l,sx} L'}{2H'} x (1-n')^2 + \frac{q'_{l,dx} L'^2}{2H'} n'^2 \frac{x}{L'} + \frac{P}{H'} x \\
z_2(x) &= \frac{q'_c x}{2H'}(L'-x) + \frac{q'_{l,sx} L'^2}{2H'} n'^2 \left(1 - \frac{x}{L'}\right) + \frac{q'_{l,dx} L'^2}{2H'} n'^2 \frac{x}{L'} + \frac{P}{H'} n' L' \\
z_3(x) &= \frac{q'_c x}{2H'}(L'-x) + \frac{q'_{l,sx} L'^2}{2H'} n'^2 \left(1 - \frac{x}{L'}\right) + \frac{q'_{l,dx} x}{2H'}(L'-x) - \\
&\quad - \frac{q'_{l,dx} L'}{2H'}(L'-x)(1-n')^2 + \frac{P}{H'}(L'-x)
\end{aligned}
\tag{4.66}
$$

These equations can be differentiated, thus obtaining:

$$
\begin{aligned}
\frac{\partial z_1(x)}{\partial x} &= \frac{q'_c}{2H'}(L'-2x) + \frac{q'_{l,sx}}{2H'}(L'-2x) - \frac{q'_{l,sx} L'}{2H'}(1-n')^2 + \frac{q'_{l,dx} L'^2}{2H'} n'^2 \frac{1}{L'} + \frac{P}{H'} \\
\frac{\partial z_2(x)}{\partial x} &= \frac{q'_c}{2H'}(L'-2x) + \frac{q'_{l,sx} L'^2}{2H'} n'^2 \left(-\frac{1}{L'}\right) + \frac{q'_{l,dx} L'^2}{2H'} n'^2 \frac{1}{L'} \\
\frac{\partial z_3(x)}{\partial x} &= \frac{q'_c}{2H'}(L'-2x) + \frac{q'_{l,sx} L'^2}{2H'} n'^2 \left(-\frac{1}{L'}\right) + \frac{q'_{l,dx}}{2H'}(L'-2x) - \\
&\quad - \frac{q'_{l,dx} L'}{2H'}(-1)(1-n')^2 + \frac{P}{H'}(-1)
\end{aligned}
\tag{4.67}
$$

Even in this case there would be a variation of the cable geometry, but they are negligible and we can assume that the geometry remains unchanged. Note that now not only changes the applied horizontal tension (which is defined as $H' = H + \Delta H$), but also the total span of the cable that can be expressed as $L' = L + \delta$, where δ stands for the assigned displacement. Furthermore, the integration limits of the formula for l_{tot} need to be redefined. To ease the discussion, we proceed with the same assumption seen in section 4.2.3, i.e. that the central section of the cable is sub-horizontal. Therefore, we can approximate the span variation of this section as:

$$
\Delta L_2 = L'_2 - L_2 = \Delta l_{el,2} = \frac{\Delta \widetilde{N_2}}{EA} l_2 \tag{4.68}
$$

Considering the assigned displacement δ, the terms included in the integration borders, that correspond to the increased span of each section, can be redefined as:

$$\begin{aligned} L'_1 &= L_1 + \Delta L_1 = L_1 + \frac{\delta}{2} - \frac{\Delta l_{el,2}}{2} = L_1 + \frac{\delta}{2} - \frac{\Delta \widetilde{N_2}}{EA}\frac{l_2}{2} \\ L'_2 &= L_2 + \Delta L_2 = L_1 + \Delta l_{el,2} = L_2 + \frac{\Delta \widetilde{N_2}}{EA} l_2 \\ L'_3 &= L_3 + \Delta L_3 = L_3 + \frac{\delta}{2} - \frac{\Delta l_{el,2}}{2} = L_3 + \frac{\delta}{2} - \frac{\Delta \widetilde{N_2}}{EA}\frac{l_2}{2} \end{aligned} \tag{4.69}$$

The non-dimensional parameter n' is also redefined as:

$$n' = \frac{L'_1}{L'} = \frac{L'_1}{L + \delta} \tag{4.70}$$

The last aspect that we need to analyse concerns the load redistribution. Since we have approximated the catenary with a parabolic curve, $q_{l,sx}$, $q_{l,dx}$ and q_c are applied over the initial span of each section. Hence, the loads must be redistributed over a different span as the applied horizontal tension varies. For this reason, once a value for ΔH has been assigned to each iteration, the redistributed load must be recalculated as:

$$\begin{aligned} {q'}^1{}_c &= {q'}_c \frac{L}{L'} = {q'}_c \frac{L}{L + \delta} \\ {q'}^1{}_{l,sx} &= {q'}_{l,sx} \frac{L_1}{L'_1} = {q'}_{l,sx} \frac{l_1}{L_1 - \frac{1}{2}\frac{\Delta \widetilde{N_2}}{EA} l_2} \\ {q'}^1{}_{l,dx} &= {q'}_{l,dx} \frac{L_3}{L'_3} = {q'}_{l,sx} \frac{l_3}{L_3 - \frac{1}{2}\frac{\Delta \widetilde{N_2}}{EA} l_2} \end{aligned} \tag{4.71}$$

Now considering the geometric symmetry of the cable, the problem can be simplified. The equation for cable's length can be developed as:

$$\begin{aligned} l_{tot} + \Delta l_{el} &= l'_{tot} \\ l_1 + l_2 + l_3 + \Delta l_{el,1} + \Delta l_{el,2} + \Delta l_{el,3} &= l'_1 + l'_2 + l'_3 \end{aligned} \tag{4.72}$$

Because of the symmetry we can simplify:

$$l_1 + \frac{l_2}{2} + \Delta l_{el,1} + \frac{\Delta l_{el,2}}{2} = l'_1 + \frac{l'_2}{2} \tag{4.73}$$

l_1 and l_2 are already known, while the other terms are a function of the only unknown ΔH. The problem can be solved using the same procedure applied in the case of a load

increase. Thus, the expression is reconfigured as:

$$l_1 + \frac{l_2}{2} + \Delta l_{el,1} + \frac{\Delta l_{el,2}}{2} - l'_1 + \frac{l'_2}{2} = 0 \tag{4.74}$$

And we can set an iterative process with the aim to minimize the residual term.

4.2.6 Analysis of the variation due to a restraint displacement

In this section we will show the cable behaviour under a horizontal displacement of one of its ends, that cause a variation of its net span. This could happen due to a generic failure of the cantilever stand, as well as following a seismic solicitation. The seismic combination involves only permanent loads as static actions(the coefficients for concomitant actions nullify all the variable actions), giving the same loads of the State 0 combination, therefore we can consider only one situation for both cases, and we take as reference the loads presented in table 4.4.

Since the external loads are already known, and since the tension under permanent loads is already known from the State 0 (determined in section 4.2.2), the only unknown is the horizontal tension variation ΔH. As the equations defined in the previous section cannot be solved explicitly, the horizontal tension variation has been determined with an iterative process set on an Excel spreadsheet. The equation 4.74 has been solved using the "seek goal" function in Excel, with the aim to find value of ΔH that minimize its residual term. The deformed geometry is then determined by calculating the vertical displacement at defined intervals. The results have been compared with the maximum design force (shown in table 4.1), trying to assess the displacement that would cause the cable failure.

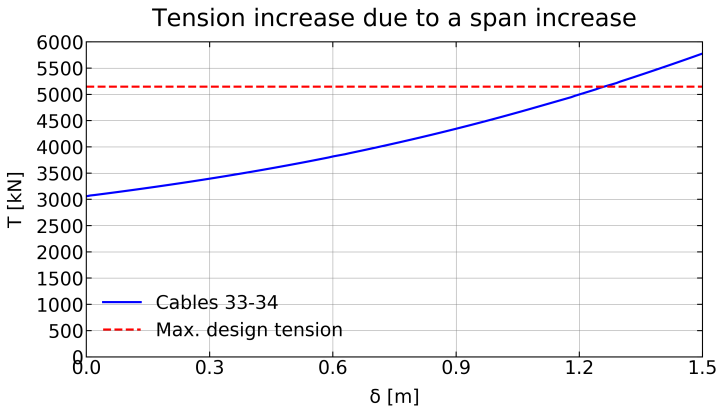

Figure 4.16: Tension increase due to a span variation of the cable, compared with the maximum design tension. Source: Excel, own elaboration

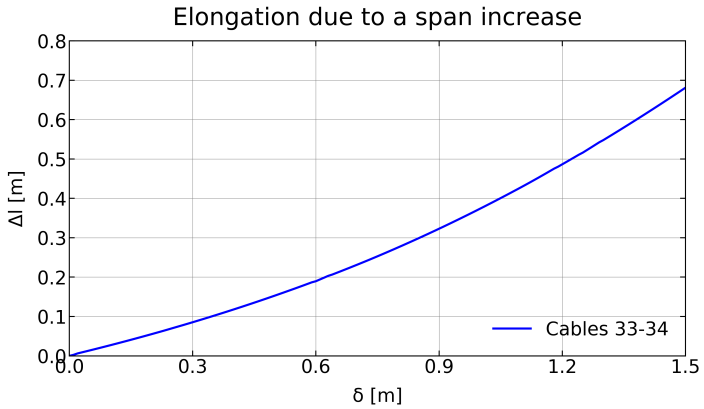

Figure 4.17: Elastic elongation due to a span increase of the cable. Source: Excel, own elaboration

Based on what has been observed in section 4.2.4, more precisely in figure 4.13, not all cables have the same strength margin: to carry on the analysis we have chosen cables 33-34, that have the higher tension if compared to its maximum design tension. Figure 4.16 shows the trend of the horizontal tension component for an assigned span variation δ. It is constant along the cable and is the only component that varies due to a span increase. We can observe that, starting from the State 0 tension, there is an exponential increase of the applied tension. However, this behaviour is considerably "flattened" by the elastic elongation, which will be further explained in section 4.2.7. The same trend can be observed for the elastic elongation (figure 4.17). The numerical results for this analysis have been summarized in annex D.

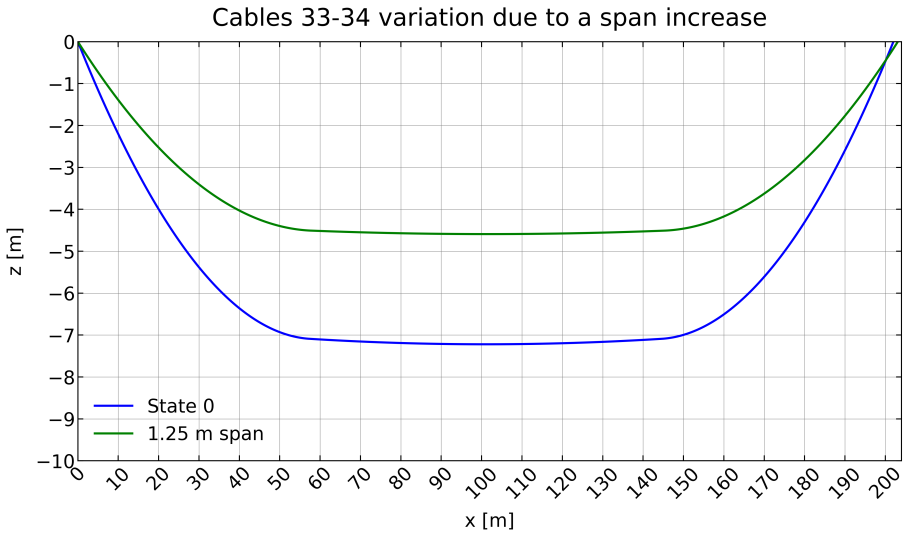

Figure 4.18: Comparison between the initial geometry at State "0" and under a 1.25m displacement. Note that the horizontal and vertical axes do not have the same proportions, to better show the cable variation. Source: Excel, own elaboration

Once the horizontal tension is known, the geometric configuration of each cable is defined by calculating $z_i(x)$ for intervals of 0,5m. In this case we can compare the State 0 configuration with the geometric configuration for the 1.25m displacement that cause the cable to fail (figure 4.18). In such situation we should consider also other aspects that have been neglected. Namely, the behaviour of the precast concrete slabs: with such displacements the variation of the geometric configuration is more evident, with the slab not following the elastic elongation of the cable.

4.2.7 Consequences of the elastic elongation

When a tension increment is applied there is a consequent elastic elongation of the cable, whose effect is noteworthy as we will briefly explain in this section. We might consider the two cases that have been already studied in section 4.2.3 and 4.2.5:

- Supposing that the tension variation has been caused by a load increase, the elastic elongation makes the cable longer but with the same span. Therefore, the maximum sag is higher, thus the horizontal tension component won't increase linearly with its vertical counterpart. Hence does the total tension, that will be lower than expected because of this elastic elongation.

- We can also consider the case of a tension variation caused by an increase of the net span. The comparison now is with a cable of the same initial length but stretched over a larger span, and therefore with a lower sag. However, the elastic elongation causes the cable to be longer, so that the maximum sag is higher than expected and the horizontal tension component lower.

In both cases we can see that because of the elastic elongation there is an effect over the horizontal component, that can be assessed by comparing the results of section 4.2.6 with the same situation on a non-elastic cable. The static solution is similar to what is seen in section 4.2.5 and with equation 4.61, with the only difference that now we do not consider the elastic elongation term in the congruence equation.

$$l_{tot} + \cancel{\Delta l_{el}} = l'_{tot} \tag{4.75}$$

The other terms are the same previously exposed. While the results are reported in detail in annex D at the end of this document, the consequences can be clearly observed on graph, 4.19.

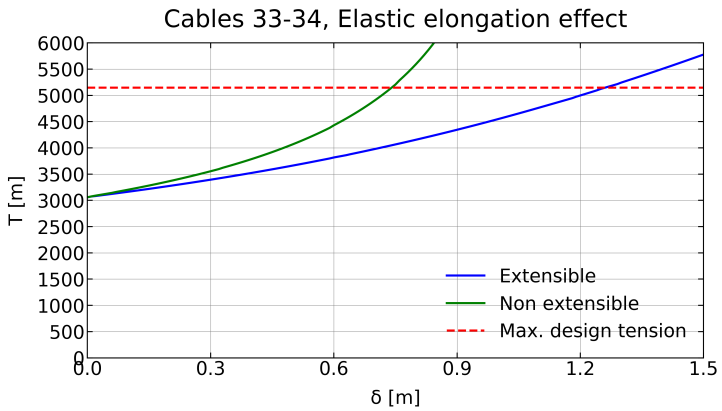

Figure 4.19: Different maximum tension behaviour between the real cable and an equivalent non-extensible cable. Source: Excel, own elaboration

Note how the cable behaviour improves: the elastic cable curve is significantly flattened, allowing the cable to resist larger displacements before reaching the breaking point. While for the non-extensible case limit is reached with a displacement of 73cm, for the real extensible cable the same point is reached only with a 125cm displacement. The same conclusions can be obtained by studying the case of a load variation: the cable will have a better response since it will be able to undergo higher loads before collapsing.

Finally, we want to point out that the results obtained in this chapter analytically, by applying simplified formulations (for example by approximating the cable geometry with a parabola) and Excel sheets have been verified by means of the structural calculation software SAP2000 (which uses a formulation based on the catenary equation). With this software, using the same data of applied loads and maximum sag of each portion, we proceeded to verify the tension over the cables (that have been modeled as described in section 6.1.3, but in this case they have been hinged to a restraint at both their ends). The results thus obtained verified the results presented in this chapter.

Chapter 5

Structural analysis of the Cantilever East stand

In this chapter we will present a brief analysis of the structural behavior of the East stand. As already described in chapter 3, this is made up of a series of reinforced concrete cantilevered uprights, linked by means of horizontal concrete plates and the cable support beam. Given the complexity of the structure, the analysis has been carried out with a 2D finite element model (assembled using the SAP2000 structural modelling software, version 21.0.2, build 1491, [11]) which will then be useful in defining the parameters for the simplified models in chapter 6.

5.1 Load analysis of the East stand

The 2D model of the East stand comprehends the upright, the cable support beam and the steel beams that carry the horizontal slabs across the uprights. Other elements (such as the stands, stairs, concrete horizontal slabs) have been be included only as static loads, as we evaluated that their contribution does not affect the structural response of the upright. Note that in the external uprights some components have a different size, since they carry slightly larger loads. However, to perform this analysis we have considered the middle uprights, since as already seen in chapter 4, we will focus on the middle cables (33, 34, 35 and 36), that are the most loaded ones, and therefore we will model the 8^{th} upright.

5.1.1 Permanent structural and non-structural loads

As we are going to create a finite element model, we can distinguish between structural elements that will be included in the model (whose load will be automatically calculated) and other structural and non-structural elements that will not be included. About these, we need to assess their equivalent static action on the elements included, and then introduce this action into the model. The contribution of such elements is related to their

weight, so that to assess them we have measured their section from the designs provided in [15] and [16], and we have evaluated their equivalent static action considering a spacing of 7.5m between each upright, as well as the material weights suggested by [29] (i.e. 25kN/m^3 for reinforced concrete and 76.97kN/m^3 for steel).

This procedure is not particularly interesting for our purposes, so we briefly report the equivalent loads without showing the step-by-step calculation. For the bleachers, their supports, seats and stairs we had to make some assumptions about their dimensions, as these were not measurable from the designs provided. These loads are therefore approximate values, that however we can still apply to get an idea of the effect of these components over the uprights.

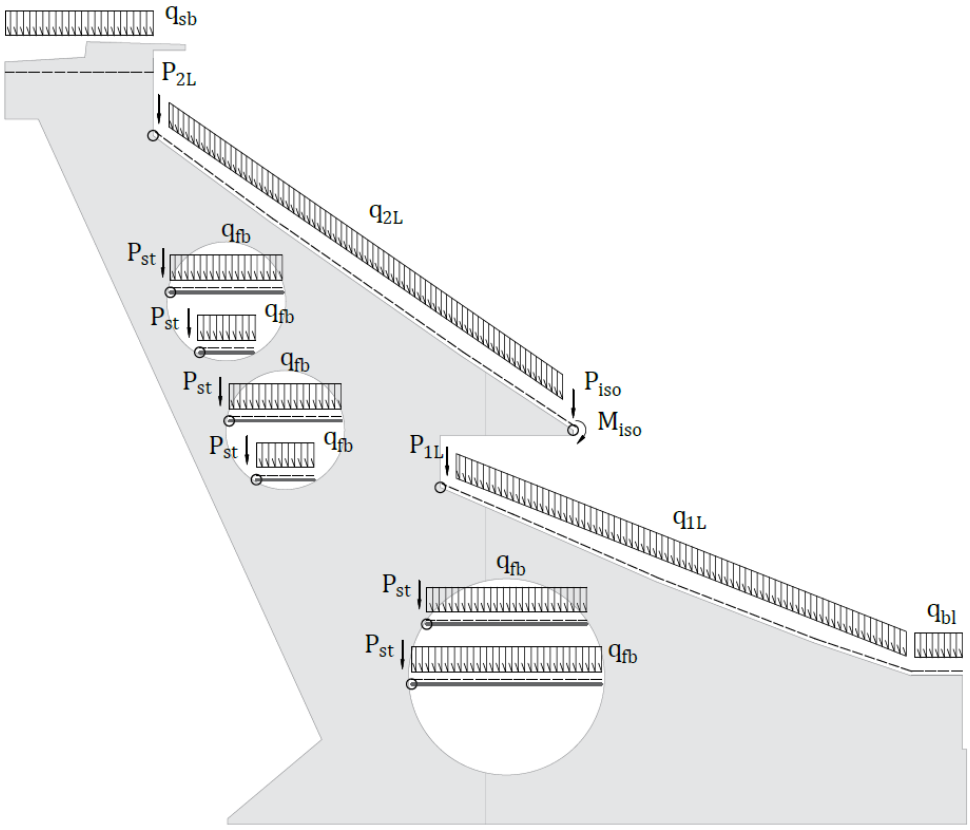

Figure 5.1: Assigned permanent structural and non-structural loads due to non-modeled elements. Source: AutoCAD, own elaboration

Table 5.1: Summary of the equivalent static actions of non-modeled members. Source: Excel, own elaboration

Static load for the non-modeled permanent constructive elements

Id.	value		cat.	description
q_{sb}	248,3	kN/m	G1	cable supporting beam
q_{2L}	65,3	kN/m	G1	concrete slab and precast concrete supports of the 2nd level
	46,2	kN/m	G2	handrails, seats, precast concrete bleachers
q_{1L}	64,9	kN/m	G1	concrete slab and precast concrete supports of the 1st level
	43,6	kN/m	G2	handrails, seats, precast concrete bleachers
P_{2L}	125	kN	G1	jutting floor at the upper end of the stand 2nd level
P_{1L}	199	kN	G1	jutting floor at the upper end of the stand 1st level
q_{bl}	40,6	kN/m	G1	concrete floor of the 1st level front balcony
q_{fb}	56,3	kN/m	G1	reinforced concrete inner floor slab
	10,8	kN/m	G2	concrete inner floor pavement
P_{iso}	185,8	kN	G1	equivalent shear force of the 2nd level front balcony structural members
	70,6	kN	G2	equivalent shear force of the 2nd level front balcony non-structural members
M_{iso}	285,8	kNm	G1	equivalent bending moment of the 2nd level front balcony structural members
	63,6	kNm	G2	equivalent bending moment of the 2nd level front balcony non-structural members
P_{st}	105	kN	G1	equivalent action of the stairs over the concrete slabs

All the non-modeled elements are listed in table 5.1, that contains a brief description of the elements to which belongs each load, its value (note that some are considered as distributed loads, others as concentrated loads), their category, and the identification code of the load itself for the scheme in figure 5.1. As we will see in section 5.2.1, the upright will be modeled with a mesh of shell finite elements. While the concentrated loads are transmitted directly to the mesh nodes, the uniformly distributed linear loads needed to be converted into concentrated loads (by multiplying them for the spacing between adjacent border nodes), and were then applied to the nodes themselves.

5.1.2 Roof equivalent static action

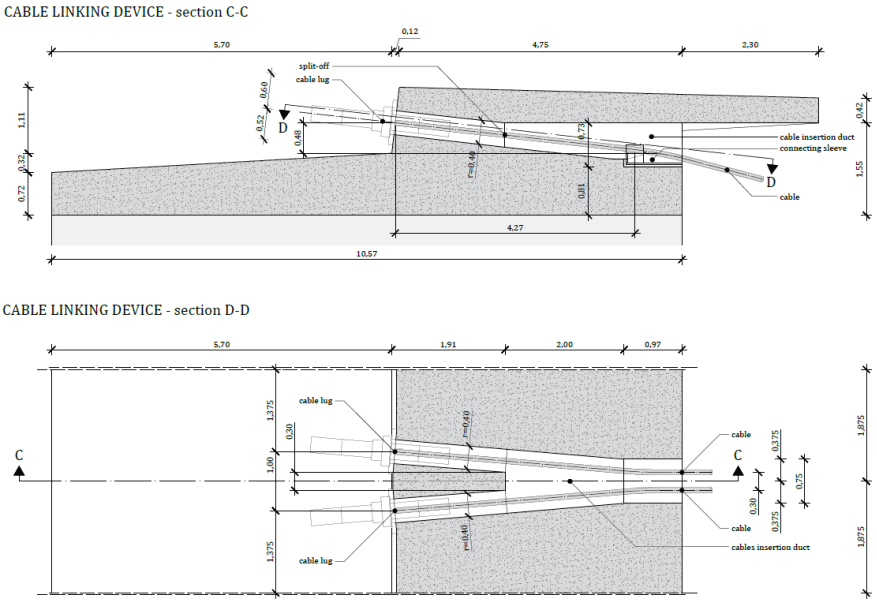

Figure 5.2: Detail of the cable anchor system (from above): horizontal section, vertical section. Source [15]

In this phase the roof has not been modeled, so we needed to define the action transmitted to the uprights. Note that each upright carries the action of 2 adjacent pairs of cables, which is transmitted by the concrete support beam. The cable action was modeled trying to reproduce the coupling system shown in figure 5.2, where each cable is inserted into a steel sleeve by means of a guide, and then anchored to the support beam at its end.

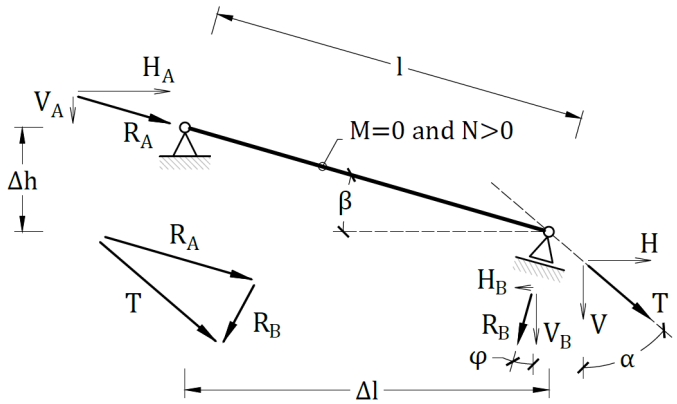

Figure 5.3: Determination of the equivalent static action of the cables over the uprights. Source: AutoCAD, own elaboration

The static action is therefore transmitted in two different points, and to assess it we can refer to the static scheme shown in figure 5.3, which reproduces the terminal

part of the cable (considered as a straight frame), the two support points (considered as hinges), and the resulting action at the coupling point (determined starting from the calculations discussed in chapter 4). Note that the terms R_i, H_i and V_i represent the cable equivalent actions, and not the restrain reactions. Since the cable can undergo only tension forces, R_A must be directed along it, while R_B is directed along the angle bisector between the external force T and the cable itself. The relation between the external action of the cable T (where $T^2 = H^2 + V^2$) and the equivalent static actions R_A and R_B defined by the formulas:

$$\begin{aligned} V_B = \frac{V\Delta l - H\Delta h}{\Delta l - \Delta h \tan\phi} \quad \text{and} \quad H_B = V_B \tan\phi \\ V_A = V - V_B \quad \text{and} \quad H_A = H - H_B \end{aligned} \tag{5.1}$$

where:

$$\phi = 45° + \beta - \frac{\alpha}{2} \quad \text{with:} \quad \beta = \arctan\frac{\Delta h}{\Delta l} \quad \text{and} \quad \alpha = \arctan\frac{H}{V}$$

where α represents the angle with the vertical axis of the external action T, β represent the angle of the anchor sleeve with the horizontal axis, l is its length, while Δl and Δh are its horizontal and vertical projection respectively.

Table 5.2: Cable attachment, geometric parameters for all pairs

Geometric parameters			
Δh [m]	Δl [m]	l [m]	β
0,48	4,27	4,29	6,45°

At this point it is sufficient to replace the numerical values: the geometric parameters are the same for all the cable pairs, and are summarized in table 5.2, while the external action transmitted by the cables changes for each pair. As we will see later, in the East stand static analysis we will consider the cables separately from the other loads, and so we have to calculate their action according to each load combination. For reasons that we will explain later in this chapter, we will consider only a limited number of significant load combinations:

- Seismic Limit State, which for the roof includes only permanent loads. For the roof action it results as:

$$G_1 + G_2 \tag{5.2}$$

- Ultimate Limit State combination that maximises the upright bending towards

the inside, and so that maximises the roof action. For the roof action it results as:

$$1.35 \cdot G_1 + 1.5 \cdot G_2 + 1.5 \cdot Q_W + 1.5 \cdot 0.2 \cdot Q_S \tag{5.3}$$

- Ultimate Limit State that maximises the upright bending towards the outside, and so that minimises the roof action. For the roof action it results as:

$$G_1 + 0.8 \cdot G_2 \tag{5.4}$$

In this case we have not evaluated the accidental action from wind suction, since it would have been almost irrelevant for the upright behaviour due to its low value, and the primary live load according to our criteria is the crowd overload over the stand.

Table 5.3: Cables 33, 34, 35 and 36 equivalent actions on the upright for the seismic combination, the ULS combination that maximises cable tension and the ULS combination that minimises it. Source: Excel, own elaboration

Cables equivalent actions - Seismic combination

cable id.	cable force			equivalent action			
	H [kN]	V [kN]	T [kN]	V_A [kN]	H_A [kN]	V_B [kN]	H_B [kN]
33-34	2973,5	715,3	3058,4	325,6	2882,1	389,7	91,5
35-36	2958,1	715,3	3043,3	323,8	2865,9	391,5	92,2

Cables equivalent actions - ULS combination for max. cable tension

cable id.	cable force			equivalent action			
	H [kN]	V [kN]	T [kN]	V_A [kN]	H_A [kN]	V_B [kN]	H_B [kN]
33-34	4193,2	1141,5	4345,8	454,3	4021,1	687,2	172,1
35-36	4176,4	1141,5	4329,5	452,3	4003,4	689,1	172,9

Cables equivalent actions - ULS combination for min. cable tension

cable id.	cable force			equivalent action			
	H [kN]	V [kN]	T [kN]	V_A [kN]	H_A [kN]	V_B [kN]	H_B [kN]
33-34	2973,0	715,1	3049,9	325,6	2881,7	389,5	91,4
35-36	2958,1	715,1	3043,3	323,8	2865,2	391,3	92,1

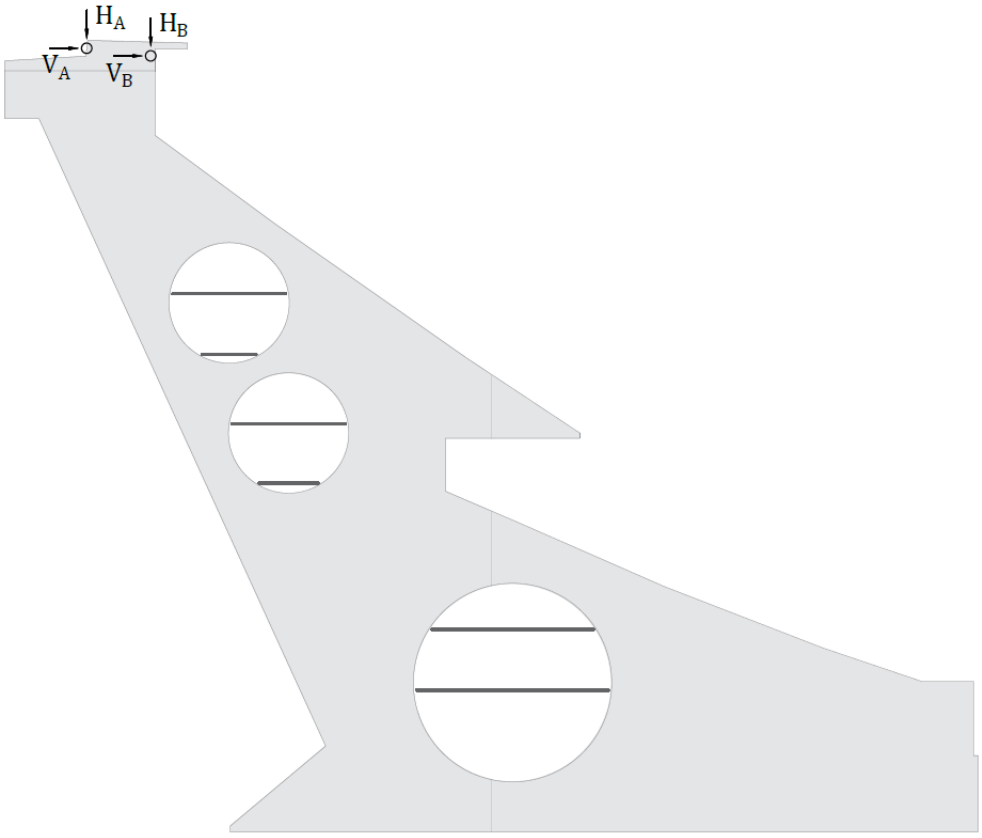

Figure 5.4: Equivalent static action of the cables applied as concentrated loads over the 2D model of the upright. Source: AutoCAD, own elaboration

Therefore we calculated the equivalent static action of the roof only for these cases, from the cable actions defined in sections 4.2.2 and 4.2.4. Since the analysis will be focused only on a specific upright (the 8^{th} one, related to cables 33, 34, 35 and 36), we reported the static equivalent actions only for the cables involved (summarized in table 5.3). These actions have been applied as concentrated loads as shown in figure 5.4. Note that, since each upright is subjected to the action of 4 adjacent cables, the terms H_A, V_A, H_B and V_B are the sum of the respective contribution of each cable for the considered load combinations.

5.1.3 Crowd overload

The stands are accessible to the public, as well as the foyers below, so they are all susceptible to crowding. According to the Eurocode prescriptions [30], the surface overload for cat. C5 is 5kN/m^2. The spacing between successive uprights is 7.5m, thus resulting in a linear overload over each stand of:

$$q_{cat.\ C5} = 5kN/m^2 \cdot 7.5m = 37.5\ kN/m \tag{5.5}$$

The distributed load thus determined is applied along the stand seats and on the HE steel beams and that support the inner foyers. The balcony at the base of the second level will not be modeled, so also the static action of the crowd overload must be calculated. This element constitutes an isostatic attachment, which can be treated as a cantilever shelf with a length of 2.55m (while the uprights have a spacing of 7.5m). The equivalent static action is therefore constituted by a shear component and a bending moment, calculated as:

$$\begin{aligned} V_Q &= q_{cat.\ C5} \cdot 2.55\ m \cdot 7.5\ m = 95.6\ kN \\ M_Q &= q_{cat.\ C5} \cdot 2.55\ m \cdot 7.5\ m \frac{2.55\ m}{2} = 121.9\ kNm \end{aligned} \tag{5.6}$$

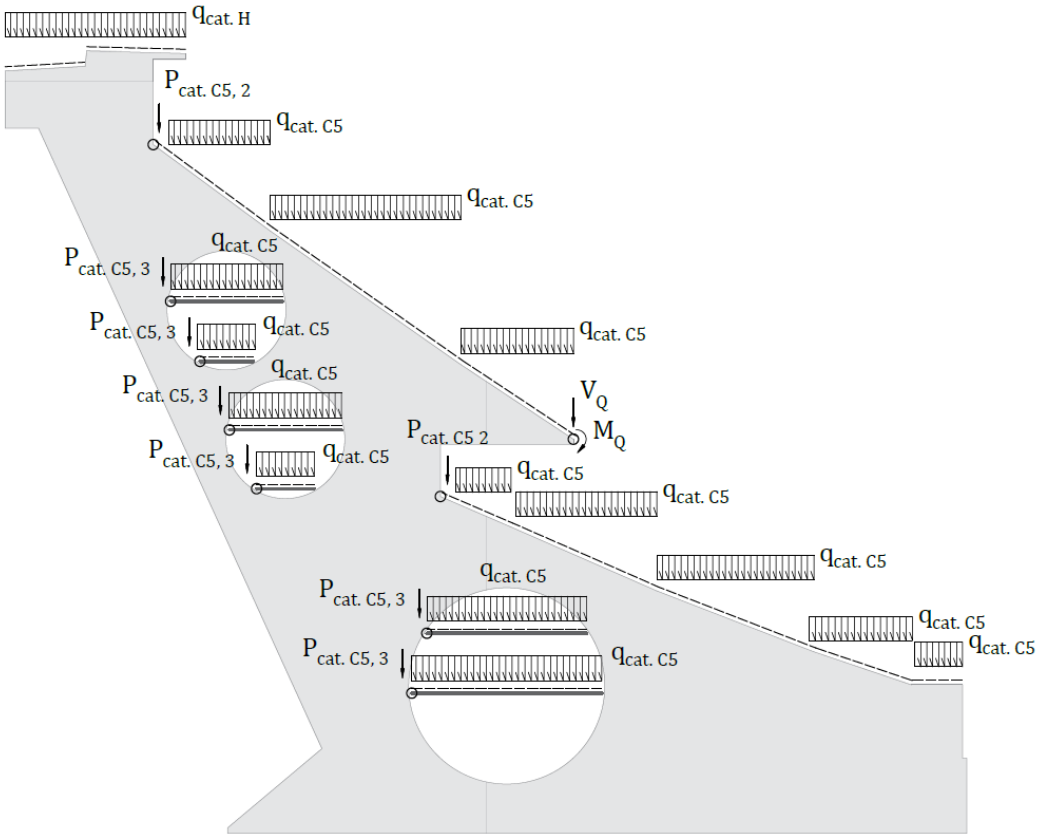

Figure 5.5: Static live loads due to crowding (cat. C5) and roof inspection (cat. H). Source: AutoCAD, own elaboration

The loads related to crowd overload thus calculated have been applied as represented in figure 5.5. Although it would not strictly comply with the Eurocode, we simplified the analysis and not included the crowd overload over the stairways, as it would be unlikely a simultaneous crowding of the stands, the internal foyers and the stairways. Instead, we can realistically expect that the crowding will occur on the stands or in the communication areas at different times during an event.

5.1.4 Roof inspection and maintenance load

We consider the same value of, 0.5kN/m^2, according to the Eurocode prescriptions in [30], related to cat. H (roof accessible only for inspection and maintenance works). Therefore, considering a spacing of 7.5m between the uprights, we can obtain a distributed load of:

$$q_{cat.\ H} = 0.5\ kN/m^2 \cdot 7.5\ m = 3.75\ kN/m \tag{5.7}$$

This load has been applied to the roof top of the East stand upright, as shown in figure 5.5.

5.1.5 Snow load

In this section we refer to the snow over the top surface of the East stand, not to the concrete slab whose snow load is already included in the cables equivalent static action. Given the reduced extension of this surface, and given that it is at the same height as the cable-suspended roof, we assign it the same uniform load determined for the roof in chapter section 4.1.4. This is equally distributed among the uprights, considering a spacing of 7.5m.

$$q_s = s \cdot 7.5\ m = 0.422 \cdot 7.5 = 3.165\ kN/m \tag{5.8}$$

This load is applied along the upper border of the upright.

5.1.6 Thermal action

Regarding the effects of thermal actions in the uprights we can observe that each one of them act as an isostatic cantilever structure. Therefore, any thermal variations could induce only deformations, about which we can make some interesting considerations. Thermal gradients and uniform thermal shifts can induce a height variation or a bending of the upright, whose consequences are of two types:

- Variation of the lever of the cable static action, thus modifying the balance of the bending moments at the uprights foundation.

- Variation of the cables net span, and therefore (as we have seen in chapter 4), a variation of the cables tension.

However, to appreciate these effects we would need unrealistic temperature shifts, such as to induce deformations with a magnitude of several centimeters. Another notable consequence of thermal actions regards the steel beams supporting the floors: these are hinged inside the uprights themselves, so any temperature increase would cause a span

reduction and at the same time an elongation of the beam itself. This would induce compression forces and bending moments over those beams. Still, we can neglect it since this is not the subject of this study, and moreover does not affect the overall behavior of the upright. For these reasons we decided to not consider thermal actions in this analysis of the uprights.

5.1.7 Wind action

The definition of the wind static action over the East stand is particularly challenging, as the cantilevered structure is inclined, it has a height of 55 m above the ground, the uprights have a spacing of 7.5m which is only partially open (so that it does not offer a smooth surface to the wind action). Therefore, the designers evaluated the wind action over the stands through the analysis of scale model in wind tunnel tests [26], as for the roof. However, even if several papers talk about this topic, we do not have information about the wind effects over the stands, nor about the calculation methods adopted.

Still, we can note that this variable load is certainly not decisive in designing the upright, since it has less influence than the static actions from cables and other permanent loads. Because of this we opted for a simplified static analysis, by assessing the static action from the Eurocode prescriptions and by applying some simplifying assumptions. Acting in favor of safety, we will treat the two facades as continuous, vertical and exposed surfaces. As stated in Eurocode [32], section 5.2, wind pressure on a generic building is determined as:

$$w_e = q_p(z_e) \cdot c_{pe} \tag{5.9}$$

Where q_p is the peak value of the wind pressure at the reference altitude z_e, while c_{pe} is the external pressure coefficient. First, q_p is calculated as:

$$q_p(z_e) = q_b \cdot c_e(z) \tag{5.10}$$

where q_b is the basic wind pressure for our location: we have already seen in chapter 4, section 4.1, that is equal to 0.46kN/m^2. To establish the reference height z we can refer to the diagram in figure 7.4, section 7.2 of the Eurocode [32], and consider the case for which $h > b$ (where h is the height of the building and b the width of the facade). In our situation the reference height is equivalent to the height of the structure (55m) and we can assume, on the safety side, a constant static wind pressure distribution along it. Making reference to equation 5.10, $c_e(z)$ is the exposure coefficient for the structure. To evaluate it we assume unitary values for the orographic factor c_o and the turbulence

factor K_I. Due to this, to assess $c_e(z)$ we can refer to the graph in figure 4.2, section 4.5 of [32]. We apply another simplification since we assume a type 0 terrain surface (which is the worst scenario), so that we obtain $c_e(z)$ equal to 4. Consequently, the peak wind pressure is:

$$q_p(z_e) = q_p(55\ m) = q_b \cdot c_e(55\ m) = 0.46 \cdot 4 = 1.84\ kN/m^2 \tag{5.11}$$

For the evaluation of c_{pe} we refer to the scheme proposed in figure 7.5, and to the values of table 7.1, section 7.2.2 of [32], and more precisely to the values assigned for zone D and zone E. Considering $h/d \approx 1$ and a loaded surface of more than 10m^2, we obtain $c_{pe} = +0.8$ for the windward facade and $c_{pe} = -0.5$ for the leeward facade. Consequently:

$$q_p(z_e) \cdot c_{pe} \cdot 7.5\ m \begin{cases} q_{p,\ side} = 1.84 \cdot 0.8 \cdot 7.5 = 11.04 kN/m & \text{windward facade} \\ q_{s,\ side} = 1.84 \cdot (-0.5) \cdot 7.5 = -6.9 kN/m & \text{leeward facade} \end{cases} \tag{5.12}$$

Note that these values are an approximation for the worst possible scenario, since they have been calculated referring to the simplified case of vertical, smooth, continuous facades. Moreover, we should also consider the action over the top surface of the East stand, that we consider as a plain roof to simplify the analysis. The peak wind pressure, determined according to Eurocode [32], is the same obtained previously for the facades (as it is referred to an altitude of 55 m).

For the pressure coefficient c_pe we will make reference to the scheme in figure 7.6, and to table 7.2, section 7.2.2 of [32]. In this case we consider the values for zone G and zone I (depending on the wind direction). We consider the case of live edges, with $h/d \approx 1$ and a loaded surface of more than 10m^2, thus obtaining a value of $c_{pe} = -1.2$ in case of windward edges and $c_{pe} = +0.2$ in case of leeward edge. Consequently, we obtain two different values:

$$q_p(z_e) \cdot c_{pe} \cdot 7.5\ m \begin{cases} q_{s,\ top} = 1.84 \cdot (-1.2) \cdot 7.5 = -16.56 kN/m & \text{windward edge} \\ q_{p,\ top} = 1.84 \cdot 0.2 \cdot 7.5 = 2.76 kN/m & \text{leeward edge} \end{cases} \tag{5.13}$$

These loads have been jointly applied as shown in figure 5.6, considering two different load patterns for the two possible wind directions.

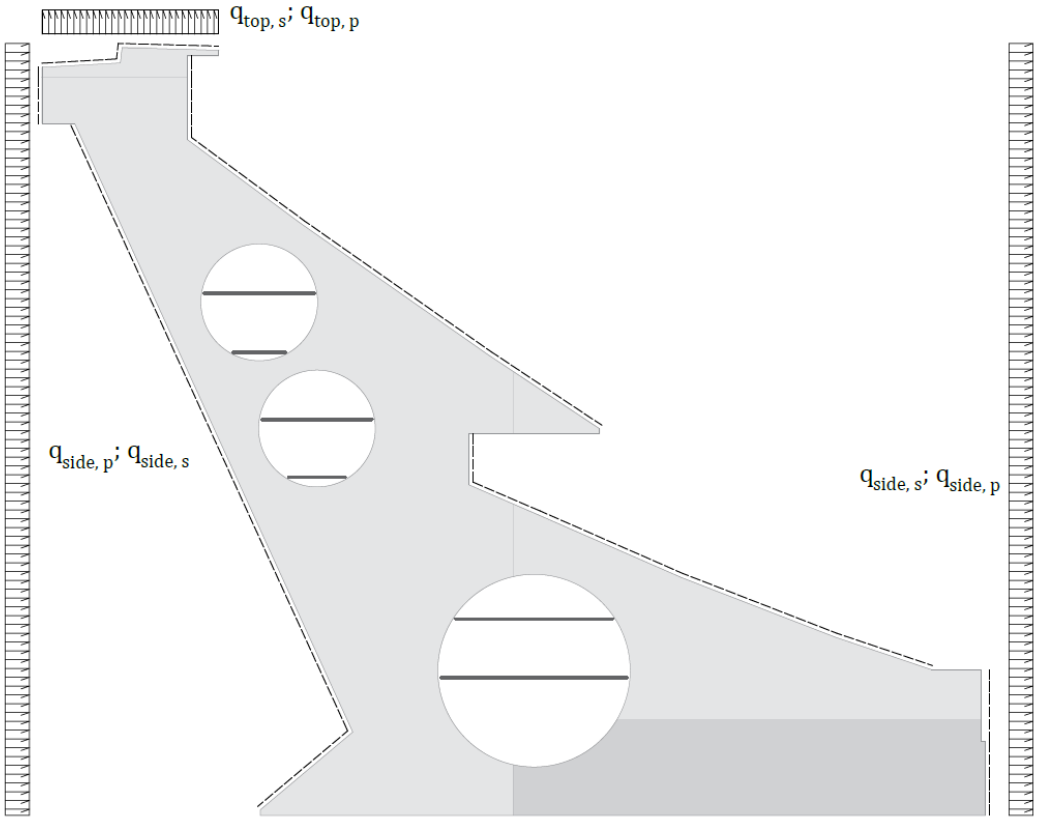

Figure 5.6: Distributed wind loads over the upright. Source: AutoCAD, own elaboration

5.1.8 Definition of ULS and SLS combinations

Each action of those just defined has been considered separately, assigning each of them to a specific load pattern and then to a specific load case, as will be shown in section 5.2.1. Then, load combination have been defined thanks to the specific tool in SAP2000. Given the level of simplification held for this analysis, it appears appropriate to briefly present these load combinations together with their results, in their respective sections of this document.

5.2 Analysis of the Upright

This section is structured by retracing the various phases followed in the development of the 2D model of the uprights. We have used the structural modelling software SAP2000 (version 21.0.2, build 1491, [11]). Then we will propose a summary of the results obtained from static and dynamic analysis. The 2D model reproduces only one upright, in particular the 8^{th} one: this can be considered as a standard case, as it has the same characteristics as the other uprights (with the exception of the first and last ones, that have some differences). This phase is preparatory for the determination the

parameters needed to define the simplified models in chapter 6, with specific regard for the modelling of the upright, with various levels of simplification.

5.2.1 2D upright model definition

To define the 2D model we referred to the information provided in the documents in the bibliography [15], [16] and [21], from which both the dimensions of the uprights, beams and other construction elements, and the materials, were extrapolated. Each upright has a thickness of 1 m and is made of concrete C35/45, while the beams are made of steel S355. These materials, whose parameters have been summarized in subsections 5.2.1.1 and 5.2.1.2, have been introduced directly from the software library.

5.2.1.1 Concrete C35/45

Table 5.4: Parameters assumed for concrete C35/45. Source [34] and SAP2000

C35/45 parameters	
Parameter	Value
$f_{ck}\ [MPa]$	35,0
$f_{ck,cubic}\ [MPa]$	45,0
$f_{cm}\ [MPa]$	43,0
$f_{ctm}\ [MPa]$	3,2
$f_{ck,0.05}[MPa]$	2,2
$f_{ck,0.95}[MPa]$	4,2
$E_{cm}\ [GPa]$	34,0
$G\ [GPA]$	14,167
Poisson - U	0,2
$\alpha\ [°C^{-1}]$	$1{,}0{\cdot}10^{-5}$
$\gamma_w\ [kN/m^3]$	24,9926

We have assumed an an elastic, linear and isotropic behaviour. We have not considered the variation of the concrete performances over time, since we do not have enough information to assess them precisely. Table 5.4 resumes its main parameters, that have been entered automatically from the SAP2000 software library, in compliance with the Eurocode [34] prescriptions.

5.2.1.2 Steel S355

Table 5.5 resumes the main parameters for steel S355, for which we have assumed an an elastic, linear and isotropic behavior. These have been entered automatically from the SAP2000 software library, in compliance with the Eurocode [36] prescriptions. We

Table 5.5: Resistance parameters for the steel used for cold-formed members according to the reference codes. Source [36]

S275 resistance parameters

Parameter	Values
$f_{yk}\ [MPa]$	355
$f_{uk}\ [MPa]$	510
$E_{cm}\ [GPa]$	210
$G\ [GPa]$	80,769
Poisson - U	0,3
$\alpha\ [°C^{-1}]$	1,2·10^{-5}
$\gamma_w\ [kN/m^3]$	76,973

did not considered the variation of the performances over time, since we do not have enough information to assess them precisely.

Subsequently we moved on to the definition of the sections. The upright consists of flat shell elements stressed along their plane: due to this it responds with a membrane behavior, while the shear deformation is not relevant in this case. From this point of view, the use of thick shell, thin shell or membrane elements in SAP2000 does not affect the results, as thick-plate or thin-plane formulation has no effect upon membrane (in plane) behaviour, only plate-bending (out of plane) behaviour. In the end, for the upright we defined a membrane-type area section named *TRIBUNE CLS - 1m*, with an overall thickness of 1m and a concrete C35/45.

Regarding the steel beams, these have been modeled as frame objects, whose sections are those of HEB beams (of type HEB 450, 500 and 600), which have been defined according to the classified parameters shown in figure 5.7 and in table 5.6.

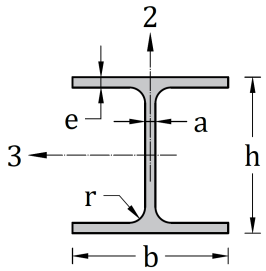

Figure 5.7: Reference scheme for the HEB section parameters shown in table 5.6 and 5.7. Source: www.oppo.it

Table 5.6: Characteristics of the employed steel HEB sections. Source: www.oppo.it

HEB sections, standard dimensions			
parameter	Section HE360B	HE450B	HE500B
h [m]	0,3600	0,4500	0,5000
b [m]	0,3000	0,3000	0,3000
e [m]	0,0225	0,0260	0,0280
a [m]	0,0125	0,0140	0,0145
r [m]	0,0270	0,0270	0,0270

For each upright there are two beams, placed side by side, supporting each horizontal slab: due to this we defined an equivalent section, whose height and flange thickness remain unchanged, while the core thickness and flange width are doubled. The resulting section is equivalent to the two side by side, since for the local axes 2 and 3 considered in the model neither the moments of inertia nor the distribution of the masses would change. The parameters of the steel beam sections thus defined are resumed in tables 5.7 and 5.8.

Table 5.7: Assigned dimensional parameters to the steel frame sections. Source SAP2000, own elaboration

Employed steel frame sections, assigned dimensions			
parameter	Section HE360B DOUBLE	HE450B DOUBLE	HE500B DOUBLE
h [m]	0,3600	0,4500	0,5000
b [m]	0,6000	0,6000	0,6000
e [m]	0,0225	0,0260	0,0280
a [m]	0,0250	0,0280	0,0290
r [m]	n.	n.	n.
material	S355	S355	S355

Table 5.8: Performances and characteristics obtained for the defined steel frame sections. Source: SAP2000, own elaboration

Employed steel frame sections, calculated parameters

parameter	unit	Section HE360B DOUBLE	HE450B DOUBLE	HE500B DOUBLE
Weight	kg/m	244	342	374
A_s	[m^2]	0,0349	0,0423	0,0465
I_{33}	[m^4]	8,351E-04	1,550E-03	2,085E-03
I_{22}	[m^4]	8,104E-04	9,367E-04	1,009E-03
I_{23}	[m^4]	0	0	0
W_3	[m^3]	4,640E-03	6,894E-03	8,340E-03
W_2	[m^3]	2,710E-03	3,122E-03	3,363E-03
$W_{pl,3}$	[m^3]	5,176E-03	7,723E-03	9,359E-33
$W_{pl,2}$	[m^3]	4,099E-03	4,758E-03	5,133E-03
ρ_3	[m]	0,1547	0,1914	0,2116
ρ_2	[m]	0,1524	0,1487	0,1473
$A_{v,3}$	[m^2]	0,0090	0,0126	0,0145
$A_{v,2}$	[m^2]	0,0225	0,0260	0,0260
J	[m^4]	6,007E-06	9,622E-06	1,198E-05

We now move on to the definition of the constituent elements of the 2D model. As previously said, the uprights were modeled with shell-thick elements: we have applied an optimized mesh, defined with the software Abaqus. With this software we have recreated the upright contour, modelling it as a shell and including the steel beams as frame elements. As boundary conditions we assigned external hinges placed with constant spacing along the base, while as external loads we have applied both the permanent loads (modeled as line loads) and the equivalent cable action (modeled as concentrated load), defined as described in sections 5.1.1 and 5.1.2. We then exploited the Abaqus meshing tool, creating a mesh of quadratic elements with in-plane behavior and quadrangular shape (or triangular, when necessary), with an average size of 80 cm. The mesh thus created was then exported to AutoCAD, refined, and imported in SAP2000. We opted for this software instead of Abaqus since it allows a better management of the load combinations, time-history simulations and data processing, as it is specifically developed for structural modelling. Special care was taken in keeping the edge nodes near the stands as equidistant as possible within each other, so as to systematically assign the concentrated loads representing the permanent action of the tribunes.

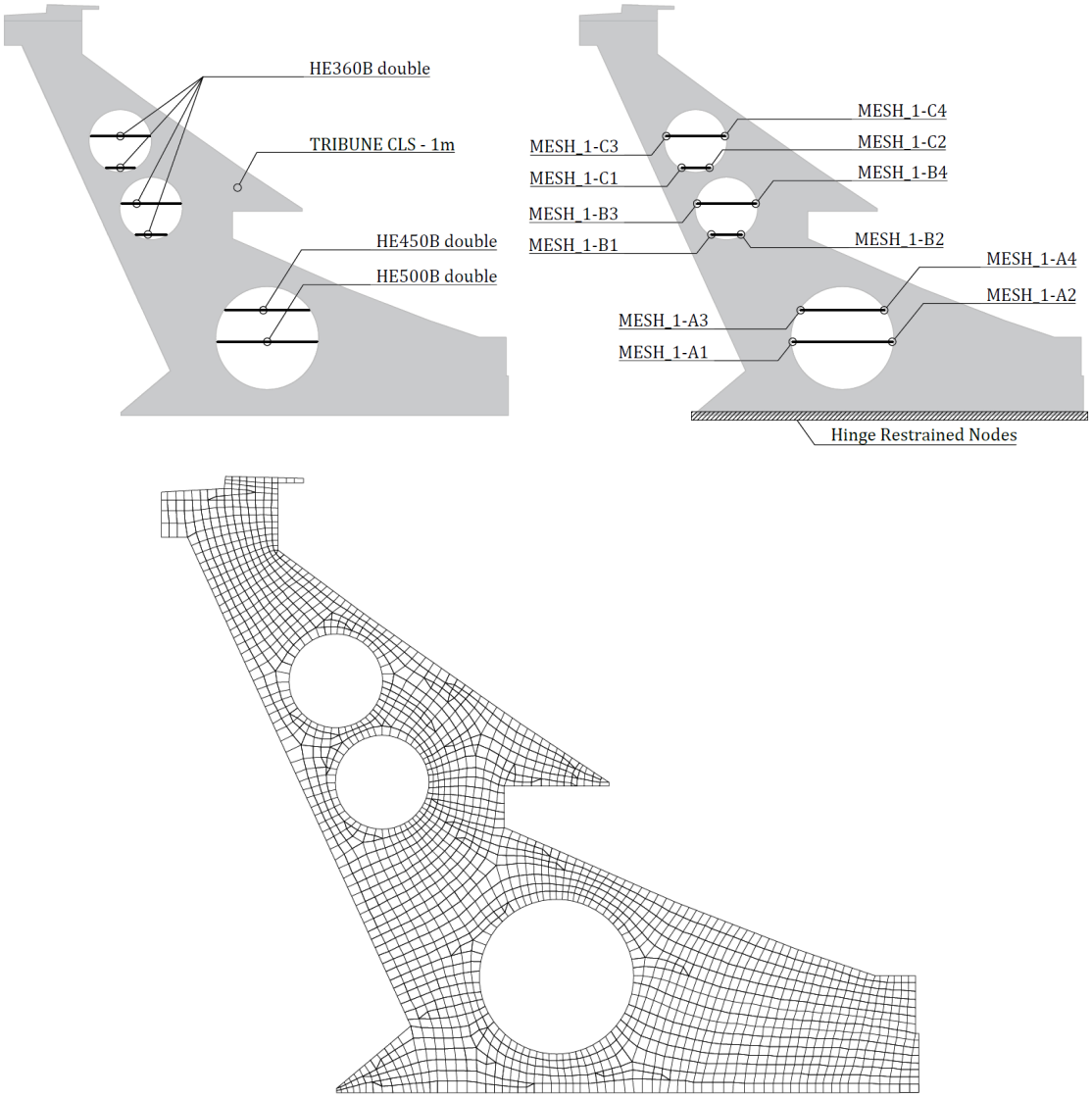

Figure 5.8: Reference scheme for the SAP200 model of the upright, showing (from above): the assigned sections, constraints and restraints, and the mesh of the upright. Source: AutoCAD; own elaboration

The beams were modeled as frame elements, each with a length of approximately 2m. Special mention should be made about the joints between beams and uprights: these are made up of steel hinges, anchored to the concrete uprights and hinged with the beams. Given their size, it was decided to consider this aspect. To do this, we defined body constraints, that can be applied to a set of joints that translate and rotate together as a rigid body to simulate rigid connections, to connect portions of a model that are defined by separate meshes, or to connect frames to shells. In this case we have assigned the body constraints between the frame end and the nearest upright node, horizontally spaced by 20cm (that is the distance between the insertion pin). The mesh, together with beams, sections and constraints, is shown in figure 5.8.

Regarding the external restraints, these are placed at the base of the uprights. Since constructive details about this part were not available, we have referred to what is stated in references [15] and [16]: the East stand is placed on a solid rock layer, in which concrete inserts have been made to tighten cracks and eventually replace lower-quality soil portions. We therefore opted to consider each upright foundation as a rigid element, for which we could expect a uniform ground response, without differential settlements. Consequently we can model the external restraints as a series of hinges at the nodes at the base of the uprights.

5.2.2 Load pattern assignment

The loads are assigned consistently with what has been seen in section 5.1. The following load patterns were then defined:

- **G1 DEAD**: contains the permanent loads of structural elements already modeled (such as beams and uprights): for this reason the self-weight coefficient is equal to 1.

- **G1 add**: contains permanent loads of structural elements that are not modeled described in section 5.1.1, because they do not significantly affect the structural response of uprights (such as stairs), or because they are omitted due to the reduction to 2 dimensions (such as the horizontal slabs). These elements are all counted as static actions.

- **G2**: contains the permanent loads of non-structural elements, which are inserted into the model in the form of static actions as described in section 5.1.1.

- **CABLE 33/34**: contains the equivalent action of the cables on the uprights, namely on the upper concrete support beam, as determined in section 5.1.2. This category is made up of both G1 and G2 type actions, already combined according to code prescriptions. This choice was made to simplify the model, since for the purposes of this analysis only a Seismic Limit State Combination is useful, as we will see later.

- **Q wind East**: contains the wind equivalent distributed load as shown in section 5.1.7. In this load pattern we refer to the case of a windward East facade and a negative pressure over the upright roof, while the West facade is consequently leeward.

- **Q wind West**: contains the wind equivalent distributed load as shown in section 5.1.7. In this load pattern we refer to the case of a windward West facade and

a positive pressure over the upright roof, while the East facade is consequently leeward.

- **Q cat. C5**: contains all the actions related to crowd overload, as determined in section 5.1.3.
- **Q cat. H**: contains the loads due to inspection and maintenance over the roof top of the East stand, as determined in section 5.1.4.
- **Q snow**: contains the snow load, as determined in section 5.1.5.

The loads have therefore been assigned consistently with what has been seen in section 5.1. The steel beams in the lower hole have an upward precamber of 0.1m, so as to counteract the action of gravitational loads and accomplish the prescriptions of the Serviceability Limit State without inducing any over-stress (as the beams are hinged). The camber was modeled by applying a thermal gradient to the frame elements, which was assessed from the static reference scheme of a hinged beam.

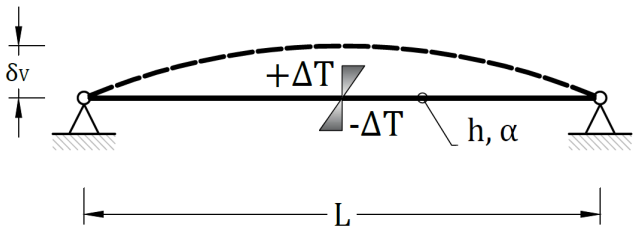

Figure 5.9: Static reference scheme for the assessment of the thermal gradient that induces an assigned precamber. Source: AutoCAD, own elaboration

By making reference to the static diagram 5.9, the curvature of the beam can be expressed as thermal curvature:

$$y''(x) = \chi(x) = -\chi_{TH} = -\frac{2\alpha\Delta T}{h} \tag{5.14}$$

Where χ is the overall beam curvature, χ_{TH} is the thermal curvature, α is the thermal expansion coefficient, and $2\Delta T/h$ is the thermal gradient applied to the beam. To solve the Euler-Bernoulli differential equation we need to integrate it 2 times:

$$y(x) = -\frac{2\alpha\Delta T}{h}\frac{x^2}{2} + Ax + B \tag{5.15}$$

And then to apply the boundary conditions, so as to determine the relation for the vertical displacement along the beam.

$$y(0) = 0 \quad \text{and} \quad y(L) = 0 \quad \longrightarrow \quad y(x) = -\frac{2\alpha\Delta T}{h}\frac{x^2}{2} + \frac{2\alpha\Delta T}{h}\frac{L}{2}x \tag{5.16}$$

The precamber is assigned: we have to calculate the vertical displacement at the middle of the beam and then reverse the resulting equation, in order to determine the unknown thermal gradient to be assigned in SAP2000, which is equal to $2\Delta T/h$.

$$y\left(\frac{L}{2}\right) = \delta_V = \frac{1}{4}\frac{\alpha \Delta T L^2}{h} \quad \longrightarrow \quad \frac{2\Delta T}{h} = \frac{8\delta_V}{\alpha L^2} \tag{5.17}$$

The precamber δ is of 0.1 m, both beams are made of steel (for which α is equal to $1.17{\cdot}10^{-5}\ C^{\circ}/m$): the only difference is the length L.

Table 5.9: Determination of the thermal gradient for an assigned precamber. Source: Excel, own elaboration

Evaluation of the thermal gradient

beam section	h [m]	δ_V [m]	L [m]	$2\Delta T/h\ [C^{\circ}/m]$
HEB450	0.45	0.1	11.41	525,32
HEB500	0.50	0.1	13.56	371,80

Results are shown in table 5.9. The steel beams are simply hinged, so that the applied thermal gradient produces only the desired precamber, without inducing any stress. Since the precamber is always present it is not affected by the scale factors related to load combinations. For this reason the thermal gradient has been aggregated to the load pattern *G1 add*, that in our case is always considered with a scale factor of 1.

5.2.3 Mass source assignment

Subsequently we moved on to the definition of the masses considered, according to the relation of Eurocode [30] for a Seismic Limit State combination:

$$G_1 + G_2 + \sum_i \psi_{2i} \cdot Q_i \tag{5.18}$$

Where the coefficients of each load type are the same exposed in table 4.3. Seismic masses are specified in the form of a mass source, that has been defined by considering the self masses from the modeled elements (such as shells and frames), together with the masses from the loads belonging to specified load patterns. In this case we can evaluate two limit situations:

- **MSSSRC1**. In the first case we consider only permanent loads, therefore the mass is defined as:

$$G_1\ DEAD + G_1\ add + G_2 \tag{5.19}$$

- **MSSSRC2**. In the second case we are going to evaluate the opposite scenario, including also the action of crowding overload, in accordance with its concomitant coefficient. Mass is defined as:

$$G_1\ DEAD + G_1\ add + G_2 + 0.6Q_C \tag{5.20}$$

In both cases the loads belonging to load pattern *G1 DEAD* are implemented as element self mass generated from the modeled elements. Thee other masses are defined from their specific load patterns, containing loads that are "converted" by the program into masses acting by dividing each load by a factor of 9.81.

5.2.4 Static analysis of the upright

Before proceeding with the static analysis of the model, it is then necessary to define the load cases. In this first phase the effects of each load were analyzed separately, thus defining a load case for each of the load patterns described in section 5.2.2. For each of them the same options have been maintained: linear analysis starting from unstressed conditions, as shown in the figure 5.10.

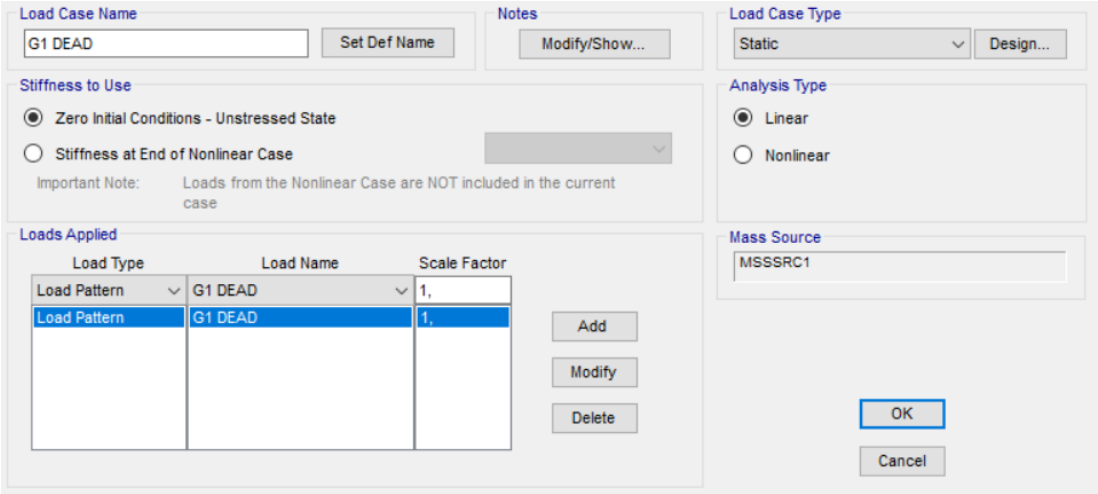

Figure 5.10: SAP200 information panel for the definition of the load case *G1 DEAD*, comprehensive of the dead loads from the modeled elements. Source: SAP2000 - own elaboration

We then moved to the definition of load combinations. As previously said, the aim of this analysis is to determine the parameters needed to define the simplified models discussed in chapter 6, that will be submitted to a seismic load combination. We thereby show and discuss in detail the results of a combination that includes only permanent loads, which are the ones that are included also in a seismic combination

(with the proper seismic action), while the results of other combinations will be briefly summarized in Annex. Considering the Eurocode prescriptions in [30], the combination results as:

$$G_1 + G_2 + S + \sum_i \psi_{2i} \cdot Q_i \tag{5.21}$$

Where G_1 are the permanent structural loads, G_2 are the permanent non-structural loads, and S is the seismic action. The crowd overload Q_{C5} has not been included in this section, since from the dynamic analysis resulted that it would have had a stabilizing effect on the oscillations, and therefore has not been considered neither in the simplified models nor their calibration.

For this reason the combination *base permanent* has been defined as shown in equation 5.22.

$$G1\ DEAD + G1\ add + G2 + CABLE\ 33/34 \tag{5.22}$$

Note that the action of the cable is calculated separately (as shown in chapter 4) and then decomposed as an equivalent static action (as shown in the 5.1.2), and is also the result of the same seismic combination. For comparison purposes, another load combination was then defined (named *G1+G2*), containing the permanent loads but without the action of the cable.

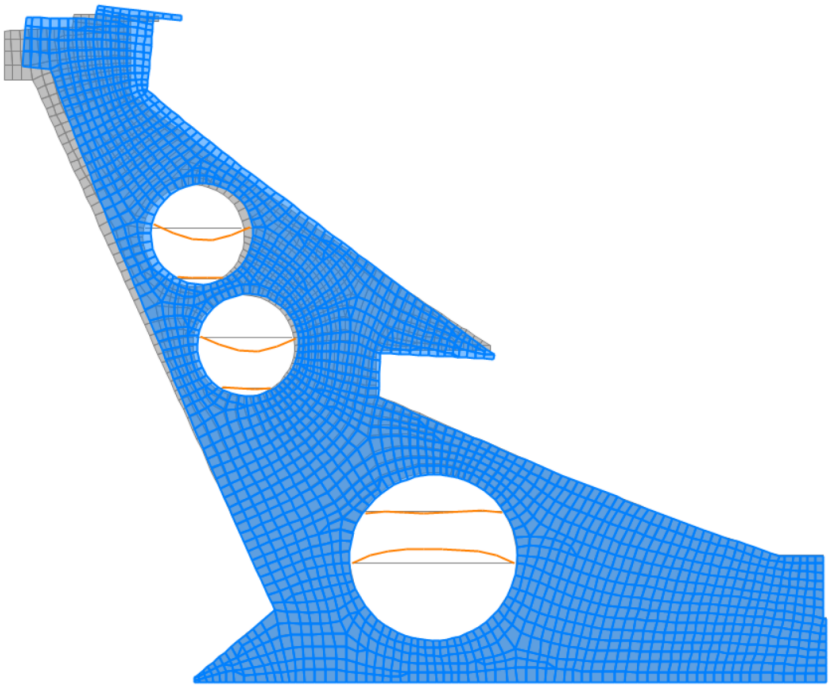

Figure 5.11: Deformed shape of the upright model under permanent loads. Displacements are amplified with a scaling factor of 50. Source: SAP2000 - own model

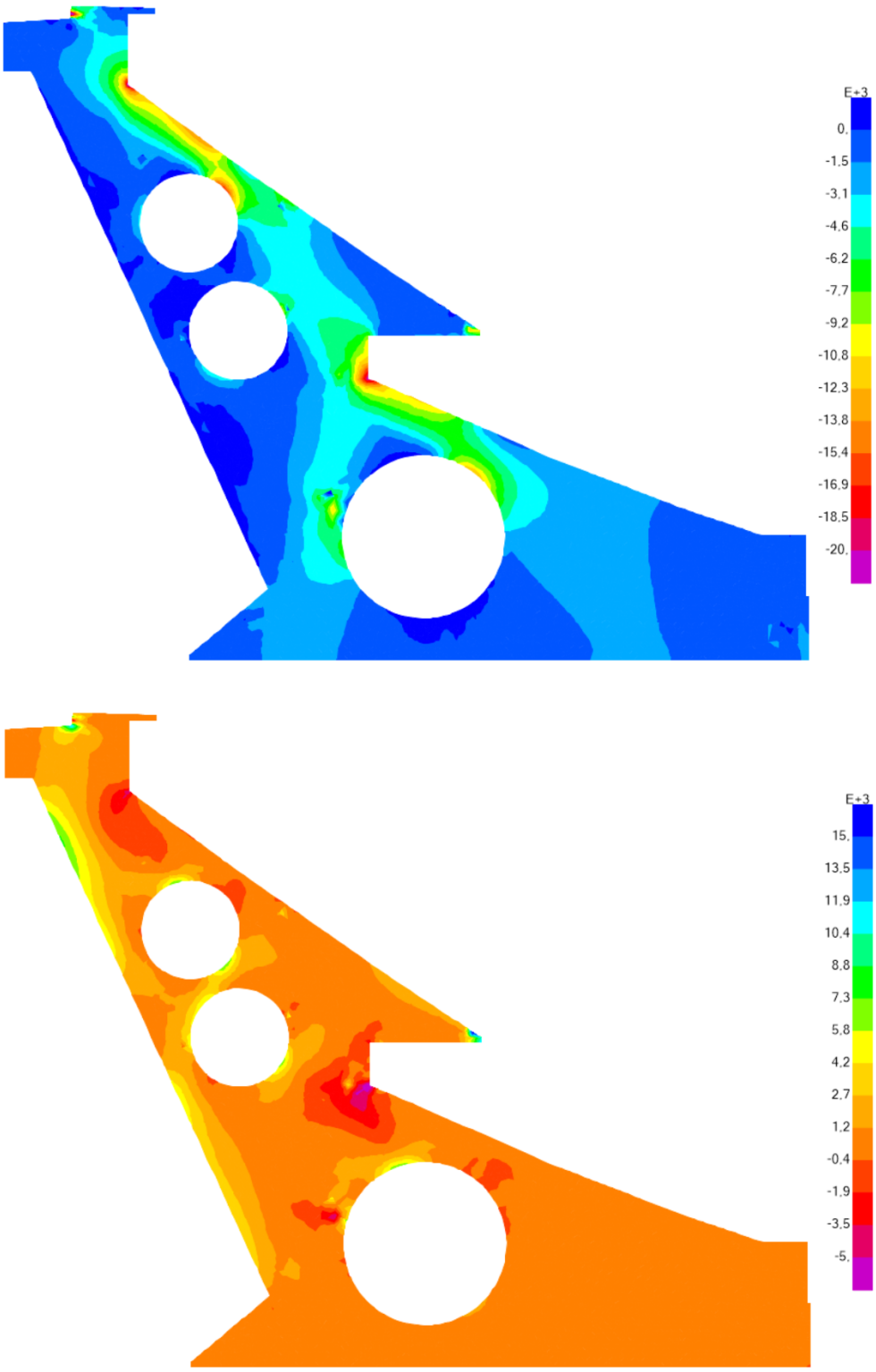

Figure 5.12: S_{min} (top) and S_{max} (bottom) stresses along the upright under permanent loads. The stresses are represented in kN/m^2. Source: SAP2000 - own model

From the results we can assess the static behavior of the upright. In the comments below, we refer to the West side of the East stand as the inside, while the East side will be referred as the outside. Regarding the steel beams, since they are not the object of this analysis we only point out that these undergo a parabolic bending moment (as expected for hinged beams), and compression forces caused by the deformation of the circular holes. From the deformed shape in figure 5.11, we can see that the beams in the lower hole have a positive sag due to their precamber, while the other ones have a negative sag. As for the upright, that same deformed shape confirms that the roof action and the gravitational loads have a mutual stabilizing effect. Without the cable action there is a displacement of 1.6cm towards the outside at the top of the upright. On the other hand, when we consider the roof action, at the same point we obtain a displacement of 3.6cm in the opposite direction. Moreover, the displacements at the first level of stands are of a lower order of magnitude when compared to the ones along the second level (about 2-3cm against 1-2mm). We can notice also that the upper part of the upright tends to retrace the behaviour of a cantilever shelf, as it progressively bends toward the inside.

From the study of the stress diagrams 5.12 we can assess how the action of the cable is transmitted along the upright, and compare it with the effects of the other static loads. We noted that, as suggested by the deformed geometry, under the action of the cable the external side undergoes positive stresses, while the internal side is compressed. The lower part of the upright is subjected to stresses of a lower magnitude than the second level, that are predominantly directed along the vertical direction. Note also the stress redistribution near the upper edge of the lower circular hole, as well as the two stress concentration points in proximity of the upper ends of each level.

This brief analysis over the 2D model confirmed that the static action of the roof affect the stress distribution, thus heavily conditioning the static behaviour of the structure, as mentioned in reference [15] and [16]. Other simulations have been carried out, with the aim to compare the cable action with the other live loads. For this purpose we have considered also a combination that includes permanent loads and also the crowd overload Q_{C5}. Moreover, 2 ULS combinations have been defined with the aim to maximize the horizontal displacement of the top of the upright toward the inside and the outside respectively. The static analysis of these combinations, whose results are briefly shown in annex E, led to the same conclusion exposed in this section.

5.2.5 Modal analysis of the upright

For the modal analysis we have defined two specific load cases, that have been named *MODAL 1* and *MODAL 2*, that perform an analysis with eigen vectors starting from unstressed initial conditions and defining the first 40 vibration modes for the structure.

- **MODAL 1** load case considers only permanent loads and their respective masses. These loads are included in the load patterns *G1 DEAD*, *G1 add* and *G2*. The results from this case were the most interesting for the purposes of this analysis and will be hereby discussed in detail.

- **MODAL 2** load case considers also the crowding overload (load pattern *Q crowd*) and its mass, multiplied by its concomitance coefficient of 0.6. It provided similar results to the first case, with the same vibration modes but slightly different periods. These have not been used in the calibration of simplified models and they will be shown in annex F.

The mass sources *MSSSRC1* and *MSSSRC2* are the same defined in section 5.2.3, and have been assigned to *MODAL 1* and *MODAL 2* respectively.

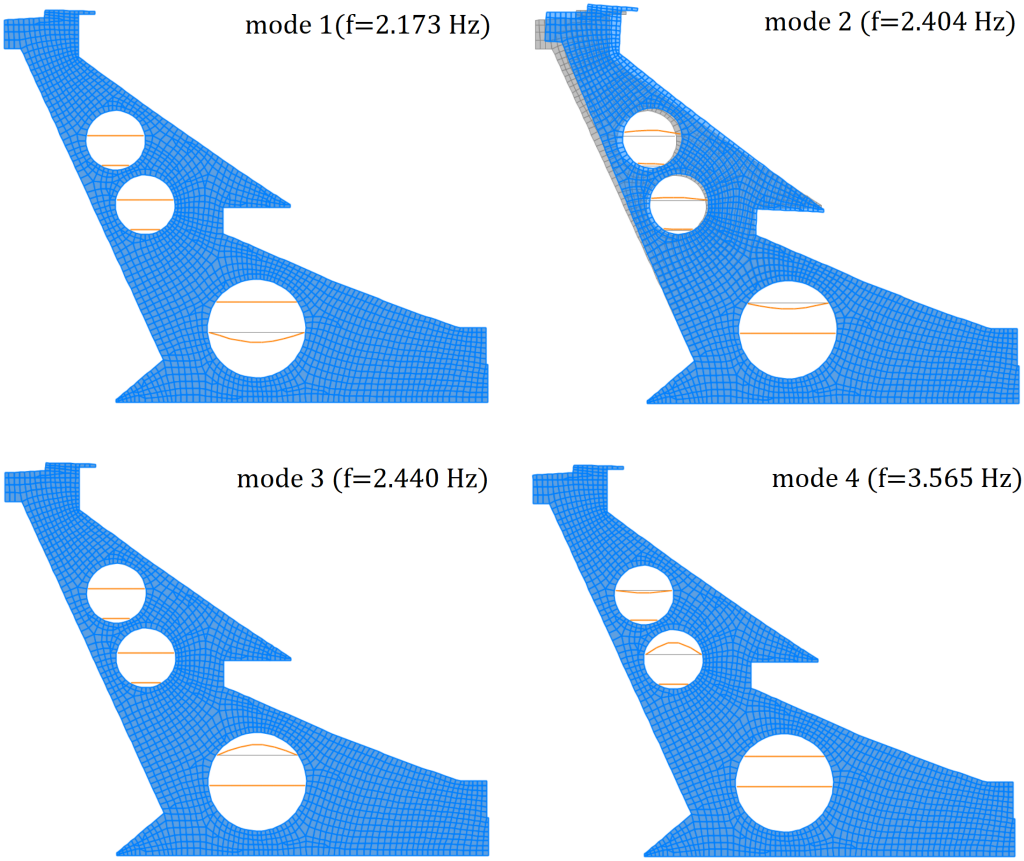

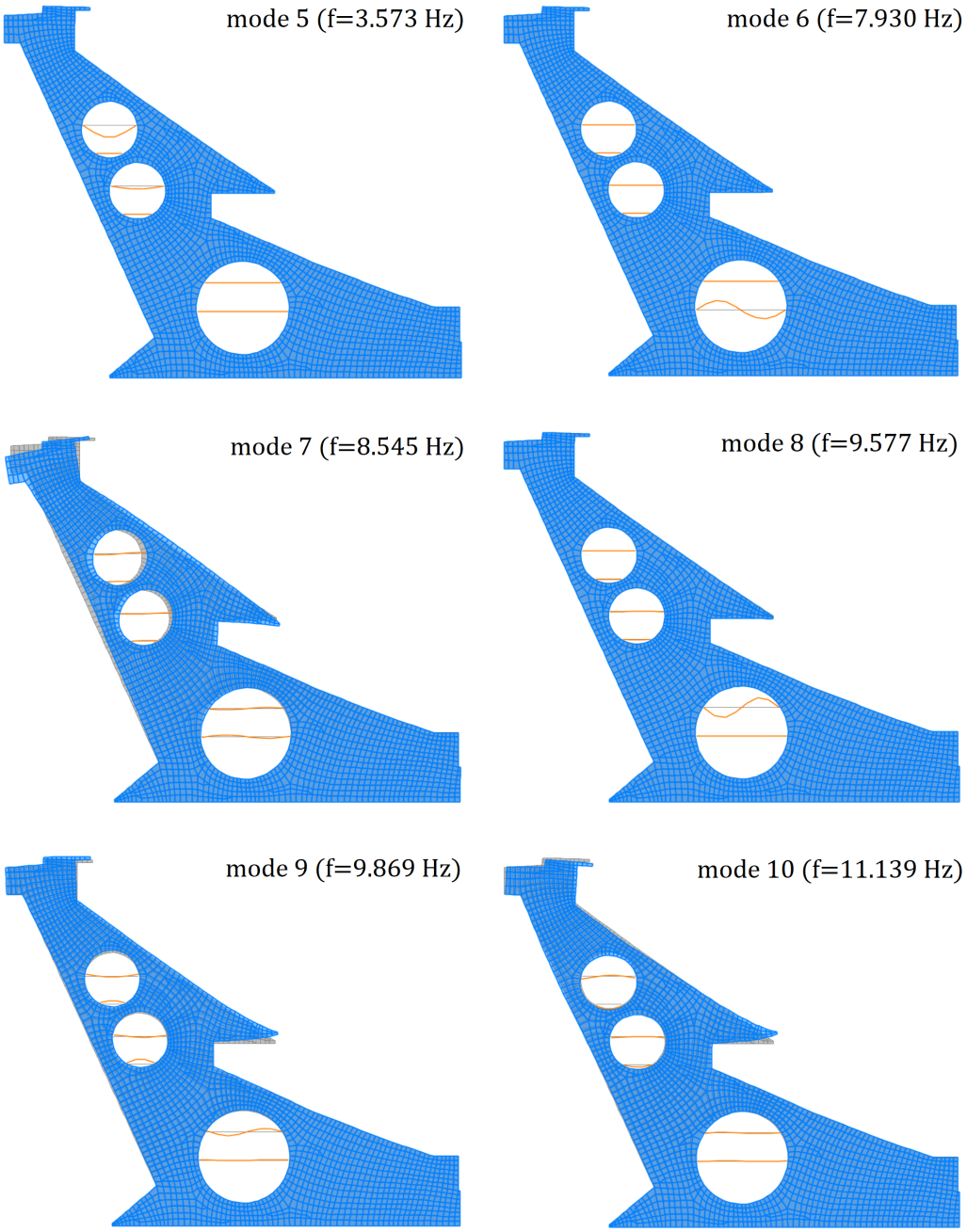

Figure 5.13: First 10 natural modes of the cantilever stand. Each mode is suitably scaled to display the deformed geometry. Source: SAP2000, own elaboration

Table 5.10: Summary of periods and modal participating mass ratios for *MODAL 1* load case, including only permanent load in seismic mass determination. Source: SAP2000, own elaboration

Modal participating mass ratios

mode	T [sec]	mass ratios U_x	$\sum U_x$	U_z	$\sum U_z$	R_y	$\sum R_y$
1	0,4602	0,0000	0,0000	0,0183	0,0183	0,0006	0,0006
2	0,4160	0,3134	0,3134	0,0356	0,0538	0,4597	0,4603
3	0,4098	0,0035	0,3169	0,0213	0,0751	0,0025	0,4628
4	0,2805	0,0003	0,3172	0,0064	0,0815	0,0002	0,4630
5	0,2799	0,0043	0,3215	0,0126	0,0941	0,0000	0,4630
6	0,1261	0,0006	0,3221	0,0003	0,0943	0,0009	0,4639
7	0,1170	0,1864	0,5085	0,0408	0,1351	0,0204	0,4842
8	0,1044	0,0004	0,5089	0,0114	0,1465	0,0013	0,4855
9	0,1013	0,0070	0,5159	0,3518	0,4983	0,0102	0,4957
10	0,0898	0,1197	0,6356	0,0401	0,5384	0,0267	0,5224
11	0,0832	0,0000	0,6356	0,0010	0,5394	0,0000	0,5224
12	0,0735	0,0001	0,6357	0,0002	0,5396	0,0000	0,5224
13	0,0735	0,0002	0,6359	0,0007	0,5402	0,0000	0,5224
14	0,0720	0,0009	0,6368	0,0004	0,5406	0,0002	0,5226
15	0,0629	0,0490	0,6858	0,0412	0,5819	0,0043	0,5269
16	0,0592	0,0001	0,6859	0,0011	0,5830	0,0001	0,5270
17	0,0511	0,0004	0,6863	0,0022	0,5852	0,0001	0,5271
18	0,0460	0,0178	0,7040	0,0523	0,6374	0,0022	0,5293
19	0,0433	0,0503	0,7543	0,0002	0,6377	0,0264	0,5557
20	0,0373	0,0000	0,7543	0,0000	0,6377	0,0000	0,5557
21	0,0372	0,0020	0,7563	0,0004	0,6381	0,0009	0,5566
22	0,0363	0,0001	0,7564	0,0005	0,6385	0,0003	0,5569
23	0,0343	0,0148	0,7712	0,0041	0,6427	0,0192	0,5761
24	0,0314	0,0173	0,7885	0,0062	0,6489	0,0009	0,5770
25	0,0309	0,0423	0,8308	0,0140	0,6629	0,0014	0,5784
26	0,0289	0,0017	0,8325	0,0307	0,6936	0,0014	0,5798
27	0,0273	0,0010	0,8334	0,0059	0,6996	0,0016	0,5814
28	0,0266	0,0099	0,8433	0,0057	0,7053	0,0107	0,5921
29	0,0257	0,0000	0,8434	0,0011	0,7064	0,0008	0,5930
30	0,0253	0,0003	0,8437	0,0002	0,7066	0,0000	0,5930
31	0,0252	0,0002	0,8438	0,0008	0,7074	0,0008	0,5938
32	0,0252	0,0000	0,8439	0,0000	0,7074	0,0001	0,5939
33	0,0244	0,0053	0,8492	0,0005	0,7079	0,0014	0,5953
34	0,0237	0,0027	0,8519	0,0025	0,7104	0,0004	0,5957
35	0,0229	0,0006	0,8525	0,0001	0,7105	0,0001	0,5957
36	0,0228	0,0003	0,8528	0,0003	0,7108	0,0008	0,5965
37	0,0228	0,0000	0,8528	0,0000	0,7108	0,0000	0,5965
38	0,0226	0,0017	0,8545	0,0006	0,7114	0,0006	0,5971
39	0,0220	0,0138	0,8683	0,0170	0,7283	0,0001	0,5971
40	0,0204	0,0001	0,8684	0,0011	0,7294	0,0003	0,5975

The most relevant modes are reproduced in figure 5.13, while a summary of the modes obtained is shown in table 5.10. From the analysis of the vibration modes emerged that numerous modes involve only the horizontal steel beams, with oscillations that are typical of hinged and uniformly loaded beams. Without considering those modes, we could see that the remaining ones retrace two different behaviours:

- The first that we found among those not related to the steel beams, retrace remotely the behaviour of a cantilever shelf (in particular mode 2). These are characterized by higher periods and higher modal masses. We noted also that mostly the upper part of the upright oscillates, while the lower portion is less involved, as it is almost not mobilized.

- Other modes have a more specific behavior for this particular structure, which is difficult to trace back to a basic static scheme. However, these ones are characterized by considerably lower periods and modal masses than the other type, and appear only from mode 15 onward.

The modes are all characterized by a rather high period (around 0.4 sec), due to the geometric conformation of the upright. Between the first 10 vibrating modes, 7 involve only these reinforcement beams: only mode 2, mode 7 and mode 10 involve part of the cantilevered concrete structure. As can be seen from table 5.10, these mobilize only a small percentage of the total mass of the upright (31% for mode 2, 18% for mode 7, 12% for mode 10). This is probably due to the fact that the lower part of the upright, which represents the largest percentage of the total mass, is not involved in these modes. Considering the first mode, although it mobilizes only 31.3% of the total mass, this is equal to about 67 % mass of the upper part of the upright, that acts as a cantilever shelf while the lower part stands still.

Chapter 6

Creation of the simplified models

In this chapter we will explain how we assembled the finite element models that we have studied, discussing the criteria applied for their development, and dealing with their assembly process. Finally, we will define the static loads applied, and we will describe how we set the simulations for the multi-support analysis of the seismic action. For the sake of brevity, we omit all the considerations already explained in previous chapters. Throughout the chapter we will refer to the direction parallel to the cables (roughly the East-West axis) as the longitudinal direction, that in the simplified models corresponds to the x axis (directed towards the West). The direction normal to the cables (roughly the North-South axis) will be referred as transverse direction, that in the simplified models is directed towards the z axis.

6.1 MODEL C - Realistic model

The first model that was developed is the the most similar to the real structure, as it acted as a reference case to assess the other ones. However, we still applied some simplifications, that were needed to reduce its complexity and the computational load. This procedure was mandatory, otherwise it would not have been possible to perform all the time-history simulations within acceptable times. Before going deep into the modelling, we explain some considerations and assumptions that allowed us to simplify the model.

6.1.1 Analysis and simplification of the structural layout

The aim of this analysis is the assessment of the response to the longitudinal component of the seismic action. We do not consider the transversal component, nor the vertical one, so that the model is optimized to retrace the structural response for the only direction considered. As a first simplification, we omitted those structural elements and

construction details whose contribution would be negligible in the structural response. The structural layout is made out from a basic portal structure repeated in parallel, that consists of an East cantilever upright, 2 adjacent cable pairs with a roof portion and the West upright, built along the hillside. This configuration counteracts both gravitational and longitudinal loads, while resistance to transversal load is ensured by means of continuous horizontal concrete slabs, connecting the uprights between them.

Furthermore, the suspended cables are linked between them and the suspended roof by 2 composite concrete slabs and 2 steel trusses: hence we can assess the structural response to longitudinal actions by simply analyzing the basic portal structure alone. Although in doing so we neglect possible differential displacements, these are limited as the uprights are linked with continuous elements. On the West side of the structure, the cable supporting beam is connected to the rocky embankment through vertical uprights, that follow its profile. Thanks to several steel tendons radially injected into the rock, the cables transmit their loads directly to the massif, so that the seismic action is directly distributed from the ground terrain to the cables' anchors. Since the rest of the West stand is built up separately and is only partially supported by the uprights, this part can be modeled as a simple hinge restrain.

Going into detail, the East stand upright can be modeled as it is (with the floor beams as well), while transversal elements, such as horizontal floors and tiers, act only as gravitational loads. Cables are linked and symmetrically placed in-between the uprights. Due to the continuous connection provided by concrete slabs and truss beams, we can assume the same response for nearby cables, thus simplifying them with an equivalent element. The concrete slabs consist of several prefabricated elements, placed in series along the cables and hinged together, and their main contribution to the structural response is the stabilizing effect due to their weight. Since their bending stiffness is extremely low due to the hinges and we do not have enough information to assess it, we acted in favour of safety and neglected it. Therefore, slabs and truss beams (that do not affect the response to longitudinal forces) have been included only as gravitational loads.

We wanted to analyse the "typical" scenario, so that we took as reference the 8^{th} upright with cable pairs 33-34 and 35-36 (which are the most stressed in relation to their design force). Figure 6.1 shows the conceptual layout of the "realistic" model, whose response has been taken as reference for the assessment of other simplified models. We should point out that it does not reproduce the overall structural response, since we were focused only on longitudinal seismic actions, thus neglecting other aspects of the structural behaviour: for instance, a transversal seismic action would involve the whole structure, that should be consequently included in the model. On the other hand, if we

want to study the effects of the vertical component we could consider the contribution of the cantilever stand as negligible, and perform a dynamic analysis of the cable roof only.

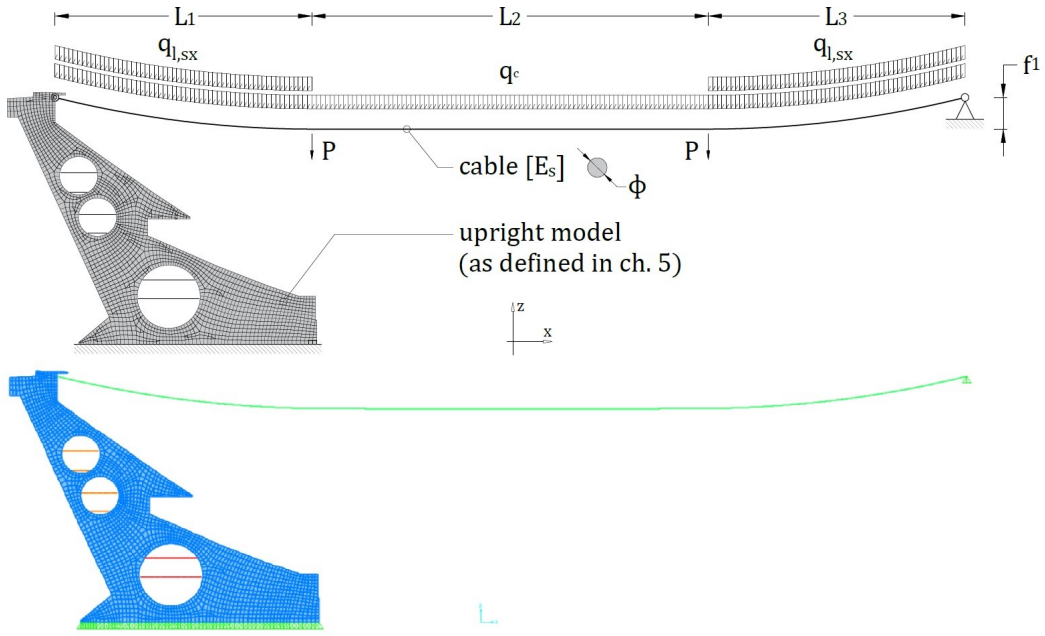

Figure 6.1: General layout of model C (realistic model) and detail of its implementation in SAP2000. Source: own design

6.1.2 Realistic model of the cantilever upright

Regarding the modelling of the upright, we are going to retrace what was previously done for the static analysis of the East stand, which was laid down and performed on the basis of these simplified models. For the sake of brevity we provide only a brief summary of the main characteristic of the upright model, making reference to what was already explained in section 5.2.1. The upright has been modeled with a mesh of 1m-thick area elements and is restrained by means of several hinges located at its base. The coupled steel beams have been included as frame elements, to which we applied a thermal gradient to reproduce the precamber. The connection between beams and upright has been modeled with body constraints. Other elements such as bleachers, stairs, and the cable linking beam are included only in the form of static actions.

6.1.3 Realistic model of the cables

As already mentioned, the model includes 2 pairs of adjacent cables that belong to the influence area of the upright. We have included both of them by means of a single

equivalent cable that has been defined, so that its stiffness module EA is equal to the sum of each cable stiffness module. Considering cables 33, 34 35 and 36, EA is equal to:

$$EA_{tot} = 4EA = 4 \cdot 821 = 3284\ MN \tag{6.1}$$

Since the cable resistant cross-section is made of steel strands we have adopted a customized material with a strength of 1575MPa, which was calculated from the data provided by the manufacturer as the ratio between the cable minimum breaking load of 7720kN and the metallic cross-section area of 4902mm^2 (both summarized in table 4.1). As for the elastic modulus E, we assumed a value of 210GPa. Supposing a circular cross-section, we calculated area and radius as:

$$A_{eq} = \frac{EA_{tot}}{E} = \frac{3284000}{2.1 \cdot 10^8} = 0.0156\ m^2 \tag{6.2}$$

$$\Phi_{eq} = \sqrt{\frac{4A_{eq}}{\pi}} = \sqrt{\frac{4 \cdot 0.0156}{\pi}} = 0.141\ m \tag{6.3}$$

With these data we defined a cable element section, called *CABLE 4D - 86mm*. Since this is an equivalent section, we had to overwrite the self defined load ans mass by assigning them a multiplication factor of 0 as property modifier.

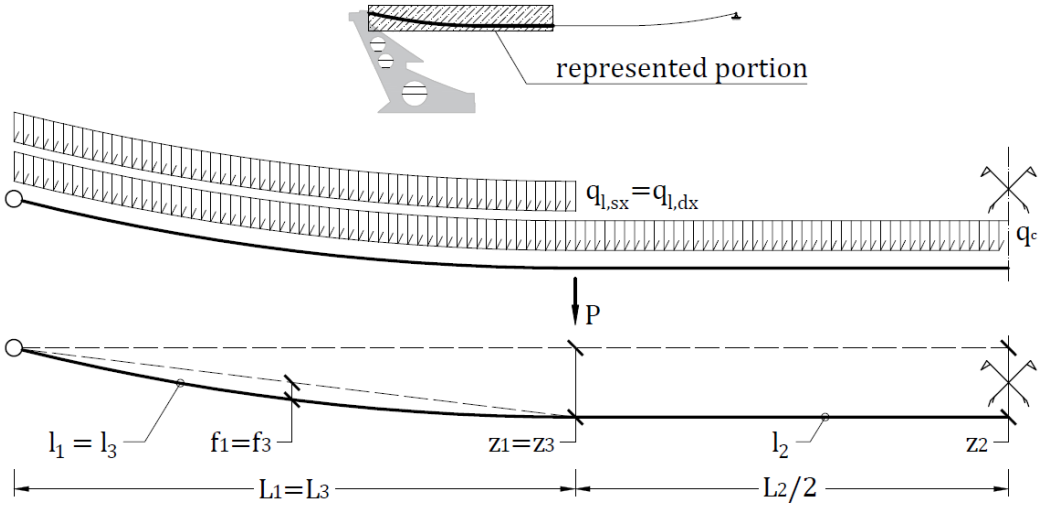

Figure 6.2: Reference scheme for the cable preliminary design values assigned in SAP2000. Source: own design

The cable's anchor system has been simplified with regard to what defined in section 5.1.2, since that level of detail is not decisive in the structural response: we directly hinged the modeled cable to a node of the upright mesh. To include the cable in the model and solve the static problem SAP2000 performs a preliminary design, calculating the cable geometry with the catenary equation. The static loads applied are those due

to a seismic combination that have been already determined in section 4.1. Cables have a decreasing sag due to the 1% roof cross-slope, and consequently are subjected to an increasing horizontal force from pair to pair. For adjacent pairs this difference is almost negligible, so we assumed in our model the lower sag between them, which in this case is the one for cables 33-34. The external loads over the equivalent cable have been multiplied by 4 with respect to what seen in 4.1, as it represents 4 cables.

Table 6.1: External loads over the cable according to a Seismic Limit State combination

Cable loads	
load id.	value
$q_{l,sx}$ [kN/m]	46,88
$q_{l,dx}$ [kN/m]	46,88
q_c [kN/m]	1,63
P [kN]	24,61

Table 6.2: Cable geometric parameters for the model assembly

Geometric parameters	
parameter id.	value
L_1 [m]	57,00
L_2 [m]	88,00
L_3 [m]	57,00
L_{TOT} [m]	202,00
f_1 [m]	1,66
f_2 [m]	0,13
f_3 [m]	1,66
z_1 [m]	7,09
z_2 [m]	7,22
z_3 [m]	7,09

Table 6.1 shows the loads applied to the cables, while table 6.2 contains the assigned geometric parameters, defined according to the notation in figure 6.2. Since the truss beams divide the cable into 3 successive catenary curves, to define its geometry in SAP2000 we had to divide it consistently. For each part we applied all the known parameters to the command window shown in figure 6.3, namely the external loads, the location of the cable ends, the maximum sag. The preliminary results shown during the preliminary design were extremely close to what obtained in section 4.2.2, thus proving once more that the the parabolic equation represents an acceptable approximation. In defining the cable we divided it into equal distinct cable elements with an horizontal projected length of about 1 m, and we adopted as reference the deformed

geometry so that displacements and deformations are measured with respect to the cable configuration under permanent loads.

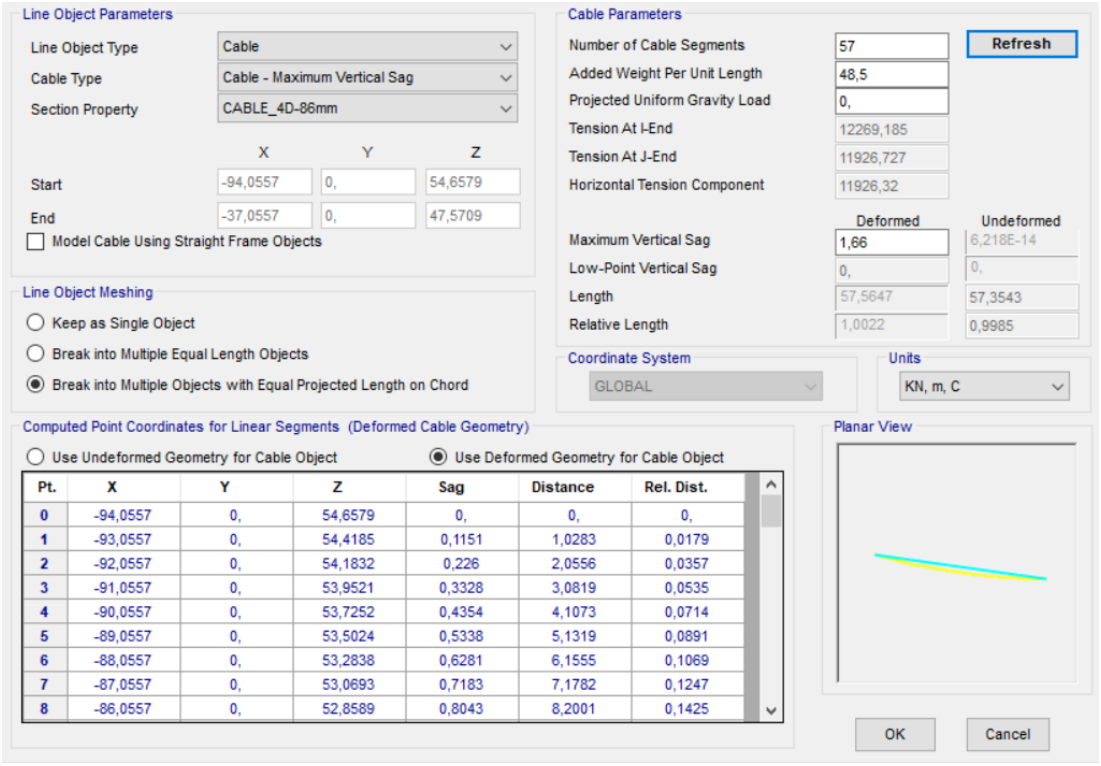

Figure 6.3: SAP2000 command window for the cable preliminary design, in this case the first part of the cable. Source: SAP2000, own design

6.1.4 Assigned static loads and masses

The static loads assigned to the model include permanent structural and non-structural loads, that have been combined according to a seismic load combination. Moreover, we had to define 2 load patterns in preparation for the multi-support analysis. This is performed by assigning a ground motion function to a given load pattern, whose loads are a unitary base displacement related to that function. We therefore created the following load patterns:

- **G1 DEAD**, that contains the permanent structural loads of the structural elements included in the model, namely the cantilever upright and the steel beams (as defined in section 5.2.1).

- **G1 add**, that contains the permanent structural loads from structural elements that have not been modeled. These have been calculated as exposed in section 5.1.1, whose values are summarized in table 5.1, making reference to the scheme in figure 5.1.

- **G2**, that contains the permanent loads due to the weight of non-structural elements acting over the East stand. These have been calculated as exposed in section 5.1.1, whose values are summarized in table 5.1, making reference to the scheme in figure 5.1.

- **CABLE 33-34 SLS**: that contains the static loads over the cable, determined according to a seismic limit state combination as shown in section 4.1. Their values are the same as defined in table 6.1 and figure 6.2 in the previous section. While naming the load pattern we referred to "SLS" as Seismic Limit State, since the Serviceability Limit State was no longer involved. This agreement has been maintained for all the simplified models defined in SAP2000.

- **EAST DISPLACEMENT**, that contains the 1m displacement towards the x axis, applied to the base of the cantilever upright.

- **WEST DISPLACEMENT**, that contains the 1m displacement towards the x axis, applied to the West support of the cable.

Once the loads have been assigned, we defined a load case that produces the static analysis of the model, thus providing the initial conditions for the multi-support analysis. We thereby created a non-linear static load case named *G1 + G2 + Cable 33-34*, that corresponds to a seismic combination defined in compliance with the Eurocode [37] requirements. As described in chapter 5 the worst scenario involves only the load patterns related to permanent loads.

Figure 6.4 shows the setting adopted in the SAP2000 command window. Note that load pattern *CABLE 33-34 SLS* includes already combined loads. For cable elements SAP2000 automatically considers large displacements and P-Delta effects in the non-linear analysis, so we did not have to specify any geometric non-linearity parameter. The results of the static analysis over all the models will be discussed in detail and compared in chapter 7. Regarding the mass source, this was defined in compliance with the Eurocode [30] prescriptions, for which we combined only permanent loads. The masses related to the load pattern *G1 DEAD* have been included as element self masses, as these are determined from the modeled elements. Other masses related to load patterns *G1 add* and *G2* are instead obtained from the applied static loads, by dividing for 9.81. The mass source thus defined was named *MSSSRC1*.

For a seismic combination live loads are multiplied by they concomitance coefficient Ψ_{2i}, which for the actions considered (wind, roof maintenance, snow, thermal) is zero, except for the crowd load. In this case is equal to 0.6, however the analyses performed over the East stand (discussed in sections 5.2.4 and 5.2.5) have shown that this action

has a stabilizing effect over the upright oscillations, thus limiting the range of increase of the cable tension (which is strictly related to the upright free-end displacements). Therefore we did not included this action in the seismic combination.

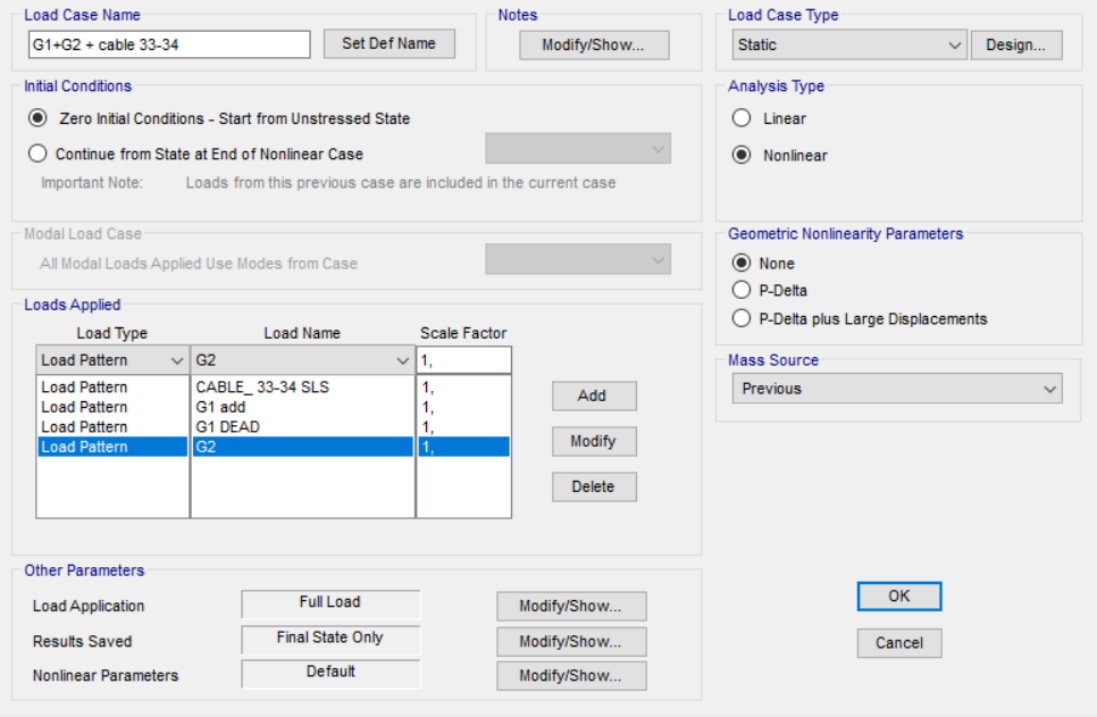

Figure 6.4: Model C, command window of the non-linear load case for the analysis of static loads. Source: SAP2000

6.2 MODEL B1 - First simplified model

Model B1 represents a first simplification of the realistic model. In this phase we tried to reduce the computational load by simplifying the support structure, leaving the cable unchanged. In fact, the cantilevered upright represents a considerably complex element, as it comprises a mesh of several hundred elements for which the software needs to determine stresses and strains at each iteration. If, as in our case, the goal is the study of the cable, these data are not useful and we can therefore find a way to reduce this data.

6.2.1 Conceptual definition of model B1

In this section our discussion continues from what previously stated in section 6.1.1. As described in sections 5.2.4 and 5.2.5 the upper part of the upright behaves like a cantilever beam, while the lower part stands still almost like a rigid basement. We

have therefore substituted the upright with a cantilevered shelf, whose dimensions, material, and other parameters have been calibrated through the results of the upright static and modal analyses performed over the 2D model of the upright in chapter 5. Since in this phase we wanted to simplify only the supporting substructure, the cable remains unchanged and is now hinged to the cantilever free end. The cantilever beam has been modeled using frame elements with constant section. To size it we made reference to the upright bending stiffness against the cable action, obtained from the static analysis of the upright model defined in section 5.2.1. The most critical point was the mass distribution, that cannot be reproduced with this method, as in the upright the mass is not uniformly distributed along its height, due to its variable width. To solve this problem we committed a rough approximation, having assigned an equivalent concentrated mass to the cantilever free end, whose value has been calibrated according to the fundamental natural period of the shelf. This simplified model was conceived assuming that the designer has already performed static analyses over rather thorough models, from which he obtained the information needed to calibrate the simplified model. This hypothesis is plausible as those analyses are easier to set up and are much less time consuming than the dynamic multi-support analysis.

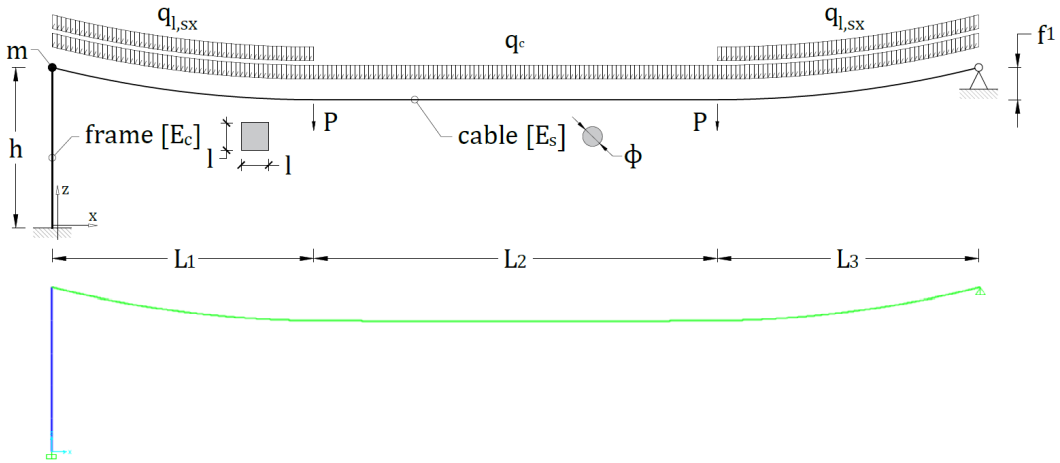

Figure 6.5: General layout of model B (with cable and equivalent cantilever beam) and detail of its implementation in SAP2000. Source: own design

6.2.2 Equivalent cantilever beam

The equivalent shelf has been sized according to the upright bending stiffness against the cable action. To assess its value we performed a static analysis of the same model defined in section 5.2.1 where we applied an horizontal incremental static concentrated load at the cable attachment point and measured the corresponding displacement of the upright.

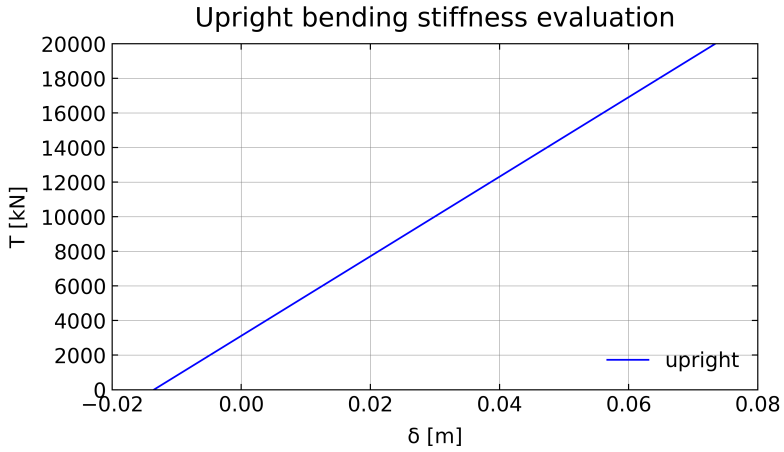

Figure 6.6: Upright load/displacement curve for an horizontal force applied at the cable attachment. Source: own design

Figure 6.6 shows the load-displacement function (its points have been gathered in a table presented in annex E). As expected, the upright has a linear behaviour with a measured stiffness of 230000kN/m. We then assumed this value as the bending stiffness of the cantilever, thus consequently determining the other parameters.

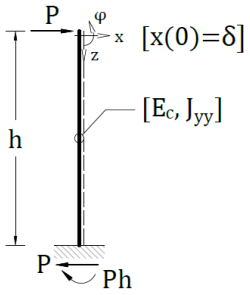

Figure 6.7: Static scheme of a cantilever beam with a orthogonal force at its free end. Source: own design

By applying the bending moment function of the cantilever structure in figure 6.7 to the Euler-Bernoulli differential equation we obtain (we adopted this formulation since we assumed that the shear deformation is negligible, compared to the deformation due to bending moment):

$$M(z) = -Pz \quad \longrightarrow \quad x''(z) = -\frac{M(z)}{E_c J_{yy}} = \frac{Pz}{E_c J_{yy}} \tag{6.4}$$

This problem can be solved by integrating twice and applying the boundary conditions related to the cantilever constraint.

$$x(h) = 0 \quad \text{and} \quad x'(h) = 0 \tag{6.5}$$

We therefore obtain:

$$x(z) = \frac{P}{6E_c J_{yy}} z^3 + Az + B \tag{6.6}$$

Where:

$$A = -\frac{Ph^2}{2E_c J_{yy}} \quad \text{and} \quad B = \frac{Ph^3}{3E_c J_{yy}}$$

We can calculate the displacement δ at the free end as:

$$\delta = \frac{Ph^3}{3E_c J_{yy}} \tag{6.7}$$

We then substitute this expression into the equation for the bending stiffness K, which is the ratio between applied force P and node displacement δ:

$$K = \frac{P}{\delta} = \frac{3E_c J_{yy}}{h^3} \tag{6.8}$$

In our case we assumed:

- As for h, we referred to what has been discovered after the static and modal analyses of the upright seen in sections 5.2.4 and 5.2.5. As previously mentioned, the lower level of the upright behaves roughly like a rigid basement, while the second level behaves like a cantilever. Therefore, we have assumed the height of that second level as the height of the equivalent shelf, thus assuming h equal to 35m.

- As mentioned, K is equal to 230000kN/m.

- As for E_c we have considered that the upright is made of reinforced concrete, and we consistently have assumed the value suggested by the Eurocode [30] of 34000MPa for C35/45 concrete.

We could calculate the inertia as:

$$J_{yy} = \frac{h^3 K}{3E_c} = \frac{35^3 \cdot 230000}{3 \cdot 34000 \cdot 10^3} = 96.68\ m^4 \tag{6.9}$$

Assuming a square section, we could define its size as:

$$J_{yy} = \frac{l^4}{12} \quad \text{and} \quad l = (12J)^{1/4} = (12 \cdot 96.68)^{1/4} = 5.84\ m \tag{6.10}$$

To summarize, the equivalent shelf has a height h of 35 m, an elastic modulus E of 34000MPa, and a square horizontal section with a side l of 5.84m. This section has been modeled with 5m length frame elements, for which we assigned a section as described

and a concrete C35/45, as described in section 5.2.1.1. A clamped support has been applied to the base node. Since this is an equivalent section, we have set as property modifiers a multiplication factor of 0 for both self mass and self weight.

6.2.3 modelling of the cables

The cable remains unchanged from what defined in model C, which is the reference case. The only variation is that now is hinged to the cantilever free end. Although in model C the cable is attached to a border node of the cable mesh, this difference should not change the cable behaviour. Therefore, for the sake of synthesis, we make reference to section 6.1.3, in which the cable modelling has been discussed and explained in detail.

6.2.4 Assigned static loads and masses

Regarding the applied loads, in this model it is not necessary to define the loads acting on the upright, while the loads acting on the cable remain as defined in model C. We also kept the load patterns defined specifically for the multi-support analysis, that contain the displacements applied to the upright base and to the western end of the cable.

- **CABLE 33-34 SLS**: that contains the static loads over the cable, determined according to a seismic limit state combination as shown in section 4.1. Their values are the same as defined in table 6.1 with reference to figure 6.2.

- **EAST DISPLACEMENT**, that contains the 1 m displacement toward the x axis applied to the base of the equivalent cantilever shelf.

- **WEST DISPLACEMENT**, that contains the 1 m displacement toward the x axis applied to the West end of the cable.

We then defined the same nonlinear static load case described in section 6.1.4, for which the only difference is that the now the only load pattern included is *CABLE 33-34 SLS*. Having modeled an equivalent cantilever in place of the upright we could not rely on the self modeled mass distribution. To account for this aspect we subsequently applied an equivalent concentrated mass to the cantilever free end, whose value has been calibrated so that the natural period of the equivalent beam as the same of the shelf-behaving upright mode. This choice is motivated by the fact that the upright vertical displacements and rotations were negligible when compared to the horizontal displacement.

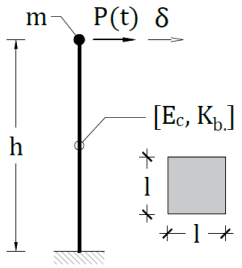

Figure 6.8: Cantilever beam with a orthogonal dynamic action at its free end. Source: own design

We therefore performed the modal analysis of the cantilever beam under a dynamic horizontal force applied at its free end, shown in figure 6.8. The system is one-dimensional so that the analysis is reduced to the resolution of a single equation.

$$det.\left(K - m\omega^2\right) = 0 \quad \longrightarrow \quad K = M\omega^2 \tag{6.11}$$

Where:

- m is the concentrated mass at the cantilever free end, which in this case is equivalent to the matrix of the masses and is unknown.

- K is the cantilever bending stiffness against the applied force. This term is already known, as seen in section 6.2.2, and is equal to 230000kN/m.

- ω is the cantilever natural pulsation, which is equal to:

$$\omega = \frac{2\pi}{T} \tag{6.12}$$

  where T is the natural period related to the oscillation mode. To assess its value we make reference to what has been obtained in the modal analysis of the upright shown in section 5.2.5. To summarize, we found that the upright fundamental mode has a natural period of 0.416s and involves 30% of the total mass, corresponding to roughly 67% of the mass of the second level, that behaves like a cantilever beam.

By solving the equation for ω, and by substituting the expression for T, we obtain the relation between mass m, bending stiffness K, and natural period T. From here it is possible to determine the mass as:

$$m = \frac{KT^2}{4\pi^2} = \frac{230000 \cdot 0.416^2}{4\pi^2} = 1010\ T \tag{6.13}$$

This value has been assigned as a horizontal translational concentrated mass to the cantilever free end. As seen previously for model C, the mass source is defined by combining the contributions from the element self and additional mass, and from the the static loads over the cable (belonging to load pattern *CABLE 33-34 SLS*). The mass source has been named *MSSSRC1*.

6.3 MODEL B2 - Beam with non-prismatic section

We have also developed an alternative to model B1, where we replaced the upright with a cantilever beam and maintained the cable. The main difference, which constitutes a notable benefit, is that this model has been assembled using only geometric data without relying on static and modal analyses to calibrate it. Therefore, a designer could potentially develop this model directly, without the need for further analyses and refinements.

6.3.1 General overview of the model

Similarly to model B1, model B2 represents an initial simplification of the reference case for which we removed the detailed supporting structure changing it by a simpler, equivalent, substructure. Despite its advantages, to calibrate the equivalent beam we exploited the results obtained from previous analyses, carried out on a more realistic model. Since these studies took a considerable time, we thereby thought about an alternative, for which we could model the upright using only data that was immediately available.

The factors that mainly affect the upright response are the mass and weight distributions (that counteracts the cable horizontal force), as well as the inertia of the transverse sections: hence we tried to maintain unaltered these characteristics in the simplified model. To do so we replaced the upright with a cantilever beam, using frame elements with variable section (also named non-prismatic sections), whose width corresponds to that of the real upright. Still, some elements were not yet included, and we had to model them as concentrated masses applied to the nearest node.

We assumed that in the real structure the transverse sections rotate rigidly, given their thickness with respect to the bending axis. Because of this, the connection between cable and upright has been modeled with a body constraint, defined between the end node of the cable and the nearest node of the equivalent beam. The model portion related to the cable remains unchanged. This does not contradict the idea on which the model is based, as to define the equivalent cable in section 6.1.3 we used only geometric data directly measured on the drawings, and the assumptions discussed are deducible

from a general overview of the project. Figure 6.9 shows the model configuration thus described.

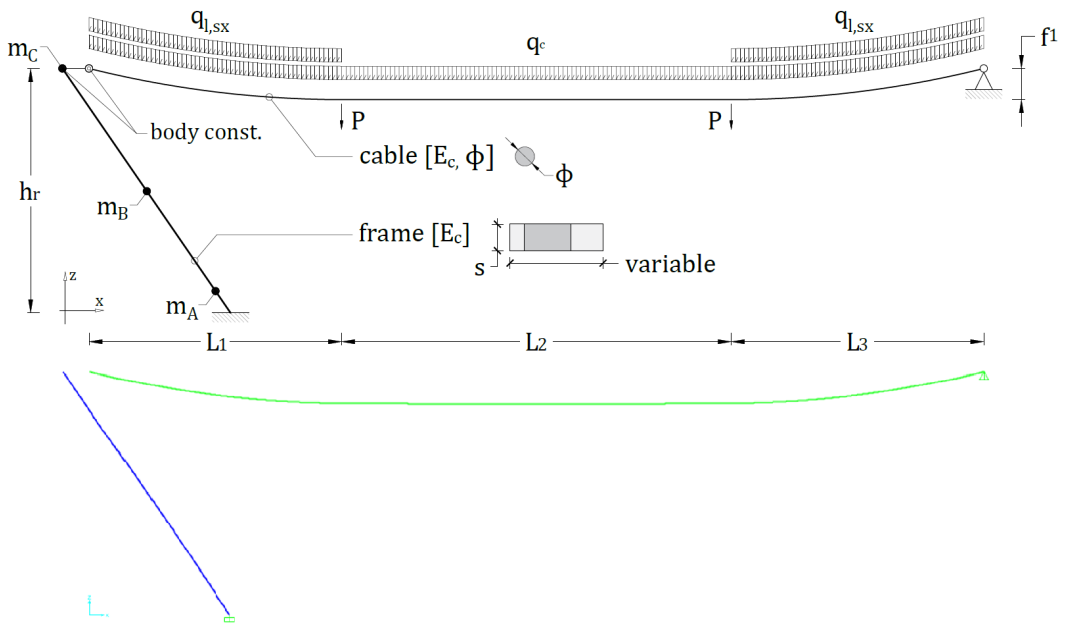

Figure 6.9: General layout of model B2 (with cable and non-prismatic cantilever beam) and detail of its implementation in SAP2000. Source: own design

6.3.2 Cantilever beam with non-prismatic sections

In this case, to model the upright we defined an equivalent cantilever beam with a non-prismatic section. The material used is the same as the upright, i.e. concrete C35/45, whose characteristics are summarized in section 5.2.1.1. We have defined the beam by means of frame elements, that act as a guiding axis and join the the upright base with its top along their centerlines. The assigned sections are orthogonal to this axis and have been defined for each variation in the upright profile, with a thickness of 1m and a variable width. Since the circular holes are placed centrally along the structure we used the gross width, as each section must have the same mass, but above all the same inertia as the real case.

The linking joints between consecutive frames are placed in correspondence of each section, so that for each element we specified the end sections, as well as the offset of their insertion points. In doing so the depth of the beam varies linearly along each frame, hence we have set a cubic variation of the moment of inertia related to the bending axis. Table 6.3 contains the node coordinates, while table 6.4 shows the section dimensions.

Table 6.3: Model B2, frame nodes coordinates for the equivalent non-prismatic cantilever beam

Frame node coordinates		
node id.	x [m]	z [m]
A	31,7100	0
B	30,6413	1,55
C	24,9945	9,74
D	23,2087	12,33
E	22,5468	13,29
F	19,5131	17,69
G	16,8793	21,51
H	15,1280	24,05
L	12,9424	27,22
M	4,1033	40,04
N	-1,4677	48,12
P	-4,0601	51,88
Q	-4,6531	52,74
R	-5,4184	53,85
S	-5,9700	54,65

Table 6.4: Model B2, frame sections for the equivalent non-prismatic cantilever beam

Non-prismatic frame section characteristics				
section id.	thickness [m]	width [m]	offset [m]	height [m]
AA	1	21,5	10,74	0
BB	1	22,82	8,68	1,55
CC	1	30,48	-1,92	9,74
DD	1	33,1	-5,18	12,33
EE	1	23,4	-1,05	13,29
FF	1	19,15	-2,24	17,69
GG	1	15,41	-3,29	21,51
HH 1	1	16,99	-1,96	24,05
HH 2	1	22,95	1,03	24,05
LL	1	20,73	0,59	27,22
MM	1	12,19	-0,94	40,04
NN	1	7,07	-1,76	48,12
PP	1	9,41	0,2	51,99
QQ	1	7,7	-0,46	52,74
RR	1	7,7	-2,42	53,85
SS	1	5,56	-2,81	54,65

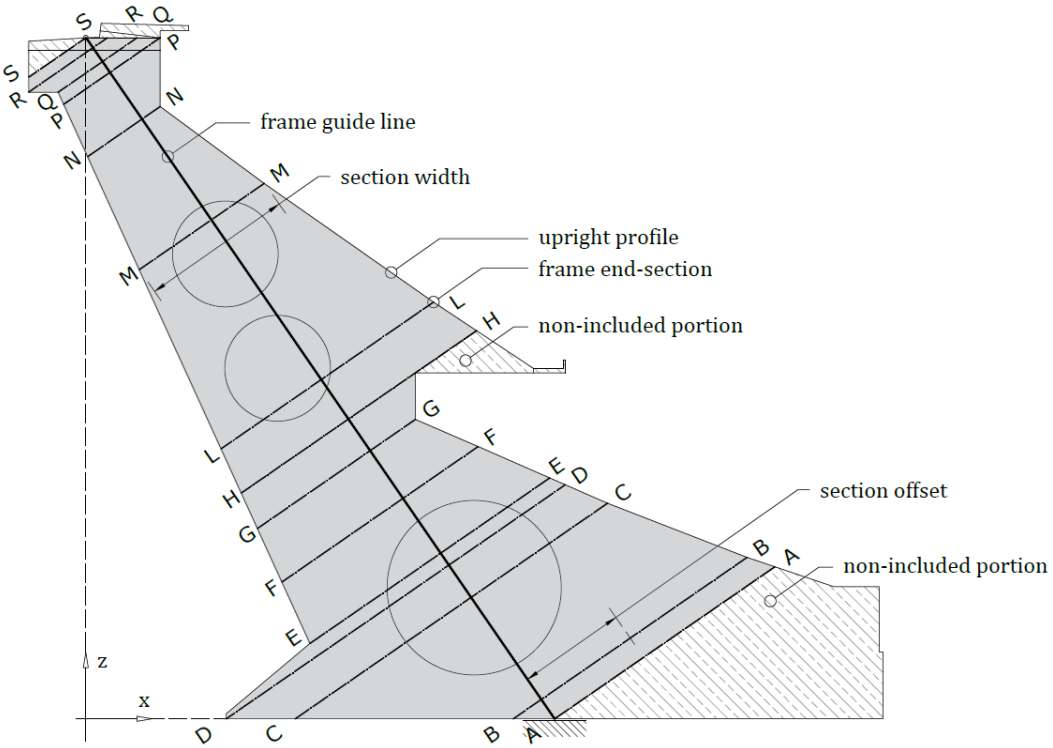

Figure 6.10: Model B2, layout of the non-prismatic frames for the cantilever upright. Source: own design

Thanks to this, the distribution of the inertia along the beam is quite close to the real case, however some approximations are inevitable, especially in the distribution of masses. To partially fix this problem, we have assigned concentrated masses to replace the missing portions. We then assigned a clamped support restrain to the base. This partly compensates for the fact that a large portion of the upright base is not included. As seen in sections 5.2.4 and 5.2.5, the missing part acts almost as a rigid basement since their displacements and oscillations are indeed negligible when compared to the rest of the structure.

The applied restraint locks any relative rotation nor displacement of the cantilever base, thus producing a similar effect. The cantilever free end does not coincide with the cable end, so it is necessary to define a link between them. Given the width of the upright cross section, we have assumed that under the cable action it rotates rigidly. Consequently, we could create a body constraint (which reproduces the rigid body behavior) between the free-end of the beam and the end of the cable. Figure 6.10 shows a rough outline of the beam layout, with the references of each section, the restraint and constraint just discussed, and the upright profile for a brief comparison.

6.3.3 modelling of the cables

The cable remains unchanged from what is defined in model C, which is the reference case. The only variation is that now is hinged to the cantilever free end. Although in model C the cable is attached to a border node of the cable mesh, this difference should not change the cable behaviour. Therefore, for the sake of synthesis, we make reference to section 6.1.3, in which the cable modelling has been discussed and explained in detail.

6.3.4 Static analysis and assigned masses

As seen previously for model C, according to the Eurocode [30] prescriptions about seismic load combinations and seismic masses we included all the loads and masses from permanent structural and non-structural elements, despite some approximation due to the simplified modelling. Regarding the applied loads, as in model B1 it is not necessary to define the loads on the upright, while the loads on the cable remain as defined in model C. We kept also the load patterns specifically created for the multi-support analysis, that contain the displacements applied to the upright base and to the cable end.

- **G1 DEAD**, containing the permanent structural self loads of the elements included in the model (in this case the cantilever non-prismatic beam).

- **CABLE 33-34 SLS**, that contains the permanent loads on the cable, determined according to a seismic limit state combination as shown in section 4.1. Their values are as defined in table 6.1, making reference to figure 6.2.

- **EAST DISPLACEMENT**, that contains the 1m displacements toward the x axis applied to the base of the equivalent cantilever shelf.

- **WEST DISPLACEMENT**, that contains the 1m displacements toward the x axis applied to the West end of the cable.

Other loads due to elements that are not included in the model such as bleachers, seats and inner floors, have been omitted as they are negligible with respect to the approximation level used here. To perform the static analysis we defined the load case *G1 + G2 + Cable 33-34* that, in compliance with a seismic combination, includes all the permanent loads belonging to load patterns *G1 DEAD* and *CABLE 33-34 SLS*. Other analysis parameters remain unchanged with respect to what defined in section 6.1.4 for model C.

Table 6.5: Model B2, equivalent concentrated masses added to the inclined beam.

concentrated masses	
mass id.	value [Tons.]
m_A	517,6
m_B	45,5
m_C	259,6

We then manually added all the masses that are not included as self masses of the frame elements. To do so we calculated the masses of the missing portions, and added them as concentrated translational masses applied to the closest node. Table 6.5 contains their values (making reference to the scheme in figure 6.9). Finally, we created a mass source named *MSSSRC1*, containing both the self masses of the modeled elements and those added later, as well as the masses from the static loads belonging to load pattern *CABLE 33-34 SLS*.

6.4 MODEL A - Second simplified model

Model A represents a further simplification when compared to models B1 and B2, as we replaced the cable with an equivalent rod. This model has been specifically developed to retrace the span variations and to reproduce the variation of the cable horizontal force. We relied on the fact that, in terms of magnitude, these are the main components that vary because of a seismic horizontal action. Therefore, we tried to assess the structural response by focusing only on these terms.

6.4.1 Conceptual definition of model A

A seismic horizontal action applied to the structure foundation consequently causes an oscillation of the upright free-end, which in turn generates a variation of the cable net span. The same happens in case of different ground motions between the stands, as for the multi-support analysis. Vertical oscillations and rotations have such low magnitude that we can neglect them and the only relevant component is the horizontal one. As previously seen, its variation implies that also the cable horizontal tension changes, while the overall vertical resultant force is almost constant as there are no variations of the applied loads. The model has been consequently simplified to retrace only the free end horizontal displacements and cable forces. However, we know that in the real structure a variation of the cable span implies a consistent variation of its sag, so that

there is a component of vertical wave motion that cause a variation of the vertical forces due to inertial effects, although we do not know the magnitude of this phenomenon.

In this model we therefore replaced the cable with an "equivalent", yet simpler, structural element. The choice of a connecting rod came out from the study of [19] and other publications about the Braga Stadium (particularly [18], in which the author briefly describes the development of a finite element model of the roof). In this specific case we started from the results of the cable static analysis discussed in section 4.2.6: these data have been exploited to calibrate the geometric and mechanical parameters of an equivalent connecting rod.

Being representative of a cable, the connecting rod only resists to tensile stresses, while the initial tension of the cable under static permanent loads has been simulated with a uniform thermal variation, thus inducing an initial prestress. Here too, it was necessary to previously define an equivalent mass distribution, as we will see later in this section. Regarding the upright, this was replaced with the same cantilever shelf defined in section 6.2.2 for model B.

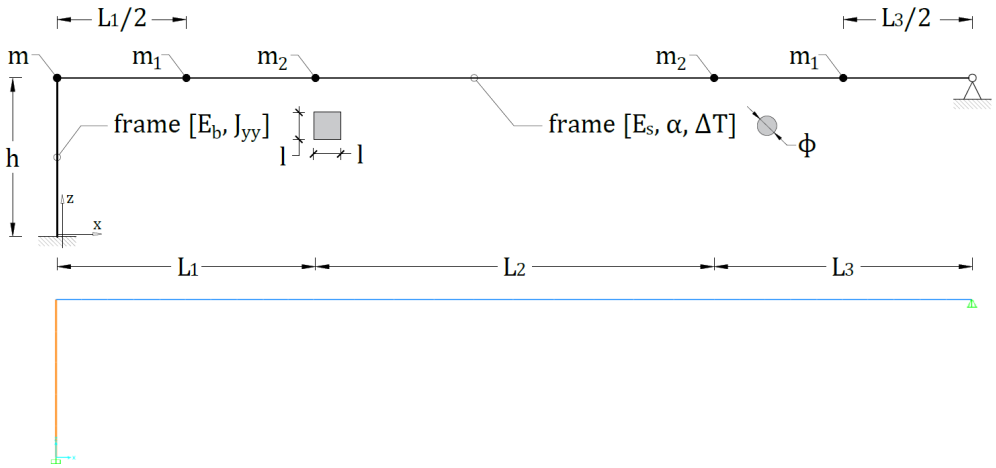

Figure 6.11: General layout of model B (with cable and equivalent cantilever beam) and detail of its implementation in SAP2000. Source: own design

6.4.2 modelling of the upright

As for the upright, this has been replaced with the same equivalent cantilevered shelf defined for model B1. For the sake of brevity we simply make reference to what has been described in sections 6.2.2, where the cantilever parameters have been calibrated using the results of the static and dynamic analyzes of the upright described in chapter 5.

6.4.3 modelling of the cables

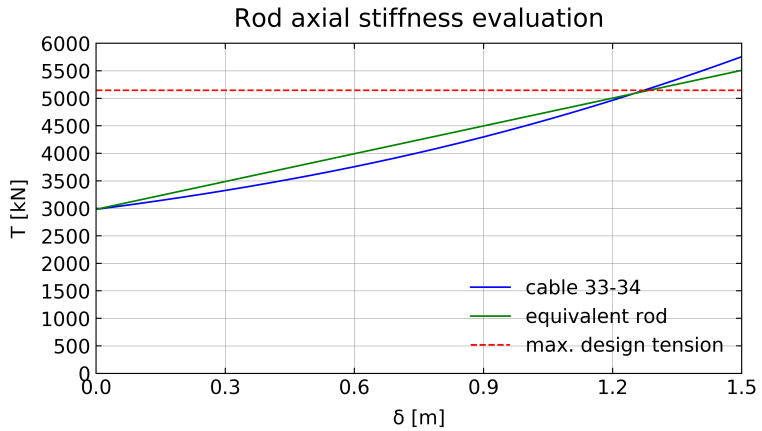

Figure 6.12: Rod equivalent axial stiffness evaluation throughout a secant line of the cable load/displacement curve determined in section 4.2.6. Source: own design

To define the technical characteristics of the equivalent rod we proceeded similarly to what was done with the upright. We evaluated the axial stiffness from the results of the static analysis of the cable discussed in section 4.2.6, where we determined its tension-displacement curve. Figure 6.12 shows that same curve, compared with the maximum design cable force. The cable has a non-linear behavior while the rod is linear elastic, so that we had to interpolate, tracing a secant line passing through the cable failure point, that corresponds to a 1.25m displacement. This choice was motivated by the fact that we want the rod to match the cable forces for both the initial state and the breaking moment, while in between we may accept a possible overestimation.

Table 6.6: Interpolation secant values for the assessment of the axial stiffness of the rod.

axial stiffness interpolation points

δ m	V [kN]	H [kN]	T [kN]
0,00	715	2973	3058
1,25	715	5074	5124

Since the model reproduces only the horizontal forces, to calculate the axial stiffness we considered this parameter and not the maximum cable tension. From the values recorded in table 6.6 we can estimate $K_{r.}$ as the ratio between the force increase and the assigned displacement.

$$K_{r.} = \frac{\Delta P}{\delta} = \frac{5074 - 2973}{1.25} = 1684\ kN/m \tag{6.14}$$

As seen previously we included 4 adjacent cables, that we approximated as equal to simplify the model. Assuming that the all rods behave like parallel springs, we could calculate the total equivalent stiffness as the sum of each cable's stiffness, thus obtaining $K_{r.}$ equal to 4·1684=6736kN/m. This hypothesis is acceptable due to the structural constraints generated by clamps, slabs links and truss beams connecting the cables. We applied a circular cross-section to the rod, thus calculating its area and diameter as:

$$K_{r.} = \frac{EA_{eq.}}{L} \quad \longrightarrow \quad A_{eq.} = \frac{K_{r.}L}{E} = \frac{6736 \cdot 202}{2.1 \cdot 10^8} = 0.00648\ m^2 \tag{6.15}$$

$$\Phi_{eq.} = \sqrt{\frac{4A_{eq.}}{\pi}} = \sqrt{\frac{4 \cdot 0.00648}{\pi}} = 0.091\ m$$

Where $E_{r.}$ is equal to 210000MPa (we assumed that this is a structural steel rod), L is equal to 202m, which is the total net span of each cable.

To summarize, the equivalent rod thus defined was modeled using straight frame elements, with a total length of 202m. We have assigned a circular 9.1cm diameter cross-section, and a strength of 1575MPa (we maintained the same value that we determined for the cable, although this rod is a different element) with an elastic modulus of 210MPa and a thermal expansion coefficient of $1.2{\cdot}10^{-5}\ °C^{-1}$. The rod is hinged on one side to the free end of the equivalent cantilever beam (not transmitting any bending moment), while on the other side is bound to an external hinge. Since this is an equivalent structural element, we have assigned a null scale factor for both its weight and mass, so that they are not included in the static analysis.

6.4.4 Assigned masses and load

Having applied a connecting rod in place of the cable, and having also replaced the upright with a cantilever beam, the external loads previously seen for model C are omitted. Subsequently it became necessary to calculate a uniform thermal load to be applied to the connecting rod, so that its initial tension is equal to the cable horizontal force due to permanent loads.

To determine the relation between thermal load and induced tension we can refer to the static scheme proposed in figure 6.13. The static problem can be solved with the displacement balance equation as we separate the structure into a cantilever beam and a connecting rod, calculating separately for both the horizontal displacement δ. Having already studied these substructures we apply the solutions explained in sections 6.2.2 and 6.4.3.

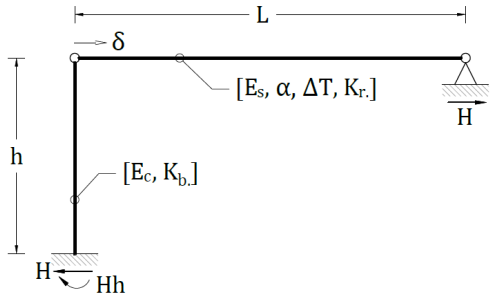

Figure 6.13: Model A reference static scheme for the assessment of the equivalent temperature decrease over the rod. Source: own design

For the cantilever beam the free end horizontal displacement is indeed equal to:

$$\delta_{b.} = \frac{Hh^3}{3E_c J_{yy}} = \frac{H}{K_{b.}} \tag{6.16}$$

where H is the tension induced over the rod, E_c is the elastic modulus, J_{yy} is the moment of inertia, h is the beam height and $K_{b.}$ represents its bending stiffness. On the other hand, for the equivalent rod δ is equal to the sum of the elastic and thermal components.

$$\delta_{r.} = \delta_{th.} + \delta_{el.} = \alpha \Delta T L - \frac{HL}{E_s A} = \alpha \Delta T L - \frac{H}{K_{r.}} \tag{6.17}$$

Where ΔT is the uniform temperature variation, L is the rod length, E_s is its elastic modulus, A is its cross-sectional area and $K_{r.}$ represents the axial stiffness. In our structure, $\delta_{b.}$ and $\delta_{r.}$ must be the same, so that we obtain:

$$\frac{H}{K_{b.}} = \alpha \Delta T L - \frac{H}{K_{r.}} \tag{6.18}$$

The thermal variation can therefore be calculated as:

$$\begin{aligned} \Delta T &= \frac{H}{\alpha L}\left(\frac{1}{K_{b.}} + \frac{1}{K_{r.}}\right) = \\ &= \frac{11778}{1.2 \cdot 10^{-5} \cdot 202}\left(\frac{1}{230000} + \frac{1}{6736}\right) = 743\ ^\circ C \end{aligned} \tag{6.19}$$

Where we adopted:

- α is the steel thermal expansion coefficient, equal to 1.2·10^{-5} °C^{-1}.
- $K_{b.}$ is the beam bending stiffness, which is already known as seen in section 6.2.2, and is equal to 230000kN/m.

- K_r is the rod axial stiffness, which is already known as seen in section 6.4.3, and is equal to 6736kN/m.

- H is known as it was determined through the cable static analysis shown in chapter 4, but we were not considering the upright deflection under permanent loads, that modifies the cable span. Although this does not implies considerable variations, we adopted the value from the static analysis of model C to avoid any initial bias of the model A results. This topic will be extensively discussed in chapter 7; for now we only state that model C provided an initial horizontal cable tension of 11778kN for the 4 cables.

We therefore applied a uniform temperature decrease of -743°C to the equivalent rod, which is included into a specific load pattern. Since in this model we have eliminated all the original elements there are no external loads, and the defined load patterns are:

- **PRESTRESS**, that contains the uniform temperature decrease applied to the equivalent rod.

- **EAST DISPLACEMENT**, that contains the 1 m displacements toward the West direction applied to the base of the equivalent cantilever shelf.

- **WEST DISPLACEMENT**, that contains the 1 m displacements toward the West direction applied to the West end of the cable.

We then have set the load case for the static analysis of the model, that acts as a basis for the simulations of the seismic actions. This load case has been simply named *PRESTRESS*, and performs a non linear analysis, without considering geometric non-linearity parameters, starting from unstressed conditions. The only load pattern included is *PRESTRESS*, containing the assigned temperature variation. Regarding the cantilever beam equivalent mass we make reference to what explained in section 6.2.4, where we defined a concentrated horizontal translational mass of 1010T applied to the free end of the beam. Regarding the equivalent rod we needed to apply the masses related to the weights acting over the cables, namely the cable itself, the truss beams and the concrete slabs.

To do so we have concentrated all the masses on 4 points located along the cable, as these account only for horizontal translations. Figure 6.14 shows the concentrated masses, that were calculated with respect to the influence zones of each point.

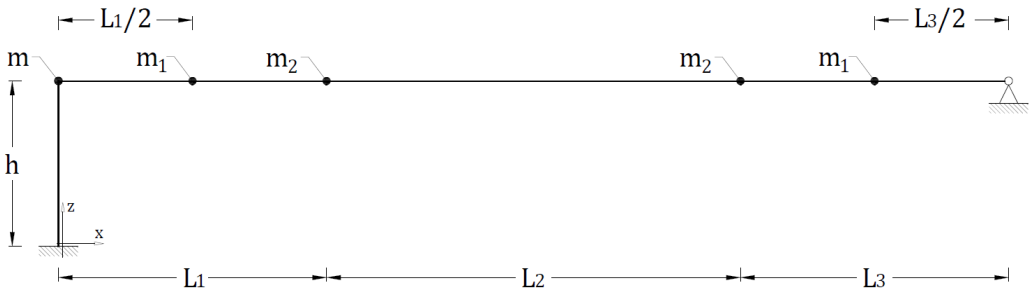

Figure 6.14: Model A equivalent concentrated masses assigned over the rod. Source: own design

$$
\begin{aligned}
m_1 &= 4\left[\frac{1}{g}\left(0.75\, q_{l,sx}\, l_1 + 0.75\, q_c\, l_1\right)\right] = \\
&= 4\left[\frac{1}{9.81}\left(0.75 \cdot 11.719 \cdot 57.65 + 0.75 \cdot 0.408 \cdot 57.65\right)\right] = 211,4\ T \\
m_2 &= 4\left[\frac{1}{g}\left(0.25\, q_{l,sx}\, l_1 + 0.25\, q_c\, l_1 + P_T\right)\right] = \\
&= 4\left[\frac{1}{9.81}\left(0.25 \cdot 11.719 \cdot 57.65 + 0.25 \cdot 0.408 \cdot 57.65 + 6.152\right)\right] = 72.9\ T
\end{aligned}
\tag{6.20}
$$

The masses were included into a specific mass source named *MSSSRC1* as element self mass and additional masses. Since the scale factor for all the element masses and weights is 0, these concentrated masses are the only ones included in the model.

6.5 Multi-support analysis set-up

The purpose of this work is a comparative analysis, for which we assess whether the simplified models just developed can provide a reliable evaluation of the seismic response of our reference case, namely model C. Therefore we must evaluate their behaviour from a probabilistic standpoint, considering the results from several simulations and comparing the main statistical parameters and the trends of the significant benchmarks, not the pointwise results from a unique case. In this section we explain in detail how we set up the multi-support analysis of both the simplified models and the reference case. For each of them we performed 100 simulations, where we applied synthetic ground motions generated from the longitudinal component of the 1940 El Centro record. In doing this analysis we considered two opposite, yet not realistic, scenarios: with perfectly correlated and with uncorrelated accelerograms.

6.5.1 El Centro - 1940 accelerograms

The seismic solicitation is characterized by high uncertainty: to constrain it, we have performed several simulations with synthetic ground motions. These have been generated from the longitudinal component of the 1940 El Centro record (similarly to what was done in [5]), through a spectral version of the Rezaiean and Der Kiureghian stochastic ground motion model (discussed extensively in [8], [9], [24] and [25]). This creates synthetic records based on significant parameters of the source record: predominant spectral content, energy content and duration. This procedure ensures the response spectrum compatibility, so that the elastic response spectra of the synthetic ground motions are statistically comparable with the response spectrum of the original (as explained in [25]).

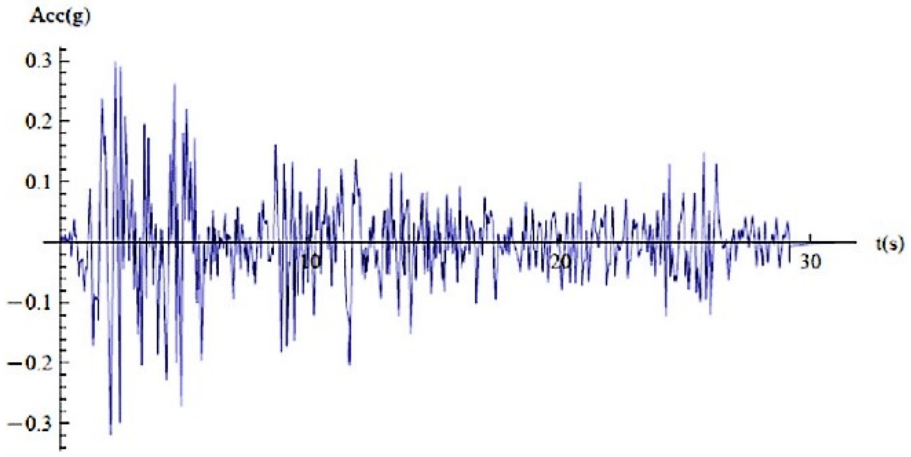

Figure 6.15: 1940 El Centro record, ground acceleration. Source: www.researchgate.net

We have been provided with a set of 1000 ground accelerograms by Professor M. Broccardo (one of the supervisors from the University of Trento and author of some of the publications just cited): each one has a duration of 48.62s with 0.02s steps, thus containing 2482 values. These have been adapted to the peak ground acceleration of the Braga area that has a value of 0.8m/s^2, or 0.081g, according to the Portuguese zonation for a type 2 seismic action (whose values have been determined in [3] for the Eurocode [37]). For the 1940 El Centro (whose original accelerogram is shown in figure 6.15) records we assumed a peak ground acceleration of 0.320g. By integrating twice the accelerograms we obtained the ground displacement functions. These have been applied to the base of the East upright and to the hinge restrain at the West end of the cable, performing different simulations for each model.

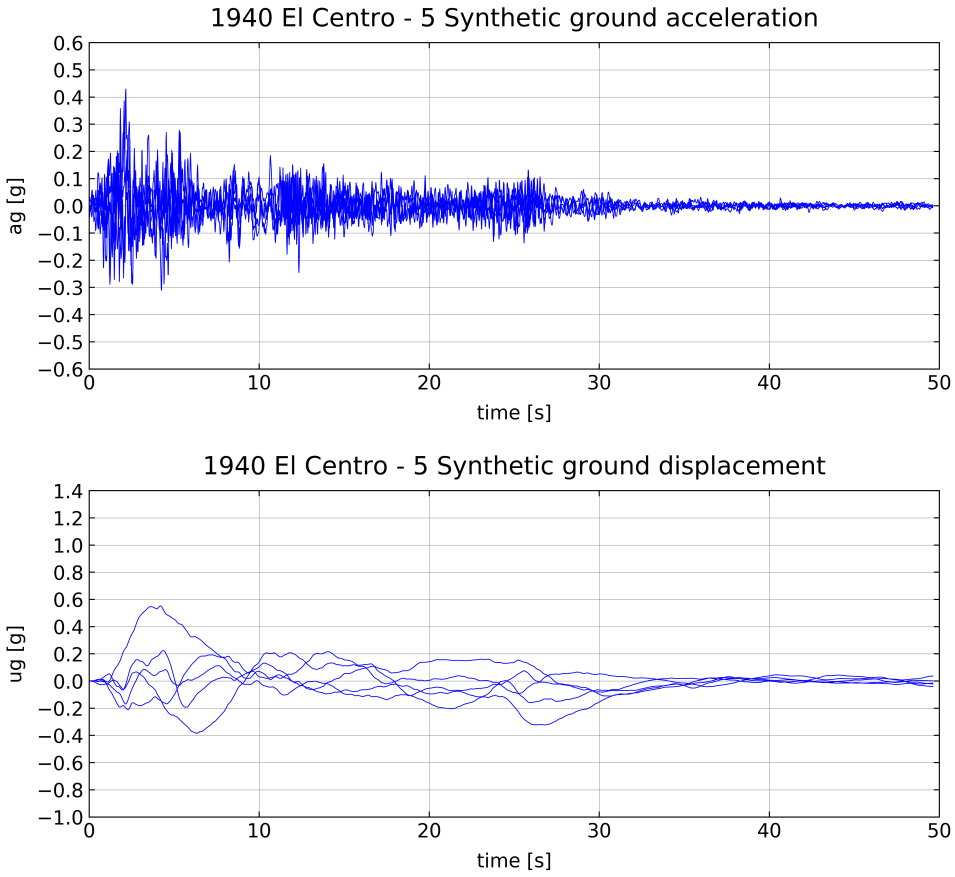

Figure 6.16: Ground accelerations and ground displacements for the first 5 synthetic ground motions provided. Source: own design

6.5.2 Perfectly correlated accelerograms

Actually, there are always factors such as a different soil composition, stratigraphy, or eventually a fault, that affect the seismic waves propagation often causing a phase shifting. The magnitude of such phenomenon on the surfaces becomes considerable for far enough points, and is studied especially in case of large span structures. To define the correlation between ground motions at different points, a correlation factor is assigned on the basis of geological and geotechnical data. Generally, the more the terrain is uniform and the structure footholds are closer, the more the ground motions are similar and consequently the correlation factor tends to 1. On the other hand, large spans and different terrains usually mean that the ground motions differ widely, so that the correlation factor tends to 0.

In our case we do not have enough information to accurately assess the correlation factor between the East and West stands, while repeating the simulations for several hypothetical values would be extremely time requiring. Since the aim of this multi-support analysis is the comparison of the response from different models we have

considered only the extreme scenarios, i.e. with correlation values of 0 and 1, thus including in this range all the possible realistic cases. The first scenario is that of perfectly correlated ground motions, that in our models are applied to the base of the East stand and to the cable West end, respectively. This represents a limit situation, yet unrealistic, for which the accelerograms are the same for both sides of the structure.

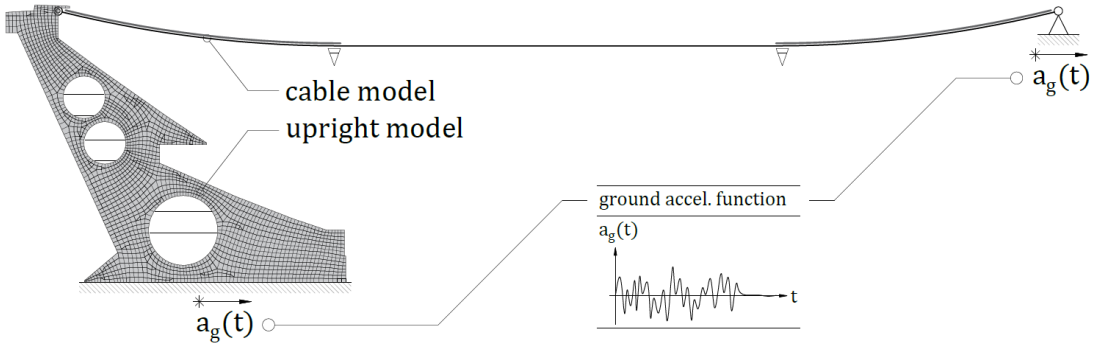

Figure 6.17: Conceptual scheme representing the applied ground acceleration for perfectly correlated ground motions. Source: own design

For each model we performed 100 simulations, for which we randomly chose 100 ground motions among the provided ensemble. Each simulation corresponds to a time-history analysis load case, that provides a nonlinear evaluation of the dynamic response under loads that vary according to a specified time function. In this case that function is one of the synthetic accelerograms defined in the previous section, and the applied load is indeed an acceleration, directed parallel to the cables. Since the accelerograms are in g-units, we assigned a scale value of 9.81 to convert them in m/s^2. The initial conditions are calculated through a non-linear load case that analyses the permanent loads (named *PRESTRESS* for model A, *G1 + G2 + Cable 33-34* for the other models), defined as shown in sections 6.1.4, 6.2.4, 6.3.4 and 6.4.4 for each model respectively. The mass source (named *MSSSRC1*) has also been defined in those sections, and includes all the masses due to structural and non-structural elements.

We have assigned the analysis parameters according to what is stated or suggested in the CSI Analysis Reference Manual [11]. The time history analysis is non linear, while the geometric non-linearity parameters of P-Delta and large displacements are automatically accounted, having included cable elements in the models. Regarding Model A, we have not considered any geometric non-linearity parameter: the model did not include cables and therefore did not require to consider also the large displacements formulation, furthermore the displacements due to the applied actions had such low magnitude that the P-delta method did not produce appreciable differences. This allowed us to further reduce the time required for its analysis. The dynamic equilibrium

equations are solved by direct integration, calculating 2500 output points with a 0.02s step. Although the manual suggests to double the output duration with respect to the load function, in our case the response peaks were within the first 15s, so that we adopted the same output duration as the load function (i.e. 50s), thus reducing the processing effort.

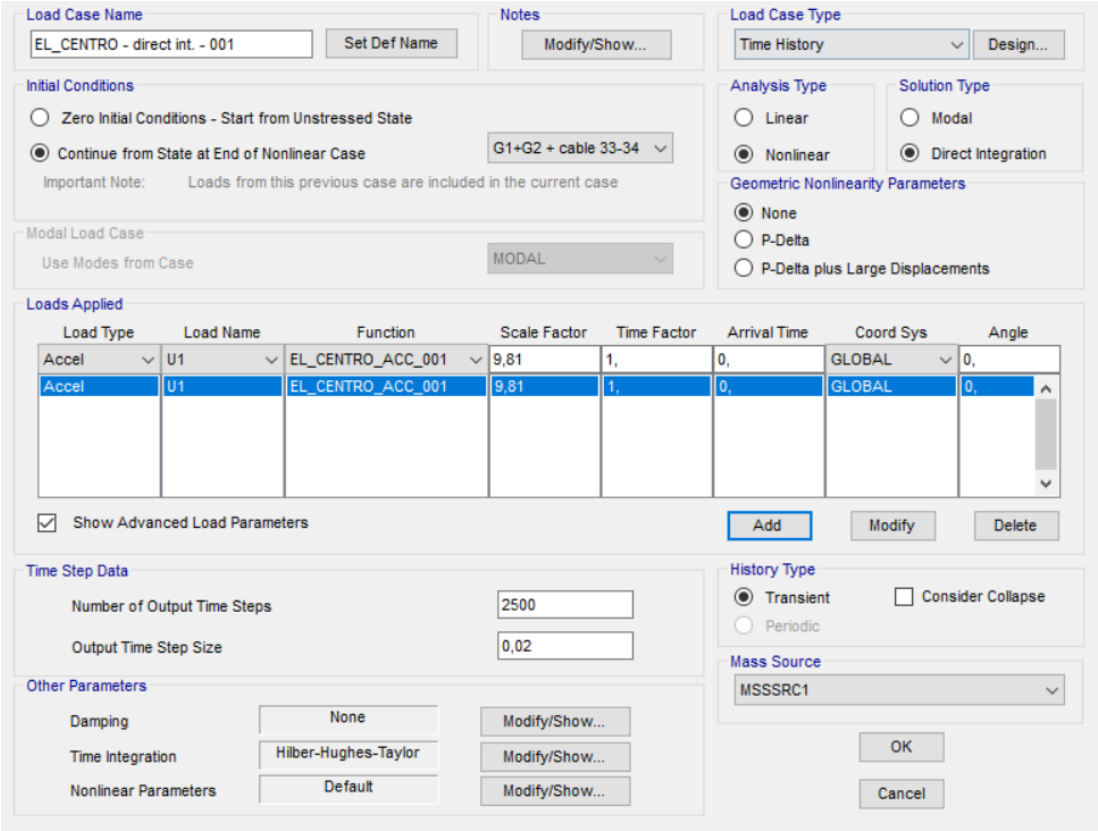

Figure 6.18: Analysis with correlated ground motions, command window for the parameters setting. Source: SAP2000

For the time integration we chose the Hilbert-Hughes-Taylor method, since it actually suffices for all problems and allows to avoid possible convergence issues. It represents an extension of the Newmark method, to which it corresponds if α=0, but by varying α between -0.333 and 0 we can introduce a numerical dissipation, while the integration scheme thus defined is second order accurate and unconditionally stable (in fact in [11] is recommended in case of poorly converging nonlinear time-history cases). As suggested in [11], after some trials we set an α value of -0.042 (while β and γ were equal to 0.271 and 0.542 respectively), so that we could add a numerical damping for the higher frequency modes without compromising the analysis results: this allowed to slightly reduce the time required for each simulation, compared to the time required with α null.

As for the damping parameters, the papers that deal with the topic (briefly reviewed

in chapter 3, section 3.3.4.5) show extremely low values. Furthermore, the synthetic ground motions from the 1940 El Centro array record are characterized by a few strong response peaks concentrated in the first moments. For these reasons the damping effect is almost negligible, and acting in favor of safety we have assumed a null value of the damping ratio. To prove this hypothesis we performed some tests on model C, comparing the answer obtained for the two cases:

- Assuming no damping ratio.
- Assigning modal damping ratios for the first 11 modes, whose values come from the data described in the reference papers.

These tests are described in detail in annex G. The results obtained have confirmed what was is assumed in this paragraph. We clarify here that, although in [20] the authors discuss a preliminary design of a damping device and in [10] is generically mentioned a damping system placed between the cables (without adding any further information), on the other publications and on the final designs there were no details regarding such devices. In absence of the necessary data we could only act in favour of safety, thus omitting any possible device system added to the structure. Still, in [22], [23], [18] and [10], are provided extremely low values of the damping ratio (obtained from full-scale tests on the final structure): it was such outcome to push some of the authors, namely M. Majowiecki and N. Cosentino, in developing the aforementioned preliminary design, although they did not specify whether it was applied to the final structure.

6.5.3 Uncorrelated accelerograms

The second scenario analyzed is that of uncorrelated ground motions, for which we performed 100 simulations applying different displacement functions to the two sides of the structure. The displacement functions were calculated by integrating twice the synthetic accelerograms defined in section 6.5.1.

For the base of the East Stand we have maintained the same 100 ground motions applied in the previous scenario (but using the displacement function instead of the acceleration one), while to the hinge restraint at the West cable support we have applied other 100 functions from the same ensemble, not related with the first ones. For each simulation we defined a time-history load case. The loads applied are the following:

- Load pattern *EAST DISPLACEMENT*, containing a 1m horizontal displacement towards x axis applied to the base of the East Stand, varying according to a synthetic time displacement function related to the same ground motion of the correlated scenario.

- Load pattern *WEST DISPLACEMENT*, containing a 1m horizontal displacement towards x axis applied to the base of the West end of the cable, varying according to a different synthetic time displacement function.

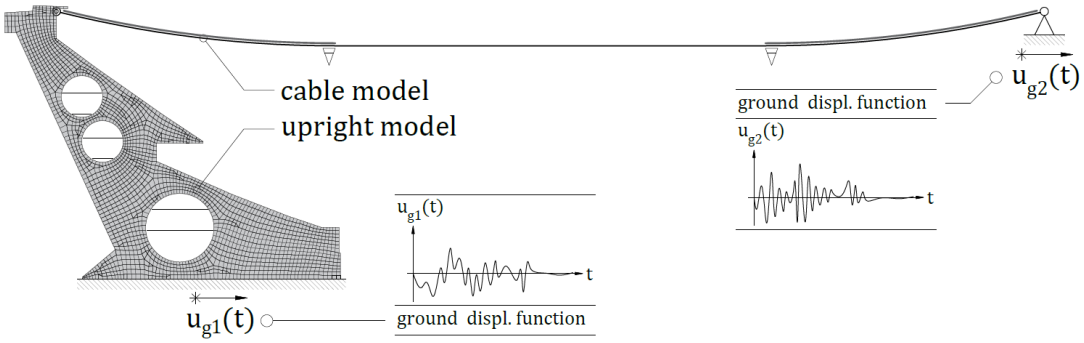

Figure 6.19: Conceptual scheme representing the applied ground displacements for uncorrelated ground motions. Source: own design

The applied loads and functions (shown in figure 6.20) are the only difference from the previous scenario. Hence, for the sake of brevity we refer to what stated in the previous section.

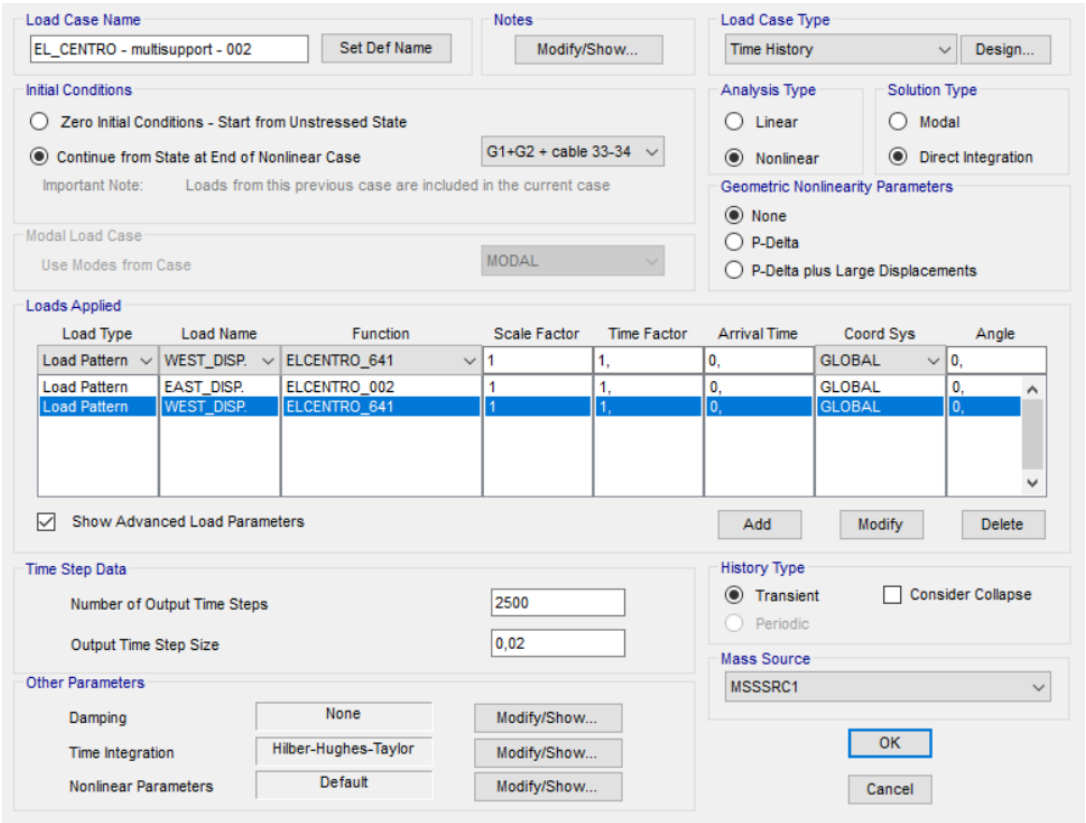

Figure 6.20: Analysis with uncorrelated ground motions, command window for the parameters setting. Source: SAP2000

Chapter 7

Analysis and comparison of the simplified models

In this chapter we will present the results of the multi-support analysis performed over the simplified models defined in chapter 6. We will briefly describe the processing of the analysis outputs, then we will compare the data obtained from the different models in terms of their main statistical parameters and trends, taking as reference model C (realistic model) and assessing whether they provide reliable values or not. Finally we will describe how the structural response changes between the two uttermost cases of perfectly correlated and uncorrelated accelerograms.

7.1 Data processing of the analysis outputs

We performed a multi-support analysis, considering the two uttermost cases of perfectly correlated and uncorrelated accelerograms as described in sections 6.5.2 and 6.5.3. For both cases we executed 100 time history simulations over each model developed in chapter 6, applying synthetic accelerograms generated using the 1940 El Centro ground motion array as seed (as described in section 6.5.1). These analyses produced arrays of stress and strain values over time for each element: among all these data we have considered only those relevant for our purposes, thus comparing the simplified models in terms of:

- **H**, cable horizontal tension component.
- **T**, maximum cable tension (that can be found at its ends).
- Δ**H**, variation of the cable horizontal tension component.
- Δ**T** variation of the maximum cable tension (that can be found at its ends).
- **u**, relative horizontal displacement of the cable East end (measured relatively to the East stand base).

- Δ**L**, cable net span variation.

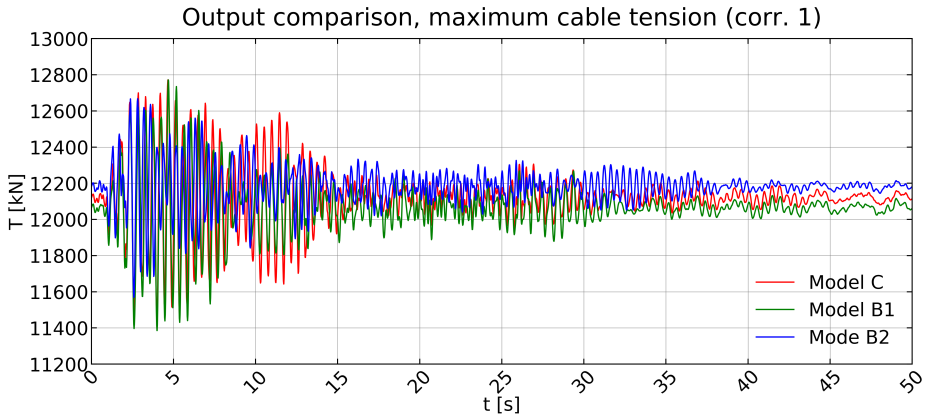

Figure 7.1: Comparison of the maximum cable tension of different models, during a simulation where we applied the same ground motion to each of them. Source: SAP2000, own elaboration

We have chosen these parameters as we want to compare the seismic response from a probabilistic standpoint, thus considering only its significant benchmarks: the behavior of the reference case and the simplified models are indeed slightly different, as shown in figure 7.1. From that same figure we can notice that the response peaks are all within a certain range. Therefore for the comparison we selected the maximum cable tension and the cable span variation (that, as seen in 4.2.6, is strictly related to it), for which we then analyzed the trend of the maximum values calculated during each simulation. The cable horizontal tension was also included as this is the predominant component in the cable maximum tension.

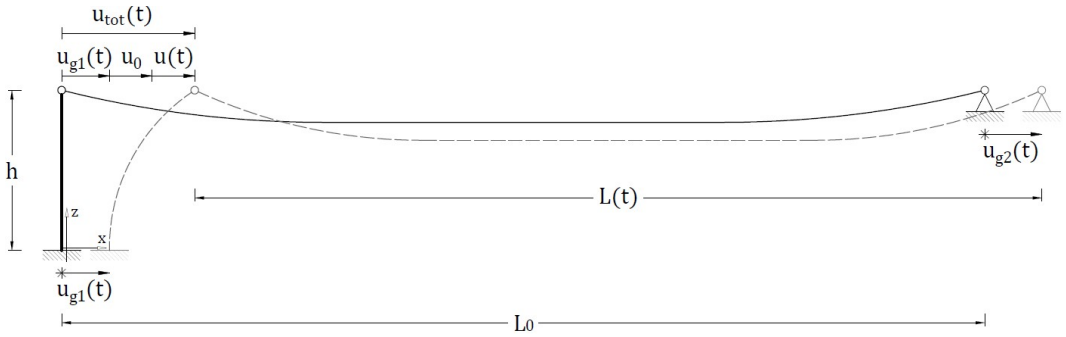

Figure 7.2: Reference scheme, applied ground displacements and measured displacements for the multi-support analysis. Source: AutoCAD, own elaboration

As for the displacement-related parameters, we briefly explain how these were determined from the SAP2000 outputs, taking as reference the scheme in figure 7.2. Here are displayed:

- $u_{g1}(t)$ is the displacement of the ground motion applied at the base of the East stand, that is known as it is a function assigned for each simulation.

- $u_{g2}(t)$ is the displacement of the ground motion applied at the cable West end, that is known as it is a function assigned for each simulation.

- $u(t)$ is the displacement of the cable East end relatively to the East stand base, and is one of the selected comparison parameters.

- $u_{tot}(t)$ is the total displacement of the cable East end, whose value is provided as output by SAP2000.

- u_0 is the displacement at the cable East end due to the permanent loads, that is known as it corresponds to the initial displacement $u_{tot}(0)$.

- L_0 is the initial cable span, also known as it is assigned.

- $\Delta L(t)$ is the cable span variation of due to the seismic action alone, and is one of the selected comparison parameters.

Knowing that:

$$u_{tot}(t) = u_0 + u_{g1}(t) + u(t) \tag{7.1}$$

The absolute maximum value of $u(t)$ was calculated as:

$$\begin{aligned} u(t) &= u_{tot}(t) - u_0 - u_{g1}(t) \\ u_{MAX} &= \max_t (|u(t)|) \end{aligned} \tag{7.2}$$

While the maximum net span variation due to the seismic action alone was calculated as:

$$\begin{aligned} \Delta L(t) &= L(t) - (L_0 - u_0) = \\ &= (L_0 + u_{g2}(t) - u_{tot}(t)) - (L_0 - u_0) = \\ &= u_{2g}(t) - u_{g1}(t) - u(t) \\ \Delta L_{MAX} &= \max_t (|\Delta L(t)|) \end{aligned} \tag{7.3}$$

From each simulation we have therefore extrapolated the maximum values of: cable tension, horizontal tension component, increase of the cable maximum tension, increase of the horizontal tension, net span increase and relative horizontal displacement, thus obtaining for each of these parameter an ensemble of 100 values. The values from each ensemble have been arranged in ascending order and plotted in the form of empirical

cumulative distribution functions (CDFs). We also calculated the main statistical parameters, i.e. mean and standard deviation. This procedure, as well as the others described in this section (also found in reference [5]), were performed on an dedicated Excel sheet for both cases studied, whose numerical results are summarized in annex H.

For model C, that is the reference case, we reported a nonparametric confidence interval based on the Dvoretzky–Kiefer–Wolfowitz (or DKW) inequality, that we briefly discuss. A confidence interval describes how close an empirically determined distribution function will be bounded to the distribution from which the empirical samples have been drawn. Given an ensemble of n independent and identically distributed random variables X_i, whose CDF is $F(x)$, we can define an associated empirical distribution function (or EDF) as:

$$F_n(x) = \frac{1}{n}\sum_{i=1}^{n} I\{X_i < x\} \quad x \in R \tag{7.4}$$

Where $F(x)$ represents the probability that a single random variable X is smaller than x, while $F_n(x)$ is the actual fraction of the random variables smaller than x. The DKW inequality bounds the probability that a random $F_n(x)$ differs from $F(x)$ by more than an assigned value ϵ for every point of its domain. This implies the two-sided relation:

$$\Pr\left(\sup_{x\in R}|F_n(x) - F(x)| > \epsilon\right) \leq 2\exp\left(-2n\epsilon^2\right) \tag{7.5}$$

From this inequality we can generate a CDF-based confidence band around $F(x)$: for every x we apply a $1-\alpha$ confidence, thus producing an envelope $B(x)$ for which the probability of $F_n(x)$ being outside the interval is less than α:

$$\Pr\left(F_n(x) \notin B(x)\ \forall x\right) \leq \alpha \tag{7.6}$$

The bandwidth ϵ can be found by solving:

$$\begin{aligned} \alpha &= 2\exp\left(-2n\epsilon^2\right) \\ \epsilon &= \sqrt{\frac{1}{2n}\ln\left(\frac{2}{\alpha}\right)} \end{aligned} \tag{7.7}$$

The interval that contains the CDF with probability $1-\alpha$ is delimited by the two functions:

$$F_{low} = \max_x\left(F_n(x) - \epsilon,\ 0\right)_x \quad \text{and} \quad F_{up} = \min_x\left(F_n(x) + \epsilon,\ 1\right) \tag{7.8}$$

In our case we took as reference the data from model C (also referred as realistic model), for which we calculated a 95% confidence band (or CI) using the formulation just discussed. We have also assessed whether we could fit a parametric continuous probability distribution functions (or PDF) to our reference case, trying different functions but achieving poor results. The best fit was provided by a lognormal distribution:

$$f(x) = \frac{1}{x\sigma\sqrt{2\pi}} \exp - \frac{(\ln x - \mu)^2}{2\sigma^2} \tag{7.9}$$

Where $f(x)$ is the PDF for the random variable x, while μ and σ are respectively the mean and the standard deviation of the variable's natural logarithm. The associated cumulative distribution function for model C parameters has been calculated with the dedicated Excel function. For the sake of completeness, we thereby specify its expression:

$$F_n(x) = \frac{1}{2}\left(1 + \text{erf}\left(\frac{\ln x - \mu}{\sigma\sqrt{2}}\right)\right) \tag{7.10}$$

Where $\text{erf}(x)$ is the error function.

7.2 Comparison of the simplified models

After having illustrated the data processing, in this section we will display and discuss the results of the multi-support analysis, making reference to the graphs and tables thus obtained. Besides discussing the two cases of perfectly correlated and uncorrelated accelerograms, we will also briefly comment the information related to the analysis time and the cable stress state under permanent loads (comparing the various models with the calculations made in chapter 4).

7.2.1 Model's initial cable tension under Seismic Limit State

Table 7.1: Initial cable tension and upright free-end displacements measured from different models and from simplified analysis. Source: Excel, own elaboration

Cable 33-34, multi-support analysis initial state

model	u [m]	H [kN]	V [kN]	T [kN]
A	0,052	11778,0	n.	n.
B1	0,051	11716,4	2877,9	12064,7
B2	0,022	11836,9	2878,2	12181,8
C	0,036	11778,1	2877,8	12119,7
Chapter 4	0,000	11894,0	2861,4	12233,3

Before comparing the seismic response of the different models, we must outline some considerations about their initial state. As previously described, this was generated by the action of permanent loads only, which were included in the combination for the Seismic Limit State. In our specific case these corresponds also to the State 0 combination, that has been already analyzed by studying the cable alone with a simplified method (in section 4.2.2). As shown in table 7.1, because of the upright bending all the models present a lower cable tension than the one calculated in chapter 4. This result is strictly related to what explained in section 4.2.5, since the upright free-end horizontal displacement causes a variation of the cable span, and therefore also of the horizontal tension component H. Vertical displacement and rotation at that point are negligible, thus complying the approximations carried out previously. In our case we do not have enough information to assess if this upright displacement is correct, since neither in the designs nor in the publications there were any data about that.

Nevertheless, the values obtained are admissible: the initial displacement u_0 for model C (which was taken as reference) is of only 3.6cm, with a maximum tension for the 4 cables of 12120kN, against the 12233kN calculated with the simplified analysis. The difference is less than 1%, while the maximum design tension for the 4 cables is of 20546kN: for such values an uncertainty around 100kN is tolerable. As for the simplified models, from table 7.1 we can note that none of them replicate exactly the initial conditions of cable tension and upright free-end displacement of the reference case (model C). For model B1 and model A this is probably due to an inaccurate calibration of parameters that define the equivalent shelf (that replaced the upright), while for model B2 the difference is simply due to our approximations in designing the non-prismatic beam using the envelope of the upright shape (this point will be clarified extensively in the following sections, where we will discuss the results of the multi-support analysis). As explained in section 6.4.3, the equivalent rod pretension in model A was calculated from the results of model C, thus avoiding any initial tension miscalculation.

We therefore decided to also analyze the tension variation, while the other comparison parameters are not affected by this difference as they do not comprehend u_0 (as explained in section 7.1). Still, the tension difference between reference case and simplified model is limited within a range of 115kN, so that also this uncertainty complies with the level of approximation held. While the results of uprights and equivalent beams are not comparable since these are different elements, the cables of different models all provide the same static response of simple traction, which was affected by horizontal displacement of the cable East end. Model A, where we have modeled an equivalent connecting rod in place of the cable, was evaluated in terms of the horizontal tension component, which is constant and analogous to the other models.

7.2.2 Results with perfectly correlated accelerograms

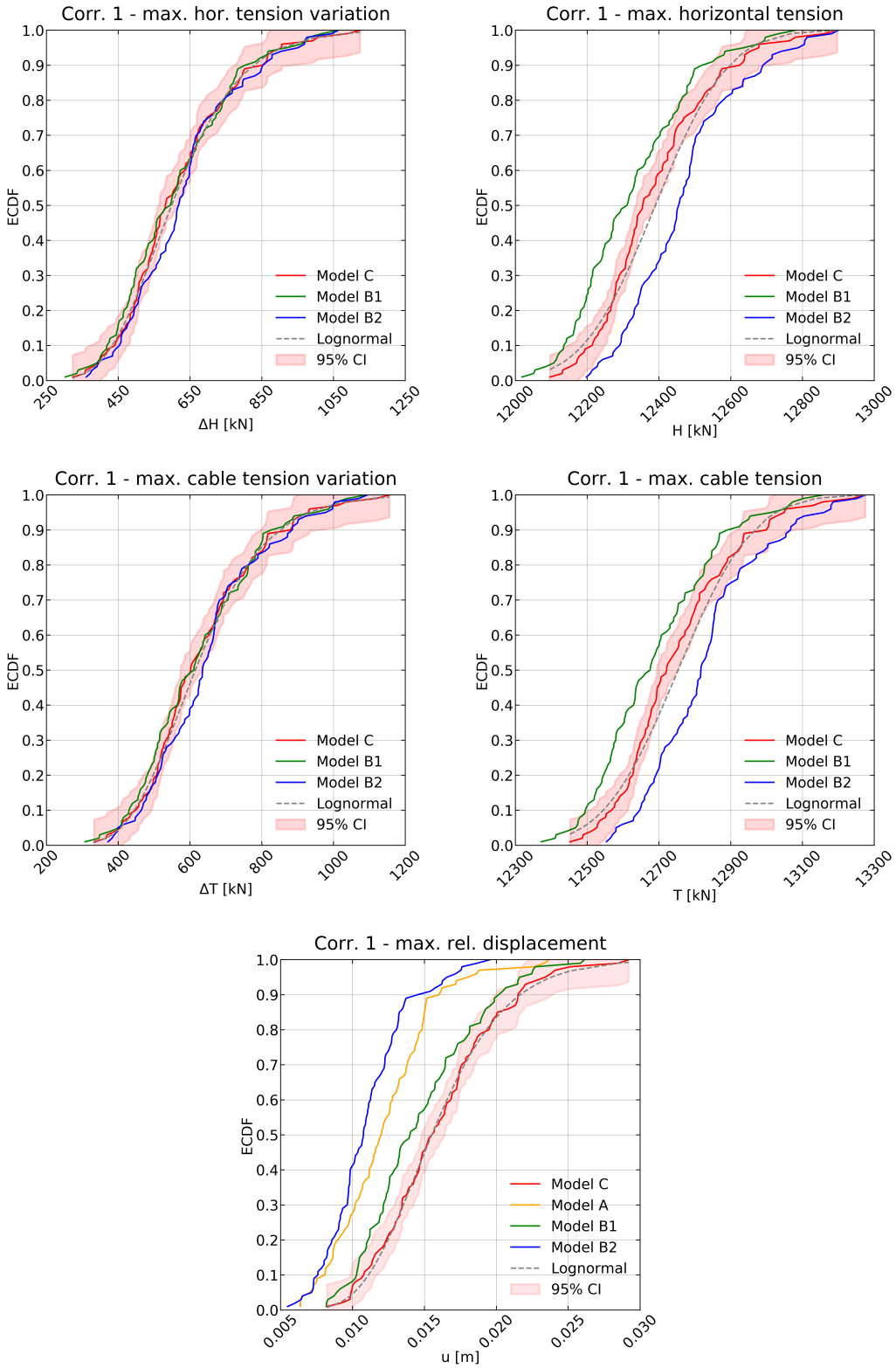

Figure 7.3: Simplified models results with correlation 1, comparison in terms of their CDFs. Source: Excel, own elaboration

Table 7.2: Simplified model results with correlation 1, comparison in terms of the main statistical parameters (mean and standard deviation). Source: Excel, own elaboration

Multi support analysis, correlation 1

		model						
		C	A		B1		B2	
		value	value	diff.	value	diff.	value	diff.
u [m]	mean	0,0194	0,0149	-23,1%	0,0180	-7,2%	0,0132	-31,9%
	std. d.	0,0031	0,0027		0,0029		0,0022	
H [kN]	mean	12514,8	12962,9	3,5%	12456,0	-0,4%	12588,0	0,5%
	std. d.	128,9	207,8		117,3		121,7	
T [kN]	mean	12881,7	n.	n.	12824,5	-0,4%	12952,8	0,5%
	std. d.	132,3	n.		120,3		125,6	
ΔH [kN]	mean	741,7	1184,9	59,7%	739,6	-0,2%	751,0	1,2%
	std. d.	128,9	207,8		117,3		121,7	
ΔT [kN]	mean	762,0	n.	n.	759,9	-0,2%	771,0	1,1%
	std. d.	132,3	n.		120,3		125,6	

In this section we analyse the seismic responses obtained from the multi-support analysis with perfectly correlated ground motions (described in detail in section 6.5.2). While comparing the different models we make reference to the graphs and tables obtained through the processing described in section 7.1, displayed in figure 7.3 and table 7.2.

- Generally, the maximum cable tension increase ranges between 360kN and 1180 kN. This variation generates maximum tensions between 12450kN and 13300kN (an increase between 5% and 10% of the initial value), whereas the relative displacement presents surprisingly low values, between 1cm and 3cm.

- Model A response is excessively different from the reference case for both the maximum horizontal tension and its variation from the initial state, to such extent that their respective CDFs could not be included in the graphs to not compromise the readability (their values are still summarized in the Annex).

- Models B1 and B2 CDFs of the maximum tension and maximum horizontal tension are regularly within the 95% CI only for non-exceedance probabilities higher than 85%, although both accurately retrace the reference trend in the graphs depicting the tension variation. Moreover, while model B1 slightly underestimates the maximum tension values of model C, model B2 provides a slight overestimation.

- Models B1 and B2 average maximum tension and average maximum tension variation are close to model C, with a difference within 70kN for the average maximum tension, and within 10kN for the average maximum tension variation.

- In terms of relative displacement, only model B1 remains within the 95% CI and only for non-excedence probabilities higher than 90% and lower than 10%, while models B2 and A do not produce an acceptable estimate. This result was also confirmed by the comparison of the mean values and the standard deviation for the different models.

- Despite always remaining within or in proximity of the 95% CI, the lognormal parametric distribution does not exactly retrace the CDFs of tension-related parameters of model C, particularly with non-exceedance probabilities lower than 70%. On the other hand it resulted particularly suitable in retracing the higher CDF values of model C and the relative displacements CDF.

In terms of relative displacement, none of the simplified models proved to be fully reliable (only model B1 remains close to the 95% CI), probably due to the difficulty in calibrating them with respect to such displacements. perhaps another factor that could have affected this result were the extremely low displacements, compared to the dimensions of the structure.

Model A failed to provide any reliable estimate of the chosen parameters. A brief comparison with the other simplified models suggests that this result might be caused by the use of a connecting rod instead of the cable. The cable net span variation indeed generates an associated sag variation, so that the cable undergoes also a vertical motion that mobilizes its masses, thus producing a variation of its vertical tension component. Model A does not consider this aspect, as it retraces only horizontal forces. The simulations provided a maximum vertical force increase between 80kN and 220kN from the initial state, that in this case resulted to be not negligible.

As for the tension-related parameters, the graphs suggest that the simplified models were affected by the different initial cable tension. In fact, by eliminating this bias the CDFs for the maximum tension of models B1, B2 and C almost overlap, similarly to what happens for the maximum tension variation. The source of this initial gap was already discussed in section 7.2.1, and while for model B1 it could have been prevented with a more accurate calibration, for model B2 could not have been avoided. However, given the magnitude of the tensions involved, the use of a highly selective formulation for the CI, the level of approximation held, we can still consider these results acceptable despite the CDFs being outside of the CI. To forestall this problem we could consider the results in terms of tension variation and calculate the initial tension separately with a static analysis, that can provide acceptable results even with simplified methods.

Regarding model B2, we must clarify why it provides good estimates of the tension-related parameters, but failing at the same time with the relative displacements. After performing a static analysis (similarly to what is described in section 6.2.2 and annex

E) we found that this model involves a 16% overestimation of the upright bending stiffness when compared to the reference case (267000kN/m against 230000kN/m). This difference is due to the use of the outer envelope to model the upright shape, when we defined the non-prismatic sections of the equivalent beam in model B2. This increase in the upright bending stiffness implies a decrease of its free-end displacements with respect to the reference case, while the cable horizontal forces are consequently higher.

As seen in section 4.2.3, cable tension does not increase evenly with the span variation, so that despite the poor approximation of model B2 in terms of relative displacements we could still obtain acceptable results in terms of tension-related parameters. This also applies to model B1, as it provides a significant underestimations of the relative displacements, while the maximum tension increase and maximum horizontal tension increase still remain within the assigned CI.

This difference in terms of bending stiffness could be eliminated by improving the upright model, for instance by including in the upright simplified model only the areas where the stresses are channeled, by taking into account the internal holes, or by switching to a tie-strut type model (that however would require some further analyses to size each element). With such arrangements model B2 could certainly provide reliable results as much as those of model B1 (but without any calibration process) in terms of both tension and displacement-related parameters: this issue could certainly be explored in a more detailed investigation.

The approximation with the lognormal parametric distribution function provided reliable results, particularly for the higher values of all the CDFs and for the relative displacements. In fact, the lognormal distribution is commonly assumed for the distribution of extremes in seismic analysis. However, the growth trend of tension-related parameters is slightly different from the CDFs of model C, especially along the intermediate sections: it would be advisable to deepen this aspect with specific statistical tests of model quality.

7.2.3 Results with uncorrelated accelerograms

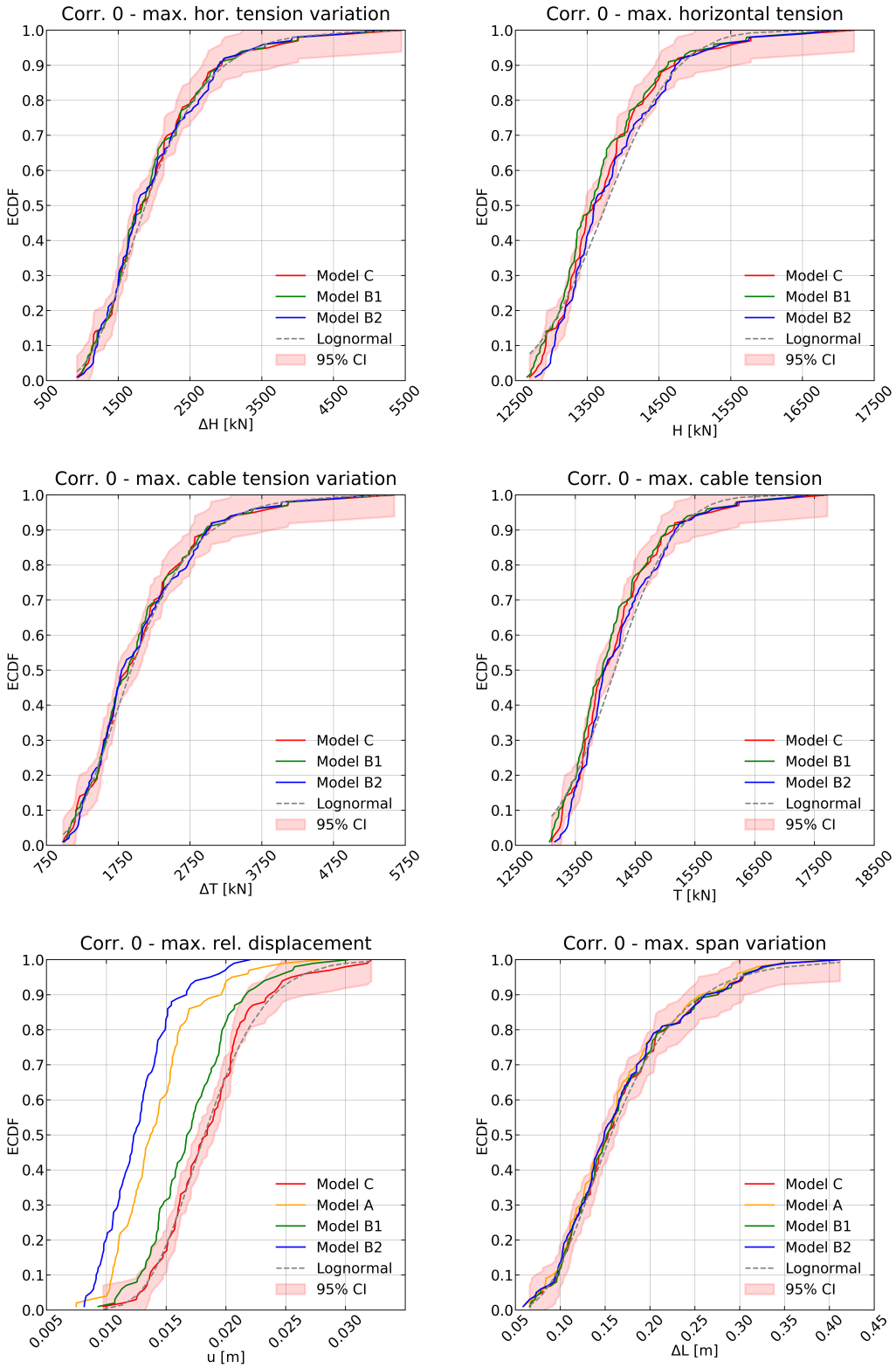

Figure 7.4: Simplified models results with correlation 0, comparison in terms of their CDFs. Source: Excel, own elaboration

Table 7.3: Simplified model results with correlation 0, comparison in terms of the main statistical parameters. Source: Excel, own elaboration

Multi support analysis, correlation 0

		model						
		C	A		B1		B2	
		value	value	diff.	value	diff.	value	diff.
u [m]	mean	0,0218	0,0169	-22,3%	0,0201	-7,6%	0,0150	-31,2%
	std. d.	0,0033	0,0030		0,0028		0,0023	
H [kN]	mean	14365,4	13661,6	-4,9%	14290,6	-0,5%	14432,4	0,5%
	std. d.	746,7	449,5		732,9		706,5	
T [kN]	mean	14778,9	n.		14707,4	-0,5%	14845,3	0,4%
	std. d.	766,4	n.		751,7		724,0	
ΔH [kN]	mean	2592,3	1883,6	-27,3%	2574,2	-0,7%	2595,5	0,1%
	std. d.	746,7	449,5		732,9		706,5	
ΔT [kN]	mean	2659,2	n.		2642,7	-0,6%	2663,4	0,2%
	std. d.	766,4	n.		751,7		724,0	

In this section we analyse the seismic responses obtained from the multi-support analysis with uncorrelated ground motions (already described in detail in section 6.5.3). While comparing the different models we make reference to the graphs and tables obtained through the processing described in section 7.1, displayed in figure 7.4 and in table 7.3.

- The maximum cable tension increase ranges between 1000kN and 5750kN, corresponding to maximum tensions between 13200kN and 17500kN (remarkably higher than the values for correlated ground motions). Also the relative displacement is higher if compared to the previous case, between 1cm and 3.3cm.

- The net span variation CDFs are quite similar for all models, and range between 6cm and 41cm: this happens mainly because of the the relative displacement between the uprights basements, since the East upright free-end horizontal displacement has a lower order of magnitude.

- As seen for the case with correlated ground motions, Model A response is excessively different from model C, so that its CDFs could not be included in the graphs (their values are still summarized in the Annex).

- Models B1 and B2 CDFs of the maximum tension and maximum horizontal tension are always within the 95% CI, thus retracing accurately the reference case. The same happens for the tension variation.

- Models B1 and B2 average maximum tension and average maximum tension variation are close to those of model C, with almost the same gaps seen for

correlated ground motions. The same happens for the standard deviations, since both simplified models give slightly lower values than the reference case.

- In terms of relative displacement we have the same outcome seen for correlated ground motions: only model B1 remains within the CI and only for non-excedence probabilities higher than 90% or lower than 10%, while models B2 and A do not produce an acceptable estimate.

- Also regarding the lognormal distribution the results are similar to those of the previous case: the lognormal parametric distribution does not exactly retrace the CDFs of model C, but still remains within or in proximity of the 95% CI.

- For all parameters the simplified models CDFs and the lognormal distribution provide increasingly accurate approximations for higher values of the non exceedance probability.

Generally, the multi-support analysis with uncorrelated ground motions confirms the outcomes seen for the case of correlated ground motions, that have been described in the previous section (to which we make reference). However, there are still some noteworthy considerations.

In terms of relative displacement we have reached the same conclusion seen for the case with correlated ground motions. As for model B2, we must remark what is stated in the previous section (7.2.2) about the reasons of such outcome and the potential improvements.

Because of the low relative displacements the span variation could not be considered to evaluate the simplified models: much of it (around 90% on average) is generated by using uncorrelated ground motions, that introduce a relative displacement between the uprights bases, which is the same among all models. Because of this, the obtained CDFs are similar and the net span variation is not a relevant parameter.

Model A failed to provide any reliable estimate of the chosen parameters, thus confirming what was seen for the previous case in section 7.2.2.

As for the tension-related parameters, in this case it appears that the CDFs were not biased by the different initial cable tension. The initial tension is indeed the same as in the case of correlated ground motion, but the initial gap is "distributed" over higher maximum values (due to the relative displacement of the uprights' bases). We can therefore confirm that simplified models B1 and B2 well reproduce the trend of the maximum tensions and maximum tension variations, while in this case the error in the initial tension estimate has less influence on the final result.

As seen in the previous section, the lognormal parametric distribution function generally provided an acceptable approximation of the reference case, specifically for

higher values of the CDFs and for the relative displacements CDF. Here too, it appears that in terms of tension-related parameters its trend is slightly different from model C, even if the function remains always within or in proximity of the CI.

7.2.4 Influence of correlation values over the seismic response

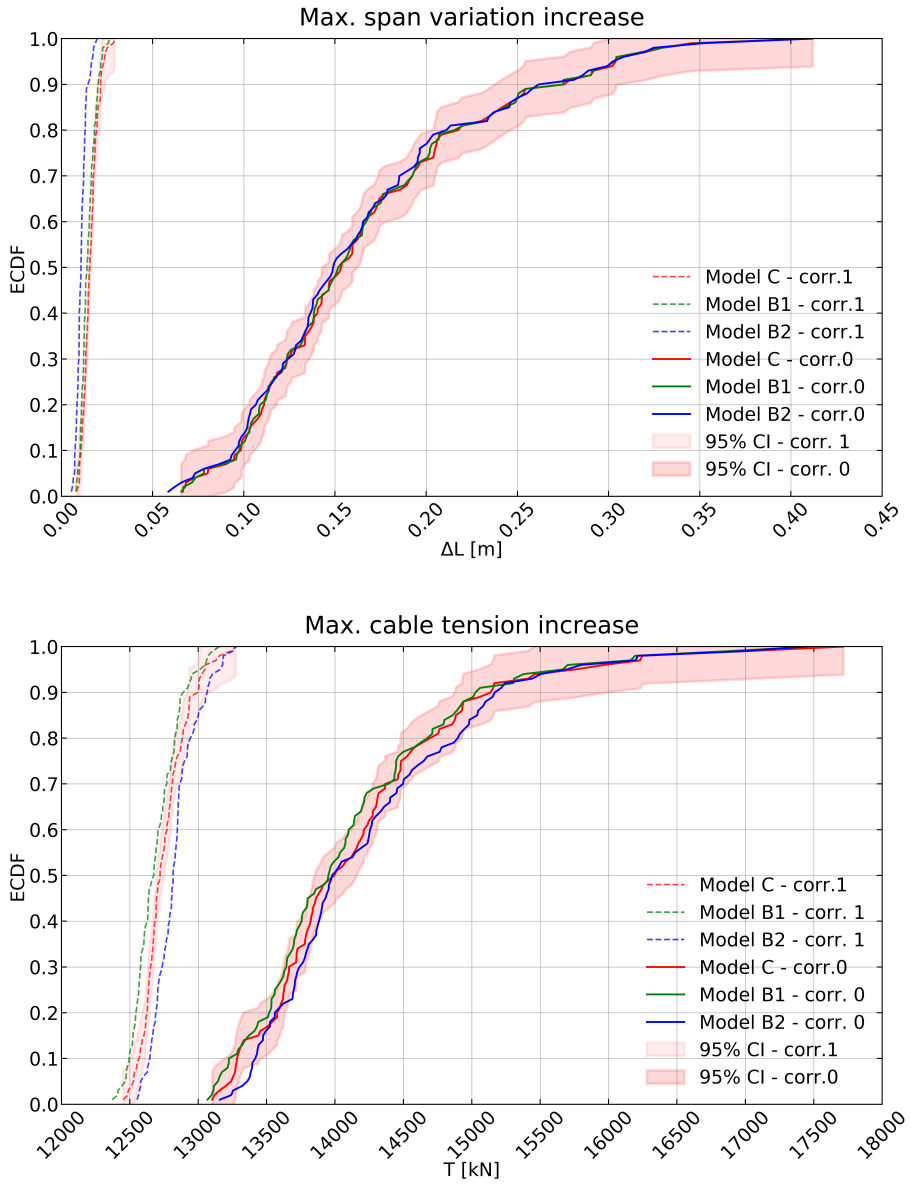

Figure 7.5: Model C multi-support analysis results, comparison between correlation 0 and 1 CDFs in terms of span variation (top) and maximum tension (bottom). Source: Excel, own elaboration

We purposely reorganized the CDFs and the statistical parameters displayed in sections 7.2.2 and 7.2.3, to set out a brief comparison between the two scenarios considered

in this multi-support analysis (perfectly correlated and uncorrelated ground motions, displayed in figure 7.5). Given the unsatisfactory results of the simplified models in terms of maximum relative displacements, for this benchmark we have only considered the reference case. For the same reason, model A was not included in any of the graphs.

The use of uncorrelated ground motions implies a considerable increase in the maximum tension (from 12% up to 31% for the highest peaks). As already discussed in section 4.2.5, the tension variation is directly related to the cable span variation: in this case we have introduced a relative displacement between the uprights' bases, so that now the span variation corresponds to the sum of this component with the relative displacement of the cable East end. When compared to the analysis with correlated ground motion, the peak amplitude of the East upright oscillation increases, but is still an order of magnitude lower than the maximum relative ground displacement (about 3cm against 15to 40cm). In none of the cases the cables reached their maximum design tension of 20456kN, although with uncorrelated motions they came close with maximums values near 17800kN. Despite being not enough to cause the cable failure, this additional term is decisive in causing a considerable increase of the maximum cable tension. Another notable effect is the dispersion of the maximum tension peaks over a larger range of values: this also is generated by the use of uncorrelated ground motions, since the relative displacements between the uprights' bases are spread over a wider interval than the relative displacements of the East upright free-end.

As described in section 6.5.2, the actual correlation factor would range between 0 and 1 (where these values represent the two uttermost, yet unrealistic, cases). However, this comparison still provides a clear idea of what is achieved by applying different accelerograms at the uprights' basements, since there is an additional component in the span variation related to the ground relative displacement. This outcome proves the sensitiveness of large span structures to this phenomenon, that consequently must be considered during the design stage.

7.2.5 Notes about the time required for the analysis

One of the main benefits of simplified models is the significant reduction of the computational load. This is essentially due to the reduction of the finite elements included in the simplified model, as well as some further simplifications that can be applied to the analysis procedure. This implies for the designer a reduction in the time required to complete each analysis cycle, as well as a reduction in the size of the output files.

We summarized in table 7.4 the data about the time required to complete 100 simulations for each model, as well as the size of the output files thus produced. Although these parameters are affected by the computer performances, a brief qualitative comparison

is still possible. Leaving aside model A (since it did not provide acceptable results), it is clear how simplified models B1 and B2 involve a considerable saving of time compared to model C, that we took as reference. The same is true for the output files size (which in model C is mainly related to the number of shell elements in the upright mesh). The use of uncorrelated ground motions instead of perfectly correlated ground motions, on the other hand, did not produce any difference in terms of time required to complete the analysis and, as expected, in terms of output file size. In conclusion, simplified models proved to be exceptionally time-saving and memory-saving.

Table 7.4: Total analysis time and output size for each model, referred to a complete cycle of 100 simulations. Source: Excel, own elaboration

Simplified models, output information for 100 simulations

	model			
	A	B1	B2	C
time	3h 30min	6h	6h	33h 30min
output file	20 Gb	85 Gb	85 Gb	960 Gb

Chapter 8

Conclusions

At the completion of this work, we have reached a number of remarkable conclusions. Once more we got confirmation that the static analysis of a suspended cable carried out using simplified methods, and specifically by approximating its geometry with a parabola, is extremely effective. The results obtained in chapter 4 were in fact verified with both the simplified and the realistic models. Even for a particular scenario, such as the case of an assigned span variation, we obtained results within an acceptable approximation limit.

Regarding the use of simplified models, as seen in chapter 7, model A did not produce satisfactory results, probably since we replaced the cable with an equivalent connecting rod, that was unable to replicate the vertical motion induced by the seismic action and related to the cable span variation. Models B1 and B2 provided excellent approximations of the structural response in terms of tension-related parameters. Even if these models have well performed with these benchmarks, in terms of displacements we have not reached the same level of approximation. Only model B1 (with the cable and a specifically calibrated equivalent cantilever beam) came close to the reference case, though remaining outside of the selected confidence band. Although tension and span variations are strictly related, such outcome was possible due to the flattening of the cable load-displacement curve, so that large displacements does not correspond to evenly large tension increases. Having low displacements, we still obtained a narrow range of values for the tension increase (compared to the maximum design tension), that was close to the reference case despite the poor approximation of the span variation. This also applies to model B2, where the overestimation of the upright bending stiffness led to an underestimation of the upright free-end displacements, while the tension-related parameters where still within the confidence interval. Given their extremely low values, it would be advisable to repeat the multi-support analysis with a more sensitive structure in terms of displacements, to assess whether or not simplified models can provide reliable results. In absence of further information, we can only remark the difficulty in calibrating such simplified models in relations to these displacements.

From the comparison described in chapter 7 it resulted that, from a probabilistic

standpoint, models B1 and B2 accurately reproduce the seismic response of model C (defined in chapter 6, as the other models) in terms of tension-related parameters. as long as we include the cable and we simplify only the supporting substructures. For these elements it is crucial to maintain the bending stiffness (and therefore the sections' inertia) and the mass distribution along the cantilever as close as possible to that of the original structure. For model B2 this was not fully achieved, although it can be improved by including only the areas of the upright were the stresses are channeled. With such arrangement it would certainly provide reliable results as those of model B1: this issue could certainly be deepened with a specific investigation. Alternatively, we can define equivalent sections and masses through a sophisticated calibration process (that began with the analyses performed in chapters 4 and 5), which however was not necessary, as by using only the geometric data available in the available design we could obtain an excellent result.

We must outline also some considerations about the outcome of the multi-support analysis, in relation to the two scenarios considered. These represent the two uttermost cases, and despite not being realistic they still allow some notable conclusions: although in none of the case we reached the failure point, the sensitiveness of the study case to the possible alteration of the ground motions is clear, particularly because of the high relative ground displacements between the uprights, that led to a considerable increase of the maximum cable tensions, even if the upright free-end displacement remained surprisingly limited. Such outcome enhances the need to perform multi-support analyses when designing large span structures, especially in case of low correlation factors, so as to prevent a potential failure.

The final judgment is that, in terms of tension-related parameters, for a large span structure (such as the study case, the Braga Stadium, described in chapter 3) it is possible to obtain reliable results from a probabilistic standpoint about its seismic response using only simplified models. In every case we must include the cable, while we can apply heavy simplifications to the supporting structures, without necessarily resorting to sophisticated calibration procedures. The studies hereby conducted underline the relevance of the multi-support analysis, particularly in case of the large span suspended roofs, whose sensitiveness against low values of the correlation factor between the applied ground motion has been once again demonstrated.

Thanks to this work it was also possible to acquire useful knowledge and experience about cable-suspended roofs. Other matters deepened while developing this thesis concern structural modelling and data analysis, without which it would not have been possible to create reliable simplified models and manage the amount of data related to the simulations performed. The research work carried out before moving on to the

development of the work just presented was very demanding, being mainly focused on the study of suspended cable structures: as for them we can't forget to mention what was learned in particular about the complex, yet peculiar, relationship between geometry, internal forces and applied loads. Besides the conclusions already discussed, due to the reasons just illustrated I can only consider the result of this work as fully satisfactory both on personal and academic levels.

Appendix A

Available drwaings of the Braga Municipal Stadium

In this annex we present some designs that contain measures and technical information taken as reference during the development of this thesis, and specifically:

- A general overview of the cable-suspended roof, from which we measured the cables' diameter.
- Transverse and longitudinal sections of the cable-suspended roof, from which we measured the cables' geometry (chapters 4, 6 and annex C).
- Side view of the truss beam composite modules.
- Side view of the East upright, containing measures, materials and sections used for the upright 2D models developed in chapters 5 and 6.
- Horizontal and vertical sections of the cable support beam, showing in detail the cables linking system (discussed in section 5.4).

The designs containing the roof and the cable support beam were kindly provided by Eng. G. Berti, of MJW-Structures (and have been granted to us for the sole didactic purposes related to this thesis). Other designs that have been taken as reference are attached to [16], more specifically: side views of the stands, planes and cross-sections of the pitch, embankments and excavations prospects, details of the rainwater drainage, the cable linking system and the steel beam hinges, as well as other technical information (such as beam sections, precamber, materials). Unfortunately they did non include all the details that we needed, so when necessary we had to make some assumptions based on our personal experience.

At the time of download (23/03/2021), this document was available online for viewing only. As of today (01/12/2021) it is no longer available, so we preferred not to include these project drawings without an explicit consent of the publisher. Because of this we have included in the following designs only the information (dimensions, materials,

sections and others) that were strictly necessary for the purposes of this work, that is the development of the East upright and cables 2D models.

EAST SIDE

WEST SIDE

D

C

C

B

B

A

A

D

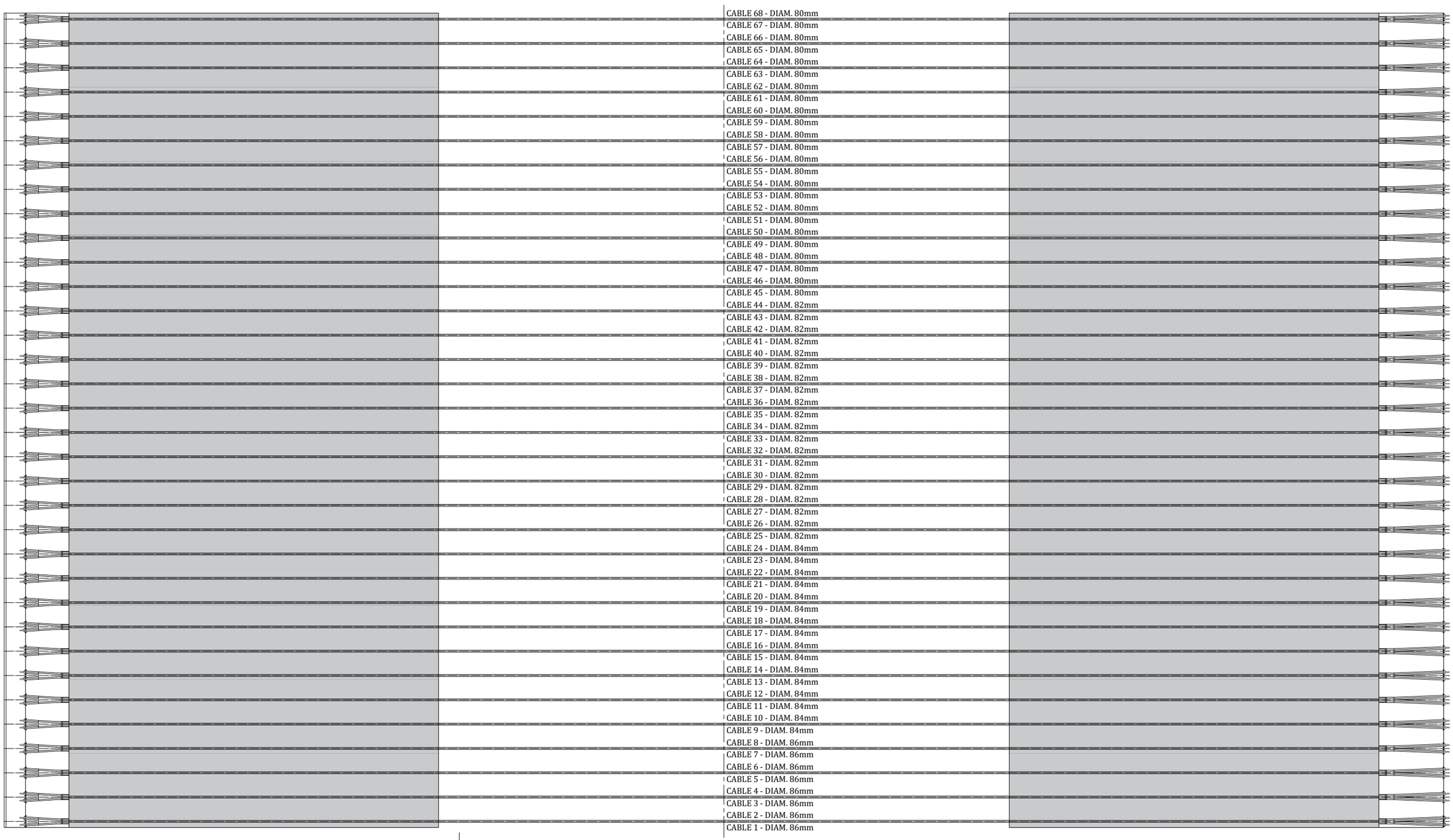

PRELIMINARY

Student: Roberto Gerussi Source: MJW Structures	Supervisors: Prof. Carlos R. Sánchez-Carratalá Prof. Marco Ballerini Prof. Marco Broccardo	Object: BRAGA MUNICIPAL STADIUM general overview of the roof	Scale: 1:600 Date: 12/12/2021	Units: [m]	Table: 1

SECTION DD

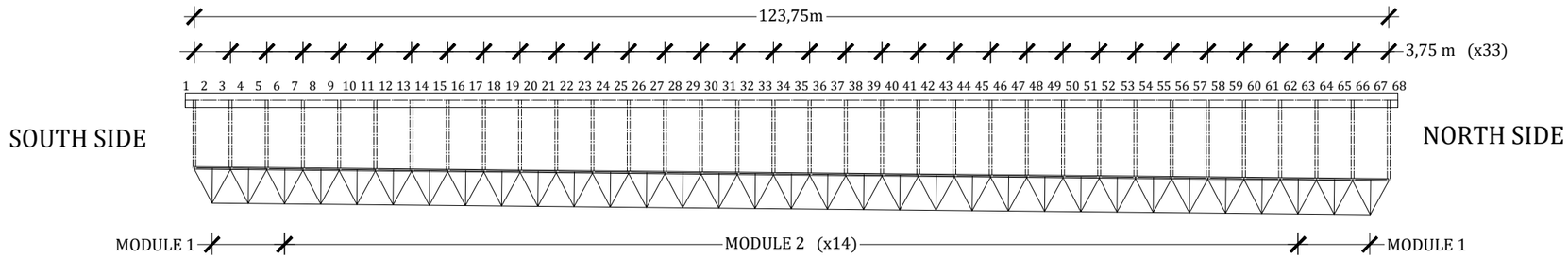

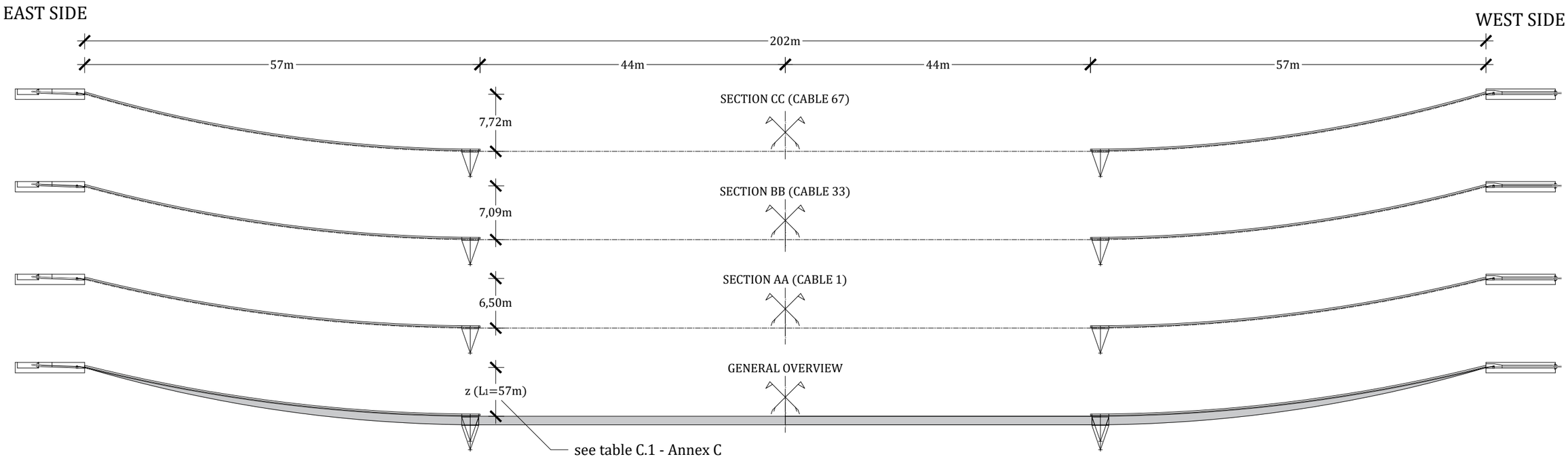

Student: Roberto Gerussi Source: MJW Structures	Supervisors: Prof. Carlos R. Sánchez-Carratalá Prof. Marco Ballerini Prof. Marco Broccardo	Object: BRAGA MUNICIPAL STADIUM longitudinal and transversal views of the cables initial geometric configuration	Scale: 1:600 Date: 12/12/2021	Units: [m]	Table: 2

TRUSS BEAM - side view of the composite modules

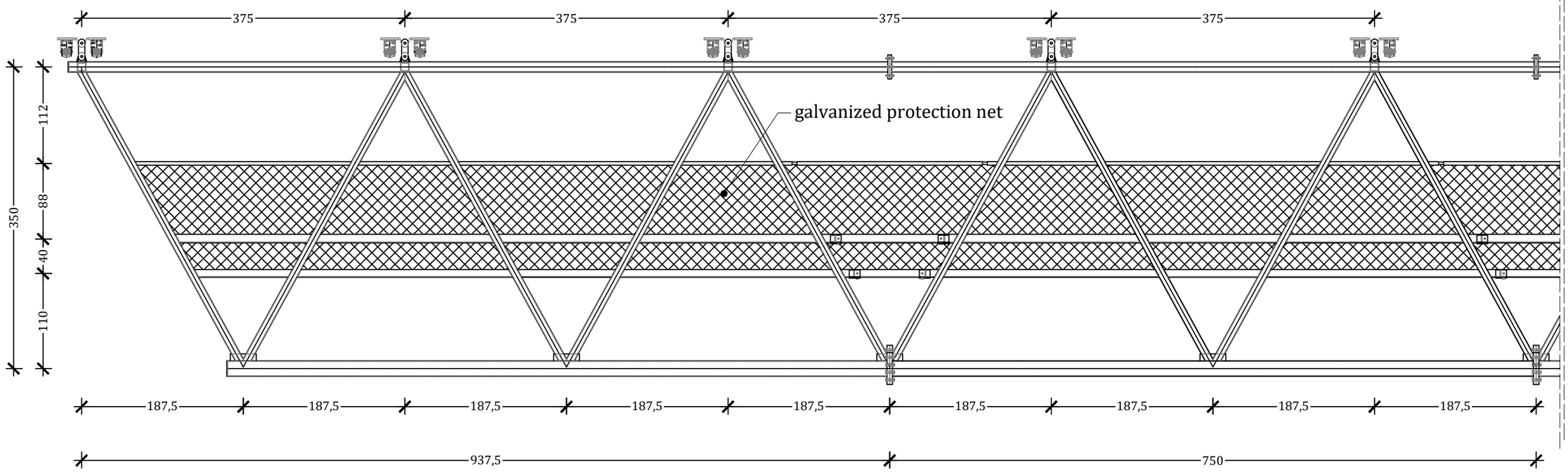

TRUSS BEAM - upper view of the composite modules

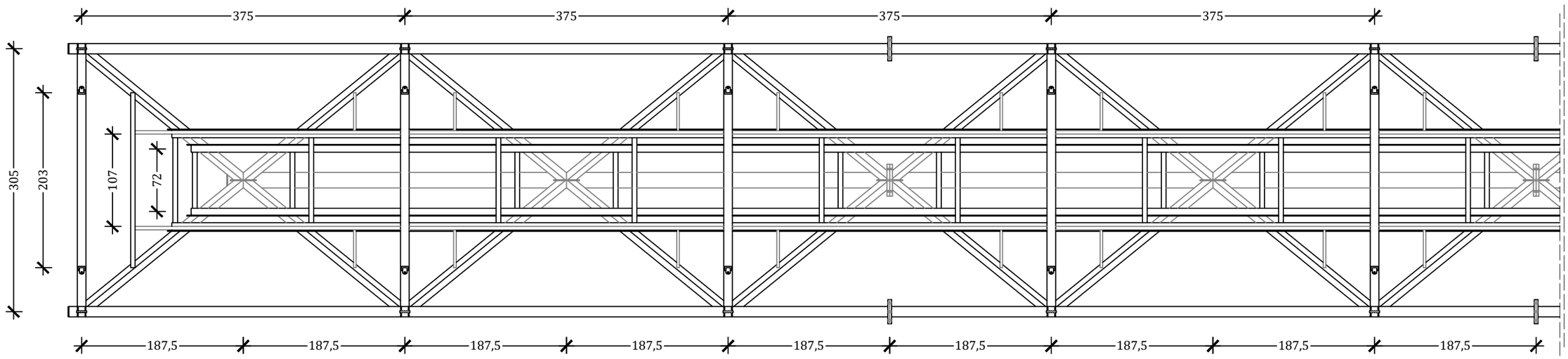

Student: Roberto Gerussi Source: MJW Structures	Supervisors: Prof. Carlos R. Sánchez-Carratalá Prof. Marco Ballerini Prof. Marco Broccardo	Object: BRAGA MUNICIPAL STADIUM longitudinal and upper views of the composite modules of the roof truss beams	Scale: 1:50 Date: 12/12/2021	Units: [cm]	Table: 3

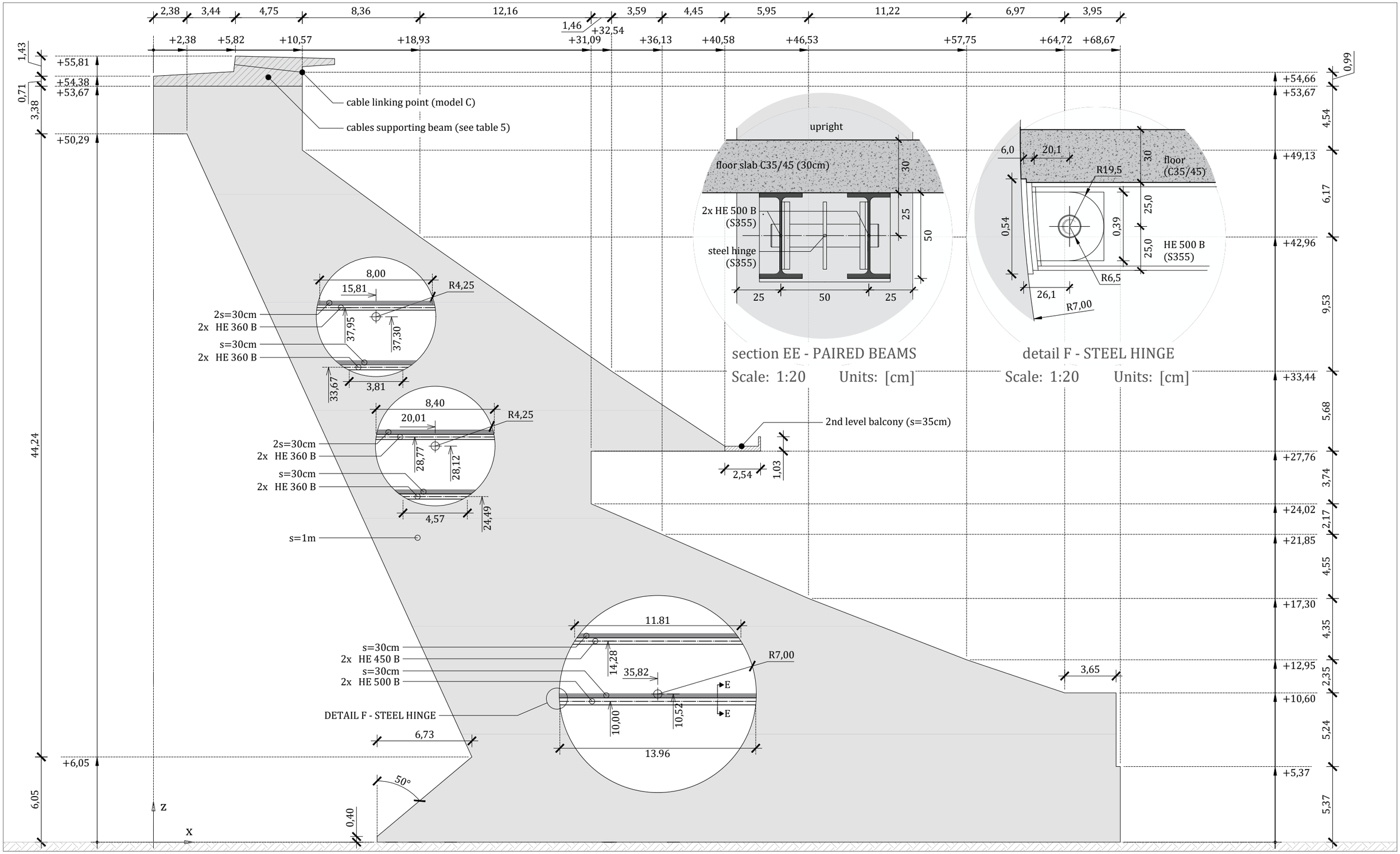

Student: Roberto Gerussi	Supervisors: Prof. Carlos R. Sánchez-Carratalá; Prof. Marco Ballerini; Prof. Marco Broccardo	Object: BRAGA MUNICIPAL STADIUM — East upright - dimensions, applied sections, details of the floors and beam hinges	Scale: 1:250	Units: [m]	Table: 4
Source: own elaboration from [16]			Date: 12/12/2021		

CABLE LINKING DEVICE - section C-C

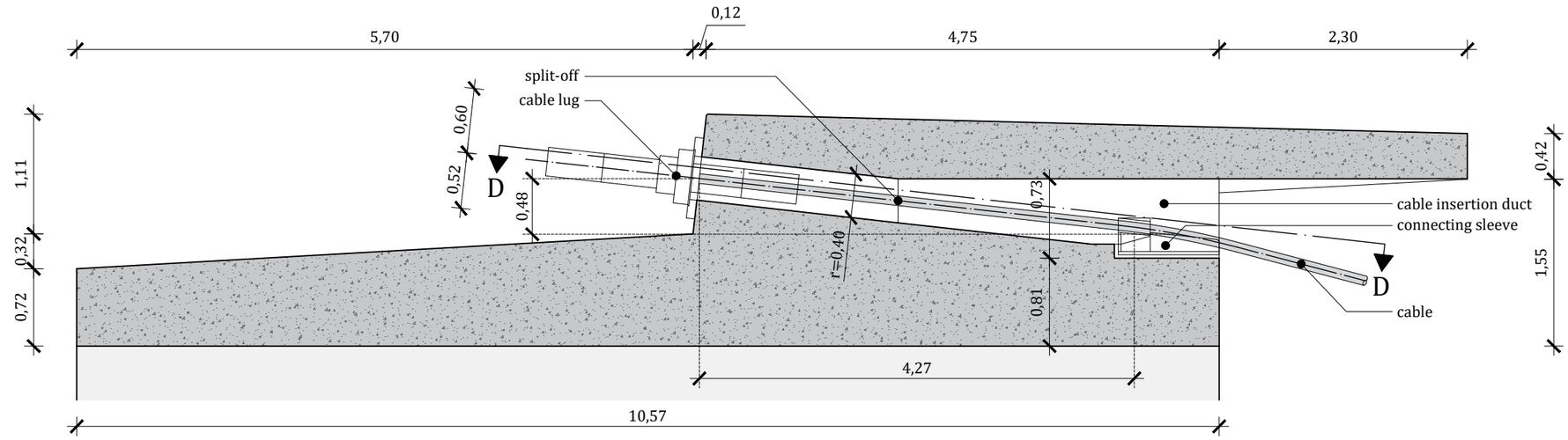

CABLE LINKING DEVICE - section D-D

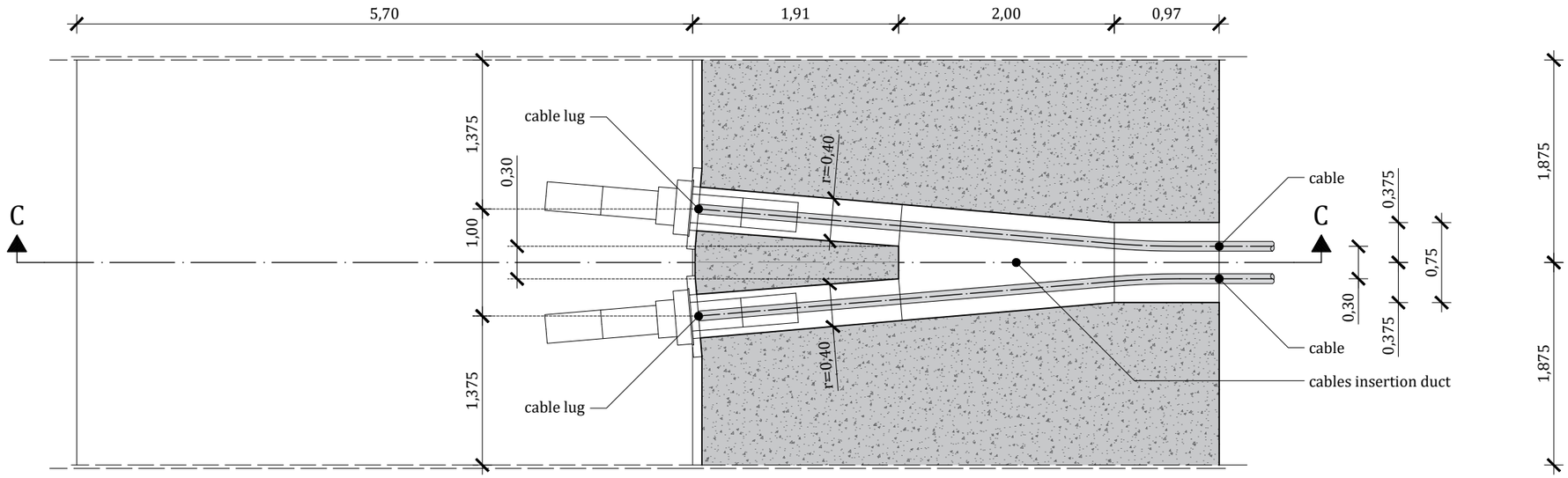

Student: Roberto Gerussi Source: MJW Structures	Supervisors: Prof. Carlos R. Sánchez-Carratalá Prof. Marco Ballerini Prof. Marco Broccardo	Object: BRAGA MUNICIPAL STADIUM East upright, significant sections of the cable linking system	Scale: 1:50 Date: 12/12/2021	Units: [cm]	Table: 5

Appendix B

Net pressure coefficient evaluation

We propose a brief outline of the net pressure coefficient estimate, that we applied to define equivalent uniformly distributed load in place of the dynamic wind action (as described in section 4.1.5) for the cable static analysis discussed in chapter 4.

Table B.1: Estimated values of mean and standard deviation of c_p, from the data displayed in figure: 4.3. Source: Excel, own elaboration.

c_p estimated statistical	
μ	σ
0,050	0,100
0,050	0,100
0,100	0,100
0,200	0,200
0,050	0,050
0,050	0,050
average:	
0,100	0,125

Referring to the mean and standard deviation values displayed in figure 4.3, we have considered the most stressed cable (which is the border one) and estimated the values of the mean and standard deviation over 6 points along it, summarized in table B.1. We defined a unique value for both of these parameters, calculated as a mean of the collected data. We then calculated the normal probability distribution function, according to:

$$f(x) = \frac{1}{\sigma\sqrt{2\pi}} \exp - \frac{(x-\mu)^2}{2\sigma^2} \tag{B.1}$$

Obtaining the values summarized in table B.2 for the normal PDF and the CDF respectively (also shown in figure 4.4). For c_p we adopted the value that corresponds almost to the 99^{th} percentile, which is equal to 0.35.

Table B.2: c_p, normal probability distribution function and cumulated distribution function determined from the estimated mean and standard deviation. Source: Excel, own elaboration.

c_p normal distribution - part. 1			c_p normal distribution - part. 2		
c_p	PDF	CDF	c_p	PDF	CDF
-0,40	0,00000	0,00000	0,10	3,86668	0,40129
-0,39	0,00001	0,00000	0,11	3,94479	0,44038
-0,38	0,00001	0,00000	0,12	3,98444	0,48006
-0,37	0,00002	0,00000	0,13	3,98444	0,51994
-0,36	0,00003	0,00000	0,14	3,94479	0,55962
-0,35	0,00005	0,00000	0,15	3,86668	0,59871
-0,34	0,00008	0,00000	0,16	3,75240	0,63683
-0,33	0,00013	0,00000	0,17	3,60527	0,67364
-0,32	0,00020	0,00000	0,18	3,42944	0,70884
-0,31	0,00031	0,00001	0,19	3,22972	0,74215
-0,30	0,00048	0,00001	0,20	3,01137	0,77337
-0,29	0,00073	0,00002	0,21	2,77985	0,80234
-0,28	0,00109	0,00003	0,22	2,54059	0,82894
-0,27	0,00163	0,00004	0,23	2,29882	0,85314
-0,26	0,00241	0,00006	0,24	2,05936	0,87493
-0,25	0,00353	0,00009	0,25	1,82649	0,89435
-0,24	0,00510	0,00013	0,26	1,60383	0,91149
-0,23	0,00732	0,00019	0,27	1,39431	0,92647
-0,22	0,01038	0,00028	0,28	1,20009	0,93943
-0,21	0,01459	0,00040	0,29	1,02265	0,95053
-0,20	0,02029	0,00058	0,30	0,86277	0,95994
-0,19	0,02794	0,00082	0,31	0,72065	0,96784
-0,18	0,03810	0,00114	0,32	0,59595	0,97441
-0,17	0,05143	0,00159	0,33	0,48792	0,97982
-0,16	0,06873	0,00219	0,34	0,39550	0,98422
-0,15	0,09094	0,00298	0,35	0,31740	0,98778
-0,14	0,11912	0,00402	0,36	0,25218	0,99061
-0,13	0,15449	0,00539	0,37	0,19837	0,99286
-0,12	0,19837	0,00714	0,38	0,15449	0,99461
-0,11	0,25218	0,00939	0,39	0,11912	0,99598
-0,10	0,31740	0,01222	0,40	0,09094	0,99702
-0,09	0,39550	0,01578	0,41	0,06873	0,99781
-0,08	0,48792	0,02018	0,42	0,05143	0,99841
-0,07	0,59595	0,02559	0,43	0,03810	0,99886
-0,06	0,72065	0,03216	0,44	0,02794	0,99918
-0,05	0,86277	0,04006	0,45	0,02029	0,99942
-0,04	1,02265	0,04947	0,46	0,01459	0,99960
-0,03	1,20009	0,06057	0,47	0,01038	0,99972
-0,02	1,39431	0,07353	0,48	0,00732	0,99981
-0,01	1,60383	0,08851	0,49	0,00510	0,99987
0,00	1,82649	0,10565	0,50	0,00353	0,99991
0,01	2,05936	0,12507	0,51	0,00241	0,99994
0,02	2,29882	0,14686	0,52	0,00163	0,99996
0,03	2,54059	0,17106	0,53	0,00109	0,99997
0,04	2,77985	0,19766	0,54	0,00073	0,99998
0,05	3,01137	0,22663	0,55	0,00048	0,99999
0,06	3,22972	0,25785	0,56	0,00031	0,99999
0,07	3,42944	0,29116	0,57	0,00020	1,00000
0,08	3,60527	0,32636	0,58	0,00013	1,00000
0,09	3,75240	0,36317	0,59	0,00008	1,00000
0,10	3,86668	0,40129	0,60	0,00005	1,00000

Appendix C

Cable static analysis of State 0, ULS and SLS

In this annex we briefly summarize the results of the cable static analyses described in sections 4.2.1 and 4.2.3. In the first one we described how we solved the static problem using a simplified formulation with the parabolic approximation, calculating for each cable its tension and overall length under permanent loads only (the State 0 combination). On the second one we described how we solved the static problem in case of a load increase using that same simplified formulation, thus calculating tension and length variations for each cable for different load combinations (ULS combination that maximise the cable tension, SLS characteristic combination for non reversible loads). The outcomes of these analyses, whose values have been summarized in tables C.1, C.2 and C.3, have been extensively discussed in sections 4.2.2 and 4.2.4.

We clarify that, for the sake of synthesis and of readability, we have included in the tables presented in this annex only the most significant values for the purpose of this thesis. We have therefore omitted other parameters calculated, such as the length of each cable section, the elongation from the State 0, the cable geometry for the State 0, as well as its variations for an assigned load increase, that otherwise would have required several pages full of tables.

Table C.1: Cable tension and elongation under permanent loads only. Source: Excel, own elaboration.

State 0 - cable static analysis results

cable	Φ m	$z(L_1)$ m	H kN	V kN	T kN	l_{tot} m
1-2	86	-6,49	1739,27	353,54	1774,84	202,91
3-4	86	-6,53	3105,64	690,58	3181,49	202,94
5-6	86	-6,57	3089,99	690,58	3166,22	202,96
7-8	86	-6,60	3074,50	690,58	3151,11	202,97
9-10	84	-6,64	3047,64	688,56	3124,45	202,98
11-12	84	-6,68	3032,55	688,56	3109,74	202,99
13-14	84	-6,72	3017,59	688,56	3095,16	203,00
15-16	84	-6,75	3002,80	688,56	3080,73	203,02
17-18	84	-6,79	2988,15	688,56	3066,45	203,03
19-20	84	-6,83	2973,64	688,56	3052,32	203,04
21-22	84	-6,86	2959,29	688,56	3038,34	203,05
23-24	84	-6,90	2945,08	688,56	3024,50	203,06
25-26	82	-6,94	2921,59	686,84	3001,24	203,08
27-28	82	-6,98	2907,70	686,84	2987,72	203,09
29-30	82	-7,01	2893,95	686,84	2974,34	203,10
31-32	82	-7,05	2880,34	686,84	2961,10	203,11
33-34	**82**	**-7,09**	**2973,55**	**715,34**	**3058,39**	**203,13**
35-36	82	-7,12	2958,07	715,34	3043,33	203,14
37-38	82	-7,16	2838,75	686,84	2920,66	203,15
39-40	82	-7,20	2825,58	686,84	2907,86	203,16
41-42	82	-7,24	2812,61	686,84	2895,26	203,18
43-44	82	-7,27	2789,75	684,92	2872,60	203,19
45-46	80	-7,31	2777,01	684,92	2860,23	203,20
47-48	80	-7,35	2764,46	684,92	2848,04	203,22
49-50	80	-7,38	2752,02	684,92	2835,97	203,23
51-52	80	-7,42	2739,70	684,92	2824,02	203,24
53-54	80	-7,46	2727,74	684,92	2812,42	203,26
55-56	80	-7,50	2715,65	684,92	2800,69	203,27
57-58	80	-7,53	2703,66	684,92	2789,07	203,28
59-60	80	-7,57	2691,79	684,92	2777,56	203,30
61-62	80	-7,61	2680,03	684,92	2766,16	203,31
63-64	80	-7,64	2668,37	684,92	2754,87	203,32
65-66	80	-7,68	2663,38	685,87	2750,27	203,33
67-68	80	-7,72	1474,85	348,83	1515,54	203,32

Table C.2: Cable tension and elongation under ULS combination that maximise its tension. Source: Excel, own elaboration.

ULS - cable static analysis results

cable	Φ m	$z(L_1)$ m	H kN	V kN	T kN	l_{tot} m
1-2	86	-6,49	2508,40	560,88	2570,35	203,07
3-4	86	-6,53	4352,40	1103,77	4490,17	203,22
5-6	86	-6,57	4335,46	1103,77	4473,76	203,24
7-8	86	-6,60	4318,65	1103,77	4457,47	203,25
9-10	84	-6,64	4272,99	1101,04	4412,57	203,27
11-12	84	-6,68	4256,64	1101,04	4396,74	203,28
13-14	84	-6,72	4240,40	1101,04	4381,01	203,29
15-16	84	-6,75	4224,27	1101,04	4365,40	203,31
17-18	84	-6,79	4208,26	1101,04	4349,91	203,32
19-20	84	-6,83	4192,37	1101,04	4334,54	203,33
21-22	84	-6,86	4176,59	1101,04	4319,28	203,34
23-24	84	-6,90	4160,92	1101,04	4304,14	203,35
25-26	82	-6,94	4119,93	1098,72	4263,92	203,38
27-28	82	-6,98	4104,66	1098,72	4249,17	203,39
29-30	82	-7,01	4089,50	1098,72	4234,53	203,40
31-32	82	-7,05	4074,45	1098,72	4219,99	203,41
33-34	**82**	**-7,09**	**4193,16**	**1141,47**	**4345,75**	**203,43**
35-36	82	-7,12	4176,35	1141,47	4329,53	203,45
37-38	82	-7,16	4028,50	1098,72	4175,65	203,45
39-40	82	-7,20	4013,78	1098,72	4161,44	203,46
41-42	82	-7,24	3999,24	1098,72	4147,42	203,47
43-44	82	-7,27	3973,01	1096,13	4121,45	203,49
45-46	80	-7,31	3944,30	1096,13	4093,78	203,51
47-48	80	-7,35	3930,23	1096,13	4080,22	203,52
49-50	80	-7,38	3916,26	1096,13	4066,77	203,54
51-52	80	-7,42	3902,38	1096,13	4053,41	203,55
53-54	80	-7,46	3888,88	1096,13	4040,41	203,56
55-56	80	-7,50	3875,19	1096,13	4027,23	203,57
57-58	80	-7,53	3861,59	1096,13	4014,15	203,59
59-60	80	-7,57	3848,08	1096,13	4001,15	203,60
61-62	80	-7,61	3834,65	1096,13	3988,24	203,61
63-64	80	-7,64	3821,32	1096,13	3975,42	203,63
65-66	80	-7,68	3816,24	1097,55	3970,93	203,64
67-68	80	-7,72	2164,73	554,66	2234,66	203,49

Table C.3: Cable tension and elongation under SLS combination for non reversible effects, that maximise its tension. Source: Excel, own elaboration.

SLS, non reversible effects - cable static analysis results

cable	Φ m	$z(L_1)$ m	H kN	V kN	T kN	l_{tot} m
1-2	86	-6,49	1962,45	412,08	2005,25	202,96
3-4	86	-6,53	3474,99	807,66	3567,62	203,03
5-6	86	-6,57	3458,89	807,66	3551,93	203,04
7-8	86	-6,60	3442,93	807,66	3536,40	203,05
9-10	84	-6,64	3411,52	805,64	3505,36	203,07
11-12	84	-6,68	3395,98	805,64	3490,24	203,08
13-14	84	-6,72	3380,57	805,64	3475,24	203,09
15-16	84	-6,75	3365,30	805,64	3460,39	203,10
17-18	84	-6,79	3350,17	805,64	3445,68	203,11
19-20	84	-6,83	3335,18	805,64	3431,11	203,13
21-22	84	-6,86	3320,32	805,64	3416,67	203,14
23-24	84	-6,90	3305,60	805,64	3402,36	203,15
25-26	82	-6,94	3277,82	803,92	3374,97	203,17
27-28	82	-6,98	3263,45	803,92	3361,01	203,18
29-30	82	-7,01	3249,21	803,92	3347,18	203,19
31-32	82	-7,05	3235,09	803,92	3333,48	203,20
33-34	**82**	**-7,09**	**3325,07**	**832,42**	**3427,68**	**203,22**
35-36	82	-7,12	3309,12	832,42	3412,21	203,23
37-38	82	-7,16	3191,94	803,92	3291,62	203,24
39-40	82	-7,20	3178,22	803,92	3278,32	203,25
41-42	82	-7,24	3164,70	803,92	3265,21	203,27
43-44	82	-7,27	3141,38	802,00	3242,14	203,28
45-46	80	-7,31	3124,30	802,00	3225,59	203,30
47-48	80	-7,35	3111,21	802,00	3212,92	203,31
49-50	80	-7,38	3098,24	802,00	3200,36	203,32
51-52	80	-7,42	3085,37	802,00	3187,91	203,33
53-54	80	-7,46	3072,88	802,00	3175,82	203,35
55-56	80	-7,50	3060,23	802,00	3163,58	203,36
57-58	80	-7,53	3047,68	802,00	3151,44	203,37
59-60	80	-7,57	3035,24	802,00	3139,41	203,39
61-62	80	-7,61	3022,90	802,00	3127,48	203,40
63-64	80	-7,64	3010,66	802,00	3115,65	203,41
65-66	80	-7,68	3004,92	802,95	3110,35	203,43
67-68	80	-7,72	1675,43	407,37	1724,24	203,37

Appendix D

Cable static analysis for an assigned span increase

In this annex we briefly summarize the results of the cable static analysis described in section 4.2.5, where we illustrated the case of an assigned increase of the cable span, considering a combination with only permanent loads (the state 0). This analysis was performed on cable 33-34, considering the cases of a linear elastic cable and of an inelastic cable. The outcomes for the scenarios just described have been discussed in detail in section 4.2.6 for the case of an extensible cable with linear elastic behaviour, and section 4.2.7 for the case of a non extensible cable. The resulting values from these analyses are summarized in tables D.1 and D.2. Moreover, the results of table D.1 have also been used for the evaluation of the equivalent axial stiffness of the connecting rod defined for Model A (section 6.4.3).

We clarify that, for the sake of synthesis and of readability, we have included in the tables presented in this annex only the most significant values for the purpose of this thesis. We have therefore omitted other parameters calculated, such as the length of each cable section, the redistributed loads and the cable geometry variation for each assigned increase (that otherwise would have required several pages full of tables). We have also displayed the results with an increase step of 5cm, while the calculations have been performed with a step of 1cm.

Table D.1: Cable 33-34, calculated values of the load displacement-curve for an assigned horizontal displacement of one of its ends in case of extensible cable. Source: Excel, own elaboration

Cable 33-34, load-displacement curve for an extensible cable

δ m	H kN	ΔH kN	V kN	T kN	ΔT kN	l m	Δl m
0,00	2973,6	0,0	715,3	3058,4	0,0	203,13	0,00
0,05	3029,7	56,2	715,3	3113,0	54,7	203,14	0,01
0,10	3083,1	109,5	715,3	3165,0	106,6	203,16	0,03
0,15	3138,4	164,9	715,3	3218,9	160,5	203,17	0,04
0,20	3196,0	222,4	715,3	3275,0	216,7	203,18	0,06
0,25	3255,7	282,1	715,3	3333,3	274,9	203,20	0,07
0,30	3317,8	344,2	715,3	3394,0	335,6	203,21	0,09
0,35	3382,4	408,8	715,3	3457,2	398,8	203,23	0,10
0,40	3449,6	476,0	715,3	3523,0	464,6	203,25	0,12
0,45	3519,5	546,0	715,3	3591,5	533,1	203,26	0,14
0,50	3592,3	618,7	715,3	3662,8	604,4	203,28	0,15
0,55	3668,1	694,6	715,3	3737,2	678,8	203,30	0,17
0,60	3749,6	776,1	715,3	3817,3	758,9	203,32	0,19
0,65	3828,8	855,2	715,3	3895,1	836,7	203,34	0,21
0,70	3913,9	940,4	715,3	3978,8	920,4	203,36	0,23
0,75	4002,2	1028,6	715,3	4065,6	1007,2	203,38	0,25
0,80	4093,4	1119,8	715,3	4155,4	1097,0	203,40	0,28
0,85	4187,9	1214,4	715,3	4248,6	1190,2	203,43	0,30
0,90	4285,9	1312,3	715,3	4345,2	1286,8	203,45	0,32
0,95	4387,3	1413,7	715,3	4445,2	1386,8	203,48	0,35
1,00	4492,2	1518,6	715,3	4548,8	1490,4	203,50	0,37
1,05	4600,7	1627,1	715,3	4656,0	1597,6	203,53	0,40
1,10	4712,7	1739,1	715,3	4766,6	1708,3	203,56	0,43
1,15	4826,1	1852,5	715,3	4878,8	1820,4	203,59	0,46
1,20	4946,8	1973,2	715,3	4998,2	1939,8	203,62	0,49
1,25	**5073,7**	**2100,2**	**715,3**	**5123,9**	**2065,5**	**203,64**	**0,52**
1,30	5195,7	2222,2	715,3	5244,8	2186,4	203,68	0,55
1,35	5325,4	2351,8	715,3	5373,2	2314,8	203,71	0,58
1,40	5458,3	2484,7	715,3	5504,9	2446,6	203,74	0,61
1,45	5594,4	2620,9	715,3	5640,0	2581,6	203,78	0,65
1,50	5733,6	2760,1	715,3	5778,1	2719,7	203,81	0,68

Table D.2: Cable 33-34, calculated values of the load displacement-curve for an assigned horizontal displacement of one of its ends in case of inextensible cable. Source: Excel, own elaboration

Cable 33-34, tension and length increase for an inextensible cable

δ m	H kN	ΔH kN	V kN	T kN	ΔT kN	l m	Δl m
0,00	2973,6	0,0	715,3	3058,4	0,0	203,13	0,00
0,05	3047,2	73,6	715,3	3130,0	71,6	203,13	0,00
0,10	3123,6	150,0	715,3	3204,4	146,1	203,13	0,00
0,15	3203,3	229,8	715,3	3282,2	223,8	203,13	0,00
0,20	3289,2	315,6	715,3	3366,0	307,7	203,13	0,00
0,25	3381,8	408,2	715,3	3456,6	398,2	203,13	0,00
0,30	3481,9	508,4	715,3	3554,7	496,3	203,13	0,00
0,35	3596,5	622,9	715,3	3666,9	608,5	203,13	0,00
0,40	3718,8	745,3	715,3	3787,0	728,6	203,13	0,00
0,45	3854,1	880,5	715,3	3919,9	861,5	203,13	0,00
0,50	4004,6	1031,0	715,3	4068,0	1009,6	203,13	0,00
0,55	4173,2	1199,6	715,3	4234,0	1175,7	203,13	0,00
0,60	4372,0	1398,4	715,3	4430,1	1371,7	203,13	0,00
0,65	4594,9	1621,4	715,3	4650,3	1591,9	203,13	0,00
0,70	4853,7	1880,2	715,3	4906,1	1847,8	203,13	0,00
0,75	**5157,5**	**2184,0**	**715,3**	**5206,9**	**2148,5**	**203,13**	**0,00**
0,80	5549,3	2575,7	715,3	5595,2	2536,8	203,13	0,00
0,85	6023,0	3049,5	715,3	6065,4	3007,0	203,13	0,00
0,90	6633,7	3660,2	715,3	6672,2	3613,8	203,13	0,00
0,95	7524,0	4550,4	715,3	7557,9	4499,5	203,13	0,00
1,00	8811,9	5838,4	715,3	8840,9	5782,5	203,13	0,00
1,05	11255,1	8281,6	715,3	11277,8	8219,4	203,13	0,00
1,10	18599,7	15626,1	715,3	18613,4	15555,0	203,13	0,00
1,15	31845,9	28872,4	715,3	31854,0	28795,6	203,13	0,00
1,20	45632,7	42659,1	715,3	45638,3	42579,9	203,13	0,00
1,25	59149,2	56175,7	715,3	59153,5	56095,2	203,13	0,00
1,30	72665,7	69692,2	715,3	72669,3	69610,9	203,13	0,00
1,35	86182,3	83208,7	715,3	86185,2	83126,8	203,13	0,00
1,40	99698,8	96725,2	715,3	99701,4	96643,0	203,13	0,00
1,45	113215,3	110241,8	715,3	113217,6	110159,2	203,13	0,00
1,50	126731,8	123758,3	715,3	126733,9	123675,5	203,13	0,00

Appendix E

Upright 2D model: static analysis results

In this annex we propose, for the sake of completeness, the results of the static analysis conducted in chapter 5 (to which we refer) on the simplified 2D upright model defined in section 5.2.1. The results related to a seismic combination that includes only permanent loads, named *base permanent*, have already been discussed in section 5.2.4, while here we want to briefly summarize the results for the other combinations considered:

- Seismic Limit State combination that includes both permanent and crowd loads, analysed with a combination named *base permanent + Q cat.C5*:

$$G1\ DEAD + G1\ ADD + G2 + 0.6 \cdot Q\ cat.C5 + CABLE\ 33/34 \tag{E.1}$$

- Ultimate Limit State combination that maximise the upright bending towards outside, analysed with a combination named *ULS MAX EAST*:

$$\begin{aligned} &1.35 \cdot G1\ DEAD + 1.35 \cdot G1\ ADD + 1.5 \cdot G2 + 1.5 \cdot Q\ cat.C5 + \\ &+0.9 \cdot Q\ wind\ west + 0.75 \cdot Q\ snow + CABLE\ 33/34\ ULS\ min \end{aligned} \tag{E.2}$$

- Ultimate Limit State combination that maximise the upright bending towards inside, analysed with a combination named *ULS MAX WEST*:

$$\begin{aligned} &G1\ DEAD + G1\ ADD + 0.8 \cdot G2 + 1.5 \cdot Q\ wind\ east + \\ &+CABLE\ 33/34\ ULS\ max \end{aligned} \tag{E.3}$$

Where the load belonging to each load pattern have been accurately described in section 5.1. Figure E.1 shows the deformed shapes for the ULS combinations, while figures E.2 and E.3 show the stress state of the upright due to these same combinations.

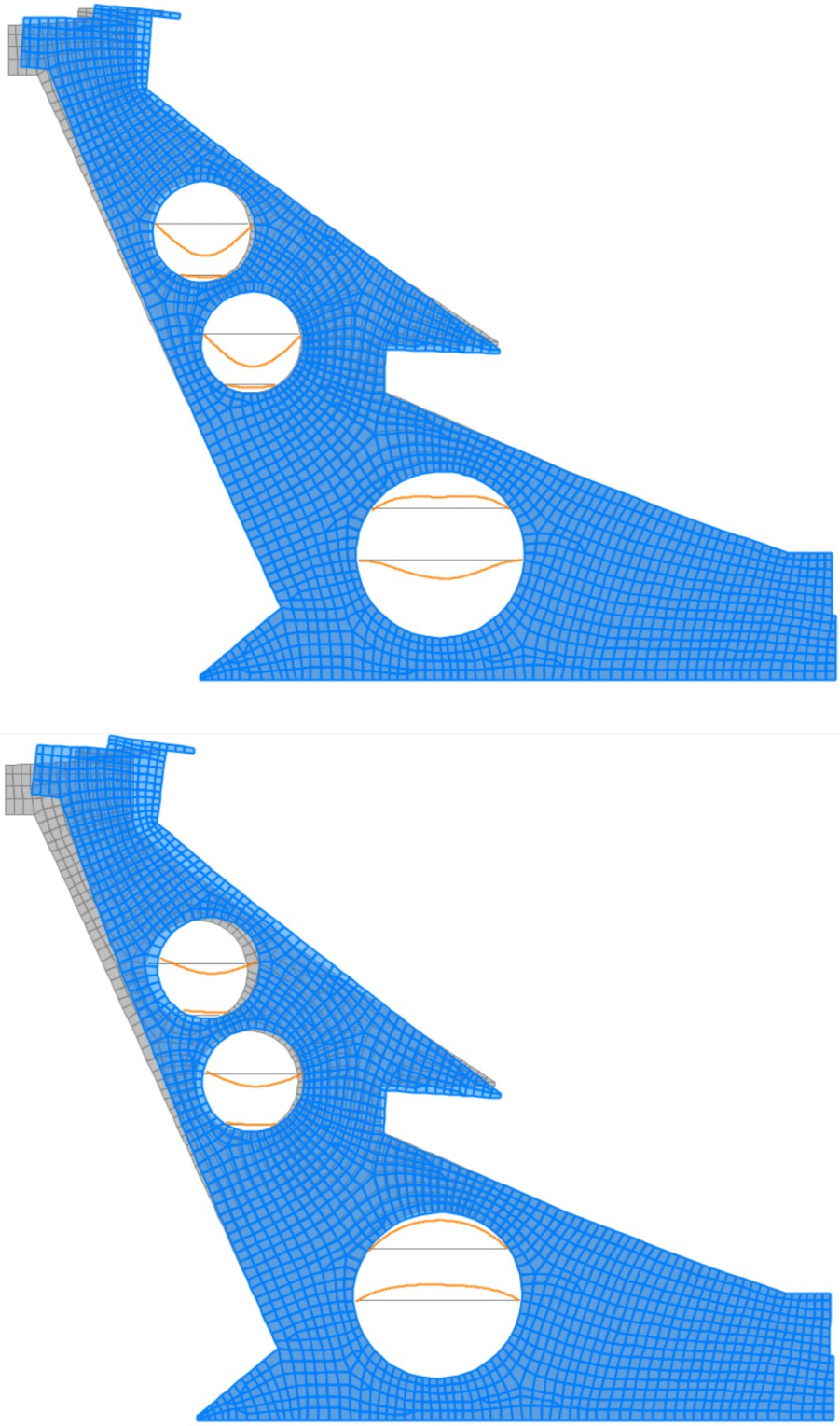

Figure E.1: Deformed shapes of the upright model under *ULS MAX EAST* (top) and *ULS MAX WEST* (bottom) combinations respectively. Displacements are amplified with a scaling factor of 50. Source: SAP2000 - own model

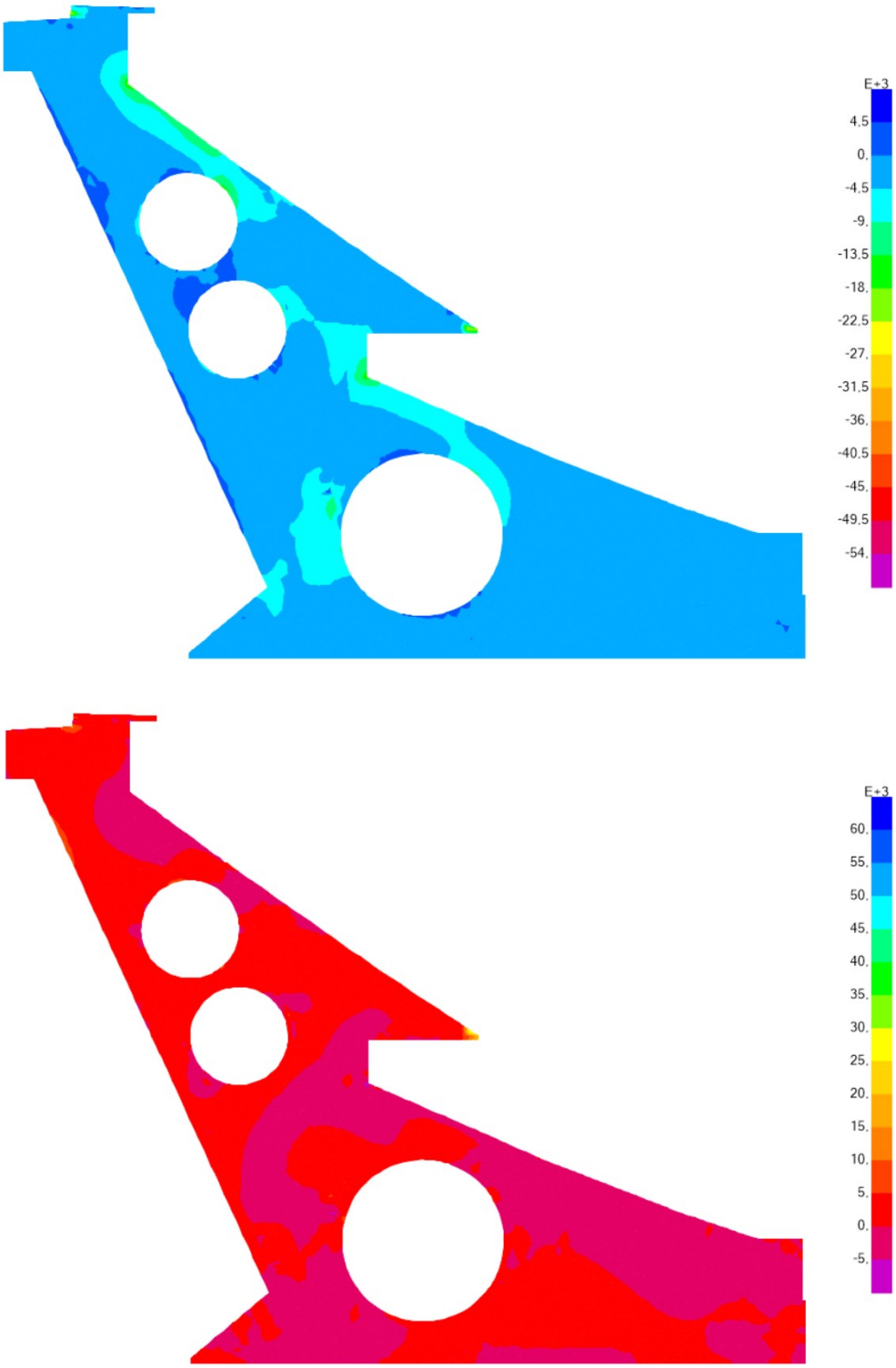

Figure E.2: S_{min} (up) and S_{MAX} (down) stresses along the upright under *ULS MAX EAST* combination. The stresses are represented in kN/m^2. Source: SAP2000 - own model

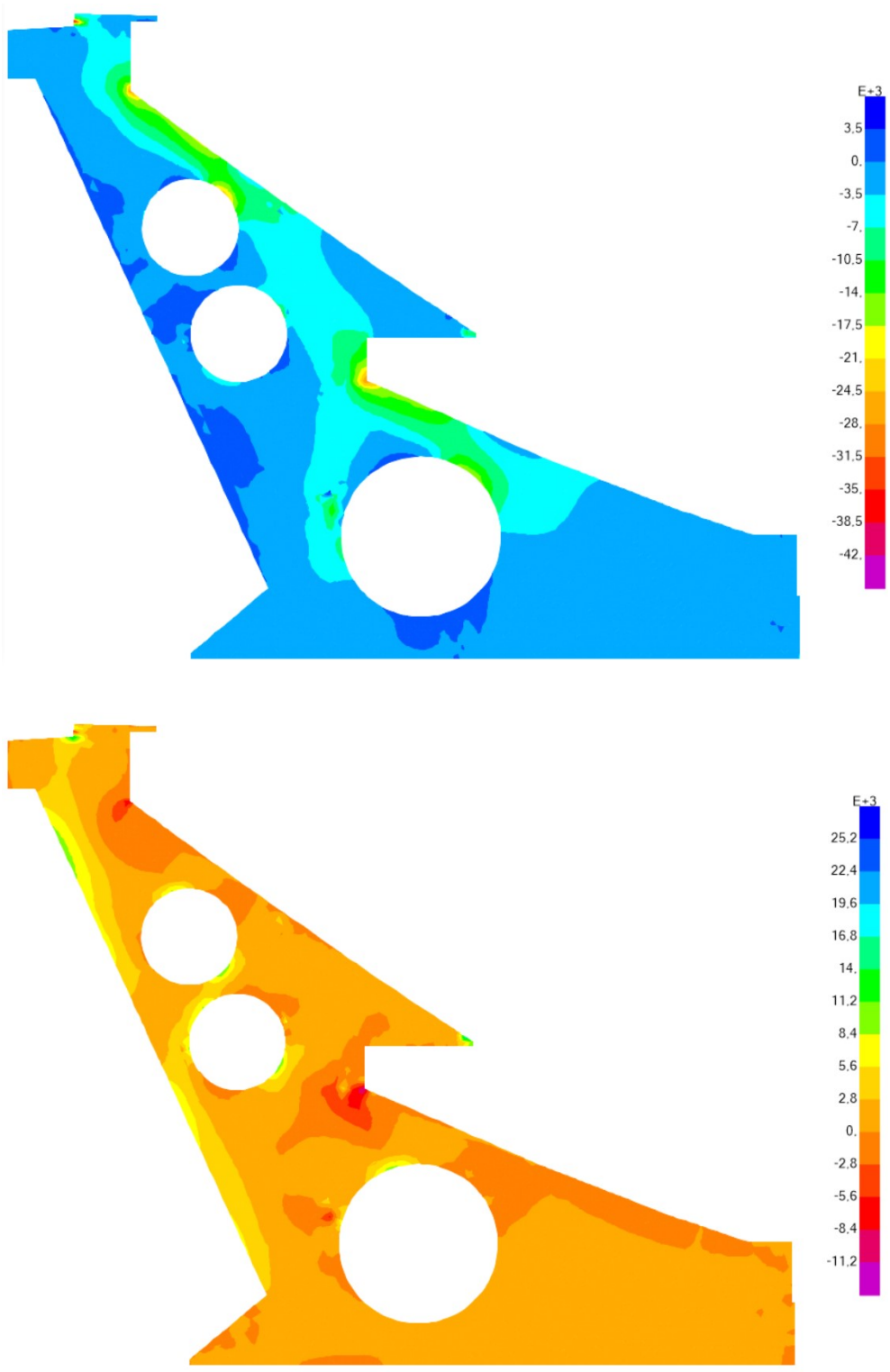

Figure E.3: S_{min} (up) and S_{MAX} (down) stresses along the upright under *ULS MAX WEST* combination. The stresses are represented in kN/m^2. Source: SAP2000 - own model

In both cases the upright remains bent toward inside, thus confirming that the cable action counterbalance the own weight of the East stand. The horizontal displacements

at the upright free-end due to these combinations are: 0.0251 m for *ULS MAX WEST*, 0.0553 m for *ULS MAX EAST*, compared to a displacement of 0.0365 m for *base permanent* (which is the Seismic Limit State combination with only permanent loads, discussed in section 5.2.4.

Regarding *base permanent+Q cat.C5*, there were no significant differences from *base permanent*: the upright free-end horizontal displacement slightly decrease from 0.0365 m to 0.0363 m, while for the upright internal stresses and deformed shape we can still make reference to those displayed in figures 5.12 an 5.11 respectively. Due to this outcome we were able to conclude that the effects of live loads are generally negligible if compared to the dead loads (an particularly the upright own weight and the cable transmitted action).

Finally, we applied a concentrated horizontal load to the node that corresponds to the cable linking point, for then measuring its horizontal displacement and evaluating the upright bending stiffness as the ratio between applied force and displacement. We started from 0 kN, and increased with steps of 500 kN up to 20000 kN. Table E.1 summarize the values of force applied and horizontal displacement, while figure 6.6 shows the load-displacement curve, that confirms its linear behaviour.

Table E.1: Applied forces and corresponding displacements of the cable linking node to the upright. Source: SAP2000, own elaboration

Upright load-displacement curve

H [kN]	u [m]	H [kN]	u [m]
0	-0,014	10000	0,030
500	-0,011	10500	0,032
1000	-0,009	11000	0,034
1500	-0,007	11500	0,036
2000	-0,005	12000	0,039
2500	-0,003	12500	0,041
3000	-0,001	13000	0,043
3500	0,002	13500	0,045
4000	0,004	14000	0,047
4500	0,006	14500	0,049
5000	0,008	15000	0,052
5500	0,010	15500	0,054
6000	0,013	16000	0,056
6500	0,015	16500	0,058
7000	0,017	17000	0,060
7500	0,019	17500	0,063
8000	0,021	18000	0,065
8500	0,023	18500	0,067
9000	0,026	19000	0,069
9500	0,028	19500	0,071
10000	0,030	20000	0,073

Appendix F

Upright 2D model: modal analysis results

We briefly summarize the results of the modal analysis performed over a 2D model of the cantilever East Stand (illustrated in section 5.2.1), considering the masses due to a seismic mass combination that include also the crowd overload (carried out with a modal load case named *MODAL 2*, described in section 5.2.5). In figure F.1 we show the upright deformed shapes for the first 10 vibration modes, while in table F.1 we summarize the modal participating mass ratios for the first 40 vibration modes.

The deformed shapes of the first 10 modes clearly resemble those found with load case *MODAL 1*, that does not include the mass related to the crowd overload. The only difference is mode 2, that in this case mobilizes only the upper steel beam of the lower upright hole, while previously it was related to the upright oscillation (that now is mobilized with mode 3). Although the natural frequencies in this case are generally higher, for mode 3 the frequency is considerably close to that of the corresponding mode 2, found with *MODAL 1*. We concluded that, for both cases considered, the modal analysis provided qualitatively similar results, and that the mass related to the crowd overload significantly affects only the modes that involve the steel beams, and not the whole upright.

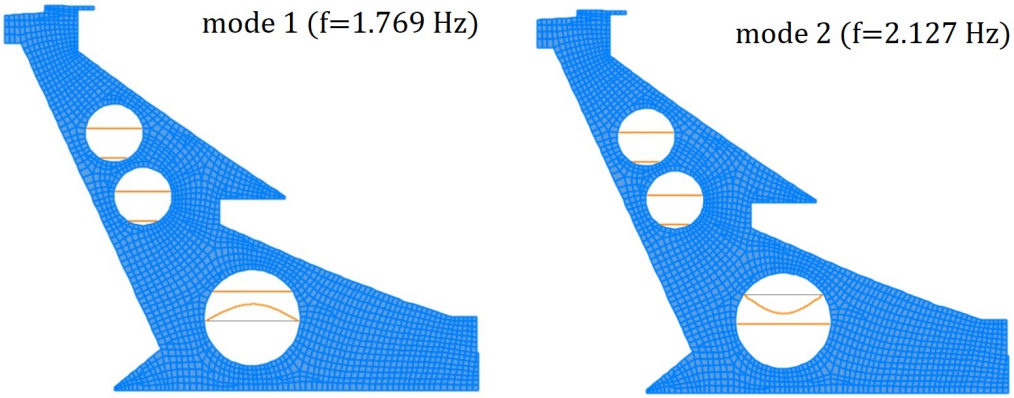

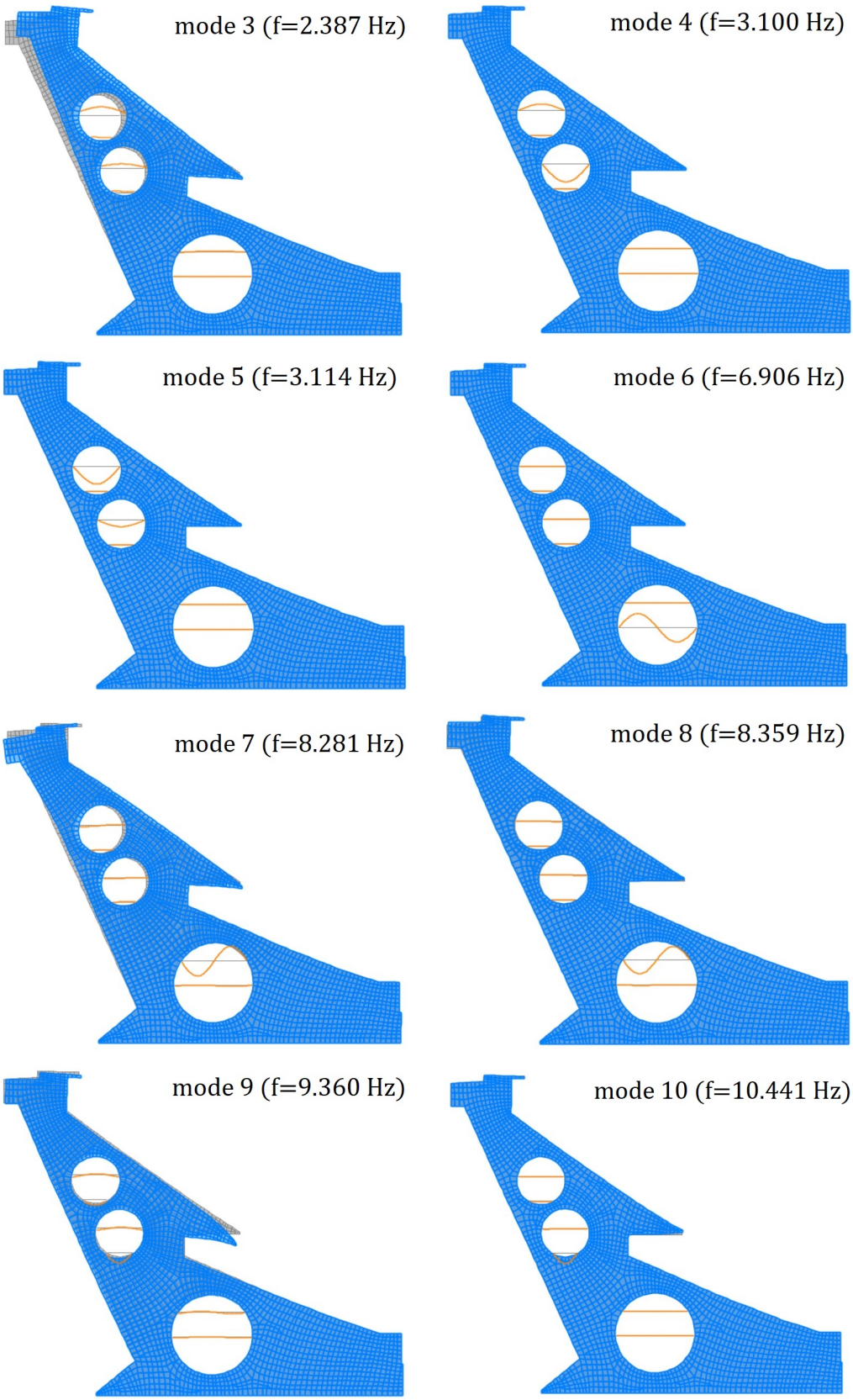

Figure F.1: First 10 natural modes of the cantilever stand for *MODAL 2* load case. Each mode is suitably scaled to display the deformed geometry. Source: SAP2000, own elaboration

Table F.1: Summary of periods and modal participating mass ratios for *MODAL 2* load case, including permanent load and crowd overload in seismic mass determination. Source: SAP2000, own elaboration

Modal participating mass ratios

mode	T [sec]	Ux	sum Ux	Uz	sum Uz	Ry	sum Ry
1	0,5653	0,0000	0,0000	0,0225	0,0225	0,0007	0,0007
2	0,4701	0,0001	0,0001	0,0181	0,0407	0,0015	0,0022
3	0,4182	0,3078	0,3079	0,0425	0,0832	0,4567	0,4589
4	0,3226	0,0001	0,3081	0,0044	0,0876	0,0001	0,4590
5	0,3212	0,0092	0,3173	0,0160	0,1036	0,0003	0,4593
6	0,1448	0,0001	0,3174	0,0001	0,1037	0,0008	0,4600
7	0,1208	0,1427	0,4602	0,0382	0,1419	0,0205	0,4805
8	0,1196	0,0446	0,5048	0,0061	0,1480	0,0025	0,4831
9	0,1068	0,0171	0,5219	0,3133	0,4614	0,0073	0,4903
10	0,0958	0,0334	0,5553	0,0015	0,4629	0,0056	0,4959
11	0,0933	0,0860	0,6413	0,0753	0,5382	0,0251	0,5210
12	0,0846	0,0001	0,6415	0,0005	0,5386	0,0000	0,5210
13	0,0845	0,0004	0,6418	0,0006	0,5392	0,0001	0,5211
14	0,0821	0,0044	0,6462	0,0088	0,5480	0,0017	0,5228
15	0,0681	0,0008	0,6469	0,0046	0,5526	0,0005	0,5233
16	0,0658	0,0537	0,7006	0,0419	0,5945	0,0048	0,5281
17	0,0586	0,0008	0,7015	0,0005	0,5950	0,0001	0,5281
18	0,0475	0,0174	0,7188	0,0488	0,6438	0,0021	0,5302
19	0,0454	0,0469	0,7657	0,0000	0,6438	0,0267	0,5569
20	0,0428	0,0002	0,7659	0,0000	0,6439	0,0001	0,5570
21	0,0426	0,0054	0,7713	0,0014	0,6453	0,0025	0,5595
22	0,0416	0,0013	0,7726	0,0005	0,6458	0,0000	0,5596
23	0,0364	0,0057	0,7782	0,0049	0,6506	0,0116	0,5712
24	0,0357	0,0106	0,7888	0,0002	0,6508	0,0074	0,5786
25	0,0327	0,0521	0,8409	0,0226	0,6734	0,0020	0,5806
26	0,0304	0,0011	0,8420	0,0074	0,6808	0,0000	0,5806
27	0,0297	0,0008	0,8428	0,0013	0,6821	0,0006	0,5811
28	0,0295	0,0030	0,8458	0,0204	0,7025	0,0044	0,5855
29	0,0290	0,0000	0,8458	0,0000	0,7025	0,0003	0,5858
30	0,0289	0,0012	0,8470	0,0013	0,7038	0,0003	0,5861
31	0,0289	0,0000	0,8470	0,0001	0,7039	0,0000	0,5861
32	0,0282	0,0001	0,8471	0,0090	0,7129	0,0079	0,5940
33	0,0264	0,0010	0,8481	0,0001	0,7130	0,0002	0,5942
34	0,0262	0,0000	0,8481	0,0002	0,7132	0,0001	0,5943
35	0,0256	0,0025	0,8506	0,0002	0,7134	0,0001	0,5944
36	0,0255	0,0084	0,8590	0,0018	0,7152	0,0005	0,5949
37	0,0245	0,0021	0,8611	0,0008	0,7160	0,0020	0,5969
38	0,0236	0,0067	0,8678	0,0091	0,7251	0,0001	0,5970
39	0,0230	0,0088	0,8766	0,0092	0,7344	0,0000	0,5970
40	0,0226	0,0001	0,8768	0,0000	0,7344	0,0002	0,5972

Appendix G

Modal damping effects

Before proceeding with the analysis of the simplified models, we wanted to evaluate the effects of modal damping (making reference to: [18],[22], [23], [20], [21] and [10]). To do this we performed 5 simulations on model C, where we applied the same synthetic ground motions defined in section 6.5.1, also including the modal damping. We then compared the response with that obtained from the same simulations, but without damping.

Table G.1: Damping ratios applied to each vibration mode, according to is what identified in [18]. Source: [18]

applied modal damping		
mode	f [Hz]	damp.
1	2,186	0,51%
2	2,421	0,48%
3	2,496	0,39%
4	2,702	0,33%
5	3,014	0,53%
6	5,432	0,47%
7	6,675	0,73%
8	7,955	0,30%
9	8,363	0,31%
10	8,785	0,29%
11	9,352	0,38%

At first, we purposely defined a specific load case named *MODAL*, that performs a modal analysis with eigenvectors, calculating 11 vibration modes. Regarding the masses and the loads applied, we maintained the same ones defined for model C in section 6.1.4, namely the mass source *MSSSRC1* and load patterns *G1 DEAD*, *G1 add*, *G2* and *CABLE 33-34 SLS*, in compliance with the Eurocode [37] prescriptions for a seismic load combination. Similarly to what was described in section 6.5.2, we then created 5 time-history load cases, for which we applied perfectly correlated accelerograms.

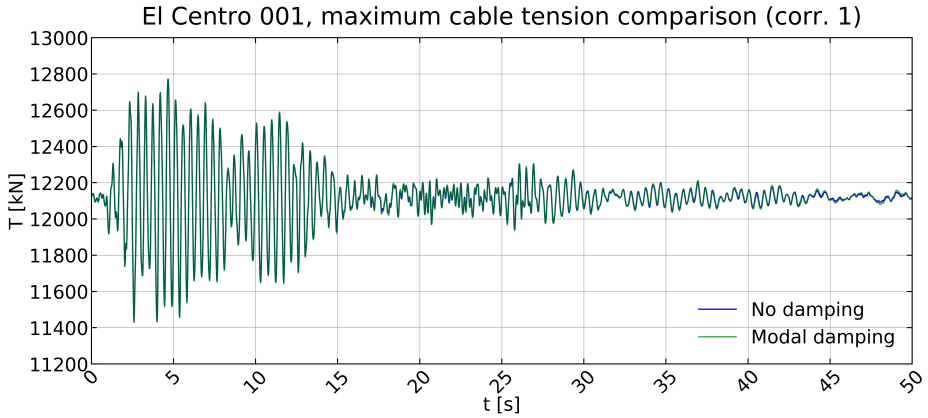

Figure G.1: Multi-support analysis with correlated ground motions, comparison between damped and undamped response in terms of maximum cable tension. Source: Excel, own elaboration

For the modal damping ratio we relied on the reference publications (summarized in 3.3.4.5), selecting the highest among the provided values (determined with the SSI-DATA method in [18], and summarized in table G.1). All the other parameters (applied loads, geometric non-linearity effects, mass source, resolution method) remain unchanged.

Table G.2: Model C, comparison between undamped and damped peak response for multi-support analysis with correlated ground motions. Source: Excel, own elaboration

Response peak, difference between no damping an modal damping

load case	Max. T [kN]			Max. ΔT [kN]
	no damping	modal damping	diff.	
El Centro - 001	12772,23	12769,99	2,24	12,68
El Centro - 002	12847,29	12845,07	2,22	13,82
El Centro - 003	12889,88	12886,53	3,35	10,80
El Centro - 004	12452,13	12451,25	0,88	8,06
El Centro - 005	12744,73	12742,25	2,49	16,05

We then compared the results of the 2 scenarios (with and without damping). For all the simulations the seismic response is almost the same (as shown in figure G.1). From table G.2 it appears that modal damping is almost negligible, as it implies a reduction of the maximum cable tension of less than 3 kN (the overall maximum difference is around 15 kN, slightly higher but still negligible). The response in terms of displacement-related presented differences of less than 0.3 mm and has not been displayed. Such outcome confirms what stated in [20], i.e. that the damping effects are extremely low, so that we neglected them.

Appendix H

Multi-support analysis data processing

In this annex we briefly propose the results obtained from the output processing described in section 7.1, in which we have determined (from the simulations outputs) the EDFs of the comparison parameters for each one of the models that we developed (described in detail in chapter 6. For model C we also calculated a 95% confidence band with the DKW formulation, as well as a lognormal parametric distribution starting from the mean and standard deviation values for each of the parameters considered.

The results have been shown in graphic form in sections 7.2.2 and 7.2.3 (for the cases of perfectly correlated and uncorrelated accelerograms respectively), while for the sake of completeness we propose in the following tables their summarized values.

Table H.1: Output processing for the maximum relative displacement measured with perfectly correlated ground motions. Source: Excel, own elaboration

Max. relative horizontal displacement with correlated ground motions - part.1

u [m]					95% CI		
model A	model B1	model B2	model C	EDF	upper b.	lower b.	lognorm
0,0064	0,0082	0,0055	0,0082	0,010	0,073	0,000	0,007
0,0064	0,0082	0,0060	0,0092	0,020	0,083	0,000	0,023
0,0064	0,0083	0,0064	0,0098	0,030	0,093	0,000	0,039
0,0065	0,0087	0,0065	0,0099	0,040	0,103	0,000	0,041
0,0070	0,0089	0,0071	0,0099	0,050	0,113	0,000	0,042
0,0072	0,0091	0,0073	0,0100	0,060	0,123	0,000	0,045
0,0073	0,0095	0,0073	0,0100	0,070	0,133	0,007	0,046
0,0075	0,0099	0,0073	0,0102	0,080	0,143	0,017	0,053
0,0075	0,0102	0,0073	0,0106	0,090	0,153	0,027	0,072
0,0081	0,0103	0,0076	0,0108	0,100	0,163	0,037	0,081
0,0081	0,0103	0,0076	0,0108	0,110	0,173	0,047	0,085
0,0081	0,0104	0,0078	0,0111	0,120	0,183	0,057	0,102
0,0084	0,0104	0,0080	0,0113	0,130	0,193	0,067	0,114
0,0085	0,0105	0,0080	0,0114	0,140	0,203	0,077	0,117
0,0086	0,0105	0,0082	0,0115	0,150	0,213	0,087	0,124
0,0086	0,0107	0,0082	0,0116	0,160	0,223	0,097	0,132
0,0087	0,0109	0,0083	0,0118	0,170	0,233	0,107	0,149
0,0087	0,0110	0,0084	0,0121	0,180	0,243	0,117	0,171
0,0088	0,0110	0,0085	0,0122	0,190	0,253	0,127	0,182
0,0090	0,0111	0,0086	0,0123	0,200	0,263	0,137	0,191
0,0091	0,0112	0,0088	0,0125	0,210	0,273	0,147	0,200
0,0093	0,0112	0,0089	0,0126	0,220	0,283	0,157	0,210
0,0095	0,0112	0,0090	0,0128	0,230	0,293	0,167	0,234
0,0097	0,0115	0,0090	0,0129	0,240	0,303	0,177	0,244
0,0098	0,0118	0,0091	0,0130	0,250	0,313	0,187	0,248
0,0098	0,0119	0,0092	0,0131	0,260	0,323	0,197	0,262
0,0099	0,0119	0,0092	0,0133	0,270	0,333	0,207	0,276
0,0101	0,0121	0,0093	0,0133	0,280	0,343	0,217	0,278
0,0101	0,0121	0,0093	0,0134	0,290	0,353	0,227	0,290
0,0102	0,0121	0,0096	0,0134	0,300	0,363	0,237	0,291
0,0103	0,0122	0,0097	0,0135	0,310	0,373	0,247	0,292
0,0105	0,0123	0,0097	0,0135	0,320	0,383	0,257	0,296
0,0105	0,0124	0,0097	0,0138	0,330	0,393	0,267	0,326
0,0106	0,0125	0,0097	0,0138	0,340	0,403	0,277	0,331
0,0107	0,0125	0,0097	0,0139	0,350	0,413	0,287	0,342
0,0107	0,0126	0,0098	0,0142	0,360	0,423	0,297	0,371
0,0109	0,0126	0,0098	0,0143	0,370	0,433	0,307	0,375
0,0111	0,0126	0,0098	0,0144	0,380	0,443	0,317	0,388
0,0112	0,0128	0,0098	0,0145	0,390	0,453	0,327	0,400
0,0112	0,0129	0,0098	0,0146	0,400	0,463	0,337	0,411
0,0113	0,0131	0,0100	0,0146	0,410	0,473	0,347	0,413
0,0114	0,0132	0,0101	0,0147	0,420	0,483	0,357	0,422
0,0115	0,0132	0,0102	0,0148	0,430	0,493	0,367	0,425
0,0115	0,0133	0,0102	0,0148	0,440	0,503	0,377	0,430
0,0116	0,0133	0,0104	0,0149	0,450	0,513	0,387	0,435
0,0116	0,0133	0,0104	0,0151	0,460	0,523	0,397	0,457
0,0117	0,0134	0,0106	0,0152	0,470	0,533	0,407	0,464
0,0118	0,0136	0,0107	0,0152	0,480	0,543	0,417	0,473
0,0119	0,0139	0,0107	0,0153	0,490	0,553	0,427	0,480
0,0120	0,0140	0,0108	0,0155	0,500	0,563	0,437	0,499

Table H.2: Output processing for the maximum relative displacement measured with perfectly correlated ground motions. Source: Excel, own elaboration

Max. relative horizontal displacement with correlated ground motions - part.2

u [m]					95% CI		
model A	model B1	model B2	model C	EDF	upper b.	lower b.	lognorm
0,0120	0,0140	0,0108	0,0157	0,510	0,573	0,447	0,518
0,0121	0,0144	0,0108	0,0157	0,520	0,583	0,457	0,518
0,0122	0,0145	0,0109	0,0160	0,530	0,593	0,467	0,545
0,0122	0,0146	0,0109	0,0161	0,540	0,603	0,477	0,553
0,0124	0,0146	0,0110	0,0162	0,550	0,613	0,487	0,570
0,0126	0,0146	0,0110	0,0164	0,560	0,623	0,497	0,585
0,0126	0,0149	0,0111	0,0164	0,570	0,633	0,507	0,586
0,0126	0,0151	0,0111	0,0165	0,580	0,643	0,517	0,592
0,0126	0,0152	0,0111	0,0165	0,590	0,653	0,527	0,598
0,0128	0,0153	0,0112	0,0168	0,600	0,663	0,537	0,623
0,0128	0,0154	0,0113	0,0169	0,610	0,673	0,547	0,629
0,0130	0,0155	0,0113	0,0169	0,620	0,683	0,557	0,631
0,0131	0,0157	0,0114	0,0172	0,630	0,693	0,567	0,656
0,0132	0,0157	0,0115	0,0173	0,640	0,703	0,577	0,660
0,0132	0,0158	0,0116	0,0173	0,650	0,713	0,587	0,662
0,0133	0,0160	0,0117	0,0174	0,660	0,723	0,597	0,668
0,0136	0,0162	0,0119	0,0174	0,670	0,733	0,607	0,670
0,0137	0,0163	0,0120	0,0174	0,680	0,743	0,617	0,671
0,0137	0,0164	0,0122	0,0175	0,690	0,753	0,627	0,679
0,0138	0,0164	0,0122	0,0176	0,700	0,763	0,637	0,684
0,0138	0,0165	0,0123	0,0179	0,710	0,773	0,647	0,706
0,0140	0,0165	0,0123	0,0179	0,720	0,783	0,657	0,707
0,0141	0,0170	0,0123	0,0182	0,730	0,793	0,667	0,729
0,0143	0,0171	0,0125	0,0183	0,740	0,803	0,677	0,736
0,0143	0,0172	0,0126	0,0184	0,750	0,813	0,687	0,745
0,0144	0,0173	0,0127	0,0184	0,760	0,823	0,697	0,747
0,0145	0,0177	0,0127	0,0186	0,770	0,833	0,707	0,757
0,0146	0,0179	0,0127	0,0187	0,780	0,843	0,717	0,762
0,0146	0,0181	0,0128	0,0189	0,790	0,853	0,727	0,779
0,0148	0,0181	0,0130	0,0195	0,800	0,863	0,737	0,809
0,0148	0,0182	0,0131	0,0196	0,810	0,873	0,747	0,814
0,0149	0,0189	0,0132	0,0197	0,820	0,883	0,757	0,819
0,0149	0,0189	0,0132	0,0198	0,830	0,893	0,767	0,824
0,0150	0,0190	0,0132	0,0200	0,840	0,903	0,777	0,835
0,0150	0,0192	0,0133	0,0201	0,850	0,913	0,787	0,839
0,0151	0,0193	0,0135	0,0209	0,860	0,923	0,797	0,872
0,0151	0,0196	0,0136	0,0213	0,870	0,933	0,807	0,889
0,0151	0,0199	0,0136	0,0214	0,880	0,943	0,817	0,893
0,0151	0,0199	0,0137	0,0215	0,890	0,953	0,827	0,895
0,0160	0,0202	0,0145	0,0215	0,900	0,963	0,837	0,895
0,0161	0,0204	0,0154	0,0217	0,910	0,973	0,847	0,900
0,0162	0,0207	0,0158	0,0219	0,920	0,983	0,857	0,906
0,0172	0,0215	0,0162	0,0220	0,930	0,993	0,867	0,911
0,0172	0,0215	0,0163	0,0227	0,940	1,000	0,877	0,929
0,0180	0,0216	0,0166	0,0234	0,950	1,000	0,887	0,943
0,0186	0,0225	0,0172	0,0238	0,960	1,000	0,897	0,950
0,0188	0,0225	0,0175	0,0241	0,970	1,000	0,907	0,954
0,0227	0,0227	0,0176	0,0251	0,980	1,000	0,917	0,968
0,0233	0,0258	0,0187	0,0285	0,990	1,000	0,927	0,990
0,0237	0,0261	0,0195	0,0292	1,000	1,000	0,937	0,992

Table H.3: Output processing for the maximum horizontal tension measured with perfectly correlated ground motions. Source: Excel, own elaboration

Max. horizontal tension with correlated ground motions - part.1

H [kN]					95% CI		
model A	model B1	model B2	model C	EDF	upper b.	lower b.	lognorm
12267,2	12018,0	12197,8	12096,1	0,010	0,073	0,000	0,031
12282,2	12050,3	12208,6	12129,8	0,020	0,083	0,000	0,050
12287,0	12054,8	12214,2	12132,1	0,030	0,093	0,000	0,051
12298,5	12084,7	12227,8	12152,4	0,040	0,103	0,000	0,067
12324,4	12106,7	12230,7	12170,0	0,050	0,113	0,000	0,082
12334,8	12114,1	12242,9	12172,3	0,060	0,123	0,000	0,085
12348,2	12117,2	12270,9	12178,1	0,070	0,133	0,007	0,091
12349,5	12123,2	12272,1	12190,8	0,080	0,143	0,017	0,105
12377,6	12133,7	12279,7	12194,2	0,090	0,153	0,027	0,108
12390,6	12134,5	12290,2	12213,7	0,100	0,163	0,037	0,133
12393,3	12141,3	12294,5	12217,0	0,110	0,173	0,047	0,138
12393,7	12143,1	12294,8	12221,0	0,120	0,183	0,057	0,144
12397,2	12160,9	12296,2	12229,4	0,130	0,193	0,067	0,156
12411,4	12162,2	12300,8	12233,0	0,140	0,203	0,077	0,161
12415,7	12165,1	12310,2	12242,3	0,150	0,213	0,087	0,176
12416,9	12166,3	12313,1	12245,1	0,160	0,223	0,097	0,181
12441,7	12169,1	12318,6	12255,1	0,170	0,233	0,107	0,198
12444,2	12179,8	12326,6	12256,3	0,180	0,243	0,117	0,200
12454,5	12180,3	12330,5	12256,3	0,190	0,253	0,127	0,200
12466,4	12182,1	12330,8	12265,4	0,200	0,263	0,137	0,217
12487,3	12190,9	12334,8	12266,3	0,210	0,273	0,147	0,218
12506,5	12193,5	12342,2	12268,7	0,220	0,283	0,157	0,223
12512,6	12197,2	12342,8	12273,9	0,230	0,293	0,167	0,233
12513,2	12197,7	12345,4	12275,5	0,240	0,303	0,177	0,236
12517,4	12202,5	12348,2	12277,5	0,250	0,313	0,187	0,240
12533,2	12202,5	12349,8	12278,7	0,260	0,323	0,197	0,242
12546,4	12209,8	12353,1	12280,5	0,270	0,333	0,207	0,246
12562,8	12210,4	12359,2	12280,9	0,280	0,343	0,217	0,246
12577,8	12211,0	12369,3	12286,7	0,290	0,353	0,227	0,258
12578,2	12214,9	12376,1	12289,3	0,300	0,363	0,237	0,263
12578,3	12215,1	12381,5	12295,5	0,310	0,373	0,247	0,276
12583,8	12217,6	12391,8	12305,9	0,320	0,383	0,257	0,299
12585,0	12226,5	12393,1	12306,8	0,330	0,393	0,267	0,301
12588,8	12237,1	12399,3	12308,1	0,340	0,403	0,277	0,304
12594,5	12241,3	12404,3	12310,6	0,350	0,413	0,287	0,309
12601,1	12243,9	12405,2	12314,5	0,360	0,423	0,297	0,318
12606,3	12244,0	12418,8	12318,5	0,370	0,433	0,307	0,327
12607,8	12248,0	12419,4	12319,6	0,380	0,443	0,317	0,329
12610,9	12250,1	12420,7	12324,4	0,390	0,453	0,327	0,340
12620,2	12261,8	12427,8	12325,2	0,400	0,463	0,337	0,342
12624,0	12267,2	12431,9	12327,7	0,410	0,473	0,347	0,348
12634,2	12267,4	12436,7	12330,9	0,420	0,483	0,357	0,355
12640,6	12271,7	12442,8	12330,9	0,430	0,493	0,367	0,356
12641,2	12271,8	12443,1	12337,6	0,440	0,503	0,377	0,371
12656,8	12272,6	12445,4	12338,2	0,450	0,513	0,387	0,373
12679,2	12274,7	12448,5	12339,6	0,460	0,523	0,397	0,376
12682,5	12281,5	12449,1	12340,2	0,470	0,533	0,407	0,377
12689,2	12291,0	12449,7	12346,4	0,480	0,543	0,417	0,392
12706,2	12295,2	12451,2	12353,4	0,490	0,553	0,427	0,409
12718,8	12310,8	12454,8	12354,5	0,500	0,563	0,437	0,412

Table H.4: Output processing for the maximum horizontal tension measured with perfectly correlated ground motions. Source: Excel, own elaboration

Max. horizontal tension with correlated ground motions - part.2

H [kN]				95% CI			
model A	model B1	model B2	model C	EDF	upper b.	lower b.	lognorm
12720,4	12314,1	12457,6	12356,4	0,510	0,573	0,447	0,417
12728,8	12316,0	12458,8	12358,3	0,520	0,583	0,457	0,421
12746,5	12317,7	12467,0	12373,4	0,530	0,593	0,467	0,459
12746,5	12324,4	12468,5	12375,9	0,540	0,603	0,477	0,465
12756,4	12329,0	12469,0	12382,4	0,550	0,613	0,487	0,481
12757,1	12331,0	12475,6	12390,3	0,560	0,623	0,497	0,501
12758,4	12333,2	12476,3	12391,5	0,570	0,633	0,507	0,504
12767,6	12333,9	12483,5	12392,1	0,580	0,643	0,517	0,505
12775,9	12338,2	12485,3	12397,4	0,590	0,653	0,527	0,519
12786,5	12339,6	12485,4	12409,2	0,600	0,663	0,537	0,548
12787,9	12355,6	12485,7	12409,6	0,610	0,673	0,547	0,549
12820,0	12362,1	12488,8	12412,4	0,620	0,683	0,557	0,556
12840,8	12363,1	12490,6	12424,0	0,630	0,693	0,567	0,584
12841,0	12374,1	12492,0	12424,0	0,640	0,703	0,577	0,584
12844,5	12376,3	12493,1	12424,1	0,650	0,713	0,587	0,584
12847,8	12383,0	12494,7	12433,4	0,660	0,723	0,597	0,607
12853,9	12383,3	12496,1	12440,9	0,670	0,733	0,607	0,625
12854,2	12386,3	12500,3	12441,8	0,680	0,743	0,617	0,627
12866,2	12393,5	12501,0	12442,1	0,690	0,753	0,627	0,628
12870,4	12402,9	12504,5	12443,2	0,700	0,763	0,637	0,630
12871,4	12404,0	12513,9	12445,8	0,710	0,773	0,647	0,636
12871,9	12410,5	12516,9	12448,7	0,720	0,783	0,657	0,643
12887,4	12427,9	12522,6	12454,7	0,730	0,793	0,667	0,657
12888,5	12428,5	12524,9	12465,7	0,740	0,803	0,677	0,682
12898,9	12437,6	12538,0	12469,3	0,750	0,813	0,687	0,690
12901,7	12439,8	12551,6	12482,5	0,760	0,823	0,697	0,718
12904,4	12450,3	12557,6	12498,0	0,770	0,833	0,707	0,750
12909,9	12455,1	12559,7	12504,0	0,780	0,843	0,717	0,761
12948,7	12456,1	12567,6	12508,7	0,790	0,853	0,727	0,770
12973,1	12461,2	12578,2	12517,1	0,800	0,863	0,737	0,786
12976,6	12466,0	12588,1	12523,1	0,810	0,873	0,747	0,796
12979,1	12477,7	12603,8	12528,1	0,820	0,883	0,757	0,805
12980,5	12478,0	12605,6	12537,6	0,830	0,893	0,767	0,821
12987,9	12478,2	12633,3	12551,5	0,840	0,903	0,777	0,842
13003,6	12486,9	12633,3	12557,8	0,850	0,913	0,787	0,852
13024,1	12489,3	12635,8	12561,1	0,860	0,923	0,797	0,856
13028,7	12494,6	12667,9	12568,5	0,870	0,933	0,807	0,866
13044,5	12496,2	12683,0	12570,7	0,880	0,943	0,817	0,869
13050,8	12500,0	12685,6	12575,7	0,890	0,953	0,827	0,876
13056,5	12519,0	12689,7	12624,3	0,900	0,963	0,837	0,927
13089,9	12548,7	12701,2	12635,5	0,910	0,973	0,847	0,936
13097,1	12560,1	12715,3	12638,8	0,920	0,983	0,857	0,938
13189,8	12581,0	12715,8	12638,9	0,930	0,993	0,867	0,939
13218,6	12584,4	12741,3	12654,2	0,940	1,000	0,877	0,949
13260,1	12635,6	12787,7	12678,1	0,950	1,000	0,887	0,963
13277,4	12674,7	12805,7	12678,4	0,960	1,000	0,897	0,963
13311,0	12693,3	12806,3	12765,2	0,970	1,000	0,907	0,990
13389,0	12696,4	12812,9	12779,7	0,980	1,000	0,917	0,992
13406,9	12732,5	12881,2	12860,0	0,990	1,000	0,927	0,998
13746,3	12779,7	12899,9	12897,1	1,000	1,000	0,937	0,999

Table H.5: Output processing for the maximum cable tension measured with perfectly correlated ground motions. Source: Excel, own elaboration

Max. cable tension with correlated ground motions - part.1

T [kN]					95% CI		
model A	model B1	model B2	model C	EDF	upper b.	lower b.	lognorm
12267,2	12371,9	12553,3	12452,1	0,010	0,073	0,000	0,032
12282,2	12410,7	12564,3	12485,9	0,020	0,083	0,000	0,050
12287,0	12413,1	12570,3	12488,9	0,030	0,093	0,000	0,052
12298,5	12442,7	12579,8	12511,1	0,040	0,103	0,000	0,068
12324,4	12467,6	12580,3	12527,0	0,050	0,113	0,000	0,082
12334,8	12473,7	12598,4	12529,0	0,060	0,123	0,000	0,084
12348,2	12474,6	12628,1	12534,6	0,070	0,133	0,007	0,090
12349,5	12479,8	12630,0	12551,5	0,080	0,143	0,017	0,108
12377,6	12493,1	12638,1	12552,9	0,090	0,153	0,027	0,109
12390,6	12494,6	12646,2	12567,7	0,100	0,163	0,037	0,128
12393,3	12498,5	12650,0	12576,3	0,110	0,173	0,047	0,139
12393,7	12504,8	12652,0	12577,3	0,120	0,183	0,057	0,140
12397,2	12519,0	12659,3	12586,5	0,130	0,193	0,067	0,153
12411,4	12520,3	12660,4	12590,9	0,140	0,203	0,077	0,160
12415,7	12524,1	12667,4	12602,8	0,150	0,213	0,087	0,178
12416,9	12526,5	12671,0	12610,9	0,160	0,223	0,097	0,192
12441,7	12535,5	12675,7	12614,9	0,170	0,233	0,107	0,198
12444,2	12540,6	12685,9	12617,2	0,180	0,243	0,117	0,202
12454,5	12541,5	12686,7	12617,9	0,190	0,253	0,127	0,204
12466,4	12545,3	12691,2	12626,6	0,200	0,263	0,137	0,219
12487,3	12549,4	12695,4	12629,0	0,210	0,273	0,147	0,224
12506,5	12554,1	12700,4	12629,8	0,220	0,283	0,157	0,225
12512,6	12558,0	12702,2	12630,5	0,230	0,293	0,167	0,226
12513,2	12564,5	12703,9	12635,2	0,240	0,303	0,177	0,235
12517,4	12565,0	12704,8	12637,2	0,250	0,313	0,187	0,239
12533,2	12567,7	12707,3	12639,0	0,260	0,323	0,197	0,242
12546,4	12569,4	12713,8	12641,4	0,270	0,333	0,207	0,247
12562,8	12573,9	12716,5	12645,4	0,280	0,343	0,217	0,255
12577,8	12574,0	12728,9	12647,1	0,290	0,353	0,227	0,258
12578,2	12579,7	12736,4	12652,3	0,300	0,363	0,237	0,269
12578,3	12580,0	12741,6	12658,5	0,310	0,373	0,247	0,281
12583,8	12581,0	12750,5	12661,9	0,320	0,383	0,257	0,288
12585,0	12585,1	12752,6	12662,9	0,330	0,393	0,267	0,290
12588,8	12595,5	12758,1	12669,7	0,340	0,403	0,277	0,305
12594,5	12602,8	12766,3	12670,1	0,350	0,413	0,287	0,306
12601,1	12603,6	12767,7	12672,8	0,360	0,423	0,297	0,312
12606,3	12606,5	12779,2	12676,5	0,370	0,433	0,307	0,320
12607,8	12608,1	12780,7	12678,0	0,380	0,443	0,317	0,323
12610,9	12615,4	12781,3	12679,4	0,390	0,453	0,327	0,326
12620,2	12629,1	12790,1	12685,7	0,400	0,463	0,337	0,340
12624,0	12631,8	12791,1	12690,3	0,410	0,473	0,347	0,350
12634,2	12633,7	12796,7	12692,8	0,420	0,483	0,357	0,356
12640,6	12633,8	12804,7	12693,3	0,430	0,493	0,367	0,357
12641,2	12635,0	12804,8	12694,2	0,440	0,503	0,377	0,359
12656,8	12635,9	12805,9	12695,1	0,450	0,513	0,387	0,361
12679,2	12639,3	12808,0	12701,3	0,460	0,523	0,397	0,376
12682,5	12642,8	12808,2	12704,9	0,470	0,533	0,407	0,384
12689,2	12653,9	12815,7	12705,5	0,480	0,543	0,417	0,385
12706,2	12661,7	12816,2	12718,7	0,490	0,553	0,427	0,417
12718,8	12675,3	12816,7	12721,3	0,500	0,563	0,437	0,423

Table H.6: Output processing for the maximum cable tension measured with perfectly correlated ground motions. Source: Excel, own elaboration

Max. cable tension with correlated ground motions - part.2

T [kN]				95% CI			
model A	model B1	model B2	model C	EDF	upper b.	lower b.	lognorm
12720,4	12676,1	12817,4	12722,1	0,510	0,573	0,447	0,425
12728,8	12679,1	12820,7	12725,6	0,520	0,583	0,457	0,433
12746,5	12681,6	12827,4	12731,9	0,530	0,593	0,467	0,448
12746,5	12686,9	12831,9	12738,3	0,540	0,603	0,477	0,464
12756,4	12691,1	12833,4	12744,7	0,550	0,613	0,487	0,479
12757,1	12693,9	12837,4	12751,6	0,560	0,623	0,497	0,496
12758,4	12700,2	12839,5	12755,4	0,570	0,633	0,507	0,505
12767,6	12701,4	12844,2	12755,8	0,580	0,643	0,517	0,506
12775,9	12705,2	12846,1	12761,3	0,590	0,653	0,527	0,520
12786,5	12706,5	12847,9	12772,2	0,600	0,663	0,537	0,546
12787,9	12721,2	12848,9	12772,2	0,610	0,673	0,547	0,546
12820,0	12730,3	12850,4	12780,1	0,620	0,683	0,557	0,565
12840,8	12730,6	12850,7	12786,1	0,630	0,693	0,567	0,579
12841,0	12740,5	12852,8	12788,5	0,640	0,703	0,577	0,585
12844,5	12741,4	12854,1	12791,2	0,650	0,713	0,587	0,591
12847,8	12748,9	12854,1	12795,3	0,660	0,723	0,597	0,601
12853,9	12751,6	12857,2	12799,3	0,670	0,733	0,607	0,610
12854,2	12752,9	12858,2	12801,9	0,680	0,743	0,617	0,616
12866,2	12754,3	12860,3	12805,9	0,690	0,753	0,627	0,626
12870,4	12770,3	12864,4	12812,7	0,700	0,763	0,637	0,641
12871,4	12771,5	12878,8	12813,2	0,710	0,773	0,647	0,642
12871,9	12772,8	12882,0	12813,3	0,720	0,783	0,657	0,643
12887,4	12798,1	12884,0	12827,3	0,730	0,793	0,667	0,674
12888,5	12798,6	12887,8	12831,3	0,740	0,803	0,677	0,682
12898,9	12804,2	12900,8	12837,4	0,750	0,813	0,687	0,695
12901,7	12812,7	12919,1	12847,3	0,760	0,823	0,697	0,716
12904,4	12822,8	12920,4	12867,8	0,770	0,833	0,707	0,756
12909,9	12825,3	12922,8	12872,5	0,780	0,843	0,717	0,765
12948,7	12826,5	12926,5	12877,2	0,790	0,853	0,727	0,774
12973,1	12826,8	12942,9	12883,6	0,800	0,863	0,737	0,785
12976,6	12835,6	12959,6	12889,9	0,810	0,873	0,747	0,796
12979,1	12845,6	12971,1	12892,1	0,820	0,883	0,757	0,800
12980,5	12846,9	12971,5	12906,1	0,830	0,893	0,767	0,823
12987,9	12847,1	12991,0	12921,0	0,840	0,903	0,777	0,845
13003,6	12857,9	13002,1	12927,1	0,850	0,913	0,787	0,854
13024,1	12862,3	13003,7	12931,7	0,860	0,923	0,797	0,860
13028,7	12866,4	13036,2	12933,7	0,870	0,933	0,807	0,863
13044,5	12867,9	13053,3	12935,2	0,880	0,943	0,817	0,864
13050,8	12868,5	13054,1	12937,4	0,890	0,953	0,827	0,867
13056,5	12890,2	13066,7	12998,9	0,900	0,963	0,837	0,931
13089,9	12924,3	13067,9	13005,5	0,910	0,973	0,847	0,936
13097,1	12932,3	13081,4	13006,7	0,920	0,983	0,857	0,937
13189,8	12949,3	13084,1	13008,8	0,930	0,993	0,867	0,938
13218,6	12954,1	13105,2	13028,0	0,940	1,000	0,877	0,951
13260,1	13012,1	13159,8	13048,9	0,950	1,000	0,887	0,962
13277,4	13050,8	13179,2	13053,1	0,960	1,000	0,897	0,964
13311,0	13061,5	13179,3	13129,7	0,970	1,000	0,907	0,988
13389,0	13072,5	13185,2	13155,2	0,980	1,000	0,917	0,992
13406,9	13102,6	13252,0	13237,6	0,990	1,000	0,927	0,998
13746,3	13156,1	13275,8	13275,5	1,000	1,000	0,937	0,999

Table H.7: Output processing for the maximum horizontal tension increase measured with perfectly correlated ground motions. Source: Excel, own elaboration

Max. horizontal tension increase with correlated ground motions - part.1

ΔH [kN]					95% CI		
model A	model B1	model B2	model C	EDF	upper b.	lower b.	lognorm
504,2	334,0	371,7	356,8	0,020	0,083	0,000	0,020
509,0	338,4	377,2	359,1	0,030	0,093	0,000	0,021
520,6	368,4	390,9	379,3	0,040	0,103	0,000	0,035
546,4	390,4	393,7	397,0	0,050	0,113	0,000	0,052
556,9	397,7	405,9	399,3	0,060	0,123	0,000	0,054
570,2	400,8	434,0	405,0	0,070	0,133	0,007	0,061
571,5	406,9	435,2	417,8	0,080	0,143	0,017	0,077
599,6	417,3	442,8	421,2	0,090	0,153	0,027	0,082
612,6	418,1	453,2	440,6	0,100	0,163	0,037	0,112
615,3	424,9	457,5	443,9	0,110	0,173	0,047	0,118
615,7	426,7	457,9	447,9	0,120	0,183	0,057	0,125
619,2	444,5	459,3	456,4	0,130	0,193	0,067	0,141
633,4	445,8	463,9	459,9	0,140	0,203	0,077	0,148
637,7	448,8	473,3	469,2	0,150	0,213	0,087	0,168
638,9	449,9	476,2	472,0	0,160	0,223	0,097	0,173
663,7	452,7	481,7	482,0	0,170	0,233	0,107	0,196
666,2	463,4	489,6	483,2	0,180	0,243	0,117	0,198
676,5	464,0	493,6	483,2	0,190	0,253	0,127	0,198
688,4	465,7	493,9	492,3	0,200	0,263	0,137	0,219
709,3	474,5	497,9	493,2	0,210	0,273	0,147	0,222
728,5	477,1	505,3	495,6	0,220	0,283	0,157	0,227
734,6	480,8	505,9	500,8	0,230	0,293	0,167	0,240
735,2	481,3	508,5	502,4	0,240	0,303	0,177	0,244
739,4	486,1	511,2	504,5	0,250	0,313	0,187	0,249
755,2	486,1	512,9	505,6	0,260	0,323	0,197	0,252
768,5	493,4	516,2	507,4	0,270	0,333	0,207	0,257
784,8	494,0	522,3	507,8	0,280	0,343	0,217	0,257
799,8	494,7	532,4	513,7	0,290	0,353	0,227	0,272
800,3	498,5	539,2	516,2	0,300	0,363	0,237	0,279
800,3	498,7	544,6	522,4	0,310	0,373	0,247	0,295
805,8	501,2	554,9	532,9	0,320	0,383	0,257	0,323
807,0	510,1	556,2	533,7	0,330	0,393	0,267	0,325
810,8	520,7	562,4	535,0	0,340	0,403	0,277	0,328
816,5	524,9	567,3	537,5	0,350	0,413	0,287	0,335
823,1	527,5	568,3	541,4	0,360	0,423	0,297	0,346
828,3	527,6	581,9	545,4	0,370	0,433	0,307	0,356
829,8	531,6	582,5	546,5	0,380	0,443	0,317	0,359
832,9	533,7	583,7	551,3	0,390	0,453	0,327	0,372
842,2	545,4	590,9	552,1	0,400	0,463	0,337	0,375
846,0	550,9	595,0	554,6	0,410	0,473	0,347	0,381
856,2	551,1	599,7	557,8	0,420	0,483	0,357	0,390
862,6	555,3	605,9	557,9	0,430	0,493	0,367	0,390
863,2	555,5	606,2	564,5	0,440	0,503	0,377	0,408
878,8	556,2	608,5	565,1	0,450	0,513	0,387	0,410
901,2	558,3	611,6	566,5	0,460	0,523	0,397	0,414
904,5	565,1	612,2	567,1	0,470	0,533	0,407	0,415
911,2	574,6	612,7	573,3	0,480	0,543	0,417	0,432
928,2	578,8	614,3	580,4	0,490	0,553	0,427	0,451
940,8	594,4	617,9	581,4	0,500	0,563	0,437	0,454

Table H.8: Output processing for the maximum horizontal tension increase measured with perfectly correlated ground motions. Source: Excel, own elaboration

Max. horizontal tension increase with correlated ground motions - part.2

ΔH [kN]				95% CI			
model A	model B1	model B2	model C	EDF	upper b.	lower b.	lognorm
942,4	597,7	620,7	583,3	0,510	0,573	0,447	0,459
950,8	599,6	621,9	585,2	0,520	0,583	0,457	0,464
968,5	601,4	630,1	600,3	0,530	0,593	0,467	0,505
968,5	608,0	631,6	602,8	0,540	0,603	0,477	0,511
978,4	612,6	632,1	609,3	0,550	0,613	0,487	0,528
979,1	614,6	638,7	617,3	0,560	0,623	0,497	0,549
980,4	616,9	639,4	618,4	0,570	0,633	0,507	0,552
989,6	617,5	646,6	619,0	0,580	0,643	0,517	0,553
997,9	621,9	648,4	624,3	0,590	0,653	0,527	0,566
1008,5	623,2	648,5	636,1	0,600	0,663	0,537	0,595
1010,0	639,2	648,8	636,5	0,610	0,673	0,547	0,596
1042,0	645,7	651,9	639,3	0,620	0,683	0,557	0,603
1062,8	646,7	653,7	650,9	0,630	0,693	0,567	0,630
1063,0	657,7	655,1	650,9	0,640	0,703	0,577	0,630
1066,5	659,9	656,2	651,0	0,650	0,713	0,587	0,630
1069,8	666,6	657,7	660,3	0,660	0,723	0,597	0,652
1075,9	666,9	659,2	667,8	0,670	0,733	0,607	0,668
1076,2	669,9	663,3	668,7	0,680	0,743	0,617	0,670
1088,2	677,1	664,1	669,1	0,690	0,753	0,627	0,671
1092,4	686,6	667,6	670,1	0,700	0,763	0,637	0,673
1093,4	687,6	677,0	672,7	0,710	0,773	0,647	0,678
1093,9	694,1	680,0	675,6	0,720	0,783	0,657	0,684
1109,4	711,6	685,7	681,6	0,730	0,793	0,667	0,697
1110,5	712,1	688,0	692,6	0,740	0,803	0,677	0,719
1120,9	721,2	701,0	696,2	0,750	0,813	0,687	0,725
1123,7	723,4	714,7	709,5	0,760	0,823	0,697	0,750
1126,4	734,0	720,7	724,9	0,770	0,833	0,707	0,776
1132,0	738,7	722,7	730,9	0,780	0,843	0,717	0,786
1170,7	739,7	730,7	735,6	0,790	0,853	0,727	0,793
1195,1	744,8	741,3	744,1	0,800	0,863	0,737	0,806
1198,6	749,6	751,2	750,0	0,810	0,873	0,747	0,814
1201,1	761,3	766,9	755,0	0,820	0,883	0,757	0,821
1202,5	761,6	768,7	764,5	0,830	0,893	0,767	0,834
1209,9	761,8	796,4	778,5	0,840	0,903	0,777	0,851
1225,7	770,6	796,4	784,7	0,850	0,913	0,787	0,858
1246,1	772,9	798,8	788,0	0,860	0,923	0,797	0,862
1250,7	778,2	830,9	795,4	0,870	0,933	0,807	0,870
1266,5	779,9	846,1	797,6	0,880	0,943	0,817	0,872
1272,8	783,6	848,7	802,6	0,890	0,953	0,827	0,877
1278,5	802,7	852,8	851,3	0,900	0,963	0,837	0,919
1311,9	832,3	864,3	862,4	0,910	0,973	0,847	0,926
1319,1	843,7	878,4	865,7	0,920	0,983	0,857	0,928
1411,8	864,6	878,8	865,8	0,930	0,993	0,867	0,928
1440,6	868,0	904,4	881,1	0,940	1,000	0,877	0,937
1482,1	919,2	950,8	905,0	0,950	1,000	0,887	0,949
1499,4	958,4	968,8	905,4	0,960	1,000	0,897	0,949
1533,0	977,0	969,4	992,2	0,970	1,000	0,907	0,977
1611,0	980,0	975,9	1006,6	0,980	1,000	0,917	0,980
1628,9	1016,1	1044,2	1087,0	0,990	1,000	0,927	0,991
1968,3	1063,3	1063,0	1124,0	1,000	1,000	0,937	0,994

Table H.9: Output processing for the maximum tension increase measured with perfectly correlated ground motions. Source: Excel, own elaboration

Max. tension increase with correlated ground motions - part.1

ΔT [kN]				95% CI			
model A	model B1	model B2	model C	EDF	upper b.	lower b.	lognorm
489,2	307,3	371,5	332,4	0,010	0,073	0,000	0,007
504,2	346,1	382,5	366,2	0,020	0,083	0,000	0,020
509,0	348,4	388,5	369,2	0,030	0,093	0,000	0,022
520,5	378,1	398,0	391,4	0,040	0,103	0,000	0,037
546,4	402,9	398,4	407,4	0,050	0,113	0,000	0,052
556,9	409,0	416,5	409,3	0,060	0,123	0,000	0,054
570,2	410,0	446,3	414,9	0,070	0,133	0,007	0,060
571,5	415,2	448,2	431,8	0,080	0,143	0,017	0,081
599,6	428,5	456,3	433,2	0,090	0,153	0,027	0,083
612,6	430,0	464,4	448,0	0,100	0,163	0,037	0,105
615,3	433,8	468,1	456,6	0,110	0,173	0,047	0,120
615,7	440,1	470,2	457,6	0,120	0,183	0,057	0,121
619,2	454,4	477,5	466,8	0,130	0,193	0,067	0,138
633,4	455,6	478,6	471,2	0,140	0,203	0,077	0,146
637,7	459,5	485,6	483,1	0,150	0,213	0,087	0,170
638,9	461,8	489,2	491,2	0,160	0,223	0,097	0,187
663,7	470,9	493,9	495,2	0,170	0,233	0,107	0,196
666,2	475,9	504,1	497,5	0,180	0,243	0,117	0,201
676,5	476,9	504,9	498,2	0,190	0,253	0,127	0,203
688,4	480,6	509,4	506,9	0,200	0,263	0,137	0,223
709,3	484,8	513,6	509,4	0,210	0,273	0,147	0,228
728,5	489,5	518,6	510,1	0,220	0,283	0,157	0,230
734,6	493,4	520,3	510,8	0,230	0,293	0,167	0,232
735,2	499,8	522,1	515,5	0,240	0,303	0,177	0,243
739,4	500,4	523,0	517,5	0,250	0,313	0,187	0,248
755,2	503,1	525,5	519,3	0,260	0,323	0,197	0,252
768,5	504,7	532,0	521,7	0,270	0,333	0,207	0,258
784,8	509,3	534,6	525,7	0,280	0,343	0,217	0,268
799,8	509,3	547,0	527,4	0,290	0,353	0,227	0,272
800,3	515,1	554,5	532,6	0,300	0,363	0,237	0,285
800,3	515,3	559,8	538,8	0,310	0,373	0,247	0,301
805,8	516,4	568,7	542,2	0,320	0,383	0,257	0,310
807,0	520,5	570,8	543,2	0,330	0,393	0,267	0,312
810,8	530,9	576,3	550,0	0,340	0,403	0,277	0,330
816,5	538,2	584,5	550,4	0,350	0,413	0,287	0,331
823,1	538,9	585,9	553,1	0,360	0,423	0,297	0,338
828,3	541,8	597,4	556,8	0,370	0,433	0,307	0,348
829,8	543,5	598,9	558,3	0,380	0,443	0,317	0,352
832,9	550,7	599,5	559,7	0,390	0,453	0,327	0,355
842,2	564,5	608,2	566,0	0,400	0,463	0,337	0,372
846,0	567,1	609,3	570,6	0,410	0,473	0,347	0,384
856,2	569,1	614,9	573,1	0,420	0,483	0,357	0,391
862,6	569,1	622,9	573,6	0,430	0,493	0,367	0,392
863,2	570,3	623,0	574,5	0,440	0,503	0,377	0,395
878,8	571,2	624,1	575,4	0,450	0,513	0,387	0,397
901,2	574,7	626,2	581,6	0,460	0,523	0,397	0,413
904,5	578,1	626,3	585,2	0,470	0,533	0,407	0,423
911,2	589,3	633,9	585,8	0,480	0,543	0,417	0,424
928,2	597,0	634,4	599,0	0,490	0,553	0,427	0,459
940,8	610,6	634,8	601,7	0,500	0,563	0,437	0,466

Table H.10: Output processing for the maximum tension increase measured with perfectly correlated ground motions. Source: Excel, own elaboration

Max. tension increase with correlated ground motions - part.2

ΔT [kN]				95% CI			
model A	model B1	model B2	model C	EDF	upper b.	lower b.	lognorm
942,4	611,5	635,6	602,4	0,510	0,573	0,447	0,468
950,8	614,4	638,9	605,9	0,520	0,583	0,457	0,477
968,5	617,0	645,6	612,2	0,530	0,593	0,467	0,494
968,5	622,2	650,1	618,6	0,540	0,603	0,477	0,510
978,4	626,4	651,6	625,0	0,550	0,613	0,487	0,526
979,1	629,2	655,6	631,9	0,560	0,623	0,497	0,544
980,4	635,6	657,7	635,8	0,570	0,633	0,507	0,553
989,6	636,8	662,4	636,1	0,580	0,643	0,517	0,554
997,9	640,5	664,3	641,6	0,590	0,653	0,527	0,567
1008,5	641,9	666,1	652,5	0,600	0,663	0,537	0,594
1010,0	656,6	667,0	652,5	0,610	0,673	0,547	0,594
1042,0	665,6	668,5	660,4	0,620	0,683	0,557	0,612
1062,8	666,0	668,9	666,4	0,630	0,693	0,567	0,626
1063,0	675,8	671,0	668,8	0,640	0,703	0,577	0,631
1066,5	676,7	672,3	671,5	0,650	0,713	0,587	0,637
1069,8	684,3	672,3	675,6	0,660	0,723	0,597	0,646
1075,9	686,9	675,4	679,6	0,670	0,733	0,607	0,655
1076,2	688,2	676,3	682,2	0,680	0,743	0,617	0,660
1088,2	689,6	678,4	686,2	0,690	0,753	0,627	0,669
1092,4	705,7	682,6	693,0	0,700	0,763	0,637	0,683
1093,4	706,9	696,9	693,5	0,710	0,773	0,647	0,684
1093,9	708,2	700,2	693,6	0,720	0,783	0,657	0,684
1109,4	733,4	702,2	707,6	0,730	0,793	0,667	0,711
1110,5	733,9	706,0	711,6	0,740	0,803	0,677	0,719
1120,9	739,6	718,9	717,7	0,750	0,813	0,687	0,730
1123,7	748,0	737,3	727,6	0,760	0,823	0,697	0,748
1126,4	758,1	738,6	748,1	0,770	0,833	0,707	0,782
1132,0	760,7	741,0	752,8	0,780	0,843	0,717	0,789
1170,7	761,8	744,7	757,5	0,790	0,853	0,727	0,796
1195,1	762,1	761,1	763,9	0,800	0,863	0,737	0,805
1198,6	771,0	777,7	770,2	0,810	0,873	0,747	0,814
1201,1	781,0	789,3	772,4	0,820	0,883	0,757	0,817
1202,5	782,2	789,7	786,4	0,830	0,893	0,767	0,836
1209,9	782,4	809,2	801,3	0,840	0,903	0,777	0,853
1225,7	793,2	820,3	807,4	0,850	0,913	0,787	0,860
1246,1	797,7	821,9	812,0	0,860	0,923	0,797	0,865
1250,7	801,7	854,4	814,0	0,870	0,933	0,807	0,867
1266,5	803,3	871,4	815,5	0,880	0,943	0,817	0,869
1272,8	803,9	872,2	817,7	0,890	0,953	0,827	0,871
1278,5	825,6	884,9	879,2	0,900	0,963	0,837	0,922
1311,9	859,6	886,0	885,8	0,910	0,973	0,847	0,926
1319,1	867,6	899,6	887,0	0,920	0,983	0,857	0,927
1411,8	884,6	902,3	889,1	0,930	0,993	0,867	0,928
1440,6	889,4	923,3	908,3	0,940	1,000	0,877	0,939
1482,1	947,4	978,0	929,2	0,950	1,000	0,887	0,949
1499,4	986,2	997,4	933,4	0,960	1,000	0,897	0,951
1533,0	996,9	997,5	1010,0	0,970	1,000	0,907	0,975
1611,0	1007,9	1003,4	1035,5	0,980	1,000	0,917	0,981
1628,9	1037,9	1070,1	1117,9	0,990	1,000	0,927	0,991
1968,3	1091,5	1094,0	1155,8	1,000	1,000	0,937	0,994

Table H.11: Output processing for the maximum relative displacement measured with uncorrelated ground motions. Source: Excel, own elaboration

Max. relative horizontal displacement with uncorrelated ground motions - part.1

u [m]					95% CI		
model A	model B1	model B2	model C	EDF	upper b.	lower b.	lognorm
0,0075	0,0093	0,0082	0,0097	0,010	0,071	0,000	0,002
0,0075	0,0107	0,0082	0,0114	0,020	0,081	0,000	0,015
0,0086	0,0107	0,0082	0,0125	0,030	0,091	0,000	0,041
0,0100	0,0109	0,0083	0,0126	0,040	0,101	0,000	0,043
0,0102	0,0111	0,0087	0,0128	0,050	0,111	0,000	0,052
0,0103	0,0113	0,0089	0,0132	0,060	0,121	0,000	0,068
0,0103	0,0117	0,0090	0,0134	0,070	0,131	0,009	0,077
0,0104	0,0126	0,0091	0,0135	0,080	0,141	0,019	0,080
0,0104	0,0126	0,0092	0,0136	0,090	0,151	0,029	0,088
0,0105	0,0128	0,0092	0,0136	0,100	0,161	0,039	0,091
0,0106	0,0130	0,0093	0,0137	0,110	0,171	0,049	0,097
0,0106	0,0133	0,0093	0,0140	0,120	0,181	0,059	0,109
0,0107	0,0133	0,0095	0,0142	0,130	0,191	0,069	0,126
0,0107	0,0134	0,0096	0,0145	0,140	0,201	0,079	0,145
0,0108	0,0136	0,0096	0,0147	0,150	0,211	0,089	0,163
0,0109	0,0137	0,0097	0,0147	0,160	0,221	0,099	0,164
0,0110	0,0137	0,0098	0,0151	0,170	0,231	0,109	0,189
0,0110	0,0138	0,0098	0,0151	0,180	0,241	0,119	0,191
0,0110	0,0140	0,0098	0,0151	0,190	0,251	0,129	0,196
0,0111	0,0142	0,0100	0,0152	0,200	0,261	0,139	0,197
0,0111	0,0142	0,0101	0,0153	0,210	0,271	0,149	0,213
0,0112	0,0142	0,0101	0,0155	0,220	0,281	0,159	0,228
0,0115	0,0143	0,0105	0,0157	0,230	0,291	0,169	0,247
0,0118	0,0143	0,0105	0,0158	0,240	0,301	0,179	0,251
0,0119	0,0144	0,0105	0,0158	0,250	0,311	0,189	0,253
0,0119	0,0144	0,0106	0,0158	0,260	0,321	0,199	0,257
0,0120	0,0144	0,0106	0,0160	0,270	0,331	0,209	0,270
0,0122	0,0144	0,0106	0,0160	0,280	0,341	0,219	0,273
0,0122	0,0145	0,0109	0,0160	0,290	0,351	0,229	0,275
0,0123	0,0147	0,0110	0,0161	0,300	0,361	0,239	0,283
0,0124	0,0148	0,0110	0,0162	0,310	0,371	0,249	0,289
0,0124	0,0153	0,0111	0,0162	0,320	0,381	0,259	0,292
0,0125	0,0154	0,0111	0,0162	0,330	0,391	0,269	0,295
0,0125	0,0154	0,0111	0,0166	0,340	0,401	0,279	0,335
0,0127	0,0154	0,0112	0,0167	0,350	0,411	0,289	0,346
0,0127	0,0154	0,0114	0,0167	0,360	0,421	0,299	0,349
0,0128	0,0155	0,0114	0,0169	0,370	0,431	0,309	0,361
0,0130	0,0158	0,0115	0,0171	0,380	0,441	0,319	0,381
0,0130	0,0158	0,0116	0,0171	0,390	0,451	0,329	0,382
0,0131	0,0158	0,0117	0,0171	0,400	0,461	0,339	0,383
0,0131	0,0159	0,0118	0,0171	0,410	0,471	0,349	0,385
0,0131	0,0159	0,0119	0,0173	0,420	0,481	0,359	0,405
0,0132	0,0163	0,0120	0,0175	0,430	0,491	0,369	0,423
0,0132	0,0164	0,0120	0,0176	0,440	0,501	0,379	0,436
0,0133	0,0165	0,0121	0,0177	0,450	0,511	0,389	0,449
0,0133	0,0166	0,0122	0,0177	0,460	0,521	0,399	0,452
0,0134	0,0166	0,0122	0,0178	0,470	0,531	0,409	0,454
0,0135	0,0167	0,0122	0,0180	0,480	0,541	0,419	0,478
0,0136	0,0167	0,0123	0,0180	0,490	0,551	0,429	0,480
0,0137	0,0167	0,0123	0,0184	0,500	0,561	0,439	0,522

Table H.12: Output processing for the maximum relative displacement measured with uncorrelated ground motions. Source: Excel, own elaboration

Max. relative horizontal displacement with uncorrelated ground motions - part.2

u [m]					95% CI		
model A	model B1	model B2	model C	EDF	upper b.	lower b.	lognorm
0,0139	0,0170	0,0125	0,0184	0,510	0,571	0,449	0,522
0,0139	0,0171	0,0125	0,0185	0,520	0,581	0,459	0,527
0,0141	0,0171	0,0127	0,0187	0,530	0,591	0,469	0,548
0,0142	0,0172	0,0128	0,0189	0,540	0,601	0,479	0,568
0,0142	0,0173	0,0128	0,0189	0,550	0,611	0,489	0,573
0,0143	0,0173	0,0129	0,0190	0,560	0,621	0,499	0,581
0,0144	0,0174	0,0129	0,0191	0,570	0,631	0,509	0,583
0,0144	0,0175	0,0130	0,0193	0,580	0,641	0,519	0,608
0,0145	0,0176	0,0130	0,0193	0,590	0,651	0,529	0,610
0,0145	0,0177	0,0131	0,0195	0,600	0,661	0,539	0,625
0,0149	0,0179	0,0131	0,0195	0,610	0,671	0,549	0,627
0,0151	0,0180	0,0131	0,0196	0,620	0,681	0,559	0,631
0,0151	0,0181	0,0132	0,0196	0,630	0,691	0,569	0,635
0,0152	0,0182	0,0133	0,0197	0,640	0,701	0,579	0,646
0,0153	0,0184	0,0133	0,0198	0,650	0,711	0,589	0,650
0,0153	0,0185	0,0134	0,0199	0,660	0,721	0,599	0,655
0,0153	0,0186	0,0135	0,0202	0,670	0,731	0,609	0,685
0,0154	0,0188	0,0138	0,0204	0,680	0,741	0,619	0,697
0,0154	0,0188	0,0139	0,0204	0,690	0,751	0,629	0,698
0,0155	0,0190	0,0140	0,0204	0,700	0,761	0,639	0,698
0,0155	0,0192	0,0140	0,0204	0,710	0,771	0,649	0,699
0,0155	0,0193	0,0141	0,0204	0,720	0,781	0,659	0,700
0,0156	0,0194	0,0142	0,0204	0,730	0,791	0,669	0,703
0,0157	0,0194	0,0142	0,0205	0,740	0,801	0,679	0,712
0,0158	0,0195	0,0142	0,0206	0,750	0,811	0,689	0,712
0,0159	0,0195	0,0143	0,0206	0,760	0,821	0,699	0,719
0,0159	0,0196	0,0143	0,0207	0,770	0,831	0,709	0,723
0,0160	0,0196	0,0145	0,0208	0,780	0,841	0,719	0,730
0,0160	0,0196	0,0147	0,0209	0,790	0,851	0,729	0,738
0,0161	0,0197	0,0149	0,0209	0,800	0,861	0,739	0,741
0,0162	0,0199	0,0150	0,0211	0,810	0,871	0,749	0,754
0,0165	0,0200	0,0150	0,0212	0,820	0,881	0,759	0,759
0,0167	0,0201	0,0150	0,0216	0,830	0,891	0,769	0,784
0,0168	0,0202	0,0151	0,0216	0,840	0,901	0,779	0,788
0,0169	0,0204	0,0151	0,0218	0,850	0,911	0,789	0,795
0,0169	0,0207	0,0151	0,0219	0,860	0,921	0,799	0,805
0,0179	0,0207	0,0154	0,0222	0,870	0,931	0,809	0,822
0,0181	0,0213	0,0154	0,0232	0,880	0,941	0,819	0,871
0,0186	0,0214	0,0160	0,0233	0,890	0,951	0,829	0,875
0,0196	0,0216	0,0167	0,0236	0,900	0,961	0,839	0,886
0,0197	0,0219	0,0167	0,0241	0,910	0,971	0,849	0,902
0,0199	0,0224	0,0169	0,0243	0,920	0,981	0,859	0,910
0,0199	0,0228	0,0171	0,0246	0,930	0,991	0,869	0,917
0,0201	0,0232	0,0175	0,0247	0,940	1,000	0,879	0,922
0,0205	0,0240	0,0186	0,0255	0,950	1,000	0,889	0,940
0,0218	0,0248	0,0194	0,0266	0,960	1,000	0,899	0,961
0,0219	0,0256	0,0199	0,0287	0,970	1,000	0,909	0,982
0,0232	0,0257	0,0202	0,0300	0,980	1,000	0,919	0,990
0,0249	0,0274	0,0207	0,0318	0,990	1,000	0,929	0,995
0,0280	0,0302	0,0220	0,0322	1,000	1,000	0,939	0,996

Table H.13: Output processing for the maximum cable span variation measured with uncorrelated ground motions. Source: Excel, own elaboration

Max. cable span variation with uncorrelated ground motions - part.1

ΔL [m]					95% CI		
model A	model B1	model B2	model C	EDF	upper b.	lower b.	lognorm
0,0585	0,0666	0,0587	0,0658	0,010	0,071	0,000	0,014
0,0636	0,0669	0,0620	0,0678	0,020	0,081	0,000	0,017
0,0688	0,0717	0,0657	0,0683	0,030	0,091	0,000	0,018
0,0709	0,0735	0,0719	0,0728	0,040	0,101	0,000	0,026
0,0758	0,0782	0,0733	0,0802	0,050	0,111	0,000	0,045
0,0819	0,0783	0,0782	0,0806	0,060	0,121	0,000	0,046
0,0828	0,0891	0,0863	0,0902	0,070	0,131	0,009	0,081
0,0837	0,0957	0,0927	0,0946	0,080	0,141	0,019	0,101
0,0838	0,0962	0,0934	0,0949	0,090	0,151	0,029	0,103
0,0915	0,0975	0,0953	0,0983	0,100	0,161	0,039	0,119
0,0956	0,0979	0,0971	0,0988	0,110	0,171	0,049	0,122
0,0992	0,1006	0,0975	0,0988	0,120	0,181	0,059	0,122
0,1004	0,1015	0,0987	0,1004	0,130	0,191	0,069	0,130
0,1009	0,1027	0,1007	0,1031	0,140	0,201	0,079	0,145
0,1016	0,1037	0,1019	0,1032	0,150	0,211	0,089	0,145
0,1024	0,1040	0,1022	0,1055	0,160	0,221	0,099	0,158
0,1035	0,1055	0,1027	0,1078	0,170	0,231	0,109	0,172
0,1065	0,1083	0,1034	0,1094	0,180	0,241	0,119	0,182
0,1079	0,1084	0,1040	0,1100	0,190	0,251	0,129	0,185
0,1080	0,1089	0,1066	0,1112	0,200	0,261	0,139	0,193
0,1088	0,1120	0,1076	0,1113	0,210	0,271	0,149	0,194
0,1106	0,1126	0,1099	0,1122	0,220	0,281	0,159	0,200
0,1108	0,1134	0,1126	0,1137	0,230	0,291	0,169	0,209
0,1109	0,1135	0,1143	0,1142	0,240	0,301	0,179	0,212
0,1113	0,1158	0,1159	0,1151	0,250	0,311	0,189	0,218
0,1153	0,1167	0,1175	0,1180	0,260	0,321	0,199	0,237
0,1161	0,1206	0,1198	0,1183	0,270	0,331	0,209	0,239
0,1175	0,1220	0,1213	0,1227	0,280	0,341	0,219	0,269
0,1177	0,1232	0,1214	0,1235	0,290	0,351	0,229	0,274
0,1226	0,1235	0,1243	0,1237	0,300	0,361	0,239	0,275
0,1254	0,1240	0,1272	0,1256	0,310	0,371	0,249	0,289
0,1258	0,1258	0,1282	0,1267	0,320	0,381	0,259	0,297
0,1262	0,1311	0,1286	0,1334	0,330	0,391	0,269	0,343
0,1266	0,1323	0,1314	0,1336	0,340	0,401	0,279	0,344
0,1274	0,1327	0,1326	0,1336	0,350	0,411	0,289	0,344
0,1282	0,1336	0,1338	0,1356	0,360	0,421	0,299	0,358
0,1330	0,1350	0,1349	0,1372	0,370	0,431	0,309	0,369
0,1344	0,1379	0,1354	0,1383	0,380	0,441	0,319	0,377
0,1346	0,1383	0,1354	0,1385	0,390	0,451	0,329	0,378
0,1347	0,1385	0,1365	0,1404	0,400	0,461	0,339	0,391
0,1357	0,1389	0,1376	0,1406	0,410	0,471	0,349	0,393
0,1360	0,1400	0,1379	0,1425	0,420	0,481	0,359	0,406
0,1392	0,1406	0,1380	0,1428	0,430	0,491	0,369	0,408
0,1397	0,1435	0,1403	0,1429	0,440	0,501	0,379	0,409
0,1424	0,1463	0,1416	0,1466	0,450	0,511	0,389	0,434
0,1459	0,1471	0,1434	0,1467	0,460	0,521	0,399	0,435
0,1460	0,1484	0,1454	0,1470	0,470	0,531	0,409	0,437
0,1482	0,1498	0,1474	0,1503	0,480	0,541	0,419	0,459
0,1483	0,1510	0,1486	0,1525	0,490	0,551	0,429	0,474
0,1491	0,1517	0,1489	0,1534	0,500	0,561	0,439	0,480

Table H.14: Output processing for the maximum cable span variation measured with uncorrelated ground motions. Source: Excel, own elaboration

Max. cable span variation with uncorrelated ground motions - part.2

ΔL [m]					95% CI		
model A	model B1	model B2	model C	EDF	upper b.	lower b.	lognorm
0,1491	0,1537	0,1496	0,1539	0,510	0,571	0,449	0,483
0,1520	0,1561	0,1509	0,1576	0,520	0,581	0,459	0,507
0,1527	0,1573	0,1535	0,1595	0,530	0,591	0,469	0,519
0,1594	0,1582	0,1567	0,1596	0,540	0,601	0,479	0,520
0,1613	0,1587	0,1589	0,1596	0,550	0,611	0,489	0,520
0,1613	0,1603	0,1613	0,1621	0,560	0,621	0,499	0,535
0,1619	0,1647	0,1624	0,1639	0,570	0,631	0,509	0,547
0,1631	0,1650	0,1641	0,1646	0,580	0,641	0,519	0,551
0,1631	0,1654	0,1650	0,1651	0,590	0,651	0,529	0,554
0,1633	0,1672	0,1654	0,1657	0,600	0,661	0,539	0,558
0,1635	0,1684	0,1678	0,1679	0,610	0,671	0,549	0,571
0,1637	0,1696	0,1684	0,1715	0,620	0,681	0,559	0,592
0,1666	0,1705	0,1709	0,1727	0,630	0,691	0,569	0,599
0,1682	0,1749	0,1719	0,1738	0,640	0,701	0,579	0,605
0,1696	0,1760	0,1765	0,1743	0,650	0,711	0,589	0,608
0,1740	0,1762	0,1785	0,1769	0,660	0,721	0,599	0,622
0,1767	0,1818	0,1788	0,1858	0,670	0,731	0,609	0,668
0,1768	0,1881	0,1845	0,1895	0,680	0,741	0,619	0,687
0,1826	0,1901	0,1850	0,1906	0,690	0,751	0,629	0,692
0,1846	0,1924	0,1853	0,1925	0,700	0,761	0,639	0,700
0,1884	0,1934	0,1893	0,1934	0,710	0,771	0,649	0,704
0,1894	0,1946	0,1933	0,1955	0,720	0,781	0,659	0,714
0,1916	0,1961	0,1953	0,1969	0,730	0,791	0,669	0,720
0,1923	0,2009	0,1955	0,2039	0,740	0,801	0,679	0,749
0,1952	0,2019	0,1965	0,2044	0,750	0,811	0,689	0,751
0,1954	0,2021	0,1965	0,2049	0,760	0,821	0,699	0,753
0,1990	0,2031	0,2002	0,2057	0,770	0,831	0,709	0,756
0,2017	0,2069	0,2020	0,2061	0,780	0,841	0,719	0,757
0,2042	0,2070	0,2038	0,2084	0,790	0,851	0,729	0,766
0,2123	0,2154	0,2111	0,2176	0,800	0,861	0,739	0,799
0,2139	0,2202	0,2134	0,2195	0,810	0,871	0,749	0,804
0,2245	0,2331	0,2334	0,2303	0,820	0,881	0,759	0,837
0,2288	0,2346	0,2344	0,2345	0,830	0,891	0,769	0,847
0,2311	0,2378	0,2374	0,2380	0,840	0,901	0,779	0,856
0,2373	0,2432	0,2456	0,2417	0,850	0,911	0,789	0,865
0,2377	0,2488	0,2460	0,2458	0,860	0,921	0,799	0,874
0,2416	0,2500	0,2498	0,2505	0,870	0,931	0,809	0,884
0,2449	0,2505	0,2552	0,2535	0,880	0,941	0,819	0,889
0,2508	0,2543	0,2580	0,2544	0,890	0,951	0,829	0,891
0,2558	0,2753	0,2617	0,2758	0,900	0,961	0,839	0,925
0,2730	0,2753	0,2811	0,2787	0,910	0,971	0,849	0,928
0,2829	0,2904	0,2858	0,2902	0,920	0,981	0,859	0,941
0,2843	0,2910	0,2888	0,2919	0,930	0,991	0,869	0,943
0,2950	0,2994	0,2994	0,3021	0,940	1,000	0,879	0,952
0,2969	0,3032	0,3022	0,3039	0,950	1,000	0,889	0,954
0,2974	0,3047	0,3081	0,3043	0,960	1,000	0,899	0,954
0,3094	0,3173	0,3192	0,3198	0,970	1,000	0,909	0,965
0,3201	0,3297	0,3248	0,3293	0,980	1,000	0,919	0,970
0,3471	0,3482	0,3520	0,3455	0,990	1,000	0,929	0,978
0,4058	0,4114	0,4116	0,4118	1,000	1,000	0,939	0,993

Table H.15: Output processing for the maximum horizontal tension measured with uncorrelated ground motions. Source: Excel, own elaboration

Max. horizontal tension with uncorrelated ground motions - part.1

H [kN]					95% CI		
model A	model B1	model B2	model C	EDF	upper b.	lower b.	lognorm
12095,3	12661,4	12777,1	12697,7	0,010	0,071	0,000	0,076
12157,8	12715,9	12855,7	12747,9	0,020	0,081	0,000	0,086
12219,0	12718,3	12889,1	12788,3	0,030	0,091	0,000	0,096
12240,5	12753,0	12951,8	12811,0	0,040	0,101	0,000	0,101
12297,0	12761,9	12987,6	12854,6	0,050	0,111	0,000	0,112
12342,6	12785,3	12989,1	12870,3	0,060	0,121	0,000	0,117
12392,8	12794,9	12995,7	12876,8	0,070	0,131	0,009	0,118
12430,8	12838,9	13007,5	12901,9	0,080	0,141	0,019	0,125
12460,0	12842,2	13014,5	12911,6	0,090	0,151	0,029	0,128
12520,9	12854,8	13045,2	12923,6	0,100	0,161	0,039	0,132
12535,7	12901,4	13049,2	12924,7	0,110	0,171	0,049	0,132
12577,6	12919,4	13057,1	12929,0	0,120	0,181	0,059	0,133
12582,6	12923,5	13058,6	12929,5	0,130	0,191	0,069	0,133
12604,7	12925,1	13070,5	12951,7	0,140	0,201	0,079	0,140
12612,1	13016,3	13094,1	13067,9	0,150	0,211	0,089	0,178
12628,1	13018,5	13105,3	13088,9	0,160	0,221	0,099	0,186
12634,8	13042,7	13143,5	13103,7	0,170	0,231	0,109	0,191
12649,0	13088,2	13181,5	13148,7	0,180	0,241	0,119	0,209
12665,9	13094,8	13181,7	13185,8	0,190	0,251	0,129	0,223
12668,0	13123,2	13194,9	13185,9	0,200	0,261	0,139	0,223
12680,7	13125,8	13198,8	13197,4	0,210	0,271	0,149	0,228
12684,5	13137,1	13239,6	13204,9	0,220	0,281	0,159	0,231
12687,3	13163,3	13287,8	13229,1	0,230	0,291	0,169	0,241
12699,4	13178,3	13301,7	13237,8	0,240	0,301	0,179	0,245
12723,3	13182,2	13304,7	13239,0	0,250	0,311	0,189	0,245
12759,4	13195,2	13313,4	13260,9	0,260	0,321	0,199	0,255
12763,2	13217,6	13336,6	13267,6	0,270	0,331	0,209	0,258
12795,0	13230,5	13340,2	13270,3	0,280	0,341	0,219	0,259
12801,2	13243,5	13342,7	13273,6	0,290	0,351	0,229	0,260
12802,5	13247,8	13344,2	13291,6	0,300	0,361	0,239	0,268
12909,3	13249,9	13348,7	13319,9	0,310	0,371	0,249	0,281
12918,6	13261,3	13368,3	13333,3	0,320	0,381	0,259	0,287
12921,8	13287,1	13397,2	13338,0	0,330	0,391	0,269	0,289
12926,9	13317,5	13404,2	13340,3	0,340	0,401	0,279	0,290
12943,4	13322,1	13407,5	13387,7	0,350	0,411	0,289	0,312
12948,2	13330,3	13454,6	13399,2	0,360	0,421	0,299	0,317
12954,8	13335,5	13461,8	13400,4	0,370	0,431	0,309	0,318
12990,0	13348,0	13476,4	13401,0	0,380	0,441	0,319	0,318
13000,2	13348,3	13478,8	13411,6	0,390	0,451	0,329	0,323
13007,5	13350,5	13489,4	13417,1	0,400	0,461	0,339	0,326
13011,1	13356,5	13493,3	13432,3	0,410	0,471	0,349	0,333
13017,2	13358,5	13510,8	13459,0	0,420	0,481	0,359	0,346
13021,2	13368,1	13532,6	13467,3	0,430	0,491	0,369	0,350
13036,8	13410,2	13544,0	13477,9	0,440	0,501	0,379	0,355
13050,4	13413,1	13572,3	13482,5	0,450	0,511	0,389	0,358
13052,7	13440,3	13579,3	13483,9	0,460	0,521	0,399	0,358
13060,5	13444,7	13583,2	13490,9	0,470	0,531	0,409	0,362
13065,9	13529,8	13584,8	13519,1	0,480	0,541	0,419	0,376
13099,6	13537,5	13593,3	13576,0	0,490	0,551	0,429	0,405
13153,6	13553,0	13595,5	13579,3	0,500	0,561	0,439	0,406

Table H.16: Output processing for the maximum horizontal tension measured with uncorrelated ground motions. Source: Excel, own elaboration

Max. horizontal tension with uncorrelated ground motions - part.2

H [kN]				95% CI			
model A	model B1	model B2	model C	EDF	upper b.	lower b.	lognorm
13166,4	13557,4	13617,0	13630,3	0,510	0,571	0,449	0,432
13187,3	13594,1	13625,4	13682,2	0,520	0,581	0,459	0,459
13190,6	13599,9	13649,6	13706,5	0,530	0,591	0,469	0,472
13193,7	13607,1	13734,3	13708,7	0,540	0,601	0,479	0,473
13233,9	13647,7	13739,3	13739,5	0,550	0,611	0,489	0,489
13236,0	13656,7	13802,8	13747,1	0,560	0,621	0,499	0,493
13257,7	13668,4	13812,1	13756,6	0,570	0,631	0,509	0,497
13259,3	13676,3	13843,6	13780,9	0,580	0,641	0,519	0,510
13285,0	13692,5	13853,9	13797,6	0,590	0,651	0,529	0,519
13292,3	13693,5	13856,7	13807,7	0,600	0,661	0,539	0,524
13296,4	13709,2	13861,3	13820,4	0,610	0,671	0,549	0,530
13305,3	13726,7	13880,6	13843,3	0,620	0,681	0,559	0,542
13313,7	13729,8	13881,0	13869,1	0,630	0,691	0,569	0,555
13319,7	13767,5	13915,5	13891,9	0,640	0,701	0,579	0,567
13325,7	13768,5	13981,4	13905,8	0,650	0,711	0,589	0,574
13326,3	13770,0	13986,0	13907,1	0,660	0,721	0,599	0,574
13330,4	13805,4	14047,7	13909,8	0,670	0,731	0,609	0,576
13350,6	13834,1	14050,8	13913,4	0,680	0,741	0,619	0,578
13360,0	13895,4	14062,8	13917,7	0,690	0,751	0,629	0,580
13387,0	14021,0	14080,8	13956,1	0,700	0,761	0,639	0,599
13400,2	14022,9	14101,7	14057,8	0,710	0,771	0,649	0,648
13492,2	14029,3	14143,5	14070,9	0,720	0,781	0,659	0,654
13495,3	14044,1	14147,5	14077,1	0,730	0,791	0,669	0,657
13502,0	14047,2	14194,0	14088,1	0,740	0,801	0,679	0,662
13509,2	14081,8	14260,0	14113,5	0,750	0,811	0,689	0,674
13519,5	14082,3	14266,7	14127,8	0,760	0,821	0,699	0,680
13539,0	14091,7	14355,7	14151,2	0,770	0,831	0,709	0,691
13608,7	14175,4	14387,6	14168,2	0,780	0,841	0,719	0,698
13630,6	14211,5	14450,9	14271,8	0,790	0,851	0,729	0,742
13635,2	14279,1	14456,9	14284,9	0,800	0,861	0,739	0,747
13653,3	14283,3	14499,0	14331,0	0,810	0,871	0,749	0,765
13751,1	14301,0	14537,4	14372,9	0,820	0,881	0,759	0,781
13777,9	14351,8	14592,3	14412,4	0,830	0,891	0,769	0,795
13803,9	14392,5	14592,4	14449,6	0,840	0,901	0,779	0,808
13834,0	14442,1	14602,8	14457,2	0,850	0,911	0,789	0,810
13835,4	14450,8	14656,5	14494,0	0,860	0,921	0,799	0,822
13848,9	14494,8	14668,5	14514,6	0,870	0,931	0,809	0,829
13879,5	14496,1	14673,3	14528,7	0,880	0,941	0,819	0,833
13890,8	14583,3	14716,7	14617,8	0,890	0,951	0,829	0,859
13937,8	14622,3	14727,9	14711,7	0,900	0,961	0,839	0,883
14001,6	14634,8	14783,4	14720,2	0,910	0,971	0,849	0,885
14018,4	14847,1	14812,5	14764,2	0,920	0,981	0,859	0,895
14043,7	14861,6	15000,1	14975,3	0,930	0,991	0,869	0,934
14087,7	14936,3	15117,5	15013,1	0,940	1,000	0,879	0,939
14409,4	15255,7	15250,2	15365,5	0,950	1,000	0,889	0,975
14459,1	15268,2	15362,3	15527,2	0,960	1,000	0,899	0,984
14490,8	15707,8	15742,9	15780,0	0,970	1,000	0,909	0,993
14659,7	15721,5	15767,4	15780,7	0,980	1,000	0,919	0,993
14787,8	16403,8	16517,4	16530,5	0,990	1,000	0,929	0,999
14959,1	16986,5	16951,0	17218,3	1,000	1,000	0,939	1,000

Table H.17: Output processing for the maximum cable tension measured with uncorrelated ground motions. Source: Excel, own elaboration

Max. cable tension with uncorrelated ground motions - part.1

T [kN]					95% CI		
model A	model B1	model B2	model C	EDF	upper b.	lower b.	lognorm
12095,3	13068,6	13159,2	13102,7	0,010	0,071	0,000	0,082
12157,8	13098,2	13241,7	13119,3	0,020	0,081	0,000	0,086
12219,0	13111,4	13255,1	13156,1	0,030	0,091	0,000	0,094
12240,5	13115,0	13321,4	13201,7	0,040	0,101	0,000	0,105
12297,0	13144,7	13359,0	13241,0	0,050	0,111	0,000	0,115
12342,6	13156,2	13378,3	13255,3	0,060	0,121	0,000	0,119
12392,8	13172,9	13383,7	13269,5	0,070	0,131	0,009	0,122
12430,8	13215,1	13394,7	13273,4	0,080	0,141	0,019	0,123
12460,0	13223,9	13395,6	13280,0	0,090	0,151	0,029	0,125
12520,9	13224,5	13417,1	13283,9	0,100	0,161	0,039	0,126
12535,7	13282,8	13430,2	13293,4	0,110	0,171	0,049	0,129
12577,6	13293,7	13434,3	13303,9	0,120	0,181	0,059	0,132
12582,6	13322,9	13442,9	13317,6	0,130	0,191	0,069	0,136
12604,7	13342,7	13473,3	13333,3	0,140	0,201	0,079	0,141
12612,1	13370,2	13474,6	13438,8	0,150	0,211	0,089	0,175
12628,1	13411,6	13494,5	13453,7	0,160	0,221	0,099	0,180
12634,8	13430,1	13524,6	13508,3	0,170	0,231	0,109	0,199
12649,0	13439,4	13525,6	13540,2	0,180	0,241	0,119	0,211
12665,9	13508,6	13559,4	13576,4	0,190	0,251	0,129	0,225
12668,0	13519,1	13560,1	13577,0	0,200	0,261	0,139	0,226
12680,7	13534,1	13590,5	13596,5	0,210	0,271	0,149	0,233
12684,5	13535,5	13622,4	13604,8	0,220	0,281	0,159	0,237
12687,3	13536,4	13688,5	13621,1	0,230	0,291	0,169	0,243
12699,4	13559,2	13692,5	13622,0	0,240	0,301	0,179	0,244
12723,3	13560,9	13698,6	13628,1	0,250	0,311	0,189	0,246
12759,4	13584,5	13705,8	13631,2	0,260	0,321	0,199	0,248
12763,2	13605,6	13707,8	13650,0	0,270	0,331	0,209	0,255
12795,0	13623,3	13717,3	13655,8	0,280	0,341	0,219	0,258
12801,2	13627,5	13725,1	13663,8	0,290	0,351	0,229	0,261
12802,5	13644,4	13740,5	13663,8	0,300	0,361	0,239	0,261
12909,3	13647,3	13766,5	13715,8	0,310	0,371	0,249	0,284
12918,6	13651,8	13780,1	13718,6	0,320	0,381	0,259	0,285
12921,8	13673,2	13788,2	13719,7	0,330	0,391	0,269	0,286
12926,9	13691,6	13799,4	13726,5	0,340	0,401	0,279	0,289
12943,4	13699,7	13810,1	13780,0	0,350	0,411	0,289	0,313
12948,2	13702,6	13839,9	13782,7	0,360	0,421	0,299	0,314
12954,8	13715,1	13862,5	13789,1	0,370	0,431	0,309	0,317
12990,0	13721,3	13864,2	13797,5	0,380	0,441	0,319	0,321
13000,2	13740,6	13873,9	13812,5	0,390	0,451	0,329	0,328
13007,5	13756,7	13882,8	13822,4	0,400	0,461	0,339	0,333
13011,1	13758,4	13891,2	13827,0	0,410	0,471	0,349	0,335
13017,2	13766,4	13899,6	13836,5	0,420	0,481	0,359	0,339
13021,2	13794,1	13904,8	13839,6	0,430	0,491	0,369	0,341
13036,8	13798,7	13909,9	13854,1	0,440	0,501	0,379	0,348
13050,4	13799,3	13930,8	13860,5	0,450	0,511	0,389	0,351
13052,7	13846,5	13940,3	13881,7	0,460	0,521	0,399	0,361
13060,5	13860,6	13954,1	13901,1	0,470	0,531	0,409	0,370
13065,9	13920,6	13956,0	13915,6	0,480	0,541	0,419	0,377
13099,6	13946,6	13971,0	13955,0	0,490	0,551	0,429	0,397
13153,6	13951,9	13978,8	13996,3	0,500	0,561	0,439	0,417

Table H.18: Output processing for the maximum cable tension measured with uncorrelated ground motions. Source: Excel, own elaboration

Max. cable tension with uncorrelated ground motions - part.2

T [kN]					95% CI		
model A	model B1	model B2	model C	EDF	upper b.	lower b.	lognorm
13166,4	13960,5	14008,4	14010,5	0,510	0,571	0,449	0,424
13187,3	13968,9	14030,2	14056,0	0,520	0,581	0,459	0,447
13190,6	13991,5	14048,1	14077,5	0,530	0,591	0,469	0,458
13193,7	14025,5	14128,5	14118,9	0,540	0,601	0,479	0,479
13233,9	14037,7	14147,4	14139,7	0,550	0,611	0,489	0,489
13236,0	14067,0	14190,8	14158,5	0,560	0,621	0,499	0,499
13257,7	14076,6	14237,8	14170,2	0,570	0,631	0,509	0,505
13259,3	14077,9	14245,0	14191,3	0,580	0,641	0,519	0,515
13285,0	14097,1	14250,9	14207,5	0,590	0,651	0,529	0,523
13292,3	14100,0	14256,0	14211,2	0,600	0,661	0,539	0,525
13296,4	14135,4	14268,7	14237,2	0,610	0,671	0,549	0,538
13305,3	14140,7	14272,8	14248,6	0,620	0,681	0,559	0,544
13313,7	14146,2	14300,5	14275,8	0,630	0,691	0,569	0,557
13319,7	14190,1	14334,5	14276,1	0,640	0,701	0,579	0,558
13325,7	14198,6	14358,7	14299,4	0,650	0,711	0,589	0,569
13326,3	14211,8	14400,7	14306,7	0,660	0,721	0,599	0,573
13330,4	14215,8	14403,4	14311,0	0,670	0,731	0,609	0,575
13350,6	14231,1	14449,9	14319,6	0,680	0,741	0,619	0,579
13360,0	14282,5	14454,9	14366,1	0,690	0,751	0,629	0,602
13387,0	14390,8	14497,4	14367,1	0,700	0,761	0,639	0,602
13400,2	14433,5	14503,0	14458,7	0,710	0,771	0,649	0,645
13492,2	14435,1	14544,3	14462,5	0,720	0,781	0,659	0,647
13495,3	14443,3	14562,1	14479,2	0,730	0,791	0,669	0,655
13502,0	14446,8	14602,1	14480,2	0,740	0,801	0,679	0,655
13509,2	14447,1	14648,4	14482,6	0,750	0,811	0,689	0,656
13519,5	14461,2	14675,1	14527,2	0,760	0,821	0,699	0,676
13539,0	14498,6	14765,0	14552,4	0,770	0,831	0,709	0,687
13608,7	14578,5	14779,9	14581,5	0,780	0,841	0,719	0,700
13630,6	14624,8	14867,7	14637,8	0,790	0,851	0,729	0,723
13635,2	14674,6	14897,4	14694,8	0,800	0,861	0,739	0,746
13653,3	14711,8	14913,9	14754,9	0,810	0,871	0,749	0,769
13751,1	14713,0	14946,2	14764,2	0,820	0,881	0,759	0,772
13777,9	14793,0	14979,6	14855,9	0,830	0,891	0,769	0,804
13803,9	14800,4	14982,1	14877,1	0,840	0,901	0,779	0,811
13834,0	14859,4	15039,9	14883,5	0,850	0,911	0,789	0,813
13835,4	14890,0	15046,2	14929,2	0,860	0,921	0,799	0,828
13848,9	14916,0	15082,6	14932,8	0,870	0,931	0,809	0,829
13879,5	14936,9	15101,2	14939,5	0,880	0,941	0,819	0,831
13890,8	15010,3	15151,7	15058,7	0,890	0,951	0,829	0,864
13937,8	15026,3	15168,7	15138,1	0,900	0,961	0,839	0,884
14001,6	15061,4	15216,7	15157,0	0,910	0,971	0,849	0,888
14018,4	15302,8	15242,2	15164,6	0,920	0,981	0,859	0,890
14043,7	15308,9	15441,7	15412,7	0,930	0,991	0,869	0,935
14087,7	15378,4	15504,3	15460,3	0,940	1,000	0,879	0,942
14409,4	15665,1	15692,2	15754,7	0,950	1,000	0,889	0,972
14459,1	15700,8	15800,3	15968,1	0,960	1,000	0,899	0,984
14490,8	16161,5	16198,7	16231,6	0,970	1,000	0,909	0,993
14659,7	16193,6	16213,1	16246,4	0,980	1,000	0,919	0,993
14787,8	16866,3	16980,2	16994,9	0,990	1,000	0,929	0,999
14959,1	17483,4	17432,0	17715,8	1,000	1,000	0,939	1,000

Table H.19: Output processing for the maximum horizontal tension variation measured with uncorrelated ground motions. Source: Excel, own elaboration

Max. horizontal tension variation with uncorrelated ground motions - part.1

ΔH [kN]					95% CI		
model A	model B1	model B2	model C	EDF	upper b.	lower b.	lognorm
317,3	945,0	940,2	924,6	0,010	0,071	0,000	0,025
379,8	999,5	1018,8	974,9	0,020	0,081	0,000	0,035
441,0	1001,9	1052,2	1015,2	0,030	0,091	0,000	0,044
462,5	1036,6	1114,9	1037,9	0,040	0,101	0,000	0,050
519,0	1045,5	1150,7	1081,5	0,050	0,111	0,000	0,063
564,6	1068,9	1152,2	1097,2	0,060	0,121	0,000	0,068
614,8	1078,5	1158,7	1103,7	0,070	0,131	0,009	0,070
652,8	1122,6	1170,6	1128,8	0,080	0,141	0,019	0,079
682,0	1125,8	1177,6	1138,5	0,090	0,151	0,029	0,083
742,9	1138,5	1208,3	1150,5	0,100	0,161	0,039	0,087
757,7	1185,0	1212,3	1151,6	0,110	0,171	0,049	0,088
799,6	1203,0	1220,2	1155,9	0,120	0,181	0,059	0,089
804,6	1207,2	1221,7	1156,4	0,130	0,191	0,069	0,090
826,8	1208,7	1233,6	1178,6	0,140	0,201	0,079	0,098
834,1	1299,9	1257,2	1294,8	0,150	0,211	0,089	0,151
850,1	1302,2	1268,4	1315,8	0,160	0,221	0,099	0,162
856,8	1326,3	1306,5	1330,6	0,170	0,231	0,109	0,170
871,0	1371,9	1344,6	1375,6	0,180	0,241	0,119	0,194
887,9	1378,4	1344,8	1412,8	0,190	0,251	0,129	0,215
890,0	1406,8	1358,0	1412,8	0,200	0,261	0,139	0,215
902,7	1409,4	1361,8	1424,3	0,210	0,271	0,149	0,222
906,5	1420,8	1402,7	1431,8	0,220	0,281	0,159	0,226
909,3	1446,9	1450,9	1456,1	0,230	0,291	0,169	0,240
921,4	1461,9	1464,8	1464,7	0,240	0,301	0,179	0,245
945,3	1465,8	1467,7	1465,9	0,250	0,311	0,189	0,246
981,4	1478,9	1476,5	1487,9	0,260	0,321	0,199	0,259
985,2	1501,3	1499,7	1494,6	0,270	0,331	0,209	0,263
1017,0	1514,2	1503,3	1497,2	0,280	0,341	0,219	0,265
1023,2	1527,1	1505,7	1500,5	0,290	0,351	0,229	0,267
1024,6	1531,4	1507,3	1518,5	0,300	0,361	0,239	0,278
1131,3	1533,5	1511,8	1546,8	0,310	0,371	0,249	0,295
1140,6	1544,9	1531,3	1560,2	0,320	0,381	0,259	0,304
1143,8	1570,8	1560,2	1564,9	0,330	0,391	0,269	0,306
1148,9	1601,1	1567,3	1567,2	0,340	0,401	0,279	0,308
1165,4	1605,7	1570,5	1614,6	0,350	0,411	0,289	0,337
1170,2	1613,9	1617,7	1626,1	0,360	0,421	0,299	0,345
1176,8	1619,2	1624,9	1627,4	0,370	0,431	0,309	0,345
1212,0	1631,6	1639,5	1627,9	0,380	0,441	0,319	0,346
1222,2	1631,9	1641,9	1638,5	0,390	0,451	0,329	0,352
1229,5	1634,1	1652,5	1644,0	0,400	0,461	0,339	0,356
1233,1	1640,1	1656,4	1659,2	0,410	0,471	0,349	0,365
1239,2	1642,1	1673,9	1686,0	0,420	0,481	0,359	0,382
1243,2	1651,7	1695,7	1694,2	0,430	0,491	0,369	0,387
1258,8	1693,8	1707,0	1704,9	0,440	0,501	0,379	0,394
1272,5	1696,8	1735,4	1709,4	0,450	0,511	0,389	0,397
1274,7	1723,9	1742,3	1710,8	0,460	0,521	0,399	0,398
1282,5	1728,3	1746,2	1717,9	0,470	0,531	0,409	0,402
1288,0	1813,4	1747,9	1746,0	0,480	0,541	0,419	0,420
1321,6	1821,1	1756,3	1803,0	0,490	0,551	0,429	0,455
1375,6	1836,6	1758,6	1806,2	0,500	0,561	0,439	0,457

Table H.20: Output processing for the maximum horizontal tension variation measured with uncorrelated ground motions. Source: Excel, own elaboration

Max. horizontal tension variation with uncorrelated ground motions - part.2

ΔH [kN]				95% CI			
model A	model B1	model B2	model C	EDF	upper b.	lower b.	lognorm
1388,4	1841,0	1780,1	1857,2	0,510	0,571	0,449	0,487
1409,3	1877,8	1788,5	1909,1	0,520	0,581	0,459	0,518
1412,6	1883,6	1812,7	1933,4	0,530	0,591	0,469	0,532
1415,7	1890,8	1897,3	1935,7	0,540	0,601	0,479	0,533
1455,9	1931,4	1902,3	1966,4	0,550	0,611	0,489	0,550
1458,0	1940,3	1965,9	1974,0	0,560	0,621	0,499	0,554
1479,7	1952,0	1975,2	1983,5	0,570	0,631	0,509	0,560
1481,3	1959,9	2006,7	2007,8	0,580	0,641	0,519	0,573
1507,0	1976,1	2017,0	2024,5	0,590	0,651	0,529	0,582
1514,3	1977,1	2019,8	2034,6	0,600	0,661	0,539	0,587
1518,5	1992,8	2024,4	2047,3	0,610	0,671	0,549	0,594
1527,3	2010,3	2043,7	2070,2	0,620	0,681	0,559	0,606
1535,7	2013,5	2044,1	2096,0	0,630	0,691	0,569	0,619
1541,7	2051,2	2078,6	2118,8	0,640	0,701	0,579	0,630
1547,7	2052,2	2144,5	2132,7	0,650	0,711	0,589	0,637
1548,3	2053,6	2149,0	2134,0	0,660	0,721	0,599	0,638
1552,4	2089,0	2210,8	2136,7	0,670	0,731	0,609	0,639
1572,6	2117,7	2213,8	2140,4	0,680	0,741	0,619	0,641
1582,0	2179,0	2225,8	2144,6	0,690	0,751	0,629	0,643
1609,0	2304,6	2243,9	2183,0	0,700	0,761	0,639	0,661
1622,2	2306,6	2264,8	2284,7	0,710	0,771	0,649	0,706
1714,3	2313,0	2306,5	2297,8	0,720	0,781	0,659	0,711
1717,3	2327,8	2310,5	2304,0	0,730	0,791	0,669	0,714
1724,0	2330,8	2357,0	2315,1	0,740	0,801	0,679	0,718
1731,3	2365,4	2423,1	2340,4	0,750	0,811	0,689	0,728
1741,5	2365,9	2429,7	2354,7	0,760	0,821	0,699	0,734
1761,0	2375,3	2518,8	2378,1	0,770	0,831	0,709	0,743
1830,7	2459,0	2550,6	2395,1	0,780	0,841	0,719	0,749
1852,6	2495,1	2614,0	2498,7	0,790	0,851	0,729	0,785
1857,2	2562,7	2620,0	2511,8	0,800	0,861	0,739	0,789
1875,3	2566,9	2662,1	2557,9	0,810	0,871	0,749	0,803
1973,1	2584,6	2700,5	2599,8	0,820	0,881	0,759	0,816
1999,9	2635,4	2755,4	2639,3	0,830	0,891	0,769	0,827
2025,9	2676,1	2755,5	2676,5	0,840	0,901	0,779	0,836
2056,1	2725,7	2765,9	2684,1	0,850	0,911	0,789	0,838
2057,4	2734,4	2819,6	2720,9	0,860	0,921	0,799	0,847
2070,9	2778,4	2831,6	2741,5	0,870	0,931	0,809	0,852
2101,6	2779,7	2836,4	2755,6	0,880	0,941	0,819	0,855
2112,8	2866,9	2879,8	2844,7	0,890	0,951	0,829	0,875
2159,8	2905,9	2890,9	2938,6	0,900	0,961	0,839	0,892
2223,6	2918,4	2946,5	2947,1	0,910	0,971	0,849	0,894
2240,4	3130,7	2975,6	2991,1	0,920	0,981	0,859	0,901
2265,7	3145,2	3163,1	3202,2	0,930	0,991	0,869	0,930
2309,7	3220,0	3280,6	3240,0	0,940	1,000	0,879	0,934
2631,4	3539,3	3413,3	3592,4	0,950	1,000	0,889	0,964
2681,2	3551,8	3525,4	3754,2	0,960	1,000	0,899	0,972
2712,8	3991,4	3906,0	4006,9	0,970	1,000	0,909	0,982
2881,7	4005,1	3930,5	4007,6	0,980	1,000	0,919	0,982
3009,8	4687,4	4680,5	4757,4	0,990	1,000	0,929	0,995
3181,1	5270,1	5114,1	5445,2	1,000	1,000	0,939	0,998

Table H.21: Output processing for the maximum cable tension variation measured with uncorrelated ground motions. Source: Excel, own elaboration

Max. cable tension variation with uncorrelated ground motions - part.1

ΔT [kN]					95% CI		
model A	model B1	model B2	model C	EDF	upper b.	lower b.	lognorm
317,3	1003,9	977,4	983,0	0,010	0,071	0,000	0,031
379,8	1033,6	1059,8	999,6	0,020	0,081	0,000	0,034
441,0	1046,8	1073,3	1036,4	0,030	0,091	0,000	0,042
462,5	1050,3	1139,6	1082,0	0,040	0,101	0,000	0,054
519,0	1080,0	1177,2	1121,3	0,050	0,111	0,000	0,066
564,6	1091,5	1196,5	1135,6	0,060	0,121	0,000	0,070
614,8	1108,2	1201,9	1149,8	0,070	0,131	0,009	0,075
652,8	1150,4	1212,9	1153,7	0,080	0,141	0,019	0,077
682,0	1159,2	1213,8	1160,3	0,090	0,151	0,029	0,079
742,9	1159,8	1235,3	1164,2	0,100	0,161	0,039	0,080
757,7	1218,1	1248,4	1173,7	0,110	0,171	0,049	0,084
799,6	1229,0	1252,5	1184,2	0,120	0,181	0,059	0,088
804,6	1258,3	1261,1	1197,9	0,130	0,191	0,069	0,093
826,8	1278,0	1291,5	1213,7	0,140	0,201	0,079	0,099
834,1	1305,6	1292,8	1319,1	0,150	0,211	0,089	0,145
850,1	1346,9	1312,7	1334,0	0,160	0,221	0,099	0,153
856,8	1365,4	1342,8	1388,6	0,170	0,231	0,109	0,180
871,0	1374,8	1343,8	1420,5	0,180	0,241	0,119	0,198
887,9	1443,9	1377,6	1456,7	0,190	0,251	0,129	0,218
890,0	1454,5	1378,3	1457,3	0,200	0,261	0,139	0,218
902,7	1469,4	1408,7	1476,9	0,210	0,271	0,149	0,229
906,5	1470,9	1440,5	1485,1	0,220	0,281	0,159	0,234
909,3	1471,7	1506,6	1501,4	0,230	0,291	0,169	0,243
921,4	1494,5	1510,7	1502,3	0,240	0,301	0,179	0,244
945,3	1496,2	1516,8	1508,4	0,250	0,311	0,189	0,247
981,4	1519,9	1524,0	1511,5	0,260	0,321	0,199	0,249
985,2	1540,9	1525,9	1530,3	0,270	0,331	0,209	0,260
1017,0	1558,7	1535,5	1536,1	0,280	0,341	0,219	0,263
1023,2	1562,8	1543,3	1544,1	0,290	0,351	0,229	0,268
1024,6	1579,8	1558,7	1544,1	0,300	0,361	0,239	0,268
1131,3	1582,7	1584,7	1596,1	0,310	0,371	0,249	0,299
1140,6	1587,2	1598,3	1598,9	0,320	0,381	0,259	0,301
1143,8	1608,6	1606,4	1600,0	0,330	0,391	0,269	0,302
1148,9	1627,0	1617,6	1606,8	0,340	0,401	0,279	0,306
1165,4	1635,1	1628,2	1660,3	0,350	0,411	0,289	0,338
1170,2	1638,0	1658,1	1663,0	0,360	0,421	0,299	0,340
1176,8	1650,5	1680,7	1669,4	0,370	0,431	0,309	0,344
1212,0	1656,7	1682,3	1677,8	0,380	0,441	0,319	0,349
1222,2	1676,0	1692,1	1692,8	0,390	0,451	0,329	0,358
1229,5	1692,0	1701,0	1702,7	0,400	0,461	0,339	0,364
1233,1	1693,8	1709,4	1707,3	0,410	0,471	0,349	0,367
1239,2	1701,8	1717,8	1716,8	0,420	0,481	0,359	0,373
1243,2	1729,5	1723,0	1719,9	0,430	0,491	0,369	0,375
1258,8	1734,0	1728,1	1734,5	0,440	0,501	0,379	0,384
1272,5	1734,7	1749,0	1740,8	0,450	0,511	0,389	0,388
1274,7	1781,8	1758,5	1762,0	0,460	0,521	0,399	0,400
1282,5	1796,0	1772,3	1781,4	0,470	0,531	0,409	0,412
1288,0	1855,9	1774,1	1795,9	0,480	0,541	0,419	0,421
1321,6	1882,0	1789,2	1835,3	0,490	0,551	0,429	0,445
1375,6	1887,2	1797,0	1876,6	0,500	0,561	0,439	0,469

Table H.22: Output processing for the maximum cable tension variation measured with uncorrelated ground motions. Source: Excel, own elaboration

Max. cable tension variation with uncorrelated ground motions - part.2

ΔT [kN]				95% CI			
model A	model B1	model B2	model C	EDF	upper b.	lower b.	lognorm
1388,4	1895,8	1826,6	1890,8	0,510	0,571	0,449	0,478
1409,3	1904,3	1848,4	1936,3	0,520	0,581	0,459	0,504
1412,6	1926,9	1866,3	1957,8	0,530	0,591	0,469	0,516
1415,7	1960,8	1946,7	1999,3	0,540	0,601	0,479	0,539
1455,9	1973,0	1965,6	2020,0	0,550	0,611	0,489	0,551
1458,0	2002,3	2008,9	2038,9	0,560	0,621	0,499	0,561
1479,7	2011,9	2055,9	2050,5	0,570	0,631	0,509	0,567
1481,3	2013,3	2063,2	2071,6	0,580	0,641	0,519	0,578
1507,0	2032,5	2069,0	2087,8	0,590	0,651	0,529	0,587
1514,3	2035,4	2074,2	2091,5	0,600	0,661	0,539	0,589
1518,5	2070,7	2086,9	2117,5	0,610	0,671	0,549	0,602
1527,3	2076,0	2091,0	2128,9	0,620	0,681	0,559	0,608
1535,7	2081,5	2118,7	2156,2	0,630	0,691	0,569	0,621
1541,7	2125,4	2152,7	2156,4	0,640	0,701	0,579	0,621
1547,7	2133,9	2176,9	2179,7	0,650	0,711	0,589	0,633
1548,3	2147,1	2218,9	2187,0	0,660	0,721	0,599	0,636
1552,4	2151,1	2221,6	2191,3	0,670	0,731	0,609	0,638
1572,6	2166,5	2268,0	2199,9	0,680	0,741	0,619	0,642
1582,0	2217,9	2273,1	2246,4	0,690	0,751	0,629	0,664
1609,0	2326,2	2315,6	2247,4	0,700	0,761	0,639	0,664
1622,2	2368,9	2321,2	2339,1	0,710	0,771	0,649	0,704
1714,3	2370,4	2362,5	2342,8	0,720	0,781	0,659	0,705
1717,3	2378,6	2380,3	2359,5	0,730	0,791	0,669	0,712
1724,0	2382,1	2420,3	2360,5	0,740	0,801	0,679	0,712
1731,3	2382,5	2466,6	2362,9	0,750	0,811	0,689	0,713
1741,5	2396,6	2493,3	2407,5	0,760	0,821	0,699	0,731
1761,0	2433,9	2583,2	2432,7	0,770	0,831	0,709	0,740
1830,7	2513,9	2598,1	2461,8	0,780	0,841	0,719	0,751
1852,6	2560,1	2685,9	2518,1	0,790	0,851	0,729	0,770
1857,2	2610,0	2715,6	2575,1	0,800	0,861	0,739	0,789
1875,3	2647,2	2732,1	2635,2	0,810	0,871	0,749	0,807
1973,1	2648,4	2764,4	2644,5	0,820	0,881	0,759	0,809
1999,9	2728,3	2797,7	2736,2	0,830	0,891	0,769	0,834
2025,9	2735,8	2800,2	2757,4	0,840	0,901	0,779	0,839
2056,1	2794,8	2858,1	2763,8	0,850	0,911	0,789	0,841
2057,4	2825,4	2864,4	2809,5	0,860	0,921	0,799	0,852
2070,9	2851,4	2900,8	2813,1	0,870	0,931	0,809	0,853
2101,6	2872,3	2919,4	2819,8	0,880	0,941	0,819	0,854
2112,8	2945,6	2969,9	2939,0	0,890	0,951	0,829	0,879
2159,8	2961,6	2986,8	3018,4	0,900	0,961	0,839	0,893
2223,6	2996,8	3034,9	3037,3	0,910	0,971	0,849	0,896
2240,4	3238,2	3060,4	3045,0	0,920	0,981	0,859	0,898
2265,7	3244,3	3259,8	3293,0	0,930	0,991	0,869	0,931
2309,7	3313,7	3322,4	3340,6	0,940	1,000	0,879	0,936
2631,4	3600,5	3510,4	3635,0	0,950	1,000	0,889	0,961
2681,2	3636,2	3618,5	3848,5	0,960	1,000	0,899	0,972
2712,8	4096,9	4016,9	4111,9	0,970	1,000	0,909	0,982
2881,7	4128,9	4031,2	4126,7	0,980	1,000	0,919	0,983
3009,8	4801,6	4798,4	4875,3	0,990	1,000	0,929	0,995
3181,1	5418,7	5250,2	5596,1	1,000	1,000	0,939	0,998

Bibliography

[1] Brincker R. Krenk S. Henning P. Rytter A. "Identification of Dynamical Properties from Correlation Function Estimates (1 ed.)" In: *Bygningsstatiske Meddelelser* 63(1) (1992), p. 33. URL: https://vbn.aau.dk/ws/portalfiles/portal/204328437/Identification_of_Dynamical_Properties_from_Correlation_Function_Estimates.pdf.

[2] Caetano E. Cunha A. "Numerical modelling of the structural behaviour of the new Braga Stadium roof". In: *Technical report FEUP/VIBEST*. 2001.

[3] A. Carvalho A. Campos Costa M.L. Sousa. "Seismic Zonation for Portuguese National Annex of Eurocode 8". In: *Proc. XIV World Conference on Earthquake Engineering*. Beijing, China, 2008.

[4] Bertero R.D. Carnicer R. Puppo A.H. "Sensibility wind analysis of the roof structural system - Stadium of Braga - Portugal". In: *Final report*. 2003.

[5] Bachmann J.A. Strand M. Vassiliou M.F. Broccardo M. Stojadinović B. "Is rocking motion predictable?" In: *Earthquake Engineering and Structural Dynamics* 47(2) (2017), pp. 535–552. DOI: 10.1002/eqe.2978.

[6] Andersen P. Brincker R. Ventura C. "Damping estimation by frequency domain decomposition". In: *Proc. IMAC XIX: a Conference on Structural Dynamics*. Orlando, Florida(US), 2001.

[7] Andersen P. Brincker R. Zhang L. *Modal identification from ambient response using frequency domain decomposition*. San Antonio, Texas(US), 2000.

[8] Dabaghi M Broccardo M. "A spectral-based stochastic ground motion model with a non-parametric time-modulating function". In: *Proc. XII International Conference on Structural Safety and Reliability*. Wien, Austria, 2017.

[9] Der Kiureghian A Broccardo M. "Simulation of near-fault ground motions using frequency-domain discretization". In: *Proc. X National Conference on Earthquake Engineering;* Anchorage, Alaska (US), 2014.

[10] Nuno M. Caetano E. Cunha A. "Characterisation of the aerodynamic behaviour of the Braga Stadium suspension roof from prototype monitoring". In: *Proc. 4^{th} ECCOMAS Thematic Conference on Computational Methods in Structural Dynamics and Earthquake Engineering*. Kos Island, Greece, 2014. DOI: 10.7712/120113.4542.C1340.

[11] Computers and Structures Inc. *CSi Analysis Reference Manual, for SAP2000®, ETABS®, SAFE® and CSiBridge®*. 2016. URL: https://ottegroup.com/wp-content/uploads/2021/02/ETABS2016-Analysis-Reference.pdf.

[12] Benedetti A. Cosentino N. "Use of orthogonal decomposition tools in analyzing wind effect on structures". In: *Structural Engineering International* 15(4) (2005), pp. 264–270. DOI: 10.2749/101686605777962829.

[13] Diana G. Bocciolone M. Collina A. Tosi A. Rocchi D. "Wind tunnel investigation on Braga Stadium". In: *Final report*. 2003.

[14] Magalhães F. "Stochastic modal identification for the validation of numerical models (Portuguese)". Master thesis. University of Porto, 2004.

[15] Bastos R. Furtado R. Quinaz C. "The new Braga Municipal Stadium". In: *Structural Engineering International* 15(2) (2005), pp. 72–76. DOI: 10.2749/101686605777963143.

[16] Bastos R. Furtado R. Quinaz C. "The new Braga Municipal Stadium, Braga, Portugal". In: *Proc. 2^{nd} International Congress, Fédéracion Internationale du Béton FIB*. Naples, Italy, 2006. URL: http://www.afaconsult.com/uploads/FicheirosImprensa/2412_4.pdf. (visited in: 3-23-2021).

[17] Majowiecki M. *Structural architecture for large roofs: concepts and realizations*. 2005. URL: https://www.majowiecki.com/userfiles/Progetto/files/@singleFileGallery/2005_-_Structural_architecture_for_large_roofs_concepts_and_realizations.pdf.

[18] Cunha A. Magalhães F. Caetano E. "Operational modal analysis and finite element correlation of the Braga Stadium suspended roof". In: *Engineering Structures* 30(6) (2008), pp. 1688–1698. DOI: 10.1016/j.engstruct.2007.11.010.

[19] M. Majowiecki. *Tensostrutture: progetto e verifica*. Edizioni CREA, 1994.

[20] Cosentino N. Majowiecki M. "Analysis and mitigation of the wind induced response of large span suspended roofs: the case of the new Braga Stadium". In: *Proc. 8^{th} Italian National Conference on Wind Engineering IN-VENTO*. Reggio Calabria, Italy, 2004. URL: https://www.majowiecki.com/userfiles/Progetto/files/@singleFileGallery/2005_-_Analysis_and_mitigation_of_the_wind_induced_response_of_large_span_suspended_roofs-the_case_of_the_new_Braga_Stadium.pdf.

[21] Cosentino N. Majowiecki M. "Design assisted by wind tunnel testing". In: *Proc. IABSE Symposium: Large structures and infrastructures for environmentally constrained and urbanised areas*. Venice, Italy, 2010. URL: https://www.majowiecki.com/userfiles/Pubblicazione/files/2010-IABSE-Design-assisted-by-wind-tunnel-testing.pdf.

[22] Cosentino N. Majowiecki M. "Dynamic aspects of the new Braga Stadium large span roof". In: *Proc. IASS Symposium*. Venice, Italy, 2007. URL: https://www.majowiecki.com/userfiles/Progetto/files/@singleFileGallery/2007_-_Dynamic_aspects_of_the_new_Braga_Stadium_large_span_roof.pdf.

[23] Cosentino N. Marini M. Majowiecki M. "Dynamic characterization of the New Braga Stadium large span suspension roof". In: *Proc. International Conference on Experimental Vibration Analysis for Civil Engineering Structure EVACES*. Bordeaux, France, 2005. URL: https://www.majowiecki.com/userfiles/Progetto/files/@singleFileGallery/2005_-_Dynamic_characterization_of_the_New_Braga_Stadium_large_span_suspension_roof.pdf.

[24] Der Kiureghian A Rezaeian S. "A stochastic ground motion model with separable temporal and spectral nonstationarities". In: *Earthquake Engineering and Structural Dynamics* 37(14) (2008), pp. 1565–1584. DOI: 10.1002/eqe.831.

[25] Der Kiureghian A Rezaeian S. "Simulation of synthetic ground motions for specified earthquake and site characteristics". In: *Earthquake Engineering and Structural Dynamics* 39(10) (2010), pp. 1155–1180. DOI: 10.1002/eqe.997.

[26] RWDI. "Wind tunnel study of roof wind pressures, Braga Stadium". In: *Report 01-327*. 2001.

[27] M. Seidel. *Tensile Surface Structures: A Practical Guide to Cable and Membrane Construction*. Wiley, 2009.

[28] *Stadio Comunale di Braga*. URL: https://it.wikipedia.org/wiki/Stadio_comunale_di_Braga (visited on 09/07/2021).

[29] European Committee for Standardization. *UNI EN 1990 Eurocodice 0: Criteri generali di progettazione strutturale*. 2006.

[30] European Committee for Standardization. *UNI EN 1991-1-1 Eurocodice 1: Azioni sulle strutture – Parte 1-1: Azioni in generale - Pesi per unità di volume, pesi propri e sovraccarichi per gli edifici*. 2004.

[31] European Committee for Standardization. *UNI EN 1991-1-3 Eurocodice 1: Azioni sulle strutture – Parte 1-3: Azioni in generale - Carichi da neve*. 2004.

[32] European Committee for Standardization. *UNI EN 1991-1-4 Eurocodice 1: Azioni sulle strutture – Parte 1-4: Azioni in generale - Azioni del vento*. 2010.

[33] European Committee for Standardization. *UNI EN 1991-1-5 Eurocodice 1: Azioni sulle strutture – Parte 1-5: Azioni in generale - Azioni termiche*. 2004.

[34] European Committee for Standardization. *UNI EN 1992-1-1 Eurocodice 2: Progettazione delle strutture in calcestruzzo – Parte 1-1: Regole generali e regole per gli edifici*. 2004.

[35] European Committee for Standardization. *UNI EN 1993-1-11 Eurocodice 3: Progettazione delle strutture in acciaio – Parte 1-11: Progettazione di strutture con elementi tesi*. 2007.

[36] European Committee for Standardization. *UNI EN 1993-1-3 Eurocodice 3: Progettazione delle strutture in acciaio – Parte 1-1: Regole generali - Regole supplementari per l'impiego dei profilati e delle lamiere sottili piegati a freddo*. 2004.

[37] European Committee for Standardization. *UNI EN 1998-1-11 Eurocodice 8: Progettazione delle strutture per la resistenza sismica – Parte 1: Regole generali, azioni sismiche e regole per gli edifici*. 2005.

[38] *SVS - ARTEMIS Extractor Pro, release 3.41. Structural vibration solutions*. Aalborg, Denmark, 1999.

[39] De Moor B. Van Overschee P. *Subspace identification for linear systems: Theory - Implementation - Applications*. Kluwer Academic Publishers Group, 1996. DOI: 10.1007/978-1-4613-0465-4.

Anexo al Trabajo Fin de Grado/Máster

Relación del TFG/TFM "Probabilistic structural evaluation of a cable-suspended concrete roof: the Braga Stadium (Portugal)" con los Objetivos de Desarrollo Sostenible de la Agenda 2030.

Grado de relación del trabajo con los Objetivos de Desarrollo Sostenible (ODS).

Objetivos de Desarrollo Sostenibles	**Alto**	**Medio**	**Bajo**	**No Procede**
ODS 1. **Fin de la pobreza.**			**X**	
ODS 2. **Hambre cero.**			**X**	
ODS 3. **Salud y bienestar.**		**X**		
ODS 4. **Educación de calidad.**			**X**	
ODS 5. **Igualdad de género.**			**X**	
ODS 6. **Agua limpia y saneamiento.**			**X**	
ODS 7. **Energía asequible y no contaminante.**			**X**	
ODS 8. **Trabajo decente y crecimiento económico.**		**X**		
ODS 9. **Industria, innovación e infraestructuras.**	**X**			
ODS 10. **Reducción de las desigualdades**.			**X**	
ODS 11. **Ciudades y comunidades sostenibles**.		**X**		
ODS 12. **Producción y consumo responsables.**			**X**	
ODS 13. **Acción por el clima.**			**X**	
ODS 14. **Vida submarina.**			**X**	
ODS 15. **Vida de ecosistemas terrestres.**			**X**	
ODS 16. **Paz, justicia e instituciones sólidas.**			**X**	
ODS 17. **Alianzas para lograr objetivos.**			**X**	

Descripción de la alineación del TFG/M con los ODS con un grado de relación más alto.

El resultado obtenido con este trabajo constituye un método innovador y más sencillo para el diseño y evaluación de la seguridad de las infraestructuras con respecto a las acciones del sismo, a través de modelos simplificados. Permite así de obtener construcciones más resilientes y estructuralmente eficientes, representando una innovación, aunque pequeña, en el campo de la industria, la innovación y las infraestructuras, de acuerdo con el ODS 9 y, en medida menor, con los ODS 3, 8 y 11.